Durham E-Theses

F.T.I.R. and Rheological studies of surfactant adsorption onto silica

Nunn, Nicholas Simon

F.T.I.R. and Rheological Studies of Surfactant Adsorption onto Silica

by

Nicholas Simon Nunn B.Sc.

A thesis submitted to the University of Durham

for the degree of Doctor of Philosophy

1993

DECLARATION

The work described in this thesis was carried out by me in the Chemistry Department in the University of Durham and at Shell Research, Thornton, between October 1990 and September 1993. I declare that this work has not been accepted in substance for any degree, and is not being concurrently submitted in candidature for any other degree. The work is original except where indicated by reference.

Signed

Date

FOR MY WIFE

ACKNOWLEDGEMENTS

ABSTRACT

The adsorption of four surfactants at the silica-toluene interface have been investigated by Fourier-transform infrared - attenuated total reflection (FTIR-ATR) spectroscopy. Specifically, hexadecylamine, 1,12-diaminododecane, didecylamine and sorbitan monopalmitate were studied. The silica surface for the spectroscopic experiments was provided by the native oxide layer on a silicon ATR prism. In order to study the CH_2 stretching vibrations, the solvent was fully deuterated.

Careful calibration of the ATR experiment enabled the contribution to the ATR spectrum made by adsorbed species to be calculated. The surface excess concentration of the amines were calculated over a range of bulk solution conentrations, enabling adsorption isotherms to be constructed.

The use of polarized radiation allowed the orientation of the molecules within the adsorbed layer to be studied. The adsorbed layer of hexadecylamine showed some ordering of the aliphatic chains. There is some spectral evidence that the chains in the adsorbed layer of 1,12-diaminododecane adopt a 'looped' configuration.

The effect of adsorbed layers of the molecules listed above upon the rheological behaviour of Aerosil 200 dispersions in toluene was investigated. Differences in the rheological behaviour of these dispersions have been correlated to differences in adsorbed layer structure as determined by FTIR-ATR. Due to differences in the Aerosil and ATR surface these correlations must be treated cautiously.

Table of Contents

Chapter 1   Introduction

Introduction

The purpose of this preliminary chapter is to establish a contextual framework in which to set the rest of the thesis. The body of work described in the following chapters is an investigation of the formation and structure of adsorbed layers of model surfactants at the solid/liquid interface and the effect such layers have on the rheology of solid-in-liquid colloidal dispersions. The first part of this introduction outlines the importance of solid-in-liquid colloidal dispersions and the effect adsorbed molecules have on their macroscopic behaviour. There exists a large body of knowledge of such macroscopic behaviour and the reader will be referred to several excellent comprehensive texts on the subject. The microscopic structure of adsorbed layers of surfactants is rather less well known. Interest in such structures has grown over the past two decades. Spectroscopic techniques have been developed to investigate adsorption behaviour at the molecular level. As the thesis is centred around such an investigation, the second, and major, part of this introductory chapter, presents a literature review of the favoured spectroscopic techniques and the important results which they have generated. An in-depth description of the theory of the particular technique employed extensively throughout this thesis is not given until chapters 2 and 3.

The aim of the work described in the following chapters is to correlate adsorption behaviour at the molecular level to the macroscopic properties of solid-in-liquid dispersions.

1.1   Colloidal Dispersions

A colloidal dispersion consists of a continuous phase, or *dispersion medium*, throughout which are distributed small particles of a discontinuous, or *dispersed phase*. The particles of the dispersed phase typically have at least one dimension in the size range 1nm to 1μm. Below 1nm the particles are so small that they are of molecular dimensions and the distinction between a colloidal dispersion and a true solution become irrelevant. Dispersions of particles larger than 1μm are usually referred to as *suspensions*. The continuous phase and the dispersed phase may be either solid, liquid or gaseous and all combinations are known apart, of course, from gas-in-gas. Table 1.1 gives a few examples of colloidal systems [1]. Such is the range and importance of colloidal systems that an entire branch of science, *colloid science*, is devoted to their study. There are a number of excellent texts on the subject [1,2] and it is beyond the scope of this introduction to give more than a brief outline of the issues pertinent to this thesis. Here we shall be concerned solely with dispersions of solid particles in a liquid continuous phase, commonly called *sols*. Sols can be differentiated on the basis of the dispersion medium. When the continuous phase is aqueous the sol is termed a *hydrosol* whereas dispersions in organic liquids are called *organosols*. It is with these organosols that this thesis is primarily concerned. Much of the effort in colloidal science is devoted to the study of the stability of sols. This subject is introduced in the following section.

<u>Table 1.1</u>   <u>Some Colloidal Systems</u>

Dispersed Phase	Dispersion Medium	Name	Examples
Gas	Solid	Solid Foam	Insulating foam
Gas	Liquid	Foam	Shaving foam
Liquid	Liquid	Emulsion	Milk
Liquid	Gas	Aerosol	Mist
Solid	Solid	Solid Dispersion	Alloys
Solid	Liquid	Sol	Ink, Paint
Solid	Gas	Aerosol	Smoke

1.2   The Stability of Sols

A dispersion of uncharged, non-sterically stabilized particles undergoes rapid

coagulation. The reason for the inherent instability of sols is that attractive dispersion

forces operate between the dispersed particles. The particles undergo rapid Brownian

motion and may collide. As a result of the attractive forces operating between the

particles, these collisions are "sticky" and result in the formation of particle pairs and

higher aggregates. The process proceeds until the previously dispersed phase is

present as a single lump. This process is described as *coagulation* if it results in a

tightly-bound coagulum or *flocculation* if a loosely bound, open, aggregate is formed.

However, some sols remain dispersed for a long time. Such sols are described as being

stable.

1.1.1   The Origin of the Attractive Forces between Colloidal Particles

In 1934 F. London proposed that transitory dipole-transitory dipole (i.e. dispersive) interactions served as attractive forces between gas molecules [3]. Such forces are responsible for the liquefaction of gases such as argon and helium. A few years later, H.C. Hamaker extended the theory to calculate the forces of attraction between colloidal particles [4]. Hamaker's theory was based upon the pairwise summation of dispersion forces. The theory is fraught with approximations and has been largely superseded by the macroscopic continuum theory of Lifshitz [5]. The Hamaker theory is considerably simpler than the Lifshitz theory and provides useful insight into the magnitude of forces between particles. For a pair of spheres of radii a_1 and a_2 separated by a centre-to-centre distance R, the Hamaker theory predicts that if $R >> a_1 + a_2$ the potential energy, $V_A(R)$, is given by:

$$V_A(R) \approx -(16A_{12}/9)(a_1^3 a_2^3 / R^6) \qquad\qquad 1.1$$

where A_{12} is the Hamaker constant. A_{12} is a function of the nature of the particles. Like, uncharged, particles always attract. The attractive force falls off to the sixth power of particle separation. For latex dispersions A_{12} is of the order of kT but may be much larger for metallic and inorganic sols. A pair of latex particles of radii 120nm have a potential of attraction of $2kT$ at a separation of 5nm and $10kT$ at a separation of 1nm [6]. This exceeds the thermal energy available to the particles ($\approx kT$) and is therefore likely to result in coagulation. In order to impart stability to a dispersion it is therefore necessary to provide a repulsive interaction between the particles which is at least equal to the attractive force both in magnitude and range.

1.1.2 Methods of Imparting Stability

The need to provide a long-range repulsive interaction between colloidal particles severly limits the number of strategies available for the stabilization of sols. Indeed, there are only two generally applicable stabilization methods available, namely *electrostatic* stabilization and *steric* (or *polymeric*) stabilization. The general principles of imparting stability to colloidal dispersion are shown in figure 1.1. The diagram shows how potential energy varies with the separation of two stabilized particles. The potential energy curve is obtained by the superposition of the van der Waals attraction and the repulsion curves. At very close separation Born repulsion operates. One maximum and two minima can be identified. The degree of stability is governed by the height of the primary maximum; if sufficiently large the dispersion will show long-term stability.

Figure 1.1   Schematic of the Potential Energy as a Function of Separation Between Two Stabilized Particles

van der Waal's Attraction V_A

Electrostatic Repulsion V_R

Total Potential Energy $V_T = V_S + V_R$
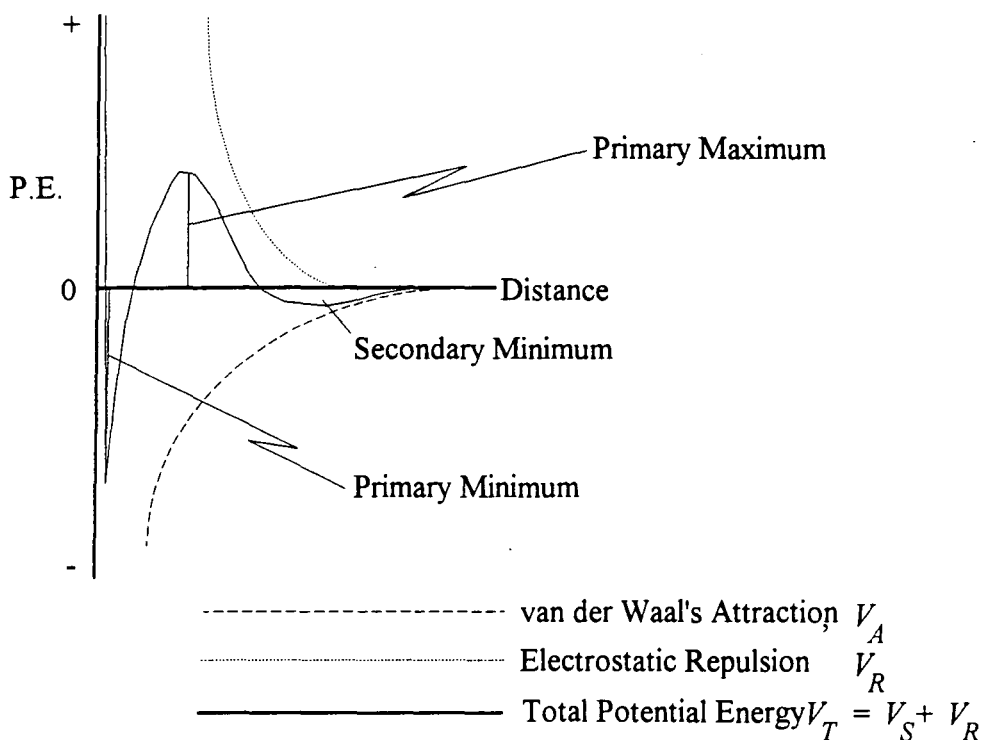
Electrostatic stabilization employs Coulombic repulsion between similarly charged colloidal particles to prevent aggregation. In aqueous solution, the particles may possess a *diffuse electrical double layer*, the electrostatic potential of which may extend sufficiently far into the surrounding medium to provide a repulsive interaction stronger than the attractive interaction due to van der Waals forces. The extent of this double layer is sensitive to electrolyte concentration. Upon increasing the electrolyte concentration the double layer "contracts" and may no longer counteract the attractive van der Waals forces. In such cases coagulation occurs. Electrostatic stabilization, then, is only applicable to hydrosols in which the electrolyte concentration in the dispersion medium is weak (e.g. $<10^{-2}M$).

Electrostatic stabilization is very well understood [1] but, because of its sensitivity to the ionic strength of the dispersion medium it has limited applicability, and therefore the second method of imparting stability to colloidal dispersions, steric stabilization, has been the subject of ever-increasing interest [6 (which also contains 17 references to review articles published between 1969 and 1982, indicating the explosion of interest in this area)]. In this technique, a layer of adsorbed polymer on each colloidal particle provides a barrier to aggregation. Polymers are able to do this because the spatial extensions of polymers molecules are, under favouable solvation conditions, are usually comparable to, or greater than the range of the van der Waals attraction. In order to cause a repulsive interaction during a Brownian encounter between two particles, the interaction between a polymer segment and the surrounding solvent must be energetically more favourable than the interaction between two polymer segments. Otherwise the polymer chains would stick together and their presense would not only have no stabilizing effect but may even promote flocculation. In terms of polymer solution thermodynamics, the dispersion medium should be better than a θ-solvent (a solvent in which the free energy of mixing the polymer and solvent is zero) if stability is to be promoted. Sterically stabilized dispersions are rather insensitive to electrolyte concentration and use of an appropriate polymer allows the technique to be employed

in both hydrosols and organosols. Flocculation can be induced by reducing the dispersion medium to a poorer-than-θ-solvent. This can be achieved by raising the temperature or adding a miscible non-solvent. Polymer-polymer contact become favoured and Brownian collisions result in aggregate formation.

The foregoing discussion of polymeric stabilization assumes that the colloidal particles are completely covered by polymer and that those polymer molecules are well-anchored to the particle surface. When the particles are incompletely covered, the possibility exists of a polymer molecule on one particle becoming attached to a second particle. This is known as *bridging flocculation*. Poor anchoring of the polymer to the particle surface may result in the chain becoming detached during a collision.

In this thesis the adsorption of polymeric molecules has not been examined. Rather, the adsorption behaviour of smaller molecules has been investigated. Specifically the adsorption of nonionic surfactants has been studied. Figure 1.2 shows a schematic representation of a nonionic surfactant molecule. There are two parts to its structure; a polar *headgroup* and an aliphatic *tail*. When placed in two-phase system consisting of a nonpolar solvent and a polar solid surface the surfactant would be expected to adsorb such that the headgoup was bound to the surface while the aliphatic tail projects into the solvent, as shown in figure 1.3.

Figure 1.2   Schematic Representation of A Nonionic Surfactant

Polar Headgroup

Aliphatic Tail
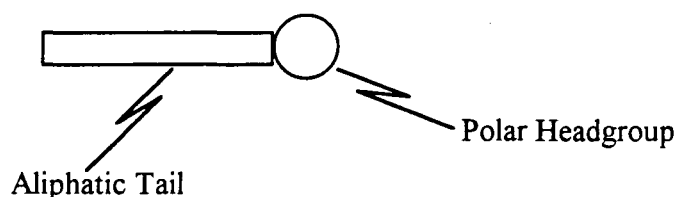
Figure 1.3   Adsorption Scheme for a Nonionic Surfactant in a Nonpolar Solvent
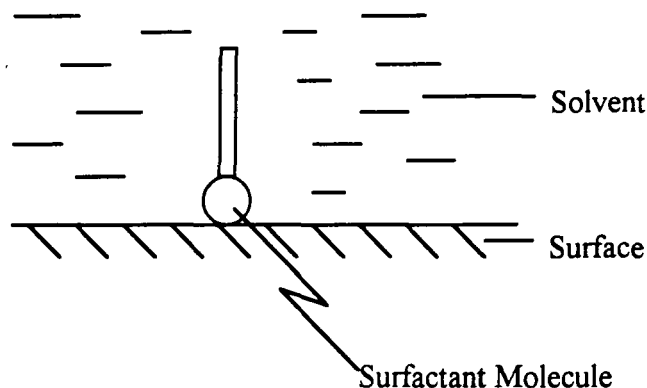
The headgroup of a nonionic surfactant is not ionised in aqueus solution, hence the term *nonionic*. The tail is typically of the order of 10-18 methylene units long. Such short chains would never be described as polymeric and hence their spatial extension may not be sufficient to impart stability to the majority of colloidal dispersions. However, if the particles of the dispersed phase are at the lower end of the colloidal size range then adsorption of nonionic surfactants may induce measureable changes in the macroscopic properties of the dispersion. Later in this thesis, this will be shown to be the case.

It is the formation and structure of such adsorbed layers which is of interest. Essentially, we wish to know three pieces of information about the adsorbed surfactant:

I.   The amount of surfactant adsorbed, i.e. the tendency of the molecule to adsorb

II.   The nature of the binding of the headgroup to the surface.

III. The stereochemistry of the tails.

Futhermore, the question arises how the above three parameters affect the macroscopic behaviour of organosols. It is to these questions that the thesis is primarily addressed. The following section describes the current state of knowledge about surfactant adsorption.

1.2   The Structure of Adsorbed Layers

The structure of layers of molecules adsorbed at interfaces has been the subject of considerable interest over the past two decades. This study is concerned with the structure of layers of small, surfactant molecules and we shall concentrate on this area in this review. However, there has been great interest in the structure of polymer layers, and the advances in the elucidation of such structures is outlined in the next two sub-sections.

1.2.1   Polymer Adsorption

The importance of adsorbed polymer layers to colloidal stability has already been mentioned. Therefore, it is unsurprising that the structure of adsorbed polymer layers has been the subject of considerable interest.

Polymeric stabilization may be described in terms of polymer solution thermodynamics and the behaviour of polymer chains may be predicted by statistical computations. A number of articles have been published which reflect the application of theoretical and computational chemistry to polymeric adsorption and stabilization [7-14].

The kinetics of polymer adsorption has been studied by a number of experimental techniques, including ellipsometry [15], reflectometry [16] and internal reflection interferometry [17].

Infrared spectroscopy can yield large amounts of chemical information about a system and has been applied widely to the study of molecular adsorption. In the context of polymer adsorption, the series of papers by Kawaguchi *et al* [18,19,20] are typical. In

this work, infrared (IR) spectroscopy is used to study the adsorption of a normally-terminated polybutadiene and a polybutadiene terminated with a highly-polar headgroup (1,1-bis(*p-N,N'*-diethylaminophenyl)methanol) onto silica from non-polar solvents. The amount of polymer adsorbed, the fraction of surface silanols covered and the bound fraction of polymer were determined. The results showed that the polar headgroup adsorbed preferentially onto the surface silanol groups compared with the carbon-carbon double-bond of the polybutadiene chain. The same group went on to study the adsorption of polystyrene and poly(methyl methacrylate) on a silica surface by IR spectroscopy [21]. Further use of IR spectroscopy was made by Cosgrove *et al*, who investigated the adsorption of linear and cyclic polymethylsiloxanes on alumina [22]. The Si-H species reacts with the hydroxyl groups associated with the alumina surface, eliminating molecular hydrogen, chemically binding the polymer to the surface. This chemisorption is preceded by physisorption. Killman *et al* studied the adsorption of ethylene oxide-propylene oxide copolymers from carbon tetrachloride onto silica by infrared spectroscopy [23]. The ethylene oxide segments were shown to be preferentially adsorbed compared with the propylene oxide segments.

1.2.2 Adsorption of Non-polymeric Molecules

Much of the early work on the adsorption of non-polymeric molecules at the solid/liquid interface was concerned with the nature of the binding between the solid surface and the molecule. One of the most widely studied solid surfaces was that of silica. The surface chemistry of silica is quite well characterised, and is the surface of interest in this thesis.

1.2.2.1 The Silica Surface

The chemistry of silica is covered comprehensively in the work by Iler [24]. The surface of a silica particle is covered by silanol (SiOH) groups. On a non-porous, amorphous, smooth silica surface which is fully hydroxylated there are 4-5 SiOH groups per nm^2. The surface is amorphous and hence the separation between adjacent

SiOH groups is variable. There exists, therefore, the possibility of hydrogen bonds of varying strengths being formed between the silanol groups. Hydrogen bonds may also form between the silanol groups and water molecules. On exposure to the atmosphere, the silica surface rapidly becomes covered with an adsorbed layer of water. Indeed, Aerosil silicas (finely divided pyrogenic silicas produced by Degussa A.G.) can take up 40% of its weight in water without losing the appearance of a dry powder [25]. Infrared spectroscopy has been used to study the surface silanol groups [26, 27, 28]. These studies have identified the following groups on the silica surface:

Table 1.2   Infrared Assignments for the Silica Surface

Type of Group	Identifying Absorption Band (cm^{-1})
Single "free" OH on surface	3750
Paired (hydrogen bonded) OH's on surface	3540
Internal hydrogen bonded OH's	3650
Molecular physisorbed water	3400

The adsorbed water may be removed by heating in dry air at 120°C or by heating at lower temperatures under reduced pressure. Heating the silica strongly will lead to condensation of the silanol groups *viz*:

$$\equiv SiOH + HOSi\equiv \rightarrow \equiv Si\text{-}O\text{-}Si\equiv + H_2O$$
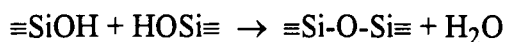
There have been numerous studies of adsorption onto the silica surface. A study of polymeric adsorption has already been mentioned [Sect 1.2.1 and refs. 18-21]. Studies of the adsorption of smaller molecules are described in the following sub-section.

1.2.2.2 Adsorption of Small Molecules onto Silica

The studies of adsorption phenomena have concentrated on the nature of the binding between the headgroup of the adsorbing molecule and the substrate and the orientation of the tails. In this section the binding interactions will be considered. Orientation studies will be described in the following section.

Much of the early work on headgroup-substrate interactions were concerned with adsorption onto powders. In the late 1960's, Low [29] designed a cell which enabled adsorption at the solid/liquid interface to be studied *in situ* by infrared spectroscopy. The solid was in the form of a powder which was compressed into a self-supporting disc. This disc could be heated in a furnace to remove adsorbed water and subjected to a vacuum to remove gases before being immersed in solvent (CCl_4) in the infrared beam. Surfactant solution was then circulated through the cell and changes in the infrared spectrum were recorded as adsorption occurred. The cell was used to examine the adsorption of stearic acid on zinc oxide [30], silica and alumina [31], decanoic acid on magnesia [31] and octadecanol, octadecylamine and octadecanedioic acid on silica [32]. Stearic acid formed a stearate with the zinc oxide and the alumina. However, stearate formation is not possible with the silica surface, and only weak, physisorption was observed, the acid adsorbing as monomers at low concentration and as dimers at higher concentration. Shifts in the frequency of the isolated silanol band were observed upon adsorption of a surfactant onto the silica surface and the amount of shift was related to the strength of the binding interaction [32]. Octadecylamine interacted strongly with the silanol groups, causing the silanol OH stretching frequency to shift to a lower frequency by approximately $750cm^{-1}$. The octadecanol interacted somewhat less strongly, causing a shift of around $275cm^{-1}$. The octadecanedioic acid interacted only weakly. The acidic character of the silanol group is evident from these observations. Interaction with an acid is only weak whereas that with an amine is strong, even though hydrogen-bonding possibilities exist with both classes of

molecules. The work of Low *et al* has been reviewed by Rochester [33], who was also involved with IR studies of molecular adsorption onto powders. This review gives an overview of the contribution infrared spectroscopy has made to the understanding of adsorption onto powders at the solid/liquid interface and covers adsorption of many classes of molecule onto silica. However, amines are of primary interest to the current work due to their strong interaction with the silica surface and so the reader is refered to Rochester's review for discussions of other classes of molecule.

1.2.2.3 Molecular Orientation

In the spectrum of stearic acid adsorbed on zinc oxide, Hasegawa and Low observed a series of weak bands in the 1350-1180cm^{-1} region [30]. These bands are associated with the disturbed wagging of methylene groups of the aliphatic chains. The methylene groups may interact so that they vibrate with each other with various phase differences if they are arranged in a coplanar, *trans* conformation. In other words, the band *progression* is only observed when the paraffinic chains are ordered in some crystalline arrangement. The band progression is therefore observed in solid stearic acid but is not apparent in the spectrum of a solution of the acid. The observation of a band progression in the spectrum of adsorbed stearic acid is evidence that the aliphatic chains in the adsorbed layer are packed in a regular arrangement. Moreover, Low used the frequency separation of the bands to obtain an approximate tilt-angle for the aliphatic chains. He concluded that the adsorbed stearate layer had a regular structure, with the chains tilted by about 60°.

In addition to the work on powders, Low also investigated adsorption by attenuated total reflection spectroscopy (ATR) [34]. He was able to study molecular orientation in an entirely different way to the progression band study. ATR is an experimental technique which has found favour with many workers in the field of thin-film technology and is the principal technique used in this thesis. The theory of ATR spectroscopy will be set out in considerable detail in the next chapter. However, it is

instructive at this stage to briefly outline the technique and set out some of the information which has been gained from its use over the past two decades.

1.3   An Introduction to Attenuated Total Reflection Spectroscopy

Attenuated total reflection (ATR) spectroscopy, also known as internal reflection spectroscopy (IRS), is a technique which was developed independently by Harrick [35, 36] and Fahrenfort [37] in the 1960's. The experimental configuration is shown in figure 1.4. Light from a spectrometer source undergoes multiple internal reflection in a prism of high refractive index. Where reflection occurs, the incident and reflected rays interfere to form a standing wave in the prism and an *evanescent* wave in the optically rarer medium. If the rarer medium contains species capable of absorbing some of the radiation in the evanescent field, the reflected beam will be of lower intensity than the incident beam, i.e. the reflection is attenuated. In other words, the propagating radiation travelling through the prism contains spectral information about the rarer medium. As a result of this process, a spectrum of the rarer medium can be obtained. ATR is usually used in conjunction with infrared spectroscopy. The probing radiation is evanescent in nature; it decays exponentially with distance into the rarer medium, becomming vanishingly small at a depth of the order of one micron. As the amount of radiation absorbed by an infrared active species is proportional to the electric field intensity (the amplitude squared) of that radiation at the point where absorption occurs, species close to the surface of the prism in the rarer medium contribute more to the spectrum than those species further away from the interface. In principle then, ATR appears to be a useful technique for studying adsorption at the liquid/solid interface, where the solid surface is provided by the ATR prism. The following section describes some of the ATR studies of molecular layers.

1.3.1 ATR Studies of Molecular Adsorption

The past decade has seen considerable activity in the field of ordered organic thin films. These have potential applications such as nonlinear optical devices, chemical, physical

Figure 1.4 The ATR Experiment

Source

Detector

ATR Prism

Standing
Wave

Prism n_1

Evanescent
Field

Sample n_2

Not to
Scale
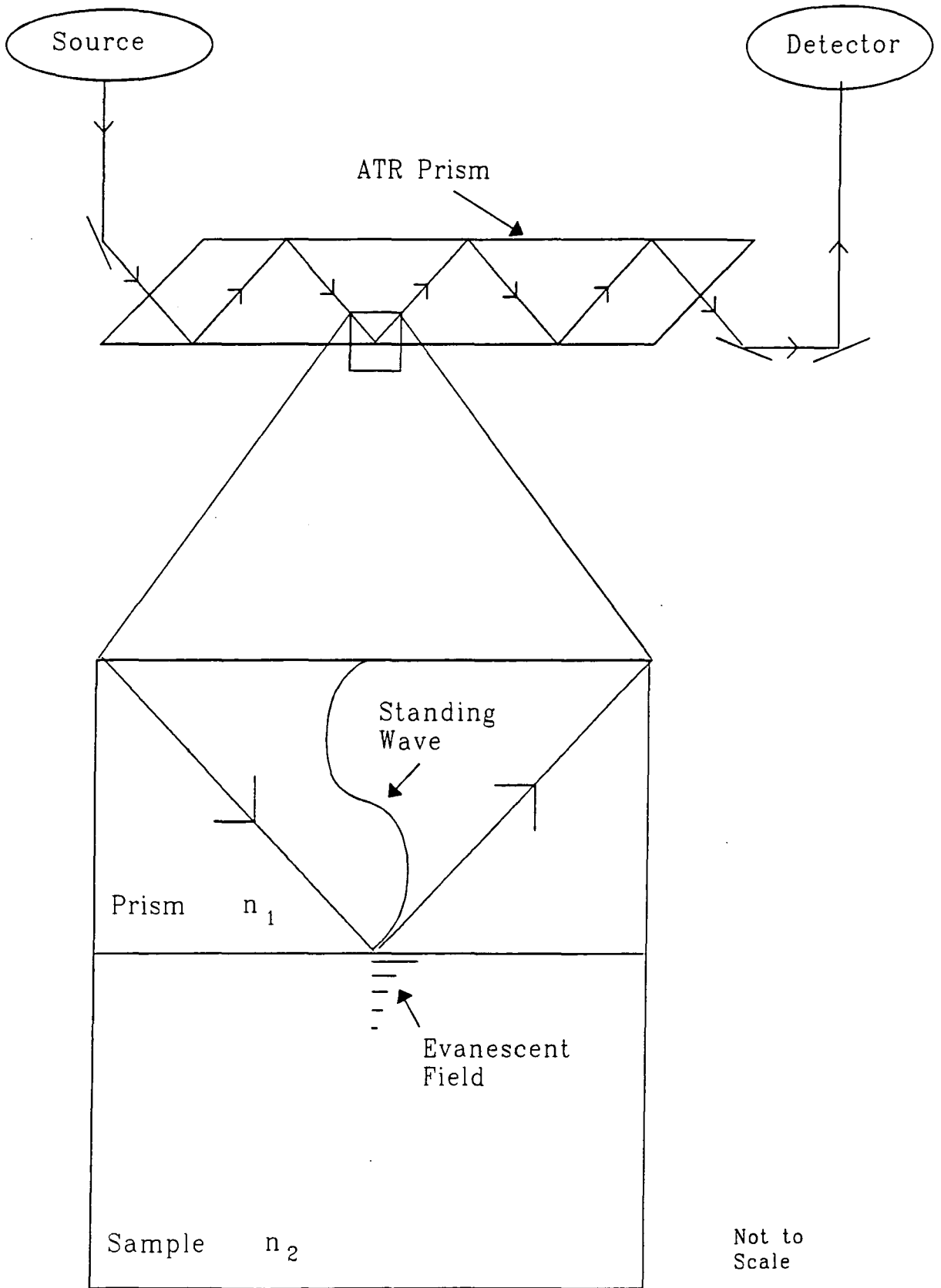
and biological sensors, protective layers, patternable materials for information storage and resist, surface tailoring and synthetic biomacromolecules [38]. Attenuated total reflection spectroscopy has been used extensively in the study of such films and the theory of ATR has been highly developed to obtain the maximum information from the spectra. In comparison to the number of papers published on the ATR spectra of thin organic films, those published on surfactant adsorption have been relatively few. Therefore, it is necessary to discuss the studies of thin films. Here we shall discuss some of the results obtained, and leave the development of ATR theory to the next chapter.

There are essentially two main routes to the formation of an ordered organic thin film, namely Langmuir-Blodgett (LB) deposition and self-assembly (SA). Langmuir-Blodgett deposition is shown schematically in figure 1.5. The deposition technique essentially involves the transfer of an ordered film from the water/air interface to a solid substrate. The ordered layer at the air/water interface is obtained by compressing a surfactant layer. As the solid substrate is repeatedly dipped through the layer, ordered layers are successively transferred to it, removing surfactant molecules from the air/water interface. The surface pressure therefore has to be maintained by reducing the area of the interface with a moving barrier. The transfer process can be followed by measuring the surface pressure as a function of area.

The self-assembly process is shown schematically in figure 1.6. The solid substrate is immersed in a solution of the molecules to be adsorbed. The headgroups physi- or chemisorb onto the surface. The process continues until a monolayer is formed. In LB deposition the chemical nature of the solid substrate is of less importance. An ordered monolayer is present (at the air/water) interface before transfer. If the solid substrate is hydrophobic, a monolayer is transferred as the plate is first dipped through the interface, as the aliphatic chains adsorb. A hydrophillic surface will pick up a layer when first withdrawn from the liquid as the headgroups adhere to the solid surface. In contrast, the chemical nature of the solid surface is pivotal to self-assembly. In order

16

Figure 1.5 Langmuir-Blodgett Deposition

Dipping Head

Moveable Barrier

Compressed Layer
(not to scale)

Solid Substrate

Water subphase

Trough
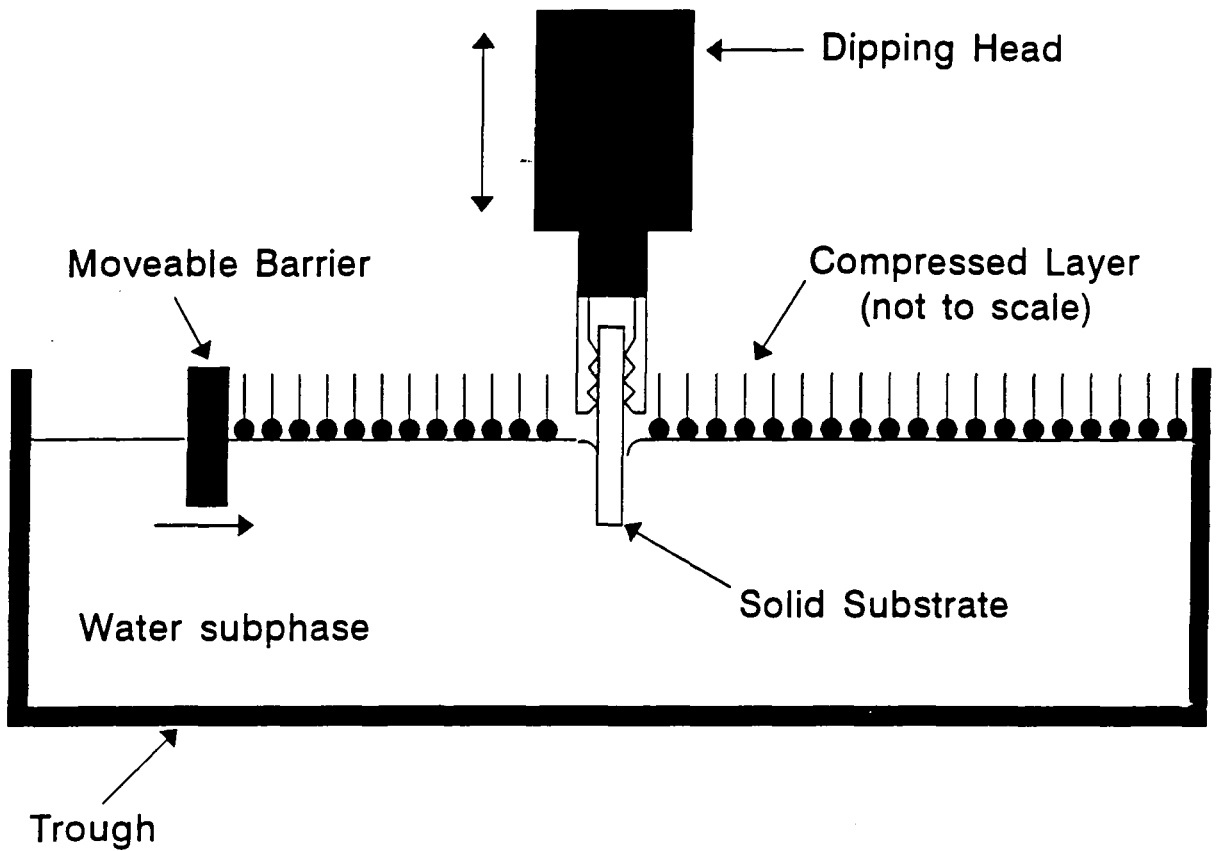
Hydrophobic Substrate

Hydrophilic Substrate
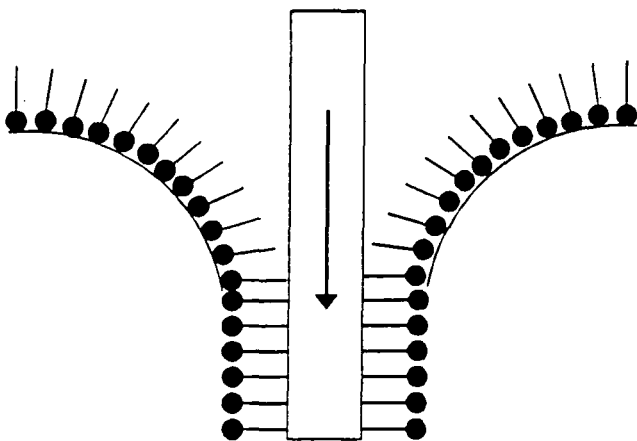
Hydrophobic chains adhere
to surface as the solid is
immersed in the water
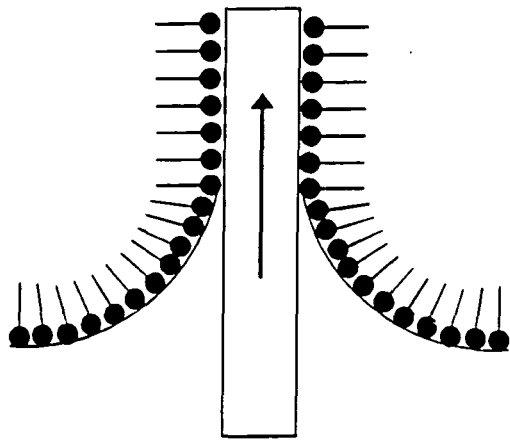
Hydrophilic headgroups adhere
to surface as the solid is
withdrawn from the water

17

Figure 1.6 Schematic of Molecular Self-Assembly

18
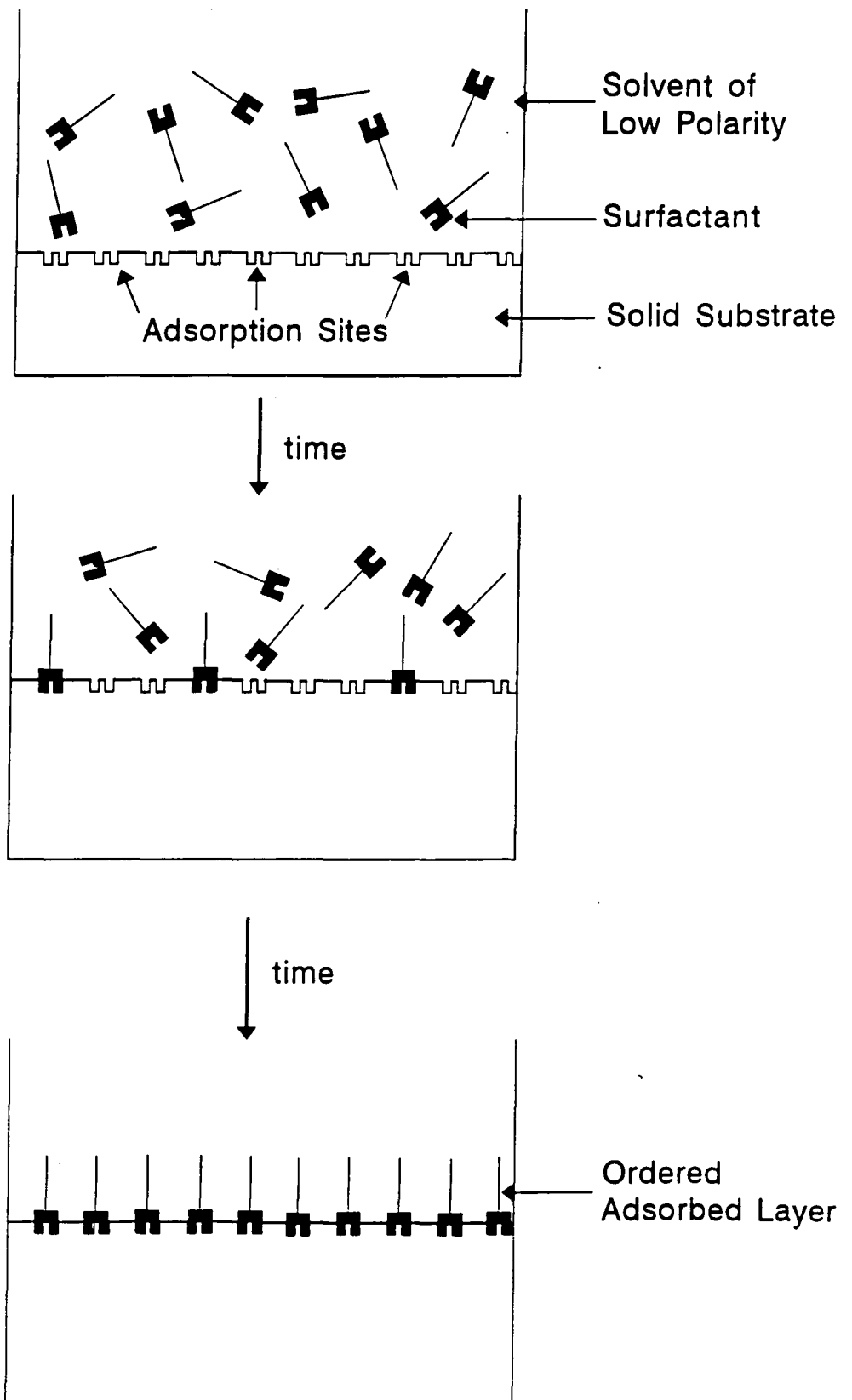
to form a well-ordered film by self-assembly it is necessary that the surfactant headgroups adsorb strongly to the surface and that the sites for adsorption are sufficiently close together to allow dense packing of the adsorbed molecules. This requirement for specific substrate-headgroup chemistry limits the number of systems to which SA can be applied. The formation of multilayers is somewhat more bothersome by SA than by LB deposition as it usually require funtionalization of the outer surface of the film prior to deposition of a second layer. However, SA has some advantages over LB depostion. The former requires less equipment and is likely to be more amenable to industrial scale-up than the latter. The SA process is the same as surfactant adsorption an so studies of SA processes are of interest to colloid science.

1.3.2 Langmuir-Blodgett Films and Model Biological Membranes

The sensitivity of ATR to adsorbed layers is illustrated by the work of Takenaka et al [39]. 1, 2, 3, 4, 5 and 9 monolayers of stearic acid were deposited by the LB technique onto a germanium ATR prism. The methylene scissoring band indicated that the hydrocarbon chains in the first layer were in a hexagonal subcell packing with the major chain axis oriented approximately perpendicular to the prism surface. In LB films consisting of more than two monolayers, the molecules in the layers above the first crystallized in a monoclinic form with the chain axis inclined at an angle of 30° to the surface normal.

Takenaka also employed ATR spectrosopy to characterize model biological membranes. These consist of phospholipid bilayers in which proteins may be incorporated. Model membranes may be prepared in a number of ways, including LB deposition; hence the inclusion here. In some early work, Takenaka et al used ATR spectroscopy to elucidate the structure of phospholipid monolayers [40] and went on to study the orientation of gramicidin D, a linear pentadecapeptide, when incorporated in phospholipid multibilayers [41]. The gramicidin produced little effect on the orientation of the phospholipid molecules, indicating that the protein penetrates the

lipid bilayers with little perturbation of layer structure. Futher use of ATR in the study of model biological membranes can be found in later papers by Takenaka *et al* [42, 43] and also by Vaughan *et al* [44].

1.3.3 Self-Assembled Films

In 1970, Haller & Rice published a paper on the use of ATR to study the adsorption of n-amyl alcohol onto single-crystal α-alumina [45]. The spectra of adsorbed n-amyl alcohol were compared with those of a calcium stearate monolayer deposited onto the crystal by the LB technique. By using polarized radiation. these workers were able to determine the orientation of the adsorbed molecules. This work was followed by a collaboration with Low [34]. In this work, stearic acid was adsorbed from CCl_4 solution onto the surfaces of Ge and Al_2O_3 internal reflection prisms. The build-up of the adsorbed layer was followed as a function of time and as a function of solution concentration. The maximum adsorbed amount was around 0.3 of a monolayer with solutions in the 10^{-4}-10^{-2}M concentration range. The lowest observed adsorbed amount was 0.03 of a monolayer. Using the Ge prism and polarized radiation it was possible to obtain orientational information about the adsorbed layer. The stearic acid was found to be randomly oriented.

The utility of ATR to the study of surfactant adsorption having been demonstrated, it is somewhat surprising that few papers on the subject were published over the next decade. The advent of relatively low-cost Fourier transform infrared spectroscopy in the 1980's caused a resurgence of interest in ATR spectroscopy, for reasons which will be given in detail in the next chapter. Sperline *et al* used ATR to study the adsorption of cetylpyridinium chloride (CPC) from water onto a zinc selenide ATR prism [46]. Careful calibration of the ATR experiment enabled these workers to determine the amount of CPC adsorbed in the presence of bulk solution. Unfortunately, whilst this work represented a leap forward in the *in situ* quantification of the amount of

surfactant adsorbed, the experimental set-up did not allow for any orientational measurements to be made.

Employing the mathematics developed by Sperline *et al*, Kellar *et al* used ATR spectroscopy to study the adsorption of oleate from water onto fluorite [47]. An adsorption isotherm was obtained over the concentration range 5×10^{-7} to 5×10^{-4} M. Monolayer coverage was observed at low surfactant concentrations ($<10^{-5}$ M). At higher concentrations, the adsorbed layer appeared to consist of surface-precipitated calcium dioleate. As with the work by Sperline, no orientational information was presented. In a later paper, Kellar *et al* followed the position of the CH_2 stretching band as a function of coverage [48]. As coverage increased, the antisymmetric stretching band moved from $2925 cm^{-1}$ to $2915 cm^{-1}$, indicating that the chains were moving to an all-*trans* conformation. Whilst this information suggests some form of crystallization is occurring, orientational information cannot be obtained in the absence of polarized data.

In order to produce a compact, well-ordered, stable self-assembled layer, it is essential that the surfactant molecules adsorb strongly to the surface. One group of compounds which have the potential to form covalent bonds with a polar surface are the silanes. The utility of silanes as coupling agents is well-known [49]. Silanes are used in the preparation of bonded-phase column packings for reversed phase high performance liquid chromatography [50]. The bonded-phase packings for HPLC are prepared from rigid silica, the surface of which is covered by silanol groups. In order to produce a non-polar packing, the surface silanol groups are reacted with an organochlorosilane *viz*:

$$-\underset{|}{\overset{|}{Si}}-OH + Cl-\underset{\underset{CH_3}{|}}{\overset{\overset{CH_3}{|}}{Si}}-R \longrightarrow -\underset{|}{\overset{|}{Si}}-O-\underset{\underset{CH_3}{|}}{\overset{\overset{CH_3}{|}}{Si}}-R$$
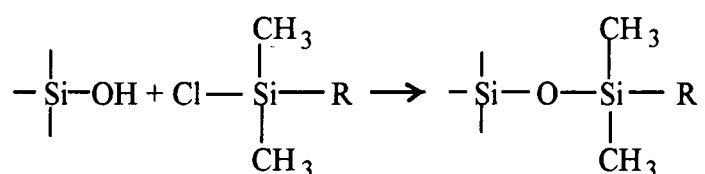
where R is generally a straight chain alkyl group. In HPLC packings, around 50% of the surface silanol groups react in this way. The remaining silanol groups do not react because of steric reasons.

The ability of silanes to form covalent bonds with polar surfaces has led to their use in the construction of self-assembled films. Much of the pioneering work in this area was conducted by Jacob Sagiv and coworkers [51-63]. Sagiv reported that well-ordered, compact monolayers of octadecyltrichlorosilane (OTS) on silica could be readily prepared under conditions of molecular self-assembly [58]. Such films are of considerable interest and were the subject of considerable research. Of particular interest was the mode of binding between the silica surface and the silane [64-67]. This work suggested that the simple reaction shown above only occurs when the silane is in the vapour phase at elevated temperatures. On a dry silica surface, a chlorosilane in water-free solvent will only physisorb [67]. Water needs to be present in order to first hydrolyse the chlorosilane to a silanol. The silanol then condenses with the silanol groups on the surface of the silica to form an Si-O-Si linkage. In the case of octadecyltrichlorosilane, where the Si atom is attached to one eighteen carbon chain and three chlorine atoms, a curing process following adsorption can lead to a crosslinked network of silanes [65]. The water necessary for this process is naturally present as a physisorbed layer on the silica surface when the silica is exposed to atmospheric water vapour. The kinetics of the reaction between dichlorophenylsilane [68] and OTS [69] and the silica surface have been studied *in situ* by ATR spectroscopy.

$$\text{H}_3\text{C(CH}_2)_{17} \overset{\overset{\displaystyle \text{Cl}}{|}}{\underset{\underset{\displaystyle \text{Cl}}{|}}{\text{Si}}}\text{-Cl} + 3\text{H}_2\text{O} \longrightarrow R\overset{\overset{\displaystyle \text{OH}}{|}}{\underset{\underset{\displaystyle \text{OH}}{|}}{\text{Si}}}\text{-OH} + 3\text{HCl}$$

Octadecyltrichlorosilane

$$R\overset{\overset{\displaystyle \text{OH}}{|}}{\underset{\underset{\displaystyle \text{OH}}{|}}{\text{Si}}}\text{-OH} + \text{HO}-\text{SiO}_2 \longrightarrow R\overset{\overset{\displaystyle \text{OH}}{|}}{\underset{\underset{\displaystyle \text{OH}}{|}}{\text{Si}}}\text{-O}-\text{SiO}_2 + \text{H}_2\text{O}$$

Silica Surface

Cure, 150°C

$$R-\overset{\overset{\displaystyle \text{O}}{|}}{\text{Si}}\text{-O}$$
$$\overset{|}{\text{O}}$$
$$R-\overset{|}{\text{Si}}\text{-O} \qquad + \text{H}_2\text{O}$$
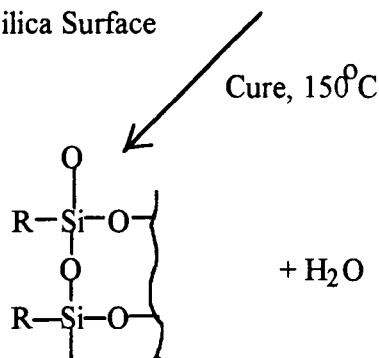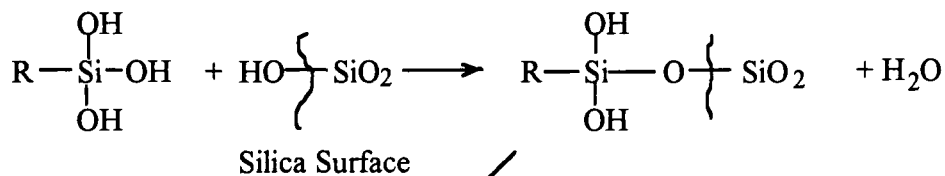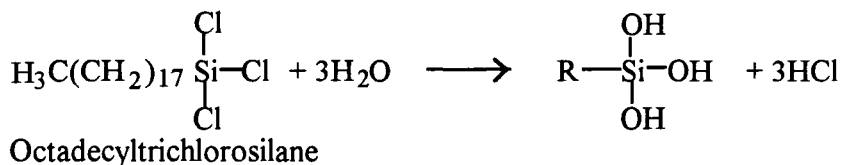
1.4   An Overview

In this introductory chapter, the importance of adsorbed molecules to the behaviour of sols has been described. An understanding of the structure of such adsorbed layers is the key to systematically tailoring the properties of sols to their application. Infrared spectroscopy has been shown to be powerful tool for elucidating the structure of adsorbed layers. The attenuated total reflection sampling technique enables the formation of adsorbed layers to be studied *in situ* and has been developed to a high degree in order to study self-assembled films. Adsorption onto silica is of primary interest in this study. Amines adsorb strongly onto silica and it is with amines that we shall be primarily concerned. The formation of covalent bonds between silanes and the silica surface enables this class of compound to form well-ordered, compact layers. The silane-silica system therefore represents the optimum system for covering a silca surface with an adsorbed layer, and will be referred to later as a comparison to the amine system.

The next two chapters cover the theory of infrared and ATR spectroscopy and explain how quantitative information about the adsorbed layer may be obtained.

Chapter 2   Principles of Fourier Transform Infrared Spectroscopy

2.1   Introduction

The utility of infrared spectroscopy for studying molecular adsorption has been described in the previous chapter. In this chapter the basic principles of infrared spectroscopy will be described. Firstly the reason why molecules absorb infrared radiation will be discussed. Secondly the method by which infrared spectra have been obtained for this thesis is described; Fourier transform infrared spectroscopy. The details of the sampling technique used throughout the current study, attenuated total reflection spectroscopy, will be described in the following chapter.

2.2   Elementary Theory of Infrared Spectroscopy

The theory of infrared spectroscopy has been covered by a number of excellent texts [70-75]. The following sub-sections are an abridged version of this theory. An infrared absorption results from the fact that an oscillating dipole absorbs radiation whose frequency is the same as the frequency of oscillation and that the oscillating dipole will transmit all other frequencies unchanged. The following sections are concerned with such oscillating dipoles.

2.2.1 The Classical Harmonic Oscillator

Consider a paricle of mass m suspended between two rigid walls by two identical springs, as shown in figure 2.1.

Figure 2.1   The Suspended Particle
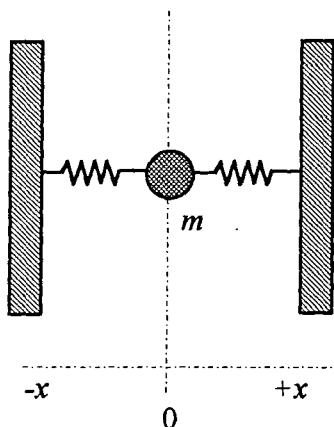
If the particle is constrained to move only in the x direction and the springs obey Hooke's law then the force exerted on the particle by the springs is proportional to the displacement from $x=0$:

$$F = -kx \qquad (2.1)$$

where k is the force constant.

When the particle is displaced from $x=0$ and released it will oscillate about $x=0$ with a frequency v given by:

$$v = \frac{1}{2\pi}\sqrt{\frac{k}{m}} \qquad (2.2)$$

Equation 2.2 shows that the frequency of oscillation depends upon m and k but is independent of amplitude.

The harmonic oscillator maintains a constant total energy, provided that there are no friction losses. The potential energy at any displacement x can be calculated thus:

$$PE = \int_0^x F dx = \int_0^x kx dx = \frac{1}{2}kx^2 \qquad (2.3)$$

Figure 2.2 shows the potential energy of the harmonic oscillator as a function of displacement. The curve is a parabola.

Figure 2.2 The PE Diagram for the Harmonic Oscillator
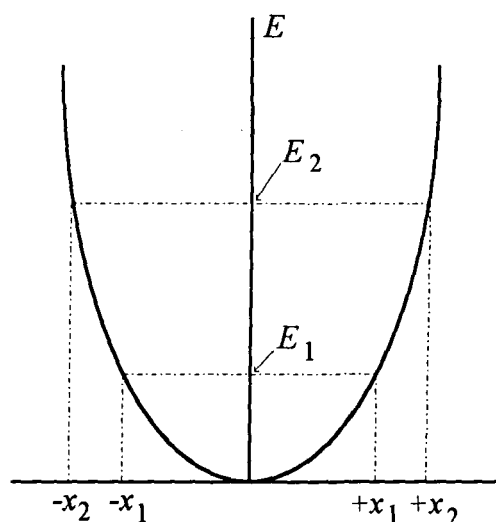
The energies E_1 and E_2 are given by $\frac{1}{2}kx_1^2$ and $\frac{1}{2}kx_2^2$ respectively. The total energy can have any value as it depends on k and the initial displacement.

2.2.2   The Quantum-Mechanical Harmonic Oscillator

The classic picture described above is inappropriate for very small particles, such as atoms. Quantum mechanics are therefore required to deal with such systems. Of prime importance to quantum mechanics is the Schrödinger equation, which may be written:

$$\hat{H}\psi(x,y,z) = E\psi(x,y,z) \qquad (2.4)$$

where $\hat{H}$ is the *Hamiltonian operator*, E is the total energy of the particle and $\psi(x, y, z)$ is the *wavefunction*. The wavefunctions may be found by solving the Schrödinger

equation, which is a second-order differential equation. Only certain discrete values of E will provide acceptable values of ψ.

For a one-dimensional harmonic oscillator the Schrödinger equation has the form:

$$\left(-\frac{h}{8\pi^2 m}\frac{d^2}{dx^2} + \frac{1}{2}kx^2\right)\psi(x) = E\psi(x) \qquad (2.5)$$

This equation, after a change of variable, is equivalent to the Hermite differential equation, which possesses solutions only for discrete values of its parameter. The solution of Hermite's equation, when applied to its form in equation in 2.5 leads to the result that E can only have certain values:

$$E = \left(n + \frac{1}{2}\right)\frac{h}{2\pi}\sqrt{\frac{k}{m}} \qquad n = 0, 1, 2, 3,\ldots\ldots \qquad (2.6)$$

Using the relationship expressed in equation 2.2 yields:

$$E = \left(n + \frac{1}{2}\right)h\nu \qquad (2.7)$$

Thus, the energy of a quatum-mechanical harmonic oscillator can only have certain discrete values; positive half-integer values of $h\nu$. The potential energy curve for the quantum mechanical harmonic oscillator looks similar to figure 2.2 except that the energy levels can only have certain values and are spaced at regular intervals equal to $h\nu$. This is shown in figure 2.3. As a result of the quantised energy levels only certain amplitudes of vibration are allowed.

Figure 2.3   Energy Levels of the Quantum Mechanical Oscillator
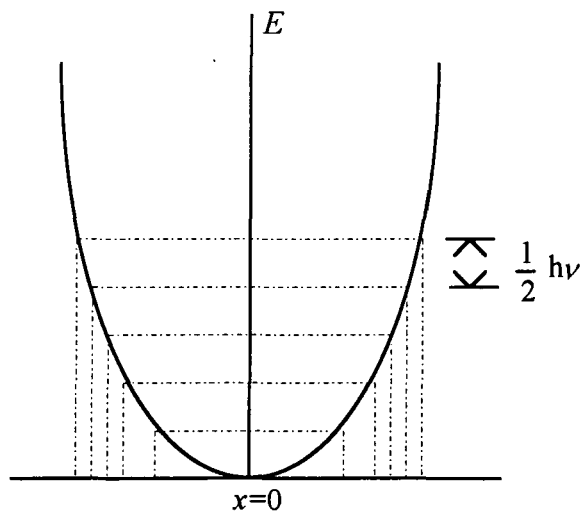
2.2.3   The Diatomic Molecule

A diatomic molecule may be pictured in a classical sense as consisting of two masses, m_1 and m_2 connected by a spring, as illustrated in figure 2.4.

Figure 2.4   The Model of a Diatomic Molecule
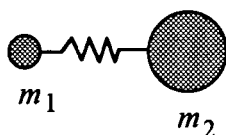
If the spring obeys Hooke's law the system will oscillate with a frequency ν given by:

$$\nu = \frac{1}{2\pi}\sqrt{\frac{k}{m_r}} \qquad (2.8)$$

where m_r is the *reduced mass*, and is given by:

$$m_r = \frac{m_1 m_2}{m_1 + m_2} \qquad (2.9)$$

The vibrational energy levels available to the diatomic molecule will be those of the quantum-mechanical harmonic oscillator, because of its small size, i.e.:

$$E = \left(n + \frac{1}{2}\right)h\nu$$

The energy levels are characteristic of a particular molecule and are the basis of identification by infrared spectroscopy.

2.2.4 Absorption of Radiation by Molecular Vibration

A vibrating heteroatomic diatomic molecule produces an oscillating dipole which in turn generates an electric field which oscillates at the same frequency as the vibration. This electric field may interact with the oscillating electric field of electromagnetic radiation (light). In order to absorb a quantum of radiation, the molecule must become excited from one vibrational energy level to a higher one by that radiation. In order that this be the case, the energy of the quantum of radiation must be exactly equal to the energy change undergone by the molecule i.e.:

$$E_{quantum} = \Delta E_{molecule}$$

The energy of the quantum is related to its frequency by Planck's equation:

$$E_{quantum} = h\nu_{quantum} \qquad (2.10)$$

and the energy of the molecule is similarly related to its frequency of vibration. Hence:

$$\nu_{quantum} = \nu_{vibration} \qquad (2.11)$$

In order for a quantum of radiation to be absorbed, the frequency of that radiation must equal the frequency of the molecular vibration. No interaction between radiation of a different frequency to that of the molecular vibration can occur. The absorption of radiation by a molecule at certain frequencies gives rise to an absorption spectrum.

2.2.5 Selection Rules

The section above discussed a transition from a vibrational energy level to an adjacent level. A consideration of quantum mechanics for the harmonic oscillator reveals that these are the only transitions allowed. A "leap" of two or more energy levels is prohibited. This is shown in figure 2.5.

Figure 2.5 Transitions Between Energy Levels in the Quantum-Mechanical Harmonic Oscillator
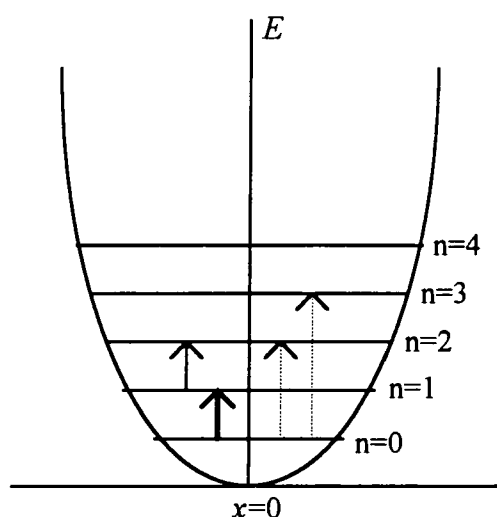
The transitions where $\Delta n = \pm 1$ are allowed and are shown by the solid arrows. These arrows correspond to a Δn of $+1$ which represent an absorption. A Δn of -1 corresponds to emission. Transitions where $\Delta n \neq \pm 1$, such as those shown by the dashed arrows, are forbidden in the quantum-mechanical harmonic oscillator.

Transitions between adjacent states other than $n=0 \rightarrow n=1$ are allowed. However, the probability of such transitions occurring is low because the ratio of molecules in state 1 to those in state 0 is very low, as predicted by the Boltzmann distribution law. If N_0 and N_1 are the number of molecules in the 0 and 1 states then:

$$\frac{N_1}{N_0} = e^{-\left(E_1 - E_0\right)/kT} = e^{-h\nu/kT} \qquad (2.12)$$

Equation 2.12 indicates that at room temperature this ratio will be less than a few percent in the mid-infrared region of the electromagnetic spectrum. The most likely transtion, therefore, is that indicated by the thick, solid arrow on figure 2.5. This transition is known as the *fundamental*. The infrared fundamentals of interest in chemistry fall between $4000cm^{-1}$ and $400cm^{-1}$.

2.2.6 Anharmonicity

The potential enegery curve for the harmonic oscillator is a parabola. This suggests that dissociation of the molecule can never take place, no matter how large the amplitude of vibration. However, the restoring force in real molecules becomes weaker as the displacement increases and when the amplitude of vibration is sufficiently large the molecule will fly apart. The potential energy curve is no longer the simple parabola, as shown in figure 2.5, but now corresponds to that for the model of an *anharmonic oscillator* as shown in figure 2.6.

Figure 2.6   Potential Energy Curve for the Anharmonic Oscillator
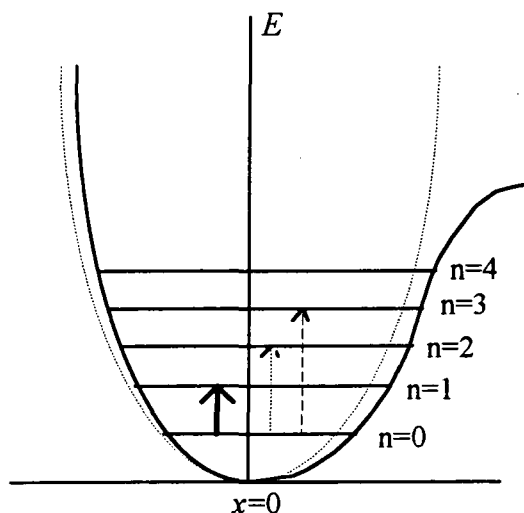
In the region of low energy, the anharmonic oscillator energy curve (solid curve) is a close approximation to the harmonic oscillator energy curve (dashed curve). In this region the real molecule approximately obeys the harmonic oscillator energy

relationship (equation 2.7). However, higher energy states are more closely approximated by:

$$E = h\nu\left[\left(n + \frac{1}{2}\right) - \left(n + \frac{1}{2}\right)^2 x_e\right]$$
(2.13)

where x_e is the *anharmonicity constant*. The energy difference between states n and $n-1$ is given by:

$$\Delta E = h\nu(1 - 2nx_e)$$
(2.14)

x_e is a positive number and so the energy spacing between successive levels decreases as n increases. The selection rule governing vibrational transition for the harmonic oscillator ($\Delta n = \pm 1$) no longer applies and other transitions with $\Delta n = \pm 2$, ± 3 etc. are now allowed. Although allowed, the probability of an *overtone* transition occurring is much lower than that of a *fundamental* transition. This intensity of a fundamental band is therefore greater than that of an overtone band. The fundamental transition is shown by the thick, solid arrow in figure 2.6 and the overtones are indicated by the dashed arrows.

Now that the molecular origins of infrared spectra have been described it is now necessary to explain how such spectra are obtained experimentally.

2.2   Fourier Transform Infrared Spectroscopy

In order to obtain an infrared spectrum it is necessary to measure the intensity of infrared radiation as a function of frequency. Infrared radiation is conveniently produced by an incandescent source and its intensity can be measured by a number of different detectors. The source produces radiation over a broad range of frequencies (i.e. it is *polychromatic*) and the detector is sensitive to these frequencies. Thus, in order to record a spectrum, there needs to be a device between the source and the detector which is capable of separating the infrared radiation frequencies with

experimentally acceptable resolution. There are two such devices commonly found in infrared spectrometers. The first is a dispersive device, such as a prism or a diffraction grating. The second is an interferometer. The latter device requires that a mathematical transformation, called a fast *Fourier transform,* be performed on the intrumentally obtained raw data before a readily comprehensible spectrum can be obtained. Infrared spectrometers are classified on the basis of which separation technique they employ, being called *dispersive* or *Fourier transform* (abbreviated FT) instruments respectively. Fourier transform spectrometers have a number of advantages over dispersive instruments which are critical to the success or otherwise of this work and these shall be described later. However, FT instruments have only gained popularity over dispersive spectrometers over the past fifteen years. This increase in popularity has been due to the advent of cheap high-speed electronics and computers which are necessary to control the optics of, and process the data obtained by, FT instruments.

There are many texts which describe Fourier transform infrared spectroscopy [76-83] and it beyond the scope of this thesis to describe the subtleties of spectrometer design and operation. However, it is of used to outline the basic principles of FT instrumentation.

2.2.1   The Michelson Interferometer

The physical device in an interferometic spectrometer which separates the frequencies is the *interferometer.* Of the several types of interferometer developed [83], the design universally used in FTIR instrumentation is that due to Michelson; the *Michelson Interferometer.* A schematic of the Michelson interferometer is shown in figure 2.7. This consists of two mirrors,one fixed, one movable, set at right-angles to each other, and, between them ,a *beamsplitter.* The beamsplitter allows light from the *source* to be partially transmitted to the movable mirror and partially reflected to the fixed mirror. Following reflection from the two mirrors, the two beams return to the

beamsplitter where they *interfere*. As a result of interference, the intensity of the beam passing to the detector depends upon the difference in the pathlengths in the two arms of the interferometer. A plot of intensity *versus* path difference is called an interferogram. The interferogram carries the spectral information. The process by which an interferogram is produced is most readily understood by considering the processes occurring in a Michelson interferometer when the source produces monochromatic radiation.

Figure 2.7   Schematic of the Michelson Interferometer
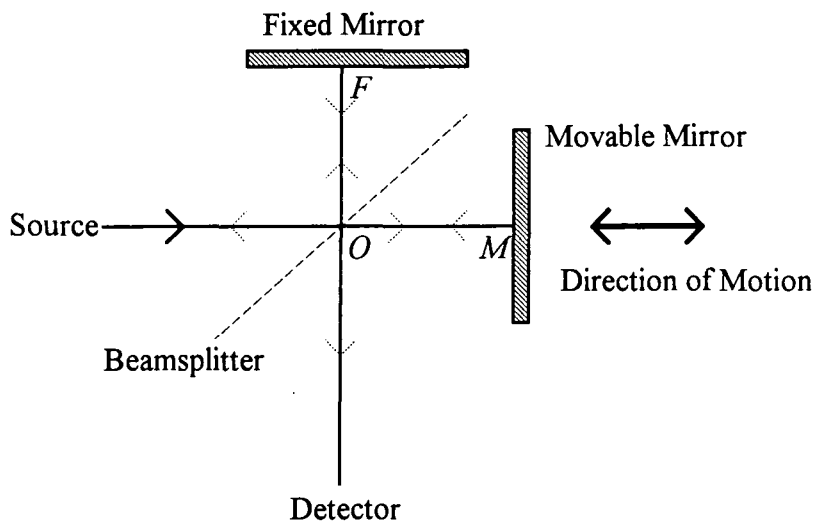
2.2.2   Monochromatic Radiation

Consider a source of radiation producing a perfectly collimated, infinitely narrow beam. If the wavelength of the radiation, in centimetres, is λ, its wavenumber, in reciprocal centimetres, is:

$$\overline{v} = \frac{1}{\lambda} \qquad (2.15)$$

The path difference between the fixed and movable mirrors (figure 2.7) is called the *retardardation*, δ, and is given by:

$$\delta = 2(OM - OF) \qquad (2.16)$$

At *zero path difference* (ZPD), i.e. when δ=0, the two beams are in phase and interfere *constructively*. The intensity of the beam passing to the detector is equal to the sum of the beams reflected from the fixed and movable mirrors. Therefore, the intensity of the light passing to the detector is at its maximum value.

When the movable mirror is moved by ¼λ, δ becomes ½λ. The beams from the fixed and movable mirrors now interfere *destructively* at the beamsplitter. The intensity of the beam passing to the detector is at a minimum. A further movement of the movable mirror of ¼λ makes δ equal to λ and the beams once again interfere constructively.

If the movable mirror is moved at constant velocity, the signal at the detector will vary sinusoidally, the signal reaching a maximum every time the condition for constructive interference is met, i.e. when $\delta = n\lambda$. FTIR spectrometers employ this phenomenon to measure the retardation of the mirror. The interference pattern produced by the interferometer from a HeNe laser source is used. Each maximum represents a retardation increment of $1\lambda_{HeNe}$.

The intensity of the beam at the detector as a function of retardation, $I'(\delta)$, is given by:

$$I'(\delta) = 0.5I(\overline{\nu})\left\{1 + \cos 2\pi \frac{\delta}{\lambda}\right\} \qquad (2.17)$$

or

$$I'(\delta) = 0.5I(\overline{\nu})\{1 + \cos 2\pi\overline{\nu}\delta\} \qquad (2.18)$$

where $I(\overline{\nu})$ is the intensity of the source. $I'(\delta)$ is composed of a constant component, $0.5I(\overline{\nu})$, and a modulated component, $0.5I(\overline{\nu})\cos 2\pi\overline{\nu}\delta$. Only the modulated component is important in spectrometric measurements, and is referred to as the interferogram, $I(\delta)$. The above arguments apply to an ideal interferometer in which the beamsplitter transmits exactly 50% of the incident energy to the movable mirror and

reflects 50% to the fixed mirror. The interferogram produced from a monochromatic source produced by an ideal interferometer is given by:

$$I(\delta) = 0.5I(\bar{v}) \cos 2\pi \bar{v} \delta \qquad (2.19)$$

The amplitude of the interferogram as recorded by the detector is proportional to the intensity of the source, the beamsplitter efficiency, detector response and amplification characteristics. For a given experimental configuration, only $I(\bar{v})$ varies from one measurement to the next. Equation 2.19 may be modified by a single wavenumber-dependent correction factor, $H(\bar{v})$:

$$I(\delta) = 0.5H(\bar{v})I(\bar{v}) \cos 2\pi \bar{v} \delta \qquad (2.20)$$

Now $0.5H(\bar{v})I(\bar{v}) = B(\bar{v})$ where $B(\bar{v})$ is the single-beam spectral intensity: the intensity of the source at a given wavenumber as modified by the instrumental characteristics. Hence:

$$I(\delta) = B(\bar{v}) \cos 2\pi \bar{v} \delta \qquad (2.21)$$

$I(\delta)$ is the cosine Fourier transform of $B(\bar{v})$. The spectrum is obtained from the interferogram by computing the cosine Fourier transform of $I(\delta)$.

In commercial FTIR instruments the interferogram is recorded as a function of time, $I(t)$ rather than as a function of retardation, $I(\delta)$. The mirror is moved at constant velocity, v, and so the two are simply related. The retardation at t seconds after ZPD is given by:

$$\delta = 2vt \text{ cm} \qquad (2.22)$$

Substitution into 2.21 yields:

$$I(t) = B(\bar{v}) \cos 2\pi \bar{v} \cdot 2vt \qquad (2.23)$$

2.2.3 Polychromatic Sources

In order to obtain an infrared spectrum it is necessary to record intensity as a function of wavenumber over a broad range of frequencies. A polychromatic source is clearly required. The interferogram of a polychromatic source is not a simple cosine wave but rather it is the resultant of the interferograms of many cosine waves. For a broad-band polychromatic source the envelope of the interferogram decays rapidly. Such an interferogram is shown in figure 2.8.

When the source is a continuum, the interferogram is represented by the integral:

$$I(\delta) = \int_{-\infty}^{+\infty} B(\bar{\nu}) \cos 2\pi\bar{\nu}\delta \cdot d\bar{\nu} \qquad (2.24)$$

which is one-half of a cosine Fourier transform pair, the other being:

$$B(\bar{\nu}) = \int_{-\infty}^{+\infty} I(\delta) \cos 2\pi\bar{\nu}\delta \cdot d\delta \qquad (2.25)$$

As $I(\delta)$ is an even function, 2.25 may be rewritten:

$$B(\bar{\nu}) = 2 \int_{0}^{+\infty} I(\delta) \cos 2\pi\bar{\nu}\delta \cdot d\delta \qquad (2.26)$$

Equation 2.26 shows that a complete spectrum of infinite resolution can only be recorded by scanning from 0 to $+\infty$ centimetres. Clearly this is impractical. Resolution is limited by the fact that mirror travel is restricted. In order to compute the Fourier transform of the interferogram using a digital computer it is necessary to digitize the (analogue) interferogram. The intervals at which the interferogram is digitized affect the resultant frequency domain spectrum. The affects the various sampling variables have on the final spectrum are described in the following sections.

Figure 2.8   Interferogram of a Broadband Source

δ_{max}
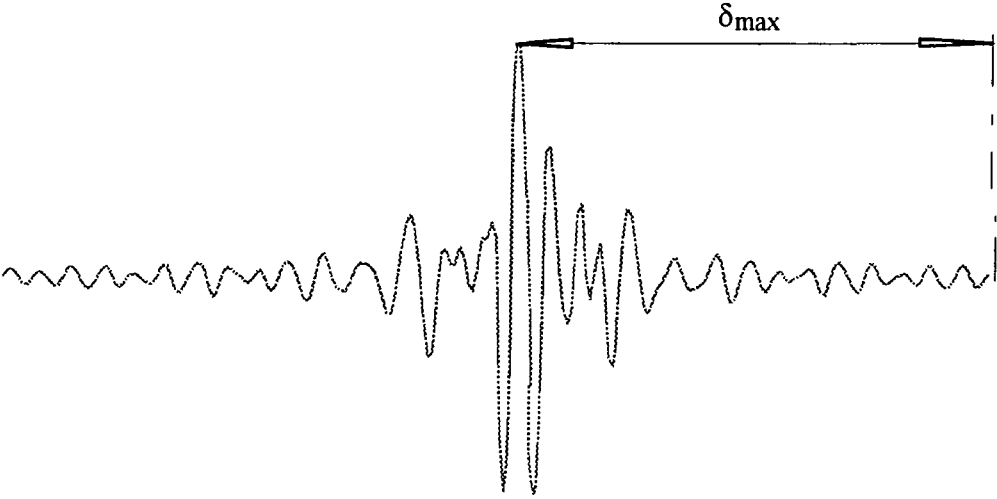
2.2.4　Resolution

In the previous section it was stated that resolution is limited by the maximum retardardation which the interferometer can achieve. If the maximum retardation is δ_{max} (as shown in figure 2.8) then the unapodized resolution, $\Delta\bar{v}$, is given by:

$$\Delta\bar{v} = 1/\delta_{max} \quad (2.27)$$

Resolution controls spectral bandwidths *and* the signal-to-noise ratio. Resolution affects the S/N ratio because the noise level of the instrument is independent of frequency and therefore the noise component of the interferogram is not a function of δ. The frequency components in the interferogram (i.e. the signal) lose amplitude as δ increases. As a proportion of the total signal, then, the noise increases as δ increases.

2.2.5　Apodization

The truncation of the interferogram resulting from finite retardation is effectively a multiplication of the infinite interferogram by a boxcar truncation function. The Fourier transform of a truncated interferogram is a convolution of the spectral line (the useful spectrum) and a sinc function; the latter resulting from the FT of the truncation function. The sinc function complicates the spectrum. In order to reduce the sinc function in the frequency domain spectrum the truncated interferogram is multiplied by an apodization function prior to transformation. An apodization function has a maximum at $\delta = 0$ and becomes zero at δ_{max}. There are several apodization functions available, the most commonly used being triangular apodization. Triangular apodization reduces the resolution by a factor of approximately $\sqrt{2}$.

2.2.6　Digital Sampling and Filtering

In order to compute the Fourier transform of the interferogram it is first necessary to digitize the interfrogram. The value of I is recorded at incremental values of δ, the size of the increment being the *sampling interval*, $\Delta\delta$. In order to accurately digitize a

waveform it is necessary to sample at least twice per cycle. Therefore, for an interferogram comprising a variety of wavelengths, the minimum wavelength which can be accurately sampled, λ_{min}, is $2\Delta\delta$. Any wavelengths which are smaller than twice the sampling interval will be incorrectly digitized and appear at longer wavelengths in the (computed) frequency domain spectrum. Such distortion is called *aliasing*. In order to prevent aliasing, high frequencies are filtered out prior to digitization.

2.2.7 Spectral Coaddition

The S/N ratio can be improved by averaging over a number of scans. Noise may be either positive or negative, with equal probability, whilst signal is positive. The signal-to-noise ratio in the final spectrum is proportional to the square root of the number of scans, i.e.:

$$S/N \propto \sqrt{N} \qquad (2.28)$$

where N is the number of scans. In order to improve the S/N ratio by a factor of 2 it is therefore necessary to quadruple the number of scans. Equation 2.28 strictly applies only to perfect systems; it suggests that one can continually increase the number of scans and continually improve the S/N ratio. In practice imperfections in the system such as interferometer instability actually degrade the spectrum as the time of acquisition increases. There is therefore an optimum number of scans beyond which the spectral quality decreases.

2.2.8 The Advantages of Fourier Transform Infrared Spectroscopy

In the previous sections the basic principles of Fourier transform infrared spectrosco have been described. From this description it is evident that FT spectroscopy requi high-speed computing if a frequency-domain spectrum is to be obtained in reasona time. The ways in which the instrumental (e.g. retardation) and computational (e apodization) parameters affect the final spectrum are not as easily (intuitively, at

understood as the parameters in dispersive spectroscopy. However, FT spectroscopy does offer a number of advantages over "conventional" dispersive spectroscopy. These advantages are listed below.

a.   The Multiplex (Felgett) Advantage.

All frequencies are measured simultaneously in a Fourier transform instrument. Consequently, a full spectrum can be recorded in a few seconds, and many spectra can be co-added (thereby improving the S/N ratio) in the time taken to record a single dispersive spectrum.

b.   The Throughput (Jacquinot) Advantage

For a given resolution, the energy throughput of an interferometer can be greater than that of a dispersive instrument where the throughput is restricted by the slits. In combination with the multiplex advantage, the throughput advantage allows an FT instrument to obtain a spectrum with the same S/N of a dispersive IR in a shorter time.

c.   The Connes Advantage

An FT instrument employs a laser in the measurement of mirror retardation. As the frequency of the laser is known very accurately the frequencies making up the interferogram can be calculated very accurately. Therefore, an FT instrument will show no frequency drift, which may occur in a dispersive instrument as components, such as the chart/grating drive, wear.

d.   Constant Resolution

The resolution in an FT instrument is independent of frequency. In a dispersive instrument the resolution is controlled by the slit-width, and may vary with frequency if a constant slit-width is employed.

The advantages of FTIR and the advent of high-speed, low-cost electronics necessary for spectrometer control and data processing have led to FT instruments largely superseding dispersive instruments, even in routine analytical applications. Manufacturers of FT instruments have turned the need for a computer into an advantage by incorporating powerful spectral manipulation packages into their spectrometer control software. The Jacquinot and Felgett advantages are of great importance where energy is unavoidably lost by the sampling technique employed.

.Attenuated total reflection (ATR) spectroscopy is a sampling technique in which much of the incident energy can be lost. The ATR technique, developed in the 1960's, has become increasingly popular as FT instrumentation has become more common. The technique is central to this thesis and is described in detail in the next chapter.

Chapter 3   Attenuated Total Reflection Spectroscopy

3.1   Introduction

Attenuated total reflection (ATR) spectroscopy is a sampling technique which is most commonly used in conjunction with infrared spectroscopy. The first chapter in this thesis indicated the importance of ATR spectroscopy in elucidating the structure of thin films. An excellent review of ATR spectroscopy was published by Harrick in 1967 [84] and much of this chapter is drawn from this text. This chapter describes the theory of ATR spectroscopy in detail and sets out the equations which enable quantitative information to be obtained from ATR spectra.

3.2   Total Internal Reflection

A ray of light travelling in a transparent medium of refractive index n_1 encountering an interface with a second transparent medium, of lower refractive index, n_2, will be partially reflected and partially transmitted, as shown in figure 3.1. The relationship between the incident angle (= reflected angle), θ, and the refracted angle, φ, is given by Snell's law:

$$n_1 \sin\theta = n_2 \sin\varphi \qquad (3.1)$$

Figure 3.1   Internal Reflection
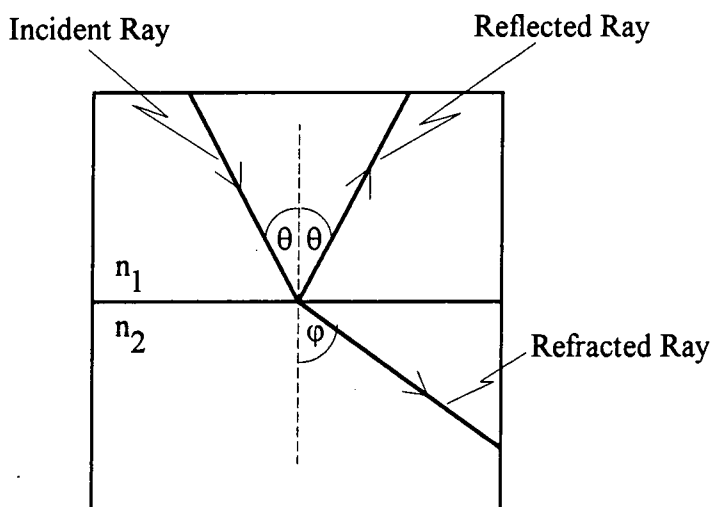
Two polarizations of light need to be defined. The incident light may be polarized such that the electric field vector vibrates in a plane which may be either parallel or perpendicular to the plane of incidence. Parallel polarization is also known as TM (transverse magnetic) or p (parallel) waves. Perpendicular polarization is also know as TE (transverse electric) or s (senkrecht) waves. In this thesis the TM/TE notation will be used. For unit incident amplitude, the reflected amplitudes of the TE and TM waves are given by Fresnel's equations:

$$r_{TM} = -\frac{\sin(\varphi - \theta)}{\sin(\varphi + \theta)} \qquad (3.2)$$

$$r_{TE} = \frac{\tan(\varphi - \theta)}{\tan(\varphi + \theta)} \qquad (3.3)$$

The reflectivity, R, is equal to the amplitude squared, i.e. $R = r^2$. For internal reflection, the value of R may take a value of 100%, i.e. all of the incident radiation is reflected. This happens when the angle of incidence is greater than or equal to the critical angle, θ_c, which is given by:

$$\theta_c = \sin^{-1}n_{21} \qquad (3.4)$$

where $n_{21} = n_2/n_1$. R_{TE} and R_{TM} both become 100% exactly when $\theta = \theta_c$ and $\varphi = \pi$ /2. When $\theta > \theta_c$, φ becomes imaginary. Fresnel interpreted this imaginary angle as meaning that no energy is transmitted to medium 2 but that all the incident energy is reflected back into medium 1. Thus, when θ lies between the critical angle and grazing incidence *total internal reflection* occurs. A totally reflecting surface is a perfect mirror, a situation which can be obtained in external reflection only when the refractive index is purely imaginary.

3.3 Electromagnetic Field Pattern Near the Reflecting Interface

Fresnel's equations, described above, give a rather limited physical picture of the electromagnetic field pattern in the vicinity of the reflecting interface. In order to gain a better appreciation of these patterns Maxwell's equations must be used. It is beyond the scope of this thesis to detail electromagnetic wave theory and so only the important results shall be discussed here. In order to describe the electromagnetic wave pattern it is necessary to define a co-ordinate system. This is shown in figure 3.2. The xy plane is the reflecting interface and the xz plane is the plane of incidence. This set of co-ordinates will be used throughout this thesis.

Figure 3.2   Definition of Rectangular Co-ordinate System

n_1

n_2

y   x

z
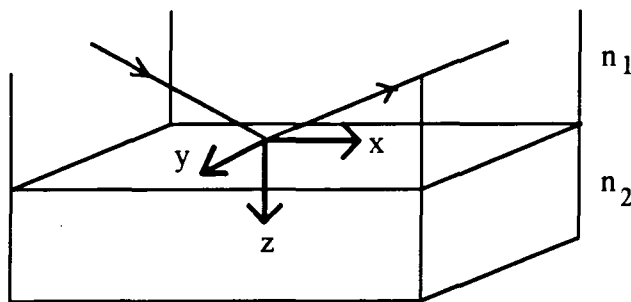
The incident and reflected waves interfere at the totally reflecting interface to form a standing wave normal to the surface in the optically more dense medium [85, 86, 87]. The electric field amplitude at the interface is non-zero and, by selecting the correct angle of incidence, it is even possible to locate an antinode at the interface. Now there must be continuity of the electric field across the interface and so the non-zero value of the amplitude of the standing wave at the interface but in the denser medium leads to the generation of an exponentially decaying *evanescent field* (evanescent = "vanishing") in the rarer medium. The form of the electric field in the vicinity of the interface is shown schematically in figure 3.3. This diagram is not the result of quantitative calculations.

Figure 3.3   Schematic of Electromagnetic Fields Near A Totally Reflecting

Interface
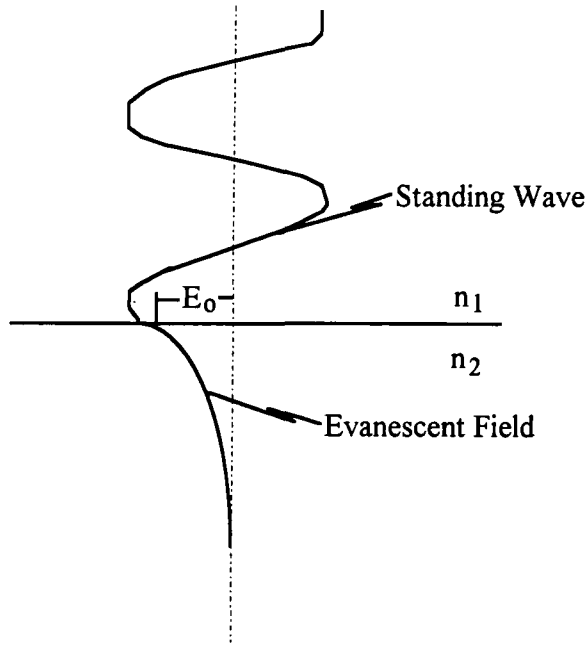
Using Maxwell's equations it is possible to calculate the electric field components in

each of the three directions; x, y and z. This has been done using a computer program

developed at Durham by Dr. Y. P. Song [88]. Figure 3.4 shows the results of these

calculations for the following system:

$\theta = 45°$

$\lambda = 3.45 \mu m$

$n_1 = 3.425$

$n_2 = 1.450$

Note that E^2 rather than E is plotted in this diagram. The negative values of z

represent the denser medium and the positive values represent the rarer medium. The

interface is represented by z=0. The values of the electric field amplitudes in the x, y

and z directions at the interface but in the rarer medium are denoted by E_{x0}, E_{y0} and

E_{z0} respectively. The values of E_{x0} and E_{y0} (and $\therefore$ E_{x0}^2 and E_{y0}^2) are continuous

across the interface because boundary conditions state that the tangential components
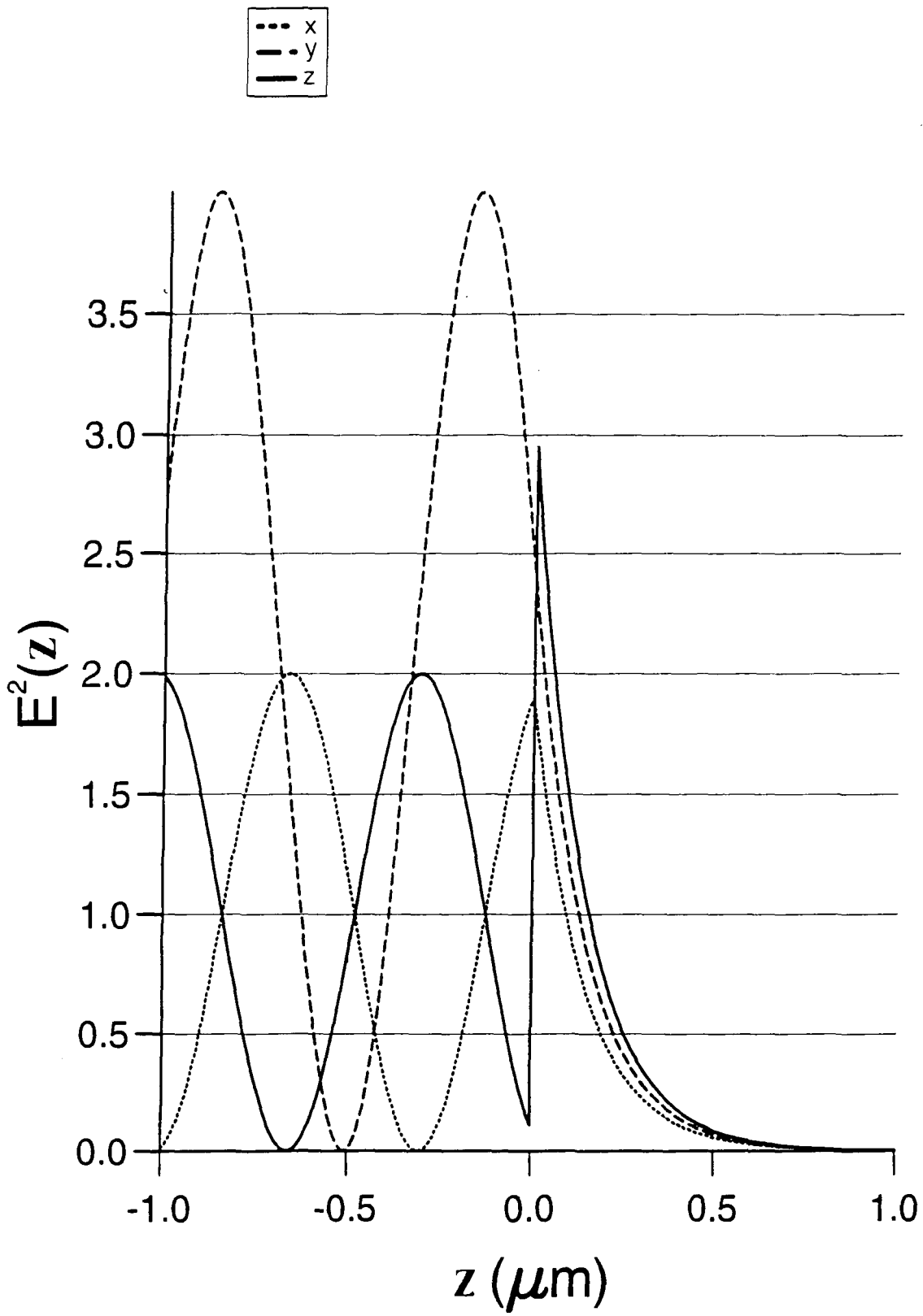
of the electric field are continuous. The normal component, E_{z0} (and $\therefore$ E_{z0}^2), is discontinuous across the interface, having a value greater by a factor of n_{21}^2 in the rarer medium. For unit incoming amplitude, the electric fields at the interface but in the rarer medium are given by:

$$E_{y0} = \frac{2\cos\theta}{\left(1 - n_{21}^2\right)^{1/2}} \qquad (3.5)$$

$$E_{x0} = \frac{2\left(\sin^2\theta - n_{21}^2\right)^{1/2}\cos\theta}{\left(1 - n_{21}^2\right)^{1/2}\left[\left(1 + n_{21}^2\right)\sin^2\theta - n_{21}^2\right]^{1/2}} \qquad (3.6)$$

$$E_{z0} = \frac{2\sin\theta\cos\theta}{\left(1 - n_{21}^2\right)^{1/2}\left[\left(1 + n_{21}^2\right)\sin^2\theta - n_{21}^2\right]^{1/2}} \qquad (3.7)$$

The TE polarized wave has only one electric field vector associated with it, the E_y. The TM wave has two electric field vectors associated with it, E_x and E_z. The total electric field amplitude of the TM wave is given by:

$$E_{TM} = \left(\left|E_{x0}\right|^2 + \left|E_{z0}\right|^2\right)^{1/2} \qquad (3.8)$$

3.3   Characteristics of the Evanescent Field

The evanescent field has components in all spatial orientations (x, y and z) and decays exponentially with distance into the rarer medium. This exponential decay can be represented by the equation:

$$E = E_0 e^{-\gamma z} \qquad (3.9)$$

48

where γ is the electric field amplitude decay coefficient, E_0 is the electric field amplitude at the interface in the rarer medium and E is the electric field amplitude at a distance z into the rarer medium. γ is given by the equation:

$$\gamma = \frac{2\pi\left(\sin^2\theta - n_{21}^2\right)^{1/2}}{\lambda_1} \qquad (3.10)$$

where λ_1 is the wavelength of the radiation in the denser medium, i.e. λ_{vacuum}/n_1. Harrick [84] defined a parameter called the *depth of penetration*, d_p, as being the depth, z, at which E falls to 1/e of its original value (E_0). Examination of 3.9 reveals that $d_p=1/\lambda$, i.e.:

$$d_p = \frac{\lambda_1}{2\pi\left(\sin^2\theta - n_{21}^2\right)^{1/2}} \qquad (3.11)$$

Examination of either 3.10 or 3.11 reveals that the rate of decay of the evanescent field depends on:

i. The wavelength of the propagating radiation, λ_1.

ii. The angle of incidence, θ.

iii. The refractive indices of the denser and rarer media, n_1 and n_2 respectively.

These parameters of of great interest in the design of ATR experiments.

Goos and Hänchen [89, 90] discovered that the reflected beam is displaced by a fraction of a wavelength from the incident beam. This effect is known as the Goos-Hänchen shift. While of interest, the Goos-Hänchen shift is of little importance in discussions of the application of ATR spectroscopy.

3.4   Absorption of the Evanescent Field

The preceding discussion has involved internal reflection occurring at an interface between two semi-infinite non-absorbing media. The incident and reflected radiation are of equal intensity because there is no net flow of energy into the rarer medium. However, if the rarer medium absorbs some of the electromagnetic radiation of the evanescent field the intensity of the reflected beam will be lower than that of the incident beam. The reflection is no longer total but *attenuated*. In other words, the reflected beam (i.e. the propagating wave) contains spectral information sensed by the evanescent wave. This is the physical basis of attenuated total reflection spectroscopy. In the presence of an absorbing rarer medium the evanescent field decays because it *is* evanescent and therefore, by nature, decays exponentially as described above <u>and</u> because it is being absorbed. Quantitative ATR spectroscopy relies on being able to predict the form of the evanescent field and modifications to the exponential decay due to absorption complicate the analysis. For example, Müller *et al* considered the effect of an absorbing rarer medium on the electric field amplitude decay coefficient, γ, [91]. These workers considered the case of an absorbing rarer medium while assuming invariant refractive index and infinite plane-wave radiation. In this case, the refractive index required for the calculations is not simply n_{21} but rather the complex refractive index:

$$\hat{n}_{21} = n_{21}(1 + ik) \qquad\qquad (3.12)$$

where k is the attenuation index. The equation for γ now becomes:

$$\gamma = \frac{\left(2\pi / 2^{1/2} \lambda_1\right)}{\left\{\left[\left(\sin^2\theta - n_{21}^2 + n_{21}^2 + n_{21}^2 k^2\right)^2 + \left(2n_{21}^2 k^2\right)\right]^{1/2} + \left(\sin^2\theta - n_{21}^2 + n_{21}^2 k^2\right)\right\}^{1/2}}$$

$$(3.13)$$

Equation 3.13 is rather more complicated than 3.10. One of the characteristics of quantitative ATR spectroscopy is that when one takes into account absorption of the evanescent field, the equations become all-but unmanagable. Fortunately, it turns out that the form of the evanescent field can be satisfactorily described by the simple equations for non-absorbing media for all but very strong absorbers, i.e. the shape of the exponential decay is only significantly modified by very strong absorbers [91]. The equations of utility in quantitative spectroscopy developed by Harrick [84] are strictly true only for non-absorbing media but are good approximations for most systems and will therefore be described in the following sections. A source of potential confusion in ATR spectroscopy is that the technique itself relies on the absorption of evanescent radiation but that the equations for quantitative ATR are based on the approximation that the rarer medium is non-absorbing. The following sections describe the non-absorbing approximation-derived equations. When these are applied to the experimental parameters used in this thesis, the results will be compared to those obtained from the Maxwell-based program developed at Durham [87]; a program which takes into account an absorbing rarer medium.

3.5   The Effective Thickness

In order to perform quantitative spectroscopy it is necessary to determine a relationship between the measured quantity, the absorbance, and the concentration of the analyte. This, in turn, relies upon being able to define a pathlength, or sample thickness. In the case of a transmission experiment the concept of a pathlength is a familiar one. The transmission experiment is shown in figure 3.5. Light from a source, of intensity I_0, falls on a sample which absorbs a fraction of this light, reducing the intensity to I.

<u>Figure 3.5</u>   <u>The Transmission Experiment</u>
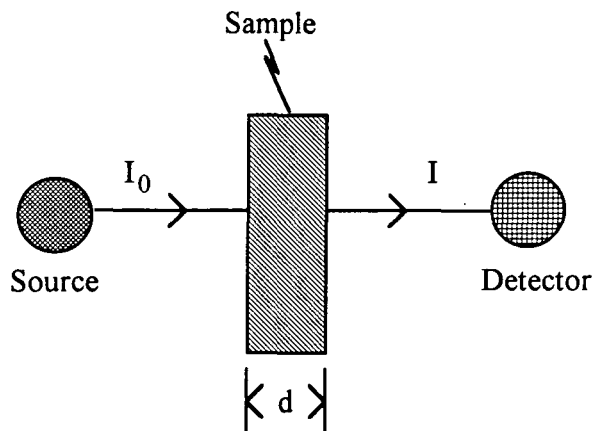
Ignoring reflection losses, the reduction in intensity follows a simple exponential law *viz*:

$$I/I_0 = e^{-\alpha d} \qquad (3.14)$$

Here, α is the absorption coefficient and d is the pathlength. The absorption coefficient, α, may be written in terms of the concentration of the sample, c, thus:

$$\alpha = \varepsilon c \qquad (3.15)$$

where ε is the molar extinction coefficient. Hence 3.14 may be re-written:

$$I/I_0 = e^{-\varepsilon c d} \qquad (3.16)$$

Taking logs:

$$-\log I/I_0 = \varepsilon c d \qquad (3.17)$$

The quantity $-\log I_0/I$ is the absorbance A, as measured in the experiment. Hence:

$$A = \varepsilon c d \qquad (3.18)$$

This is the familiar Beer-Lambert relationship.

In the ATR experiment the concept of a pathlength is somewhat more complicated than the physically measureable cell dimensions in the transmission experiment. However, for the ATR experiment we may define the reflectivity, R, as:

$$R = I/I_0 \qquad (3.19)$$

where I_0 is the intensity of the incident beam and I is the intensity of the reflected beam. A similar expression to that for the transmission experiment can be written for the reflection case:

$$R = I_0/I = e^{-\alpha d_e} \qquad (3.20)$$

Here d_e is the *effective thickness*. Comparison of 3.20 with 3.14 shows that d_e may be defined as the the thickness of sample which would be required to obtain the same absorbance in a transmission experiment as in a single reflection ATR experiment where the rarer medium is semi-infinite in thickness. For semi-infinite non-absorbing media, the effective thickness is given by:

$$d_e = \frac{n_{21}}{\cos\theta} \int_0^\infty E^2 dz \qquad (3.21)$$

$$d_e = \frac{n_{21}E_0^2 d_p}{2\cos\theta} \qquad (3.22)$$

The value of E_0^2 is different for each direction x, y and z (see equations 3.5-3.7). Substitution of the equations for E_0^2 (3.5-3.7), the relationship expressed in 3.8 and the equation for d_p (3.11) into 3.22 allows the effective thickness to be calculated for the TE amd TM polarizations:

53

TE Polarization

$$d_e = \frac{n_{21}\lambda_1 \cos\theta}{\pi\left(1 - n_{21}^2\right)\left(\sin^2\theta - n_{21}^2\right)^{1/2}}$$ (3.23)

TM Polarization

$$d_e = \frac{n_{21}\lambda_1\left(2\sin^2\theta - n_{21}^2\right)\cos\theta}{\pi\left(1 - n_{21}^2\right)\left[\left(1 + n_{21}^2\right)\sin^2\theta - n_{21}^2\right]\left(\sin^2\theta - n_{21}^2\right)^{1/2}}$$ (3.24)

For unpolarized radiation, the effective thickness is given by:

$$d_{eUP} = (d_{eTE} + d_{eTM})/2$$ (3.25)

Examination of 3.23 and 3.24 reveals that d_e is affected by the following factors. (Note that an increase in effective thickness leads to an incrase in the observed absorption intensity in an ATR spectrum).

a. Wavelength. As wavelength increases, d_e increases. When an ATR spectrum is compared to a transmission spectrum of the same material, an increase in spectral contrast towards longer wavelengths is observed in the ATR spectrum.

b. Angle of incidence, θ. As θ increases, d_e decreases. This is the basis by which depth-profiling [e.g. 110] is achieved in ATR spectroscopy.

c. Ratio of refractive indices, n_{21}. The refractive index of most samples of interest to infrared spectroscopists lies in the range 1.4-1.5. A range of ATR prisms, also called internal reflection elements (IREs), are available and range in refractive

indices, from 2.4 (KRS-5) to 4.0 (Ge). The greater the refractive index of the IRE compared to the sample, the smaller the effective thickness.

d. Electric field strength. The greater the electric field strength at the interface, the greater the effective thickness. Hence TE polarization has a lower effective thickness than TM polarization.

Control of the above four parameters allows the spectroscopist to select an appropriate effective thickness. Values of d_e typically fall in the range 0.5-3.0μm. ATR spectroscopy is often described as a "surface" technique. A sampling depth of 2μm would not be considered as surface selective by an exponent of a true surface analysis technique such as XPS. However, it will become clear in the following chapters that while ATR may not be surface specific, it is surface sensitive. In terms of infrared spectroscopy, a sample thickness of a few of microns is very thin. In order to improve the sensitivity of the technique, multiple internal reflections are commonly used. The absorbance per reflection, A/N, where A is the total absorbance and N is the number of reflections, is simply the product of the effective thickness and the absorption coefficient:

$$\frac{A}{N} = \frac{n_{21}\alpha}{\cos\theta} \int_0^\infty E^2 dz \qquad (3.26)$$

and since $\alpha = \varepsilon c$:

$$\frac{A}{N} = \frac{n_{21}\varepsilon c}{\cos\theta} \int_0^\infty E^2 dz \qquad (3.27)$$

The equations described here work well for semi-infinite, homogenous samples. However, self-assembled films in the presence of bulk solution are clearly inhomogeneous. The next section extends ATR theory to encompass such systems.

3.6   ATR and Inhomogeneous Samples

Equation 3.27 assumes that the sample probed by the evanescent field is homogenous, at least to a value of z at which E becomes vanishingly small (the semi-infinite bulk case). (In this context, the term *homogeneous* is used to describe a system in which the sample concentration is not a function of z). However, if the concentration of the analyte changes significantly within the depth sampled by the probing evanescent field the situation becomes complex and equation 3.27 does not apply. Two distinct types of inhomogeneous systems can be defined. The first is the situation in which, as a result of sample inhomogeneity, the refractive index of the sample changes significantly within the depth sampled. Such a situation arises when a sample of a few monolayers is prepared by,say , the L-B technique and then studied by ATR in air. Here, the refractive index of the film is 1.4-1.5 while that of air is 1.0. The film is sufficiently thin that the value of E remains reasonably constant throughout the sample, i.e. d, the film thickness, is much less than d_p, and the form of the evanescent decay is primarily controlled not by the film but by the air. This type of system has been the subject of much interest and was termed the *thin film* case by Harrick [84]. The effective thickness is now given by:

$$d_e = \frac{n_{21} E_0^2 d}{\cos \theta} \qquad (3.28)$$

The electric field amplitudes in the film are approximately given by:

$$E_y = \frac{2 \cos \theta}{\left(1 - n_{31}^2\right)^{1/2}} \qquad (3.29)$$

$$E_x = \frac{2 \cos \theta \left(\sin^2 \theta - n_{31}^2\right)^{1/2}}{\left(1 - n_{31}^2\right)^{1/2}\left[\left(1 + n_{31}^2\right)\sin^2 \theta - n_{31}^2\right]^{1/2}} \qquad (3.30)$$

$$E_z = \frac{2\cos\theta\sin\theta n_{32}{}^2}{\left(1-n_{31}{}^2\right)^{1/2}\left[\left(1+n_{31}{}^2\right)\sin^2\theta - n_{31}{}^2\right]^{1/2}} \qquad (3.31)$$

where n_{31} is n_3/n_1, i.e. n_{air}/n_{IRE}. The above three equations reflect the importance of medium 3, (air), to the form of the evanescent decay.

A second type of inhomogeneous system is the type in which concentration is a function of z but where the refractive index is, to a first approximation, invariant. This situation arises, for example, when a surfactant molecule adsorbs onto the surface of the internal reflection element from solution in an organic solvent. The concentration of the surfactant increases at the interface relative to the bulk solution and therefore the concentration is a function of z. However, the refractive index of the surfactant may be very similar to that of the solvent and so refractive index is not a function of z. In this case the equations for the semi-infinite bulk approximation may be used as the starting point for deriving equations to treat such systems quantitatively. The problem was first addressed by Tompkins [93] and later by Ohta and Iwamoto [94, 95]. As c is no longer constant, equation 3.27 does not apply. The concentration term now has to follow, rather than precede, the integral sign:

$$\frac{A}{N} = \frac{n_{21}E_0{}^2\varepsilon}{\cos\theta}\int_0^\infty c(z)e^{-2z/d_p}\,dz \qquad (3.32)$$

Tompkins [93] considered a step-type concentration profile such that $c=c_1$ for $z \leq t$ and $c=0$ for $z>t$, as shown in figure 3.6.

Figure 3.6   The Step-Type Concentration Profile
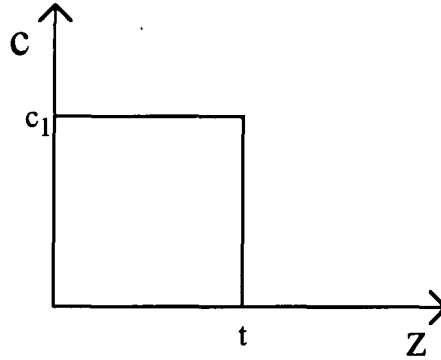
Applying this profile to equation 3.32 and performing the integration, Tompkins obtained:

$$\frac{A}{N} = \frac{n_{21}E_0^2}{\cos\theta}\varepsilon c_1 \frac{d_p}{2}\left[1 - e^{-2t/d_p}\right] \qquad (3.33)$$

and since $d_e = \dfrac{n_{21}E_0^2 d_p}{2\cos\theta}$:

$$\frac{A}{N} = \varepsilon c_1 d_e\left[1 - e^{-2t/d_p}\right] \qquad (3.34)$$

Tompkins also pointed out the limitations of resolving t and c_1. When $t > \lambda_1$, c_1 may be determined but not t. When $t < 0.05\lambda_1$ the product $c_1 t$ may be determined but the values not resolved. This latter situation applies to most surfactant adsorption studies. For example, at a wavelength of $3\mu m$ using a silicon IRE t would have to exceed 900nm before c_1 and t could be resolved. Sperline et al applied Tompkins mathematics to the study of surfactant adsorption [46]. These workers were working with a system in which there was adsorbed surfactant at the interface and free surfactant in the bulk solution. Hence a slightly different concentration profile was considered, i.e.:

$c(z) = c_i + c_b$ for $0 < z < t$ and

$$c(z) = c_b \qquad \text{for } t < z < \infty$$

The subscripts i and b denote the interface and bulk respectively. The concentration of the analyte does not fall to zero in this case. Therefore, the absorbance equation will contain terms for the adsorbed species at the interface and for the bulk surfactant. In order to evaluate 3.32, Sperline *et al* used the approximation:

$$e^{-2t/d_p} = 1 - 2t/d_p$$

since

$$2t << d_p$$

Sperline's experiment used unpolarized radiation and therefore the average value of d_e was used (i.e. 3.25). Using these approximations and substitutions Sperline arrived at the absorbance equation:

$$\frac{A}{N} = \varepsilon c_b d_e + \varepsilon\left(2d_e/d_p\right)\left(c_i t\right) \qquad (3.35)$$

This equation contains both interface and bulk terms. One important assumption and one approximation are evident in this equation. The assumption is that the value of ε is the same in both the interface and bulk terms. In other words, it is assumed that the molar absorptivity does not change upon adsorption of the surfactant. This assumption may apply to those chromophores on the molecule which do not bind to the surface of the IRE. However, the assumption is clearly unsound for those chromophores associated with the part of the molecule which binds to the surface. In order to determine c_b it is assumed that the surface area of the IRE is so low that the adsorption process reduces the bulk concentration negligibly. In other words, the bulk concentration following adsorption is, to a first approximation, the same as the original concentration of the surfactant solution. Clearly, this approximation is most accurate when there is a large volume of solution at high concentration.

Sperline was interested in surfactant adsorption and wanted to present his results in terms of the *surface excess concentration*. This quantity is used throughout colloid science [1] as a measure of surface activity and was first suggested by Gibbs. The next section defines the surface excess concentration.

3.7   The Surface Excess Concentration

A system containing an interface may be conveniently considered as consisting of three parts: two bulk phases of volumes V' and V'' and a surface, of area A separating them. The concentration of a component i in each of the bulk phases can be written as c_i' and c_i'' respectively. The number of moles of i in each of the bulk phases is given by:

$$n_i' = c_i'V' \quad \text{and} \quad n_i'' = c_i''V'' \qquad (3.36)$$

The extra number of moles which can be accommodated in the system because of the presence of an interface is given by:

$$n_i^\sigma = n_i - c_i'V' - c_i''V'' \qquad (3.38)$$

where n_i is the total number of moles of i in the system.

A surface concentration may be defined as:

$$\frac{n_i^\sigma}{A} = \Gamma_i \qquad (3.39)$$

where A is the surface area. The quantity Γ_i is called the *surface excess concentration* (or sometimes the Gibb's surface excess concentration).

In the case of the ATR experiment, one of the phases is the (solid) IRE. Therefore $c_i''=0$ and 3.38 becomes:

$$n_i^\sigma = n_i - c_i'V' \qquad (3.40)$$

Hence $\Gamma_i = \dfrac{n_i - c_i' V''}{A}$ (3.41)

The units of Γ_i are clearly moles per unit area, usually $mol.cm^{-2}$.

Sperline recognised that the $c_i t$ term in the absorbance equation (3.35) is related to Γ_i. The units of $c_i t$ are $mol.dm^{-3}.cm$ while those of Γ_i are $mol.cm^{-2}$. Therefore:

$\Gamma_i = \dfrac{c_i t}{1000}$ (3.42)

In principle, then, it is possible to determine Γ_i as defined in 3.41 from an ATR spectrum, provided that the absorbance due to bulk species can be accurately subtracted from that due to the adsorbed species. This requires careful calibration of the ATR experiment. Many workers in the field of ATR rely on geometrical measurements of the ATR sampling accessories to determine the angle of incidence, θ, and the number of sampling reflections. However, such measurements do not take into account beam divergence or the possibility of misalignment of the accessory. As a result of the need for careful calibration of the ATR experiment, Sperline *et al* developed an iterative procedure for calibrating an ATR cell [96]. This procedure is described below.

3.8   Calibration of the ATR Experiment

The method described above for determining the surface excess concentration of a surfactant in the presence of bulk solution is wholly dependent on the ability to subtract the bulk component from the surface component. This in turn relies upon an accurate knowledge of d_e (and hence also d_p). In order to calculate d_e it is necessary to know:

i.   The refractive indices of IRE and sample.

ii.   The polarization.

iii. The wavelength of the radiation.

iv. The angle of incidence, θ.

v. The number of sampling reflections, N.

Optical constants for most materials commonly used in IR spectroscopy are known over a wide range of frequencies and so (i) is known. The polarization and frequency of observation should be known to the spectroscopist and hence (ii) and (iii) are known. The angle of incidence and the number of sampling reflections are commonly obtained *via* geometrical measurements of the ATR accessory. However, such measurements do not take into account divergence of the beam or misalignment of the accessory in the spectrometer. An alternative calibration method, proposed by Sperline *et al* involves the use of a standard solution of a non-adsorbing analyte. The analyte must show no surface activity as adsorbed molecules lead to enhanced intensities in ATR spectra. Harrick's equations for the semi-infinite bulk case are used to calculate an effective pathlength for the experiment. This pathlength is then used in the Beer-Lambert equation. Successive approximation calculations converge to give an average internal incidence angle. This process is described in detail hereunder.

A standard solution of concentration c_r is prepared. The molar absorptivity of the standard solute, ε_r, is determined from a transmission measurement. The spectrum of the standard solution is then obtained by the ATR technique. The integrated absorbance, A_r, of the reference band is measured. An angle of incidence is assumed (the manufacturer's claimed θ is usually taken). Together with the refractive indices of solvent and IRE and the wavelength, the assumed θ is used to calculate an effective thickness, d_{er}, (from 3.23-3.25). A rearranged Beer-Lambert-type equation is applied to obtain the number of sampling reflections from the measured absorbance, molar absorptivity, concentration and effective thickness, *viz*:

$$N = \frac{A_r}{\varepsilon_r c_r d_{er}} \qquad (3.43)$$

For an IRE of thickness d having a sample contact length L, the number of sampling reflections is given by:

$$N = \frac{L}{d \tan \theta} \qquad (3.44)$$

The value of N obtained from equation 3.43 is inserted in equation 3.44 to obtain a value of θ_{calc}. The original value of θ that was estimated from the manufacturer's data is now θ_{old}. A new value for θ is calculated thus:

$$\theta_{new} = \frac{2\theta_{old} + \theta_{calc}}{3} \qquad (3.45)$$

The new value of θ is now used in Harrick's equations to calculate a new d_e which is then used in 3.43 to obtain a new N which is then used in 3.44 to obtain a new value of θ_{calc}. The previous value of θ_{calc} now becomes θ_{old}. The cycle is repeated until $|\theta_{new} - \theta_{calc}|/\theta_{new} < 0.0002$. Convergence is rapid, requiring less than ten cycles. The result of the process is a pair of values, N and θ, which may be used in quantitative expressions for ATR spectroscopy, such as those for determining surface excess concentration.

3.9 Orientational Measurements by ATR

In the first chapter of this thesis it was noted that in addition to quantitative information about the amount of surfactant adsorbed, ATR spectroscopy is able to yield information about the orientation of chromophores within the adsorbed layer. In order for an electromagnetic field to induce a dipole moment change in a molecule the direction of the dipole moment must have a component parallel to the electric field vector. The probability of a dipole moment change occurring is proportional to the

cosine of the angle between the dipole moment and the electric field vector. An evanescent field generated by unpolarized electromagnetic radiation has components in all spatial orientations, E_y, E_x and E_z. Therefore, the evanescent field may couple with dipoles in any orientation with respect to the surface. In other words all chromophores in range of the evanescent field will contribute to the spectrum regardless of their orientation. However, if the incident radiation is polarized, the situation changes. The incident radiation may be polarized either parallel (TM) or perpendicular (TE) to the plane of incidence. The TE wave has only one electric field vector associated with it, E_y. This vector is perpendicular to the plane of incidence and parallel to the reflecting interface. Only dipoles with a component parallel to the interface can therefore couple to this radiation and contribute to the TE spectrum. The TM wave, on the other hand, has two electric field vectors associated with it, E_x and E_z. E_x is parallel to both the plane of incidence and the reflecting surface. Therefore, as with E_y, dipoles with a component parallel to the interface can couple with the radiation and contribute to the spectrum. The E_z component is unlike the other two in that it is parallel to the plane of incidence but *perpendicular* to the interface. Thus, dipoles with a component perpendicular to the interface will contribute to the spectrum.

In order to obtain orientational information from polarized ATR spectroscopy the *dichroic ratio, D,* is measured:

$$D = \frac{A_{TE}}{A_{TM}} \qquad (3.46)$$

where A_{TE} and A_{TM} are the integrated areas of a given absorbance band in ATR spectra obtained with TE and TM polarization respectively. The strength of a given absorbance band is proportional to the intensity of the electromagnetic radiation promoting that absorption, i.e. $A \propto E^2$. Therefore, if the dipoles in the sample are completely randomly oriented then:

64

$$D = \frac{A_{TE}}{A_{TM}} = \frac{E_{y0}^2}{E_{x0}^2 + E_{z0}^2} \qquad (3.47)$$

However, if the dipoles are oriented solely parallel to the interface, the z component can no longer contribute to the TM spectrum and the dichroic ratio becomes:

$$D = \frac{A_{TE}}{A_{TM}} = \frac{E_{y0}^2}{E_{x0}^2} \qquad (3.48)$$

The above equations were derived by Haller and Rice [45]. In an ordered layer of a surfactant deposited by either the L-B or self-assembly technique, the aliphatic chains may align perpendicular to the surface. The the CH stretching vibrations of the methylene units occur at right-angles to the chain axis. Therefore chains aligned normal to the surface plane will have methylene stretching vibrations occurring parallel to the surface plane. A perfectly aligned film will have an infrared spectrum in which the dichroic ratio of the bands associated with the methylene stretching is given by 3.48. A random film will have a dichroic ratio given by 3.47. This is illustrated in figure 3.7.

The values taken for the electromagnetic field intensities may be calculated using the thin film approximation (3.29-3.31) or the semi-infinite bulk approximation (3.5-3.7) depending on the thickness of the sample. The thin film approximation is appropriate to studies of L-B films. In the case where an adsorbed surfactant layer is studied in the presence of a (thick) layer of bulk solution, the semi-infinite bulk approximation should be used as the adsorbed layer has a comparable refractive index to that of the bulk solution. Such systems have the added complication of possessing both a potentially ordered adsorbed film and a random bulk solution. However, if the surface excess concentration of the surfactant is known, it is possible to obtain a model for the expected dichroic ratio of an ordered layer/random bulk system. This is done in chapter 6.

Figure 3.7 Schematic of Dichroic Measurement

Methylene
Stretching
Dipole

a

Aliphatic Chain
Axis

b

z

x

y

TE

TM
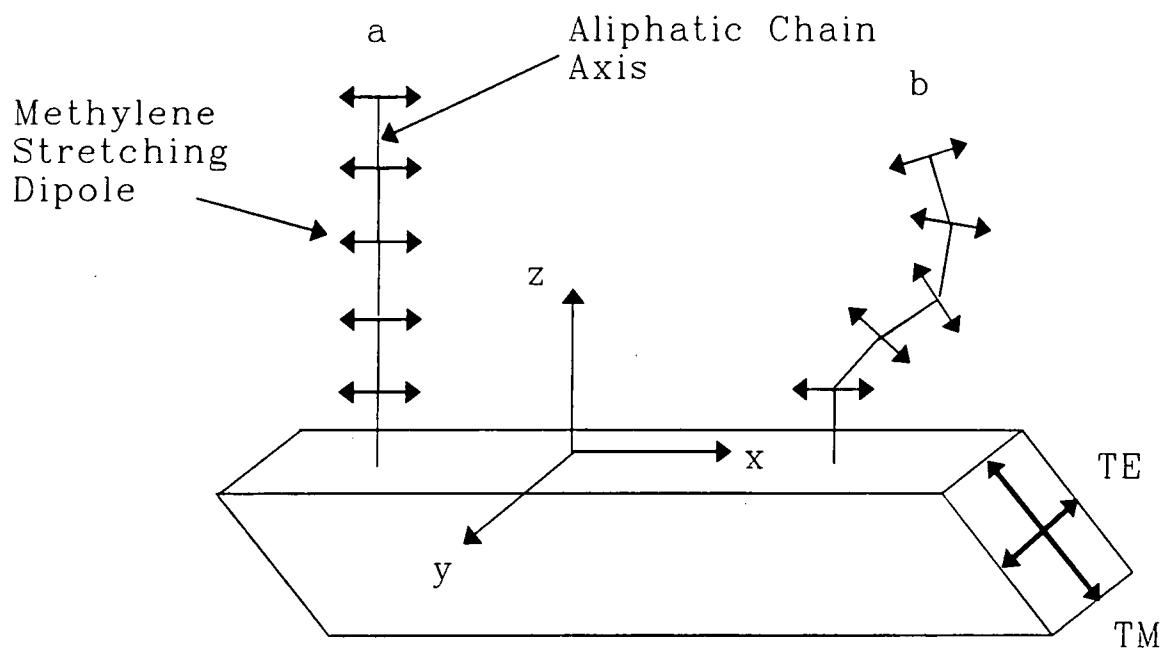
a — Perfect Alignment

$$\frac{A_{TE}}{A_{TM}} = \frac{E_{yo}^2}{E_{xo}^2}$$

b — Random Orientation

$$\frac{A_{TE}}{A_{TM}} = \frac{E_{yo}^2}{E_{xo}^2 + E_{zo}^2}$$

Chapter 4   Rheology as a Probe of Dispersion Structure

4.1   Introduction

In chapter 1 the effect that adsorbed molecules can have on the stability of colloidal dispersions was described. Chapters 2 and 3 described how infrared spectroscopy may be used to study the structure of layers of adsorbed molecules. Clearly it is desirable to study how the adsorbed layers studied by infrared spectroscopy affect the properties of real colloidal dispersions. Changes in the aggregation behaviour of colloidal particles affects the way in which dispersions of those particles respond to an applied stress. A study of the rheology of a colloidal dispersion therefore yields valuable information about its structure.

This chapter briefly outlines how rheology may be used to probe the structure of silica-in-toluene dispersions.

4.2   Introductory Rheology

4.2.1   The Response of Ideal Solids and Liquids to Shear

A shearing stress S acting on an ideal elastic solid produces a strain γ according to equation 4.1:
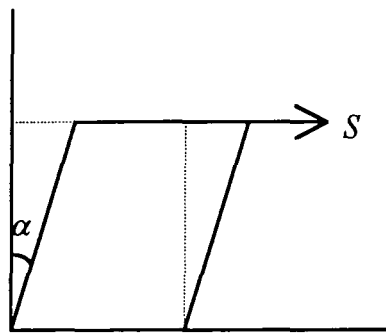
$$S = G\gamma \qquad 4.1$$

where G is the shear modulus of the material and γ is defined by figure 4.1.

Ideal liquid behaviour is shown when the applied shearing stress is directly proportional to the rate of shear or rate of strain, i.e.:

$$\dot{\gamma} = \frac{d\gamma}{dt}$$

$$\text{and} \quad S \propto \dot{\gamma} \quad \text{or} \quad S = \eta\dot{\gamma} \qquad 4.2$$

Figure 4.1   Definition of Strain in an Elastic Solid

$$\gamma = \tan\alpha$$

The proportionality constant in equation 4.2, η, is the *viscosity*. Equation 4.2 was first proposed by Isaac Newton and fluids which obey this equation are described as *Newtonian*.

4.2.2   The Response of Colloidal Dispersions to a Shearing Stress

Colloidal dispersions often consist of solid particles dispersed in a Newtonian liquid. The resulting dispersion is seldom Newtonian. Einstein considered how the addition of solid particles to a Newtonian liquid would affect the viscosity of the system and produced equation 4.3:

$$\eta_{rel} = 1 + 2.5\phi \qquad 4.3$$

where η_{rel}, the relative viscosity, is the ratio of the viscosity of the suspension to that of the pure continuous phase and ϕ is the volume concentration of the solid particles. The equation shows that the viscosity of the dispersion increases as the volume concentration of the dispersed phase increases. Einstein's equation applies only to dilute dispersions of non-interacting hard spheres. Such dispersions are expected to exhibit Newtonian behaviour, i.e. η_{rel} is independent of shear rate.

Most colloidal dispersions do not show Newtonian behaviour. In many dispersions the particles interact with one another and form aggregates. Large aggregates are less mobile than small, discrete particles and so the viscosity of a dispersion of the former will be greater than that of a dispersion of the latter for the same volume concentration of solid. As the dispersion of aggregates is subjected to increasing shear rates, the aggregates may break down, thereby lowering the viscosity of the dispersion. This process is called *shear thinning*.

Once the aggregates have been broken down to individual particles, increasing the shear rate will not produce a further reduction in the viscosity. A Newtonian region may be entered where the viscosity remains constant as the shear rate increases.

Further increases in shear rate may increase the viscosity of the dispersion. The continuous phase is forced to flow around the slower-moving particles at such a rate that small vortices may be formed on the 'down-stream' side of the particles. This

turbulent flow restricts the movement of the liquid and hence the viscosity increases. This process is called *shear thickening*.

The processes described above lead to a complex relationship between the viscosity of a dispersion and the shear rate. This relationship is shown schematically in figure 4.2. Not all colloidal dispersions show all the regions of the curve. The control of the rheological properties of dispersions is a very important area of colloid science. Silica is commonly used as a viscosity-modifying dispersed phase. In the next section the rheological properties of silica dispersions and how they may be modified by adsorbed molecules will be described.

Figure 4.2   Schematic of the Variation of Viscosity with Shear Rate for a

Dispersion of Interacting Particles
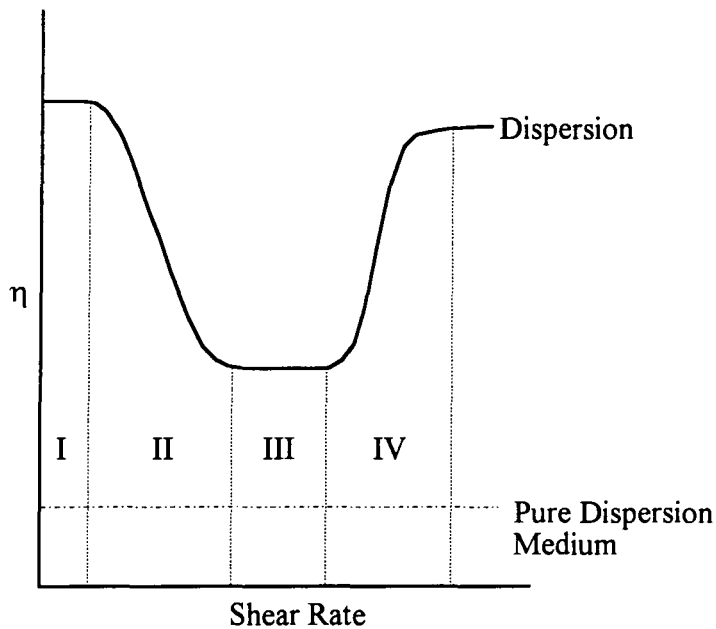
I.   Newtonian Region. Shear rate insufficient to break up aggregates. Viscosity
      remains constant as shear rate increases.

II.   Shear Thinning Region. Shear breaks down aggregates. Viscosity decreases as
      shear rate increases.

III. Newtonian Region. Increase of shear does not break down aggregates any
      further. Viscosity remains constant as shear rate increases.

IV.   Shear Thickening. Increasing shear produces turbulent flow. Viscosity increases
      as shear rate increases.

### 4.2.3   Colloidal Silica as a Viscosity Modifier

The silica chosen for this study was AEROSIL 200. Aerosil 200 is one of a range of Aerosil silica products manufactured by Degussa AG. These silicas are produced by the high temperature hydrolysis of silicon tetrachloride *viz*:

$$SiCl_4 + 2H_2 + O_2 \rightarrow SiO_2 + 4HCl$$
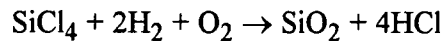
The resulting primary silica particles are almost spherical and are virtually non-porous. Aerosil 200 has a surface area of 200m²/g. The average diameter of the primary particles is 12nm. The surface of Aerosil 200 is hydrophilic as there are 3-4 silanol groups per nm². Atmospheric water adsorbs readily onto these groups.

Aerosil acts as a thickening agent by forming aggregates and larger agglomerated aggregates in the dispersion medium. Attractive dispersion forces act to bind the primary particles into aggregates. There also exists the possibility of hydrogen bonding between the silanol groups on adjacent particles, as shown in figure 4.3.

Figure 4.3   Schematic of Hydrogen Bonding between Two Aerosil Particles
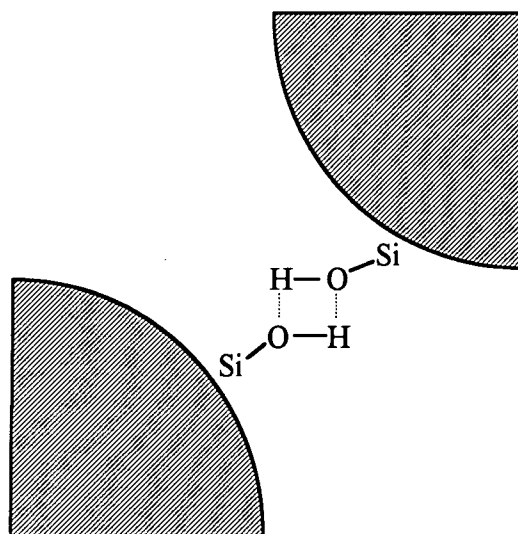

Not to Scale

Such hydrogen bonding between primary particles is not believed to be extensive [109]. Dispersion forces appear to be the main binding force in Aerosil aggregates.

The agglomeration behaviour of Aerosil 200 has been studied by electron microscopy [109]. The agglomeration characteristics of Aerosil 200 are shown schematically in figure 4.4.

Figure 4.4   Schematic of the Agglomeration Behaviour of Aerosil in Liquid Systems.
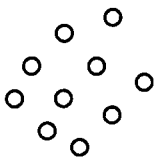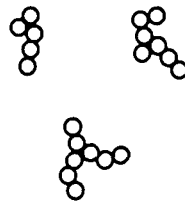
I. Primary Particles   II. Aggregates
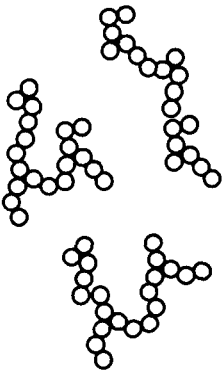
III. Agglomerated Aggregates   IV. Three-dimensional Network
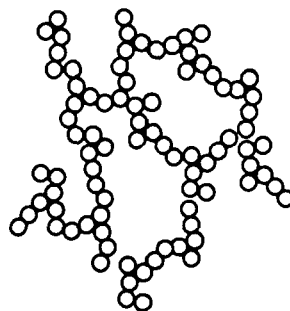
The viscosity of a dispersion of Aerosil silica increases as the agglomeration increases i.e. η I<II<III<IV. Increasing the shear rate may break down the agglomerates and thereby reduce the viscosity of the dispersion. Aerosil dispersions may therefore be expected to exhibit shear thinning. The transition from a dispersion of agglomerated aggregates to a three-dimensional network (III→IV) of silica results in a dramatic increase in the viscosity of the system.

The ability of a silica dispersion to form a three-dimensional network depends on the nature of the dispersion medium. The nature of the interaction between the silica surface and the surrounding solvent has been studied by infrared spectroscopy [33]. The hydrophilic silica surface is capable of forming hydrogen bonds with solvent molecules *via* the silanol groups. Solvents which may form hydrogen bonds with the silanol groups, such as methanol, wet the surface better than those solvents which can only interact weakly with the surface, such as carbon tetrachloride. Therefore, solvents which wet the surface well therefore tend to disperse the silica particles better than those which do not. When the dispersion medium wets the silica surface well, a larger volume fraction of silica is required to produce a three-dimensional network than when the dispersion medium wets the surface poorly. However, it should be noted that whatever the dispersion medium, the volume fraction of silica particles in systems which show a three-dimensional network is low (typically <5%).

4.2.4   Control of the Viscosity Modification Characteristics of Aerosil

In the previous section the way in which the viscosity of dispersions of Aerosil silica depends upon the aggregation of the particles was described. The aggregation behaviour is controlled by attractive dispersion forces between the particles which serve to bind the aggregates together and hydrogen bonding interactions between the silica surface and the dispersion medium. Altering either the particle-particle interactions or particle-dispersion medium interactions will therefore affect the aggregation behaviour of the silica particles and hence the rheological behaviour of the dispersion.

In chapter 1 the attractive van der Waals forces acting between colloidal particles were described. These forces lead to the aggregation of the silica particles. In order to prevent aggregation it is necessary to provide a repulsive force at least equal to the attractive van der Waals forces. This can be done electrostatically or sterically. In the (non-aqueous) systems of interest in the present study only steric (polymeric)

stabilization can be used. Figure 4.5 shows how the total potential energy, V_T, between two sterically stabilized particles is composed of an attractive potential, V_A, due to van der Waals forces and a repulsive potential due to the adsorbed steric layer, V_S.

Figure 4.5   Schematic of Total Potential Energy Between Two Sterically Stabilized Particles
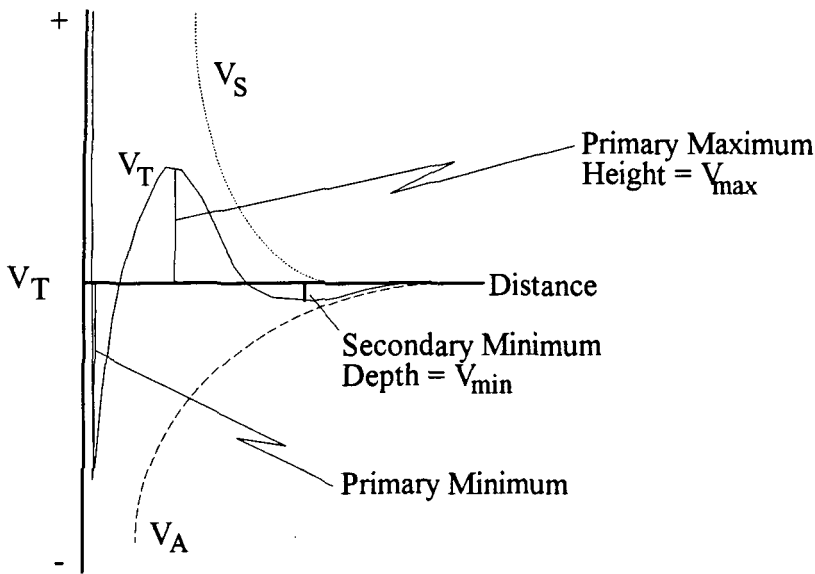
The depth of the secondary minimum, V_{min}, is dependent upon the shape of the V_S curve, which in turn, is critically dependent upon the structure of the adsorbed layer. A secondary minimum deeper than a few kT will lead to aggregation of the particles. The centre-to-centre distance of the particles in the aggregate will be greater than it would be in the absence of the adsorbed layer but an aggregate will still be formed. In order to prevent aggregation, then, the V_S curve needs to rise steeply at a great enough distance from the particle surface to prevent a significant secondary minimum being formed. The way in which the shape of the V_S curve is affected by the structure of the adsorbed layer is described below. The discussion considers surfactant molecules anchored at one end to the solid surface by a headgroup with an aliphatic chain extending into solution.

The thickness of the adsorbed layer clearly affects the distance at which the V_S curve rises steeply. The thickness of the layer depends upon the length of the adsorbed molecules and their conformation. Long chains will have greater spatial extensions than short ones. For a given chain length, well ordered chains oriented perpendicular to the surface have optimum spatial extension.

The degree of surface coverage also affects stability. If the coverage of the surface is low the adsorbed layers on two particles may interpenetrate during a collision. This does not provide a barrier to aggregation. Considering a typical adsorption isotherm, such as that presented in figure 4.6, the stability of a dispersion of particles on which is adsorbed an amount of a compound X, a molecule capable of stabilizing the dispersion, will increase as the surface excess concentration increases (section I of the curve) and remain essentially constant over the plateau region (section II).

Figure 4.6   Schematic of a Possible Adsorption Isotherm

Equilibrium Concentration
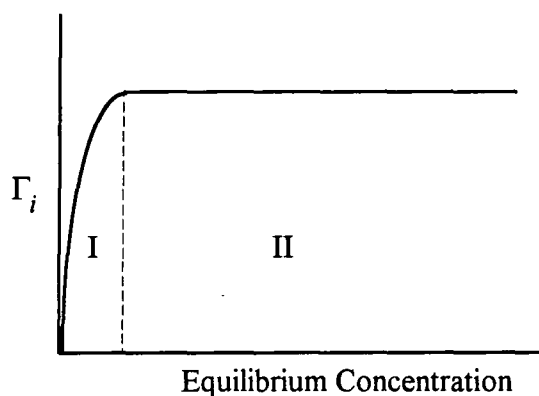
As the surface excess concentration increases, the area of surface available per adsorbed molecule decreases. The area available per molecule may decrease to such an extent that the chains become constrained and are forced into all-trans conformations with the major chain axis oriented perpendicular to the surface. The change in adsorbed layer structure with increasing surface excess concentration is shown schematically in figure 4.7.

In order to provide stability to a dispersion the adsorbed molecules need to be strongly bound to the surface, otherwise they may desorb and move away from the zone of interaction during a Brownian collision.

Figure 4.7   Change of Adsorbed Layer Structure with Increasing Γ_i
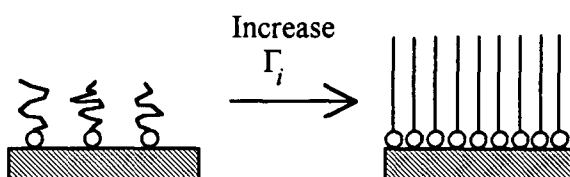
In summary, in order to produce stability in a dispersion the adsorbed layer should be tightly bound to the surface, have a sufficiently low area per molecule to prevent interpenetration of the layers and have a spatial extension such that V_{min} is less than kT.

Infrared studies of silica immersed in toluene, the solvent of choice in this study, have shown that the π-electrons of the toluene molecule interact with the surface silanol groups, leading to a shift to lower frequency of the position of the silanol OH stretching band of $155cm^{-1}$ [111]. This indicates that there is an attractive interaction between the silanol group and the toluene ring. However, this interaction is much weaker than that between a molecule capable of forming a strong hydrogen bond and the silanol group. For example, the adsorption of n-octylamine produces a shift in the frequency of the silanol OH stretching vibration of $800cm^{-1}$ to lower wavenumber [32]. From the discussion in section 4.2.3 it follows that Aerosil 200 should be 'wet' by toluene but that the dispersion medium-silica interactions are sufficiently weak to enable the formation of a three-dimensional network at low volume fraction of solid. The following discussion refers to silica-in-toluene dispersions in which the volume fraction of unstabilized silica is sufficient to form a three-dimensional network. However, if the silica particles are shrouded by an adsorbed layer capable of inhibiting aggregation, the ability of the silica to form a three-dimensional network is reduced

and hence the viscosity of the system at shear rates lower than that required to completely break down a network will be less than that of one containing such a network. As the stabilized system has less structure at zero shear than the unstabilized one, the amount of shear thinning will be less in the stabilized system. The relationship between viscosity and shear rate for the stabilized and unstabilized systems is shown in figure 4.8.

The presence of an adsorbed surfactant layer may also inhibit agglomeration by improving the wetting of the surface by the dispersion medium. An adsorbed layer of hexadecylamine will present a hydrophobic surface of aliphatic chains. This may be wet better by toluene than the original hydrophilic surface of silanol groups.

Figure 4.8   Relationship Between Viscosity and Shear Rate for Stabilized and Unstabilized Silica Dispersions
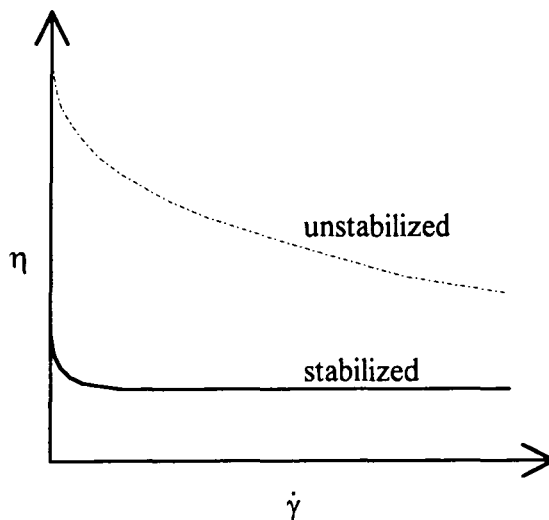
4.3   An Overview

Dispersions of hydrophilic colloidal silica in toluene undergo aggregation as a result of attractive van der Waals forces operating between the primary particles. The aggregates may form larger agglomerates which can bind together into a three-dimensional network. Such networks can arise even when the volume fraction of silica is less than 5% and lead to a dramatic increase in the viscosity of the system. The network may be broken down under shear, resulting in a lowering of the viscosity of the system.

The aggregation of the silica and hence its ability to form networks can be inhibited by the presence of an adsorbed layer on the silica surface. Such layers provide a repulsive force which opposes the van der Waals attraction. The strength of this repulsive force, and hence the ability of the adsorbed layer to inhibit aggregation, depends upon the structure of the layer. The adsorbed layer may also inhibit aggregation by improving the affinity of the dispersion medium for the particle surface.

The ability of an adsorbate to inhibit the formation of three-dimensional networks of silica may be determined by measuring the viscosity as a function of shear rate of a system in which the volume fraction of solid silica is sufficiently high to produce a network in the absence of the adsorbate.

Chapter 5   Calibration of the ATR Experiment

5.1   Introduction

The ability to perform quantitative ATR spectroscopy relies upon careful calibration of the ATR sampling accessory. The theory behind the calibration of an ATR experiment was described in section 3.8. This chapter describes the practical calibration of the ATR device which is used throughout this thesis, the Specac Squarecol™, and the results obtained. Many of the experimental details described hereunder also apply to the measurements described in the following chapters. Hence the experimental section of this chapter will be particularly comprehensive.

5.2   Experimental

5.2.1   Materials

Deuterated toluene (99+atom% D, Aldrich) was distilled prior to use. Chloroform (99.9% ACS HPLC grade, Aldrich) and 2-propanol (99.5% HPLC grade, Aldrich) were used as recieved. Hexadecane (99%, Gold Label, Aldrich) was dried over molecular sieve (4A) prior to use.

5.2.2   The Specac Squarecol

There are many ATR accessories on the market and a number of these are available at Durham. The accessory chosen for most quantitative measurements in the current work is the Squarecol cell, manufactured by Graseby Specac Ltd. This cell was chosen because it offers good reproducibility of positioning, can readily be filled with solutions, both aqueous and nonaqueous, and has an ATR prism which has a square cross section of similar dimensions to the IR beam. An ATR accessory which has found some favour for the quantitative analysis of solutions is the CIRCLE CELL [46, 96, 97, 98]. Obtaining a spectrum of a solution with this accessory is easy but the

ATR prism is circular in cross-section, the end-faces being conical. Such a geometry scrambles the polarization and therefore no orientational information can be obtained.

The Squarecol cell consists of a stainless steel trough in which the ATR prism sits. The cell is sealed by two Viton O-rings which are placed on either end of the ATR prism and clamped into place by two stainless steel plates secured by allen bolts. The Squarecol is shown in plan view in figure 5.1 together with supporting optics. A loose-fitting lid is provided by Specac for the top of the cell. However, whilst this is adequate for aqueous solutions, volatile solvents quickly evaporated. At Durham we have modified the cell by fitting a stainless steel lid which may be sealed onto the cell body by tightening four allen bolts. A Teflon gasket is fitted between the cell body and the lid to aid sealing. Two female luer joints in the lid allow the cell to be filled (using a syringe) whilst sealed. After filling, the luer joints are stoppered with Teflon plugs.

A second modification to the Squarecol cell made at Durham is the addition of a temperature control unit. This consists of a copper plate on which the cell body sits. Beneath the copper plate are two Peltier units (Farnell) which sit on top of a hollow copper box through which water can be pumped. The assembly is clamped together and heat-sink compound is used to ensure good thermal contact between the components. Power is supplied to the Peltier units by an autoranging power supply capable of supplying high current (Farnell LS 30-10). An exploded view of the assembly is shown in figure 5.2.

5.2.3 Cleaning of the Cell and ATR Prism

The stainless steel cell body was rinsed in turn with deionized water, methanol and carbon tetrachloride. The silicon ATR prism was washed with deionized water and methanol. The surface was then swabbed with a lens tissue (Whatman) soaked in carbon tetrachloride. The prism was then placed in the thimble of a Soxhlet apparatus and refluxed in 2-propanol for a minimum of four hours. The reflux treatment cleans the surface of the prism and promotes the formation of silanol groups on the surface

thereby making it more hydrophilic. Measurements of the contact angle of a water droplet on the surface of silicon wafers treated with 2-propanol for various times showed that three hours in the Soxhlet apparatus were required to reduce the contact angle to <45°.

5.2.4 Preparation of Solutions

Solutions of hexadecane in deuterated toluene were prepared by weighing an appropriate amount of hexadecane into clean 5ml volumetric flasks such that when made up to the mark concentrations of 0.0035, 0.0119 and $0.0186 mol.dm^{-3}$ (3.5, 11.9 and 18.6mM) were obtained. Hexadecane is a liquid at warm room temperature and so in order to facilitate the weighings a micropipette of adjustable volume was used.

5.2.5 Spectroscopy

A fixed-pathlength transmission cell was constructed with KBr windows and a Teflon spacer approximately 0.02cm thick. A single beam spectrum of the empty cell was recorded and was ratioed against the instrument background. The interference fringes observed in the spectrum were used to calculate the pathlength of the cell. Spectra were recorded of each hexadecane solution and ratioed against the single beam spectrum of the pure solvent.

The single beam spectrum of the empty Squarecol cell was ratioed against that of the instrument background to check for cleanliness. The single beam spectra of the hexadecane solutions were recorded in the cell and ratioed against the ATR single beam spectrum of pure solvent. The cell was taken apart and cleaned throroughly between each solution, the hexadecane, being less volatile than toluene-D8, tending to remain tenaciously in the cell.

All spectra were recorded on a Mattson Sirius 100 spectrometer with upgraded circuitry and equipped with an MCT detector. The data was processed using PC-based

FIRST software. The instrumental operating parameters used for recording the transmission and ATR spectra are given in table 5.1.

Table 5.1   Instrumental Parameters

Parameter	Transmission	ATR
Resolution	4cm^{-1}	4cm^{-1}
Number of Scans	124	512
Mirror Velocity	40kHz	40kHz
Iris	20%	95%
Apodization	Triangular	Triangular
Zerofilling	On	On

5.3   Results and Discussion

A part of the spectrum of the empty transmission cell is shown in figure 5.3. Interference fringes can clearly be seen. These may be used to determine the pathlength of the cell using the formula:

$$l = \frac{n}{2(v_1 - v_2)} \qquad 5.1$$

where l is the pathlength in centimetres, n is the number of complete fringes lying between frequencies v_1 and v_2 (where v is in reciprocal centimetres). In the case shown in figure 5.3:

$$l = \frac{12}{2(2179 - 1910)}$$

$$= \underline{0.022cm}$$

Having determined the pathlength of the cell the molar extinction coefficient of hexadecane may be determined from the spectra of the solutions. Figure 5.4 shows the transmission spectra of the three hexadecane solutions in the CH stretching region. Four fundamental bands can be seen in this region. The peak positions and their assignments are given in table 5.2.

Table 5.2   Band Assignments in the CH Stretching Region of the Spectrum of Hexadecane

Band Position (cm^{-1})	Assignment
2956	Antisymmetric CH_3 stretching
2926	Antisymmetric CH_2 stretching
2872	Symmetric CH_3 stretching
2854	Symmetric CH_2 stretching

Throughout this thesis quantitative spectral measurements will be made in terms of *integrated peak areas* rather than peak heights. The molar extinction coefficient, ε, can be calculated *via* Beer's law:

$$\varepsilon = \frac{A_{in}}{cl} \qquad 5.2$$

where A_{in} is the integrated peak area in cm^{-1}, c is the concentration of the analyte in $mol.dm^{-3}$ and l is the pathlength in centimetres. Therefore, ε has units $dm^3 mol^{-1} cm^{-2}$. The integrated peak areas from 3000-2800cm^{-1} are tabulated in table 5.3, together with the calculated values of ε.

Table 5.3   Integrated Absorbances and ε Values for Hexadecane Transmission
Spectra

Concentration (mM)	A_{in} (cm^{-1})	ε (dm^{3}mol^{-1}cm^{-2})
3.5	3.848	49974
11.9	13.272	50695
18.6	21.054	51451

The mean value of ε is 50707dm^{3}mol^{-1}cm^{-2}. This value is now used in the calibration of the ATR experiment.

The absorbance spectrum of the silicon ATR prism is shown in figure 5.5. The main feature of this spectrum is the intense series of bands below 1500cm^{-1}. These are due to vibrations of the SiO layer and are the reason that silicon ATR prisms have a narrower IR "window" than KRS-5 or ZnSE. Bands arising from the sample compound below 1500cm^{-1} cannot be studied by Si ATR.

The CH stretching regions of the spectra of the hexadecane solutions are shown in figure 5.6. These spectra show bands in the same position as in the transmission spectra but the bands are much less intense in the ATR spectra. This is because the effective pathlength in the ATR experiment is much smaller than the actual pathlength in the transmission experiment (a few microns compared with 0.02cm). In the case of the 3.5mM solution, noise makes a significant contribution to the ATR spectrum. This is why the top of the band at 2926cm^{-1} looks slightly distorted.

A BASIC computer program was written to perform the calibration calculations proposed by Sperline *et al* [96] and described in section 3.8. A listing of this program can be found in Appendix A. The physical data required in addition to the band intensities for the procedure are given in table 5.4.

Table 5.4   Physical Data Required for Calibration

Parameter	Value
Solution Contact Length of Prism (cm)	5.6
Thickness of Prism (cm)	0.6
Frequency (cm^{-1})	2900
Refractive Index of Silicon	3.425
Refractive Index of Toluene-D8	1.457
ε ($dm^3 mol^{-1} cm^{-2}$)	50707
Claimed Angle of Incidence, θ (°)	45
Claimed Number of Reflections, N	10

The physical data given in table 5.4 is used with the integrated band areas from the spectra shown in figure 5.6 to calculate the values of θ and N for each concentration. The results of these calculations are given in table 5.5.

Table 5.5   Results of Calibration Calculations

Concentration (mM)	Peak Area (cm^{-1})	θ (°)	N
3.5	0.069	41.7	10.5
11.9	0.144	47.4	8.6
18.6	0.336	42.6	10.1

Note that the iterative program produces a pair of values, θ and N, which give the best fit to the data. Hence non-integer values of N are produced. The mean value of θ is 43.9° and the mean N is 9.7. These values are close to the manufacturer's claimed angle of incidence and number of reflections (45° and 10, respectively) which are derived simply from geometrical considerations. From the data presented in table 5.5 it can be seen that scatter in the data is equivalent to a deviation in the angle of incidence from 45° by approximately ±2°.

The value of θ obtained by the calibration experiment can be used in conjunction with other physical data to calculate the *effective thickness*, d_e, for the experiment, as described in section 3.5. In order to facilitate such calculations a BASIC computer program has been written; a listing of which is given in Appendix B. In addition to the angle of incidence, the following physical data are used to calculate the effective thicknesses.

Table 5.6   Physical Data for the Calculation of Effective Thickness

Parameter	Value
Frequency (cm^{-1})	2900
Refractive Index of Silicon	3.425
Refractive Index of Toluene-D8	1.457

The data listed above have been used to calculate the effective thicknesses at several angles of incidence for TE, TM and unpolarized radiation. Values of θ have been chosen which cover a range suggested by the calibration experiment. The results of these calculations are given in table 5.7.

Table 5.7   Effective Thicknesses for the ATR Experiment

θ (°)	d_e TE (μm)	d_e TM (μm)	d_e Unpolarized (μm)
43	0.23	0.46	0.35
43.9	0.22	0.44	0.33
45	0.21	0.42	0.31
47	0.19	0.38	0.28

As the area of a band in an ATR spectrum is directly proportional to the effective thickness, any variation in effective thickness due to changes in θ will give rise to imprecision in the measured data. From the data presented in table 5.7 it is apparent that the relative standard deviation (%RSD) for the effective thickness is 8%. Therefore, in ATR experiments conducted using the Squarecol ATR cell the precision can be no better than 8%RSD.

5.4   Conclusions

The calibration experiment has given an average value for the angle of incidence of 43.9° and for the number of reflections of 9.7. These are very close to the values obtained from geometrical considerations. The scatter in the data suggests that precision of no better than 8%RSD can be achieved with the Squarecol device.
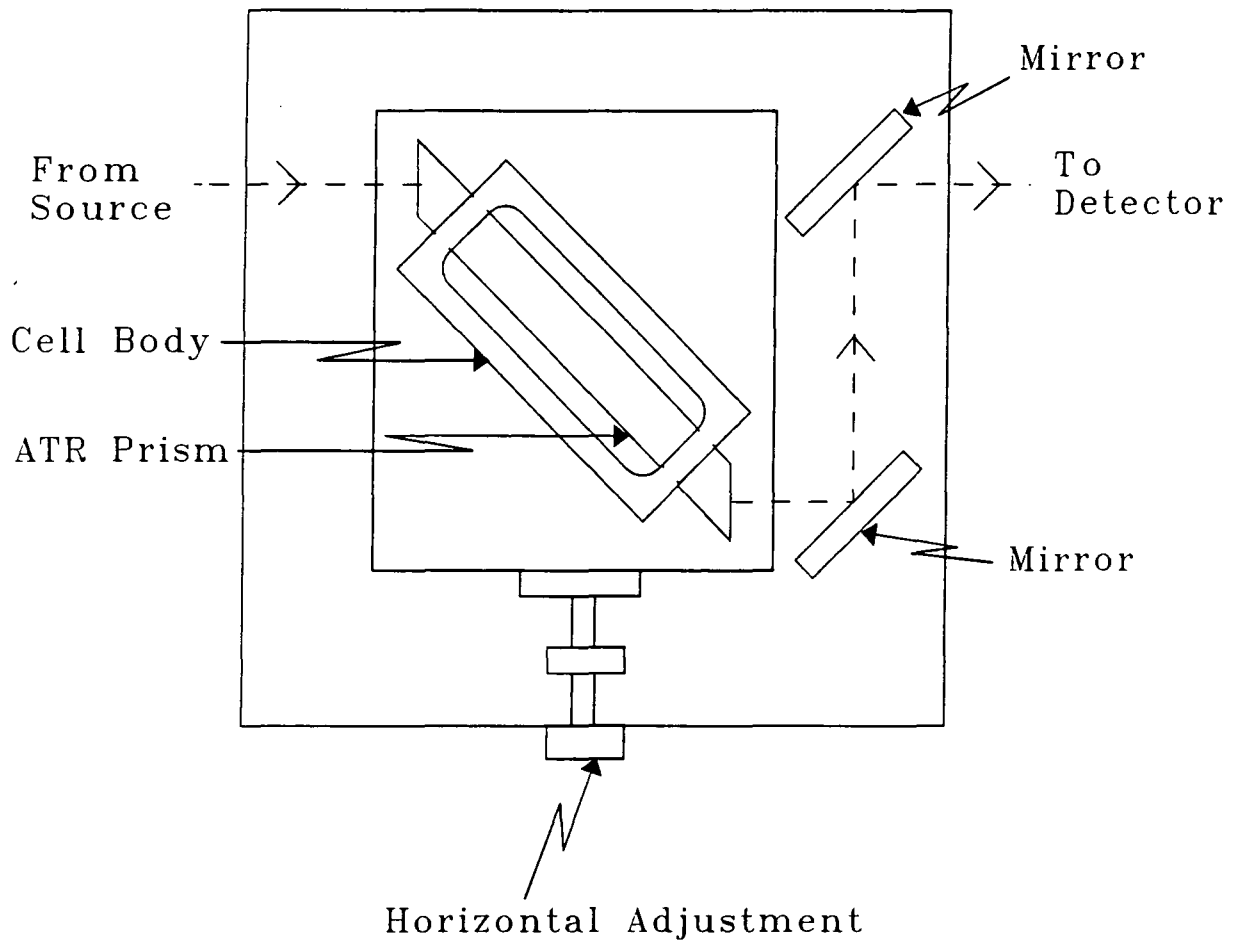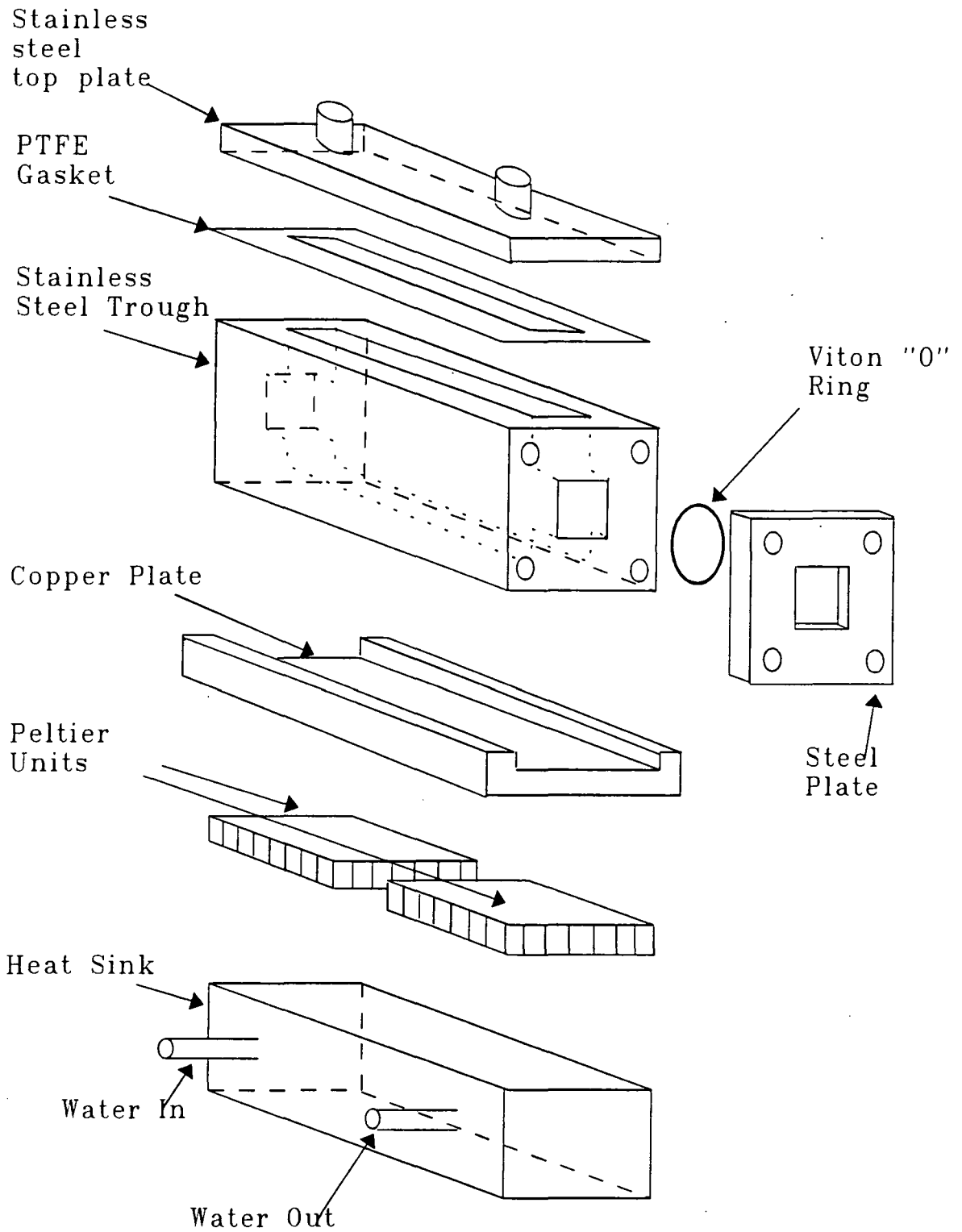
Figure 5.1 Plan View of the Squarecol
Accessory

Figure 5.1 Plan View of the Squarecol Accessory

Figure 5.2   Modified Squarecol ATR
Assembly

Stainless
steel
top plate

PTFE
Gasket

Stainless
Steel Trough

Viton "O"
Ring

Copper Plate

Steel
Plate

Peltier
Units

Heat Sink

Water In

Water Out

Note : Internal Reflection Element
and supporting optics omitted for clarity

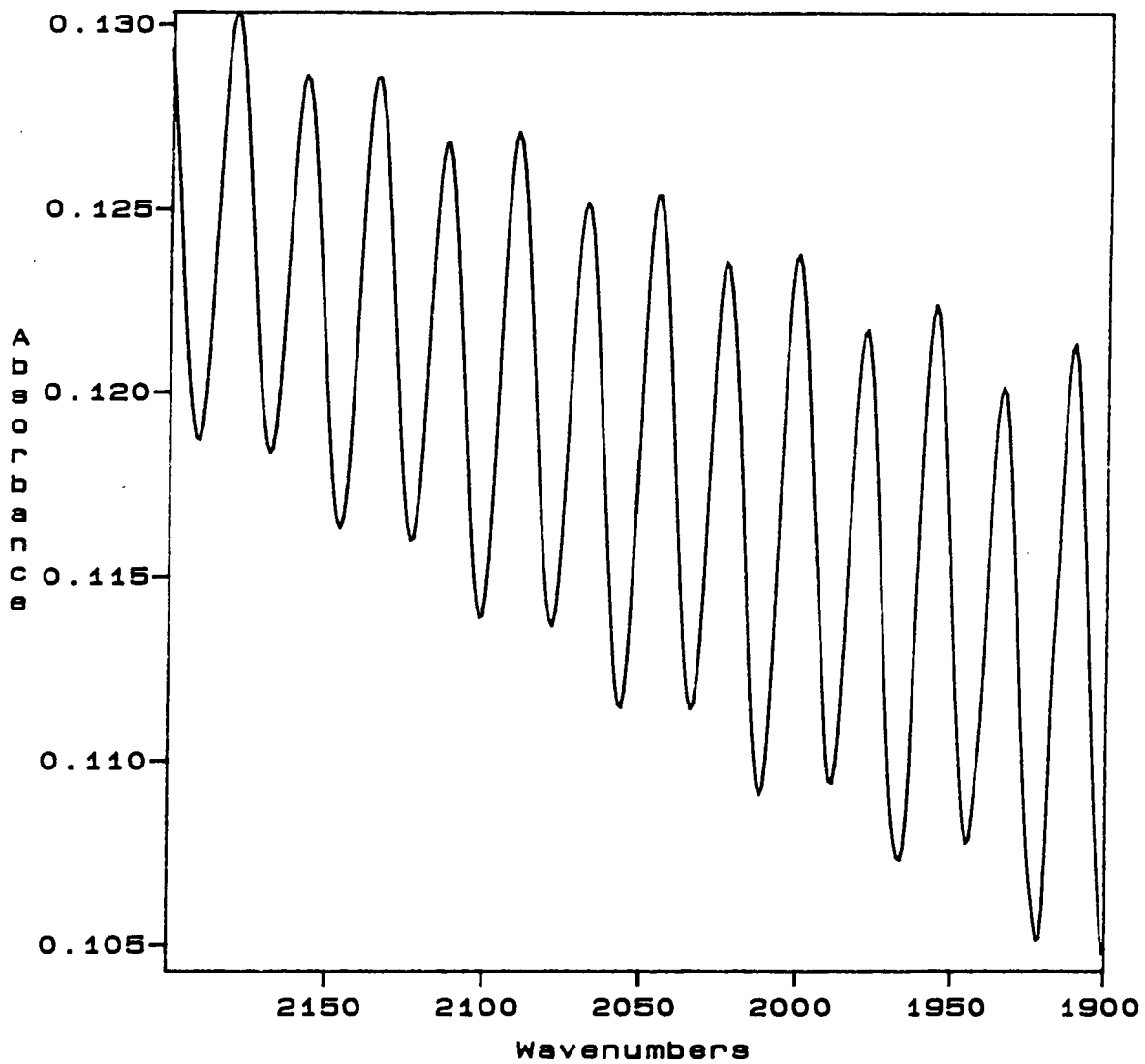Figure 5.3   Interference Fringes Produced by a Transmission Cell

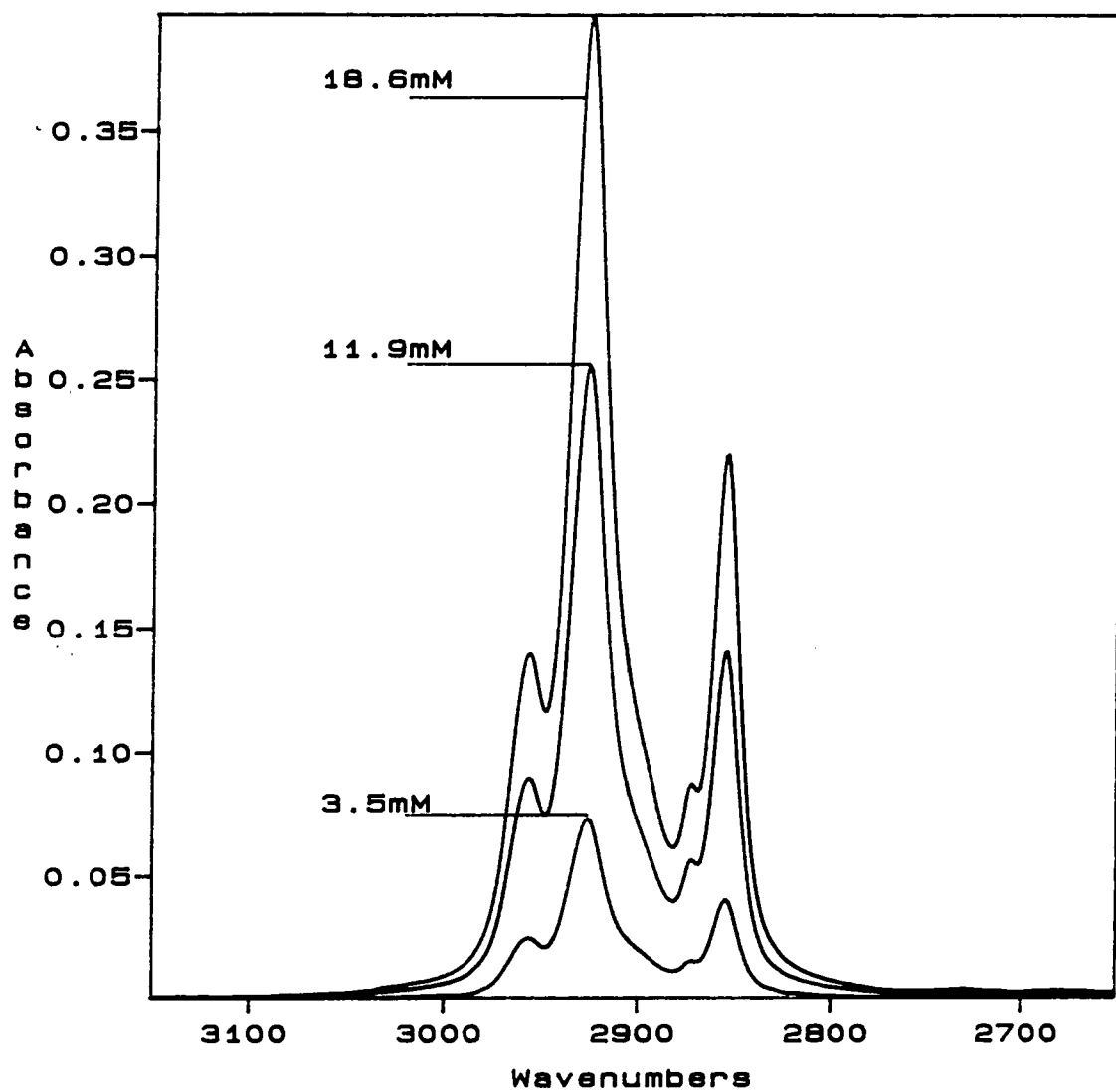Figure 5.4   Transmission Spectra of Three Hexadecane Solutions
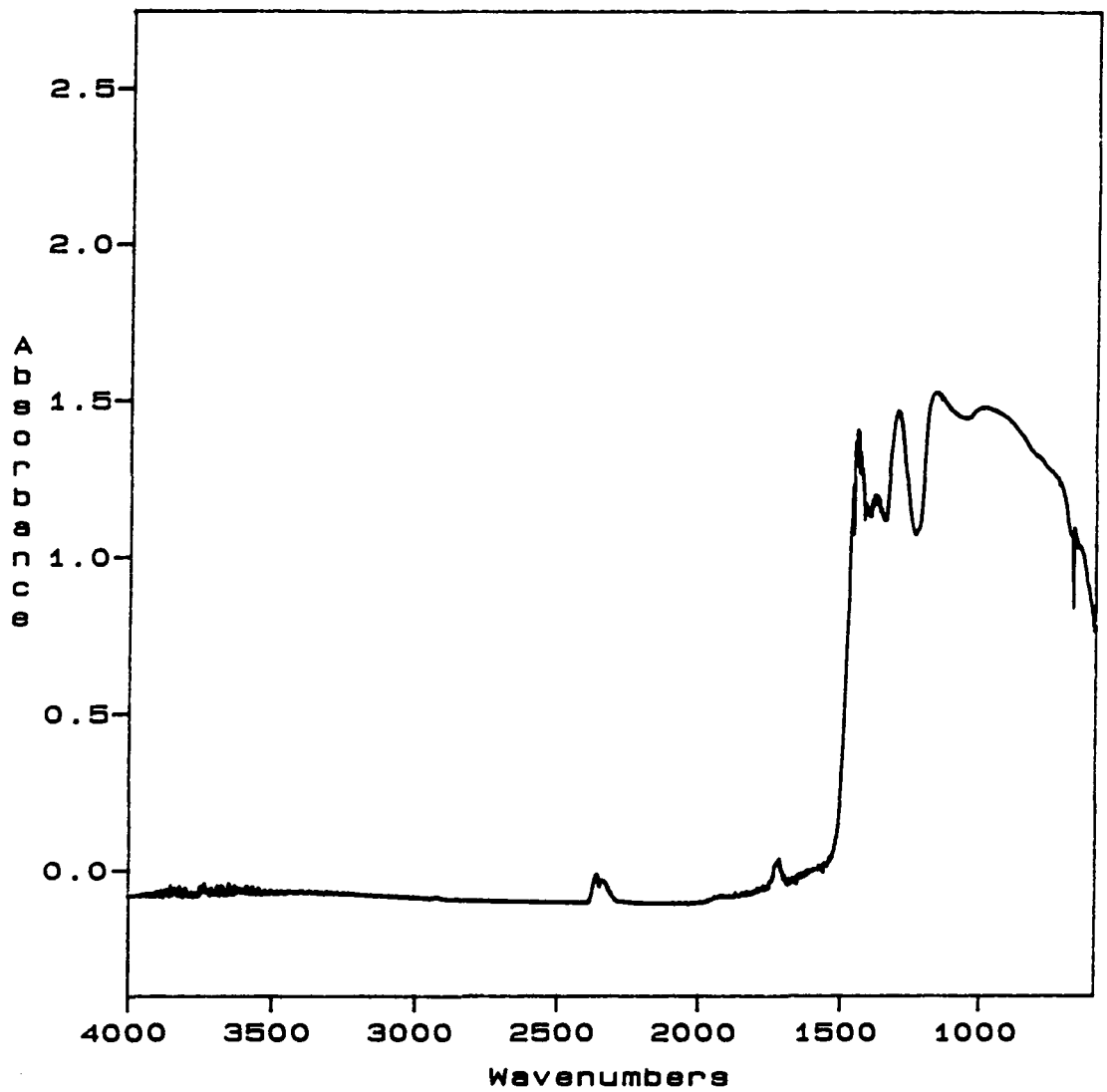
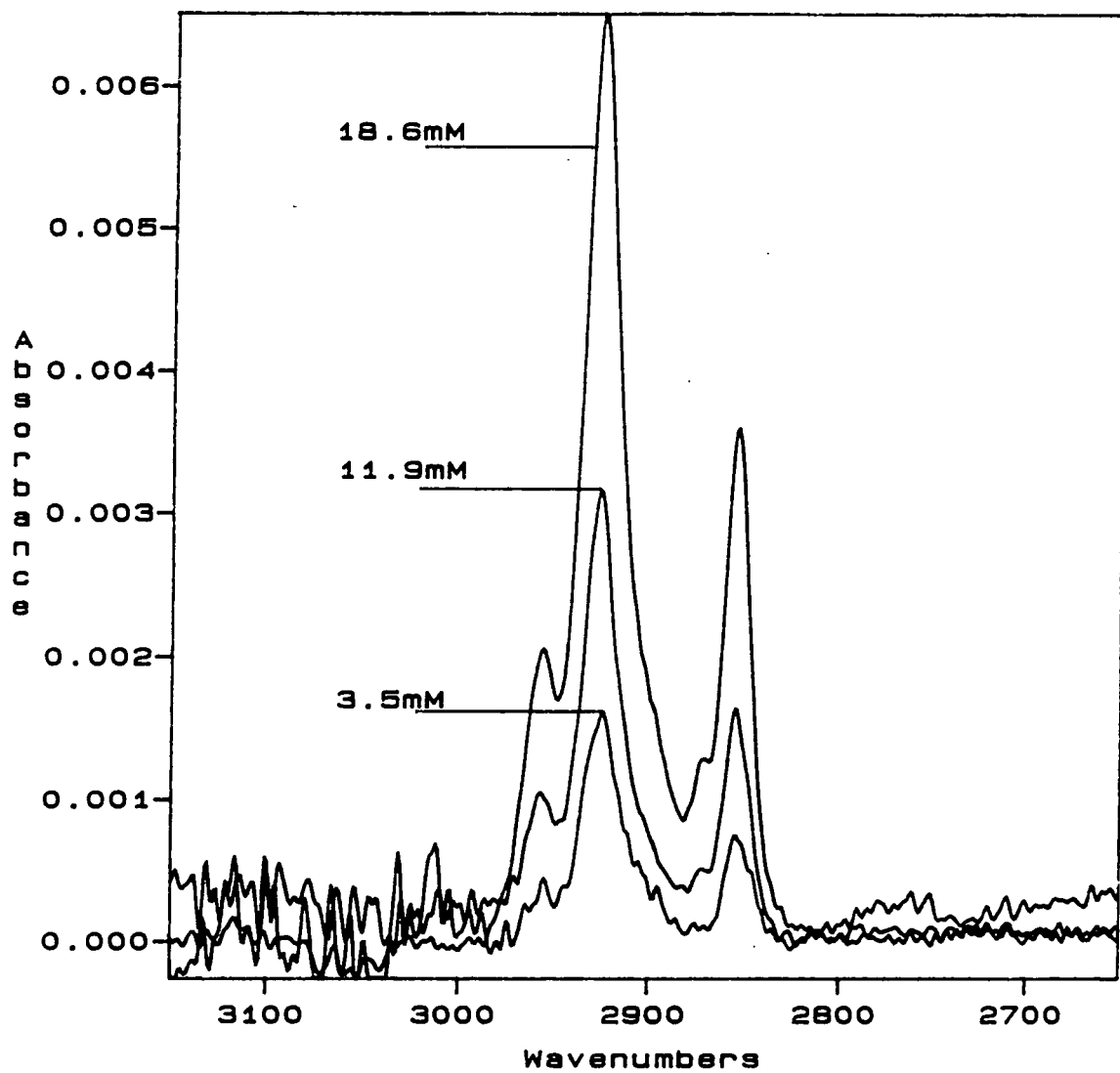Figure 5.5   Spectrum of Silicon ATR Prism

Figure 5.6   ATR Spectra of Three Hexadecane Solutions

Chapter 6   ATR Spectroscopy of Adsorbed Amines

6.1   Introduction

This chapter describes studies of the adsorption of three amines onto silica from solution in deuterated toluene by ATR spectroscopy. Hexadecylamine is the compound of principal interest. Didecylamine and 1,12-diaminododecane have also been studied. Adsorption isotherms for these amines are presented.

6.2   Experimental

6.2.1   Materials

Fully deuterated toluene (99+atom% D, Aldrich) was distilled prior to use. Chloroform (99.9% ACS HPLC grade, Aldrich) and 2-propanol (99.5% HPLC grade, Aldrich) were used as recieved. Hexadecylamine (Pfaltz & Bauer), didecylamine (Aldrich) and 1,12-diaminododecane (Aldrich) were used as received.

6.2.2   Cleaning of the Squarecol Cell

The cell body, lid, 'O'-rings and Teflon gasket were rinsed sequentially with deionized water, methanol and chloroform prior to use. The silicon ATR crystal was rinsed sequentially with dilute hydrochloric acid (approx. 0.1M), deionized water, methanol and chloroform prior to being refluxed for a minimum of four hours in 2-propanol. The dilute acid rinse was found to be effective in removing any residual amine from previous experiments.

The cell components and ATR prism were handled with polythene gloves (RS Components) during assembly. Care was taken to handle the prism by the non-sampling faces only.

All glassware was cleaned using the same series of rinses as used for the ATR prism.

6.2.3   Spectroscopy

Solutions of the amines were prepared over a range of concentrations from 0-15mM by weighing an appropriate amount of amine into a volumetric flask and diluting to the mark with freshly distilled, D8-toluene.

Transmission spectra of the solutions were obtained by ratioing the single beam spectrum of the solution in a 0.022cm pathlength cell against the single beam spectrum of the same cell filled with pure solvent. These spectra allowed the molar extinction coefficient of each amine to be determined.

A single beam spectrum of the empty Squarecol was obtained and ratioed against that of the open beam. The resulting absorbance spectrum was checked in the CH stretching region for cleanliness. If, as often happened, the prism was not completely clean, the cleaning procedure was repeated.

If the prism was clean, the cell was filled by syringe with freshly distilled D8-toluene and the single beam spectrum was recorded. In order to make dichroic measurements polarized spectra are required. Using a gold-wire polarizer (Specac), single beam ATR spectra of the solvent were recorded with the light polarized TE and then TM. This set of three spectra constitued the set of background spectra.

The cell was emptied of solvent and blown dry in a stream of dry nitrogen. A spectrum of the empty dry cell was obtained to check for cleanliness.

The sample solution was introduced to the ATR cell using a syringe. Unpolarized, TE and TM polarized single beam spectra of the solution were recorded. In some cases series of spectra were recorded at time intervals to study the time-dependence of the adsorption.

All spectra were recorded on a Mattson Sirius 100 spectrometer with upgraded circuitry and equipped with an MCT detector. The data was processed using PC-based

FIRST software. The instrumental operating parameters used for recording the transmission and ATR spectra are given in table 6.1.

Table 6.1   Instrumental Parameters

Parameter	Transmission	ATR
Resolution	$4cm^{-1}$	$4cm^{-1}$
Number of Scans	124	512 or 1024
Mirror Velocity	40kHz	40kHz
Iris	20%	95%
Apodization	Triangular	Triangular
Zerofilling	On	On

6.3   Results and Discussion

6.3.1   Hexadecylamine

Hexadecylamine is an aliphatic primary amine which has the formula $CH_3(CH_2)_{15}NH_2$.

6.3.1.1 Transmission Spectra

The full-range transmission spectrum of a 12.5mM solution of hexadecylamine is shown in figure 6.1. The main feature of this spectrum is the group of bands centred around $2900cm^{-1}$ which are associated with methyl and methylene CH stretching vibrations. The NH stretching band which may be expected at around $3400cm^{-1}$ is so weak that it is virtually invisible at this concentration. This weakness of the NH band is common to all the amines studied in the current work. The double peak at $2350cm^{-1}$ is due to carbon dioxide and results from a change in the level of atmospheric CO_2

between the background and the sample spectra. On the low wavenumber side of the CO_2 peak a series of negative bands can be seen at around $2259cm^{-1}$. These bands arise from an incomplete cancellation of the solvent bands in the background and sample spectrum. In a 0.02cm pathlength cell D8-toluene is almost opaque in this region and so incomplete cancellation may be expected. This incomplete cancellation of the solvent bands also complicates the region below $1600cm^{-1}$. As the solvent bands do not cancel exactly it would be impossible to quantify any sample bands in the region of solvent bands. This is one of the reasons why D8-toluene was chosen as the solvent; it has a "window" in the region of interest in the amine studies, i.e. the CH stretching region.

The CH stretching region of the 12.5mM hexadecylamine solution is shown expanded in figure 6.2. In this region, the spectrum of hexadecylamine resembles that of hexadecane (see figure 5.4). The band assignments are the same as those for hexadecane and are given in table 6.2.

Table 6.2   Band Assignments for the Solution of Hexadecylamine

Band Position (cm^{-1})	Assignment
2956	Antisymmetric CH_3 stretching
2926	Antisymmetric CH_2 stretching
2872	Symmetric CH_3 stretching
2854	Symmetric CH_2 stretching

In the spectrum of hexadecylamine, the bands associated with CH_3 stretching modes appear as shoulders on the high frequency side of the CH_2 bands. In the spectrum of hexadecane the methyl stretching bands are somewhat more distinct. This is because whereas hexadecylamine has one methyl group per molecule, hexadecane has two.

In order to obtain the molar extinction coefficient, the transmission spectra of a number of hexadecylamine solutions were obtained. Figure 6.3 shows a stacked plot of these spectra. The CH stretching bands were integrated from 3000-2800cm^{-1}. Using these areas and knowing that the pathlength of the cell is 0.022cm the molar extinction coefficient can be calculated for each concentration *via* equation 5.2. The results of these calculations are given in table 6.3.

Table 6.3   Determination of ε for Hexadecylamine

Concentration (mM)	Area 3000-2800cm^{-1} (cm^{-1})	ε (dm^{3}mol^{-1}cm^{-2})
0.8	0.722	41022
2.0	2.037	46295
4.0	4.106	46659
5.0	5.218	47436
10.0	11.036	50163
12.5	13.253	48192

The mean value of ε is 46628dm^{3}mol^{-1}cm^{-2}. The %RSD is 6.6%. There is no systematic variation in the values of ε. This indicates that Beer's law applies over the concentration range studied.

6.3.1.2 ATR Spectra and Determination of Isotherm

The full-range ATR spectrum of 12.5mM hexadecylamine is shown in figure 6.4. Atmospheric water vapour gives rise to two series of narrow bands in the regions 4000-3500cm^{-1} and 2000-1500cm^{-1}. No attempt was made to purge the spectrometer dry and so bands due to water vapour and CO_2 are apparent in the

spectrum. Below 1500cm^{-1} the spectrum is complicated because the Si ATR prism is opaque in this region. A band due to the incomplete cancellation of D8-toluene can be seen at 2308cm^{-1}. The bands of interest in the determination of the surface excess concentration are the CH stretching bands of hexadecylamine centred around 2900cm^{-1}.

The CH stretching region is shown expanded for a series of hexadecylamine solutions of increasing concentration in figures 6.5-6.11 inclusive. These spectra are presented sequentially rather than as a stacked plot for clarity. All these spectra were obtained at 25°C, one hour after injection into the Squarecol. This time interval allowed the system to come to equilibrium.

Figure 6.12 shows ATR spectra of 12.5mM hexadecane obtained immediately after injection and one and two hours following the injection. There is no trend towards larger or small peaks over this time period. This indicates that adsorption occurs rapidly.

The areas under the CH stretching bands were obtained using Mattson's FIRST software from 3000-2800cm^{-1}. The results of these integrations are given in table 6.4.

In chapter 5, the area under the CH stretching bands in the ATR spectrum of 11.9mM hexadecane was 0.144cm^{-1}. From table 6.4 it can be noted that the area under the peaks in the ATR spectrum of 12.5mM hexadecylamine is 0.340cm^{-1}. In other words, the absorbance from the amine is more than double that of a solution of hexadecane of comparable concentration. From transmission measurements, it is known that the molar extinction coeffiecients are similar for the two compounds. Therefore, the observed increase in absorbance must be due to adsorption of the amine onto the silica surface. This leads to an increased concentration at the prism/solution interface where the evanescent field has maximum intensity thereby leading to enhanced absorbance in the ATR spectrum, as described in chapter 3.

Table 6.4   Band Areas from the ATR Spectra of Hexadecylamine

Concentration (mM)	Spectrum Shown in Figure	Area 3000-2800cm^{-1} (cm^{-1})
0.8	6.5	0.074
2.0	6.6	0.087
3.5	6.7	0.172
4.0	6.8	0.215
10.0	6.9	0.268
12.5	6.10	0.340
15.0	6.11	0.346

In section 3.7 the way in which the surface excess concentration, Γ_i, can be calculated from the peak area was described. Once Γ_i has been calculated two other related numbers can be obtained. The first is the area available per adsorbed molecule, *Apm*. Since Γ_i has units mol.cm^{-2}, the area available per molecule, in cm^2 is given by $1/(N_A x \Gamma_i)$, where N_A is Avogadro's constant. Areas per molecule are usually quoted in Å^2. Therefore:

$$Apm = \frac{1 \times 10^{16}}{N_A \times \Gamma_i} \text{ Å}^2 \qquad (6.1)$$

A second piece of information which can be derived from Γ_i is the percentage of the absorption band which comes from the bulk solution, as opposed to the adsorbed layer. The equation used to perform this calculation was derived by Sperline *et al* [46] and is:

$$\%bulk = 100\frac{cd_p}{cd_p + 2000\Gamma_i} \quad (6.2)$$

In order to facilitate the calculations a BASIC program was written. A listing of this program may be found in Appendix C. This program was used in conjunction with the physical data obtained in chapter five and listed in table 6.5. The results of these calculations are tabulated in table 6.6.

Table 6.5 Physical Data Other than Band Areas Used for Surface Excess Calculations

Parameter	Value
Refractive Index of Prism	3.425
Refractive Index of Sample	1.457
Angle of Incidence (°)	43.9
Number of Reflections	9.7
Frequency (cm^{-1})	2900

Table 6.6   Results of Adsorption Calculations for Hexadecylamine

Concentration (mM)	$\Gamma_i \times 10^{10}$ (mol.cm^{-2})	Apm (Å^2)	%bulk
0.8	0.58 ± 0.07	286 ± 30	17 ± 2
2.0	0.52 ± 0.07	316 ± 30	36 ± 2
3.5	1.10 ± 0.16	150 ± 25	32 ± 3
4.0	1.44 ± 0.20	116 ± 17	29 ± 3
10.0	1.04 ± 0.24	160 ± 40	58 ± 7
12.5	1.35 ± 0.30	123 ± 30	58 ± 6
15.0	1.04 ± 0.31	160 ± 50	68 ± 4

An adsorption isotherm may be constructed by plotting Γ_i against the concentration. Such an adsorption isotherm is shown in figure 6.13. The isotherm rises steeply to a plateau of 1.2×10^{-10} mol.cm^{-2} when the concentration reaches 3mM. No further increase in adsorption is observed. This is Langmuirian behaviour. As the concentration of the bulk solution increases in the plateau region the percentage of the absorption spectrum attributable to bulk species increases as no further adsorption takes place. Hence the %bulk figure increases.

Clearly there is considerable scatter of data around the mean platea value. Considering the points on the plateau (i.e. where $c > 3$mM) then:

$$\overline{\Gamma}_i = 1.19 \times 10^{-10} \text{ mol.cm}^{-2}$$

and

$$\sigma_{n-1} = 0.188 \text{ for } \Gamma_i$$

which gives a %RSD of 15.7%. This figure is considerably worse than expected from the calibration experiment which suggested that an RSD of 8% could be achieved with the Squarecol cell. However, the calibration experiment did not, by definition, involve adsorbed species. Table 6.5 shows that the percentage of the absorption bands arising from the adsorbed layer is between 70 and 30 percent, depending on the bulk concentration. The calculation of Γ_i attributes any peak intensity in excess of that expected for a non-adsorbing molecule to the adsorbed layer. Hence the %RSD of 8% for peak areas inherent in the ATR experiment result in errors in Γ_i which increase as the percentage of the signal due to adsorbed species decreases. Therefore if the bulk concentration is increased indefinitely and no further adsorption occurs, there will come a point at which the contribution of adsorbed species to the spectrum will be less than the error inherent in ATR Squarecol measurements. Such a situation represents the upper concentration limit of the experiment. The lower concentration limit is governed by the sensitivity of the instrument. In the current experiment, the bands for the 0.8 and 2.0mM solutions have areas less than $0.1cm^{-1}$. These spectra are just above the sensitivity limit of our current equipment. The range of concentrations of hexadecylamine studied therefore represent the range of which the experiment is capable of measuring.

The mean value for Γ_i of $1.2x10^{-10}mol.cm^{-2}$ is equivalent to an area per molecule of $138Å^2$ (equation 6.1). A close-packed array of all-trans aliphatic chains has an area per molecule of around $25Å^2$. This indicates that the adsorbed layer of amine is by no means close-packed. The amine head-group is small and its physical size cannot explain the diffuse nature of the adsorbed layer. The surface of the ATR prism is not well characterized; the silanol group density is not known. However, it is known that a surface layer of silica of around $50Å$ thickness exists on silicon which has been exposed to the atmosphere [99] and bands associated with Si-O vibrations are evident in the spectrum of the prism below $1300cm^{-1}$ (see figure 5.5). Although the density of silanol groups on the ATR prism is not known, it is generally agreed that [24] on non-

porous, amorphous silica the area per silanol group is 20-25Å^2. Therefore, it is somewhat difficult to believe that on the ATR prism the silanol density is some five times less than this figure. However, the value of Γ_i is low and suggests that the adsorbed layer is diffuse. This may be due to either low silanol density or some of the silanol groups being blocked by some passivating species. The indentity of this species, should it exist, is uncertain as the spectrum of the clean silicon ATR prism shows only bands attributable to silica (figure 5.5).

The figure of 138Å^2 per molecule is an average value. The adsorbed molecules may be distributed uniformly over the surface or they may occupy tightly-bunched islands separated by 'bare' silica. The ATR expeiment does not have the spatial resolution capability to distiguish between the two situations. However, it is possible to distinguish between a well ordered film and a randomly orientated film by making orientational measurements with polarised light and by examining the position and shapes of the CH stretching bands. A well ordered film would suggest island formation whereas a random film would suggest a uniform distribution of adsorbed molecules.

6.3.1.3 Orientational Measurements on the Adsorbed Layer

The way in which molecular orientational information can be derived from polarized ATR data was described in chapter 3. In fact, the description of orientational measurements applied strictly only to uniform concentration profiles. In the case where an adsorbed film is present together with bulk surfactant it is clear that the situation becomes more complicated. To recap from chapter 3 and retaining the original equation numbers, the dichroic ratio, D, is defined as

$$D = \frac{A_{TE}}{A_{TM}} \qquad (3.46)$$

where A_{TE} and A_{TM} are the integrated areas of a given absorbance band in ATR spectra obtained with TE and TM polarization respectively. The strength of a given absorbance band is proportional to the intensity of the electromagnetic radiation promoting that absorption, i.e. $A \propto E^2$. Therefore, if the dipoles in the sample are completely randomly oriented then:

$$D = \frac{A_{TE}}{A_{TM}} = \frac{E_{y0}^2}{E_{x0}^2 + E_{z0}^2} \qquad (3.47)$$

However, if the dipoles are oriented solely parallel to the interface, the z component can no longer contribute to the TM spectrum and the dichroic ratio becomes:

$$D = \frac{A_{TE}}{A_{TM}} = \frac{E_{y0}^2}{E_{x0}^2} \qquad (3.48)$$

Equation 3.48 only applies to a sample of uniform concentration. When an adsorbed film is studied in the presence of bulk solution then, even if it is perfectly ordered, there will be a random contribution from the bulk surfactant. Just how much a contribution the bulk will make can be estimated from the %bulk figure. Considering a perfectly

ordered film in the presence of randomly oriented bulk solution, the equation for the dichroic ratio becomes:

$$D = \left(1 - \frac{\%bulk}{100}\right)\left(\frac{E_{y0}^2}{E_{x0}^2}\right) + \left(\frac{\%bulk}{100}\right)\left(\frac{E_{y0}^2}{E_{x0}^2 + E_{z0}^2}\right) \quad (6.3)$$

Clearly the presence of the bulk solution serves to reduce the sensitivity of the measurement to order within the adsorbed layer. In deriving equation 6.3 the implicit assumption is made that the %bulk contribution is the same in the TE and TM spectra. The value of E_0 is different in each direction x, y, and z (see figure 3.3 and equations 3.5-3.7) but the decay constant, γ, (see equations 3.9 and 3.10) is common to all directions. Consequently, the evanescent field <u>decays at the same rate in all spatial orientations</u>. Thus the %bulk contribution is the same in both the TE and TM polarizations.

In order to calculate theoretical dichroic ratios it is first necessary to calculate the various values of E_0. This can be done from first principles, using the program developed at Durham by Dr. Y. P. Song [88] or by using the approximate equations derived by Harrick [84]. We recall that Harrick derived two sets of equation using two approximations. The first was the *semi-infinite bulk* approximation in which the sample thickness d is much greater than the penetration depth, d_p. The second approximation was the *thin film* approximation in which $d \ll d_p$. In the current experiment the value of d_p is $0.29\mu m$, as calculated using the program listed in Appendix B with the physical data listed in table 6.5. Now although the film of interest in this study is, by Harrick's definition thin, the whole sample is thick (approx 2mm). The refractive indices of the film and solvent are, to a good approximation, the same and therefore the presence of the film will not significantly perturb the evanescent field. Therefore, the thick film approximation must be used when calculating E_0. The equations of use are therefore 3.5-3.7. These equations are used in the program listed

in appendix B. The data listed in table 6.5 has been used in conjunction with this program to calculate the values of $E_0{}^2$ listed in table 6.7.

Field Direction	Intensity
$E_{y0}{}^2$	2.54
$E_{x0}{}^2$	1.97
$E_{z0}{}^2$	3.15

Using the values in table 6.7 it is possible to calculate the dichroic ratios for the totally random case and for a range of ordered film/random bulk situations from equation 6.3. The results of these calculation are listed in table 6.8 The case in which the %*bulk*=0 is equivalent to a perfectly ordered film and has the dichroic ratio given by equation 3.48. The case were the bulk contribution is 100% corresponds to the completely random case and the dichroic ratio is given by equation 3.47. Between these two extremes, the dichroic ratio varies linearly with %*bulk*.

The TE and TM polarized spectra of the hexadecylamine solutions are shown in figures 6.14 to 6.20. At each concentration the TM polarized spectrum is the more intense of the two spectra. Poor signal-to-noise ratios can be seen in the spectra of the 0.8 and 2.0mM solutions. As mentioned previously, these samples represent the limit of the sensitivity of our equipment. The areas under the CH stretching peaks were integrated and the dichroic ratios calculated according to equation 3.46. The results of these measurements are given in table 6.9. The experimentally obtained dichroic ratios are listed in the column labelled D_{exptl}. The contribution made to the spectra by bulk species is known from the unpolarized data in the previous sub-section. This data can be used in conjunction with equation 6.3 to calculate the theoretical dichoric ratio that

Table 6.8   Dichroic Ratios Expected from a Number of Oriented Film/Random

Bulk Situations

%bulk	D
0	1.29
10	1.21
20	1.13
30	1.05
40	0.97
50	0.90
60	0.82
70	0.74
80	0.66
90	0.58
100	0.50

would be expected for an ordered layer. These theoretical data are listed in the column labelled D_{order}.

Table 6.9   Dichroic Ratio Measurements of Hexadecylamine Solutions

Conc. (mM)	Spectrum in Figure	A_{TE} (cm^{-1})	A_{TM} (cm^{-1})	D_{order}	D_{exptl}
0.8	6.14	0.053	0.072	1.16	0.74
2.0	6.15	0.068	0.083	1.05	0.82
3.5	6.16	0.120	0.200	1.03	0.60
4.0	6.17	0.157	0.242	1.06	0.65
10.0	6.18	0.243	0.367	0.83	0.66
12.5	6.19	0.292	0.344	0.83	0.85
15.0	6.20	0.276	0.442	0.75	0.62

For comparison purposes, the TE and TM polarized ATR spectra of 18.6mM hexadecane are shown in figure 6.21. This solution represents the completely random case as no adsorption occurs. The band areas for TE and TM polarization are 0.214 and 0.410cm^{-1} respectively. This yields a dichroic ratio of 0.52, which is very close to the theoretical value of 0.50, calculated for such a system. The experimentally determined values of D for the hexadecylamine systems suggest some partial order within the adsorbed films but not perfect alignment of the chains perpendicular to the prism surface. The value of D for the 12.5mM solution seems anomalously high.

In calculating theoretical dichroic ratios the assumption is made that the intensity of the incoming radiation (i.e. the propagating wave rather than the evanescent field) is the same for TE polarization as for TM polarization. However, as Sperline has pointed

out [100], this is not necessarily the case. Infrared spectrometers, be they dispersive or FT, cause polarization distortion. In other words, the radiation in the TE direction may be more intense than that in the TM direction, *or vice versa*. Futhermore, the degree of polarization depends upon the frequency. Therefore the measured dichroic ratio will depend upon the frequency at which it is measured. In order to assess the severity of this problem two single beam spectra were recorded with only a polarizer in the instrument. The first spectrum was recorded with the polarizer in the 0°(TE) position and the second was recorded in the 90°(TM) position. These spectra were then ratioed against the single beam spectrum of the open (unpolarized) beam. The resulting absorbance spectra are shown in figure 6.22. The upper curve is the TE curve and the lower curve is the TM curve. This indicates that there is generally more energy reaching the detector in the TM polarization than in TE polarization. The difference in the amount of energy reaching the detector is clearly shown by the separation of the curves and is dependent upon frequency. At the frequency of interest, $2900cm^{-1}$, the curves have similar absorbances, 0.30 for TE and 0.28 for TM. An absorbance value of 0.3 corresponds to a transmittance of 50%, which one would hope to achieve with a polarizer, i.e. half of the intensity is lost. The similarity of the absorbance values indicates that, at this frequency, the assumption that the TE wave and TM wave have the same intensity is approximately correct. Therefore, no corrections to the dichroic ratio calculations have been made. However, if dichroic ratios were to be measured at, say, $1800cm^{-1}$, where the curves have maximum separation, then the assumption would clearly be invalid and corrections would have to be made to the dichroic ratio calculations.

Dichroic ratio measurements give information about the orientation of dipoles with respect to the surface normal. However, the partial ordering observed in the current experiment can be interpreted as being due to either all-trans chains inclined at an angle to the surface normal or to chains with some gauche content in which slightly more of the CH stretches have their oscillating dipole moment perpendicular to the surface

normal than oscillate parallel to it. However all-trans chains can be distinguished from chains with high gauche content by the frequency of the methylene stretching vibrations [101, 102]. Aliphatic chains with a high gauche content have an antisymmetric CH_2 stretching band at 2926cm^{-1} whereas the same vibration in an all-trans chain occurs at approximately 2920cm^{-1}. The frequency of the symmetric CH_2 stretching vibration is somewhat less sensitive to conformation. Figure 6.23 shows the ATR spectra of 12mM hexadecane, 12.5mM hexadecylamine and the difference between them. The difference spectrum is effectively due to the adsorbed layer. The positions of the antisymmetric and symmetric CH_2 stretching bands are given in table 6.10.

Table 6.10   Methylene Stretching Band Positions in 12mM Spectra

Spectrum	Antisymmetric CH_2 stretching band position (cm^{-1})	Symmetric CH_2 stretching band position (cm^{-1})
Hexadecane	2926	2854
Hexcadecylamine	2923	2853
Difference (adsorbed layer)	2920	2851

From the figures in table 6.10 it can be seen that the adsorbed molecules have chain in the all-*trans* conformation. The dichroic ratio for the 12.5mM hexadecylamine sample suggested a high degree of orientation. In this case, it appears that a highly ordered film was formed. The question now arises, what is the situation for a film which the dichroic ratio indicates is less well ordered? Figure 6.24 shows the spectra of 3.5mM hexadecane (obtained by scaling the spectrum of 12mM hexadecane), 3.5mM hexadecylamine and the difference. The dichroic ratio of the amine solution suggests

that there is a low degree of order in this film (table 6.9). The methylene stretching

band positions for these spectra are given in table 6.11.

Table 6.11   Methylene Stretching Band Positions in the 3.5mM Solutions

Spectrum	Antisymmetric CH_2 stretch position (cm^{-1})	Symmetric CH_2 stretch position (cm^{-1})
Hexadecane	2926	2854
Hexadecylamine	2925	2854
Difference (adsorbed layer)	2924	2854

Clearly, the shift of the bands to lower frequency is less marked here than in the

12.5mM case. Therefore it would appear that the degree of order within the adsorbed

layer is variable; from poorly oriented chains with some gauche conformers to well

oriented all-trans chains oriented parallel to the surface normal. There appears to be

no trend of the order with bulk concentration or surface excess concentration. Quite

what controls the degree of "order" is unknown at the present time.

6.3.2   1,12-diaminododecane

1,12-diaminododecane is a primary diamine with the formula $H_2N(CH_2)_{12}NH_2$. This

is of interest because the C_{12} aliphatic chain has a primary amine headgroup at either

end.

6.3.2.1 Transmission Spectra

The transmission spectrum of a 20mM solution of 1,12-diaminodecane is shown in

figure 6.25. The principal feature of this spectrum are the two bands due to methylene

stretching vibrations either side of 2900cm^{-1}. Two peaks which may be tentatively

assigned to NH_2 stretching can be seen around $3360cm^{-1}$. The region of interest for quantitative measurements is, as before, the CH stretching region. This region is shown expanded in figure 6.26. Two bands can be readily identified in this region. These are the antisymmetic and the symmetric CH_2 stretching vibrations at 2926 and $2854cm^{-1}$ respectively. The spectrum is less complicated in this region than that of hexadecylamine or hexadecane due to the absence of methyl groups on the diamine molecule.

The area under the peaks was integrated from $3000-2800cm^{-1}$ and found to be $18.76cm^{-1}$. Knowing that the pathlength of the cell is 0.022cm, the molar extinction coefficient,ε, can be calculated to be $\underline{42,643}dm^3mol^{-1}cm^{-2}$.

6.3.2.2 ATR Spectra and Determination of Surface Excess Concentration

Expanded ATR spectra of a number of 1,12-diaminododecane solutions of increasing concentration are shown in figures 6.27 to 6.31 inclusive. These spectra were obtained without a polariser. The area under the peaks were integrated from $3000-2800cm^{-1}$. The results of these integrations are presented in table 6.12.

Table 6.12   CH Stretching Band Areas in the Unpolarized ATR Spectra of 1,12-diaminododecane.

Concentration (mM)	Spectrum Shown in Figure	Area $3000-2800cm^{-1}$ (cm^{-1})
1.9	6.27	0.136
3.7	6.28	0.159
5.8	6.29	0.213
7.4	6.30	0.236
11.7	6.31	0.302

Using these areas, the value of ε calculated in section 6.3.2.1 and the physical data presented in table 6.5, it is possible to calculate the surface excess concentrations *via* the computer program presented in appendix C. The results of these calculations are given in table 6.13.

Table 6.13   Results of Adsorption Calculations for 1,12-diaminododecane

Concentration (mM)	$\Gamma_i \times 10^{10}$ (mol.cm^{-2})	*Apm* (Å^2)	*%bulk*
1.9	1.18 ± 0.14	141 ± 19	19 ± 2
3.7	1.16 ± 0.17	143 ± 24	32 ± 3
5.8	1.43 ± 0.23	116 ± 16	37 ± 4
7.4	1.44 ± 0.25	115 ± 17	43 ± 4
11.7	1.52 ± 0.32	109 ± 19	52 ± 5

The adsorption isotherm is presented in figure 6.32. The adsorption isotherm curve ceases to rise rapidly when Γ_i is around 1.4×10^{-10} mol.cm^{-2}. This is slightly greater than but comparable to the value obtained for hexadecylamine, suggesting that both molecules adsorb to similar extent onto the silica surface. The value of Γ_i corresponds to an area per molecule of 119Å^2. As was the case with the hexadecylamine, this figure suggests that the adsorbed layer is not compact.

The question of the orientation of the adsorbed molecules now arises. This is discussed in the next sub-section.

6.3.2.3 Orientational Measurements on 1,12-diaminododecane

The TE and TM polarized ATR spectra of 1.9, 3.7, 5.8, 7.4 and 11.7mM solutions of 1,12-diaminododecane are shown in figures 6.33 to 6.37 inclusive. The spectra were

integrated from 3000-2800cm^{-1} and the dichroic ratios calculated. The results of these calculations are given in table 6.14.

Table 6.14   Dichroic Ratio Measurements of 1,12-diaminododecane Solutions

Conc. (mM)	Spectrum in Figure	A_{TE} (cm^{-1})	A_{TM} (cm^{-1})	D_{order}	D_{exptl}
1.9	6.33	0.092	0.155	1.14	0.59
3.7	6.34	0.105	0.189	1.04	0.55
5.8	6.35	0.133	0.245	1.00	0.54
7.4	6.36	0.129	0.310	0.95	0.42
11.7	6.37	0.223	0.365	0.88	0.61

The dichroic ratio calculated for the completely random and oriented cases are, as before, 0.50 and 1.29 respectively. The theoretical dichroic ratios for an ordered film in the presence of random bulk solution are listed in the D_{order} column and were calculated using the %*bulk* figures from table 6.13. The experimentally determined dichroic ratios show that there is little or no ordering in the adsorbed layer. The 1,12-diaminododecane appears to show less tendency to form ordered films than hexadecylamine. This is probably due to the ability of the diamine to anchor both ends of the molecule to the silica surface thereby preventing the aliphatic chain attaining an all-trans conformation and orienting parallel to the surface normal.

Evidence for the absence of all-trans-chains also comes from a consideration of peak frequencies in the CH stretching region of the spectrum of the adsorbed layer. Figure 6.38 shows the ATR spectra of 11.7mM 1,12-diaminododecane, 11.9mM hexadecane and the difference between them. As described in section 6.3.2.1, the transmission spectrum of 1,12-diaminododecane is somewhat different to that of hexadecane in the

116

CH stretching region as the former compound has no methyl groups. However, the antisymmetric methylene stretching band occurs at the same position in the transmission spectrum of both compounds, at $2926cm^{-1}$, as does the symmetric methylene stretching band, at $2854cm^{-1}$. In the ATR spectra, these bands are no longer coincident. Their frequencies are listed in table 6.15. Clearly the methylene stretching bands do not exhibit the shift to lower frequencies that would be expected were the chains in the adsorbed layer in an all-trans conformation. Indeed, a shift to higher frequency is observed. This indicates that the chains in the adsorbed layer have a higher proportion of gauche conformers than the chains in the bulk solution. Gauche conformations are required if the molecule is to loop such that both amine groups are hydrogen-bonded to the surface. Hence the band positions may be evidence for such a looped conformation.

Table 6.15   Methylene Stretching Band Positions in 12mM Spectra

Spectrum	Antisymmetric CH$_2$ stretch position (cm^{-1})	Symmetric CH$_2$ stretch position (cm^{-1})
Hexadecane	2926	2854
1,12-diaminododecane	2927	2854
Difference (adsorbed layer)	2930	2855

In summary, 1,12-diaminododecane appears to form somewhat diffuse adsorbed layers on the silica surface in which some of the molecules are looped over in such a way that both amine groups are hydrogen-bonded to the surface. In addition to these looped species there may also be a number molecules anchored to the surface by just one amine group. The second, 'free', amine group may then hydrogen bond to a second amine molecule.

6.3.3   Didecylamine

Didecylamine is a secondary amine with the formula $(CH_3(CH_2)_8CH_2)_2NH$.

6.3.3.1 Transmission Spectra

The transmission spectrum of a 15mM solution of didecylamine in a 0.022cm cell is shown in figure 6.39. The NH stretching band is so weak that it is not observed. The principal feature of this spectrum is the series of bands associated with CH stretching. This region is shown expanded in figure 6.40. In addition to the bands associated with the antisymmetric and symmetric methyl stretching bands (2956 and 2872cm^{-1} respectively) and the antisymmetric and symmetric methylene stretching bands (2926 and 2854cm^{-1} respectively) there is a fifth band at 2812cm^{-1}. The assignment of this

band is uncertain. It may be due to a stretching vibration of the methylene groups adjacent to the NH function.

The area under the CH stretching bands was measured and found to be $22.993cm^{-1}$, which corresponds to a value of ε of $\underline{69675}dm^3mol^{-1}cm^{-2}$.

6.3.3.2 ATR Spectra and Adsorption Calculations

The unpolarized ATR spectra of 4.5, 8.4, 11.7 and 15.0mM solutions of didecylamine are shown in figures 6.41 to 6.44 inclusive. The spectrum of the 4.5mM solution is of rather poor quality. The areas under the CH stretching bands were found by integration. The results of these measurements are given in table 6.16.

Table 6.16   CH Stretching Band Areas in the Unpolarized ATR Spectra of Didecylamine.

Concentration (mM)	Spectrum Shown in Figure	Area 3000-2800cm^{-1} (cm^{-1})
4.5	6.41	0.144
8.4	6.42	0.235
11.7	6.43	0.282
15.0	6.44	0.377

Using the value of ε obtained in the previous subsection and the physical data presented in table 6.5 it is possible to calculate the surface excess concentration values at each concentration via the program listed in Appendix C. The results of these calculations are given in table 6.17.

Table 6.17   Results of Adsorption Calculations for Didecylamine

Concentration (mM)	$\Gamma_i \times 10^{10}$ (mol.cm^{-2})	Apm (Å^2)	%bulk
4.5	0.28 ± 0.11	583 ± 290	69 ± 8
8.4	0.31 ± 0.15	535 ± 527	80 ± 10
11.7	0.14 ± 0.14	1228 ± 700	92 ± 8
15.0	0.27 ± 0.25	604 ± 290	88 ± 8

The adsorption isotherm is presented in figure 6.45. Clearly the 'plateau' value of Γ_i for didecylamine is only a fraction of that for hexadecylamine or 1,12-diaminododecane, indicating that the secondary amine has a lower affinity for the silica surface than either of the primary amines. The values of the area available per molecule show that only a small fraction of the silica surface is covered by adsorbed didecylamine. Although didecylamine has two aliphatic chains per molecule and may therefore be expected to occupy more volume than either of the primary amines, an area per molecule of 600Å² is significantly more than double the area occupied by a hexadecylamine molecule. Therefore the lower values of Γ_i for didecylamine cannot be explained in terms of excluded volume alone. The NH headgroup would appear to have a lower affinity for the silica surface than the NH$_2$ group.

6.3.3.3 Orientational Measurements

The TE and TM polarized ATR spectra of 4.5, 8.4, 11.7 and 15.0mM didecylamine solutions are shown in figures 6.46 to 6.49 inclusive. The peak areas have been integrated and the dichroic ratios calculated. The results of these measurements and calculations are given in table 6.18, together with theoretical dichroic ratios for a perfectly oredered film in the presence of bulk solution.

Table 6.18   Dichroic Ratio Measurements of Didecylamine Solutions

Conc. (mM)	Spectra in Figure	A_{TE} (cm^{-1})	A_{TM} (cm^{-1})	D_{order}	D_{exptl}
4.5	6.46	0.107	0.218	0.74	0.49
8.4	6.47	0.183	0.354	0.66	0.52
11.7	6.48	0.190	0.354	0.56	0.53
15.0	6.49	0.278	0.542	0.59	0.51

Due to the low adsorption of didecylamine the percentage of the signal due to bulk species is high and therefore the range of dichroic ratios theoretically possible is small. This is particularly true for the solutions of 11,7 and 15.0mM concentration, where the theoretical dichroic ratio for a completely random film is 0.50 and that for an ordered film is around 5.6. Hence it is difficult to differentiate between the two cases. However, all the experimentally determined dichroic ratios are of the order of 0.52, which is very close to the theoretically determined dichroic ratio for a randomly oriented film (0.50). As the area available per molecule is much larger than would be occupied by two all-trans aliphatic chains oriented parallel to the surface normal (approx. 50Å^2) it would be somewhat surprising if the chains were oriented in the all-trans conformation. Didecylamine, then, forms a disordered, 'dilute' adsorbed layer.

6.4   Conclusions

Quantitative ATR spectroscopy has been used to determine the amount of surfactant adsorbed at the silica/toluene interface and to determine the orientation of chromophores within the adsorbed layer. The NH stretching vibrations associated with the surfactants' headgroups was too weak to enable the precise nature of the interaction between the surface and the surfactant to be studied.

The adsorption isotherm of hexadecylamine follows a Langmuirian pattern; Γ_i rising rapidly with concentration and reaching a plateau at around 1.2×10^{-10} mol.cm^{-2}. This value indicates that approximately 1 in 5 of the available sites is occupied by a surfactant molecule. A certain degree of orientation is present in the adsorbed layer. In one case the aliphatic chains were in an all-trans conformation with the major chain axis aligned parallel to the surface normal. In the other cases the ordering was less perfect. Quite what controls the degree of orientation is uncertain.

The diamine, 1,12-diaminododecane, adsorbs to a similar extent. However, the 'plateau' on the isotherm exhibits a slight positive gradient which may arise from the formation of partial multilayers. Dichroic ratio measurements indicate that the adsorbed layer is less ordered than that of hexadecylamine. Measurements of the frequency of the CH stretching vibrations strongly suggest the presence of adsorbed species in which both amine groups are bonded to the surface.

The secondary amine, didecylamine, adsorbs to a lesser extent than either of the primary amines; the plateau value of Γ_i being a mere 0.3×10^{-10} mol.cm^{-2}. Orientational studies of the adsorbed layer show that it is highly disordered, as may be expected from the low value of Γ_i, which shows the adsorbed layer to be much less than a compact monolayer.

Figure 6.1   Transmission Spectrum of a 12.5mM Solution of Hexadecylamine
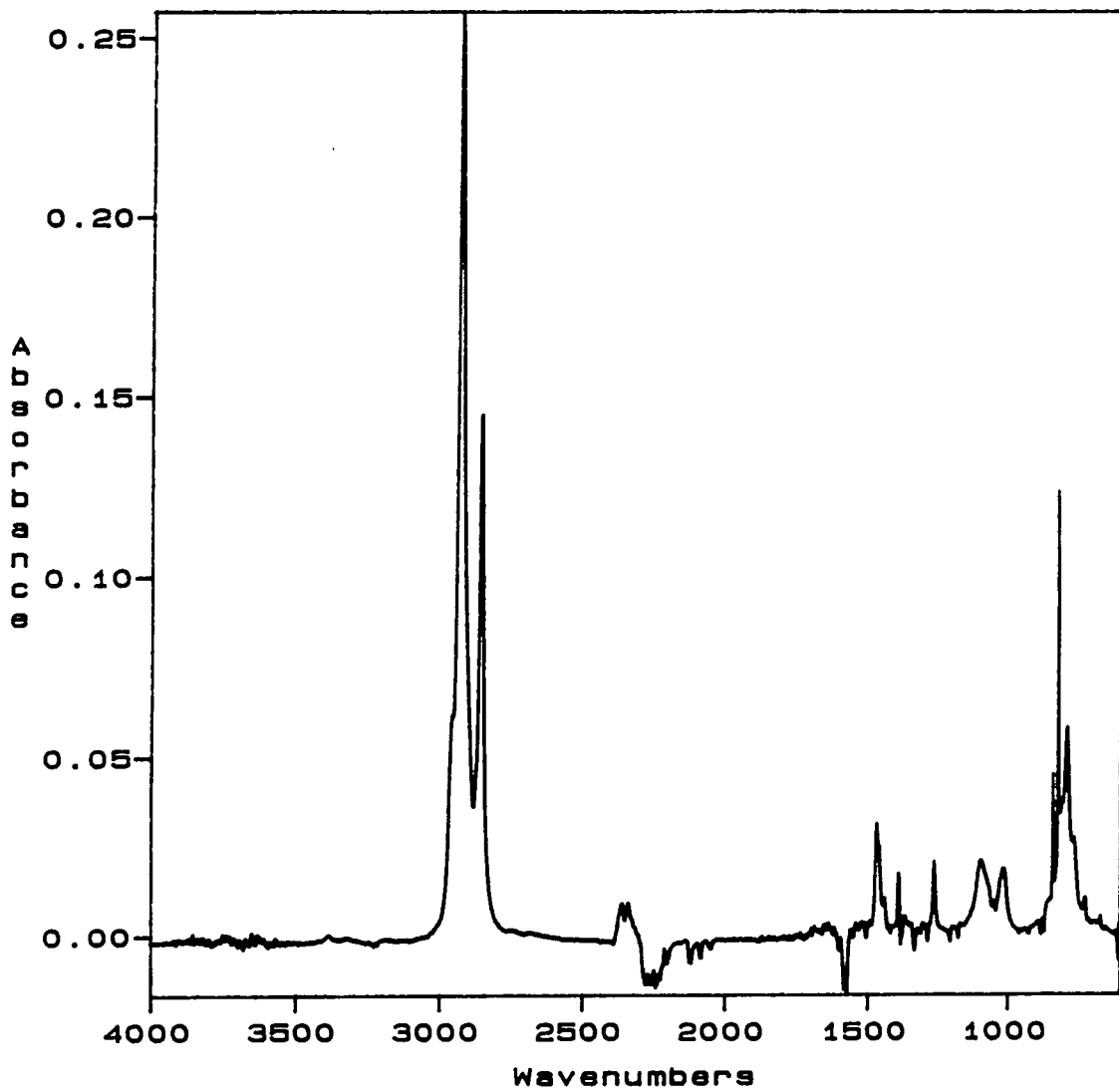
Figure 6.2   Transmission Spectrum of a 12.5mM Solution of Hexadecylamine

Expanded in the CH Stretching Region
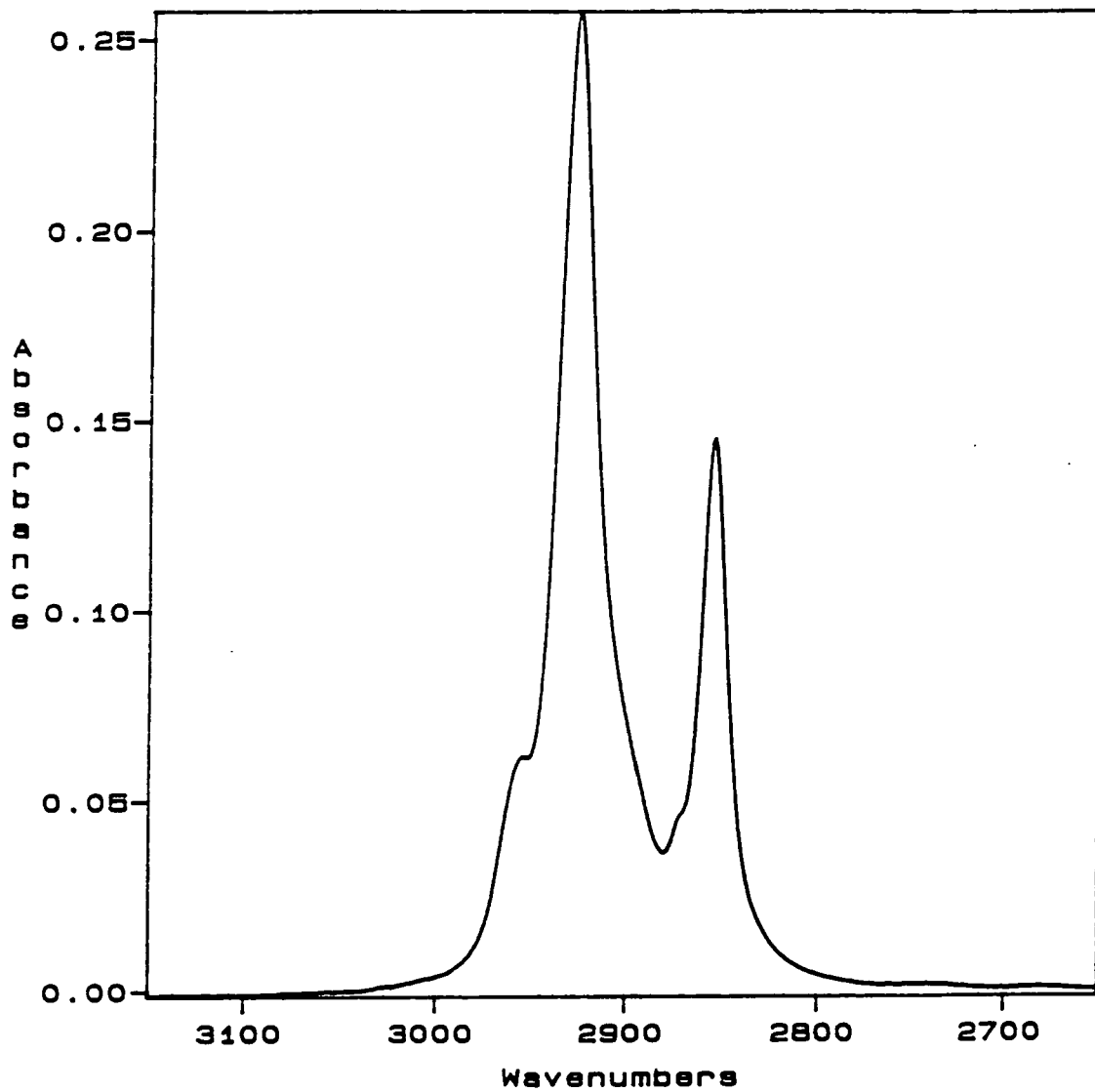
Figure 6.3   Transmission Spectra of Six Hexadecyamine Solutions
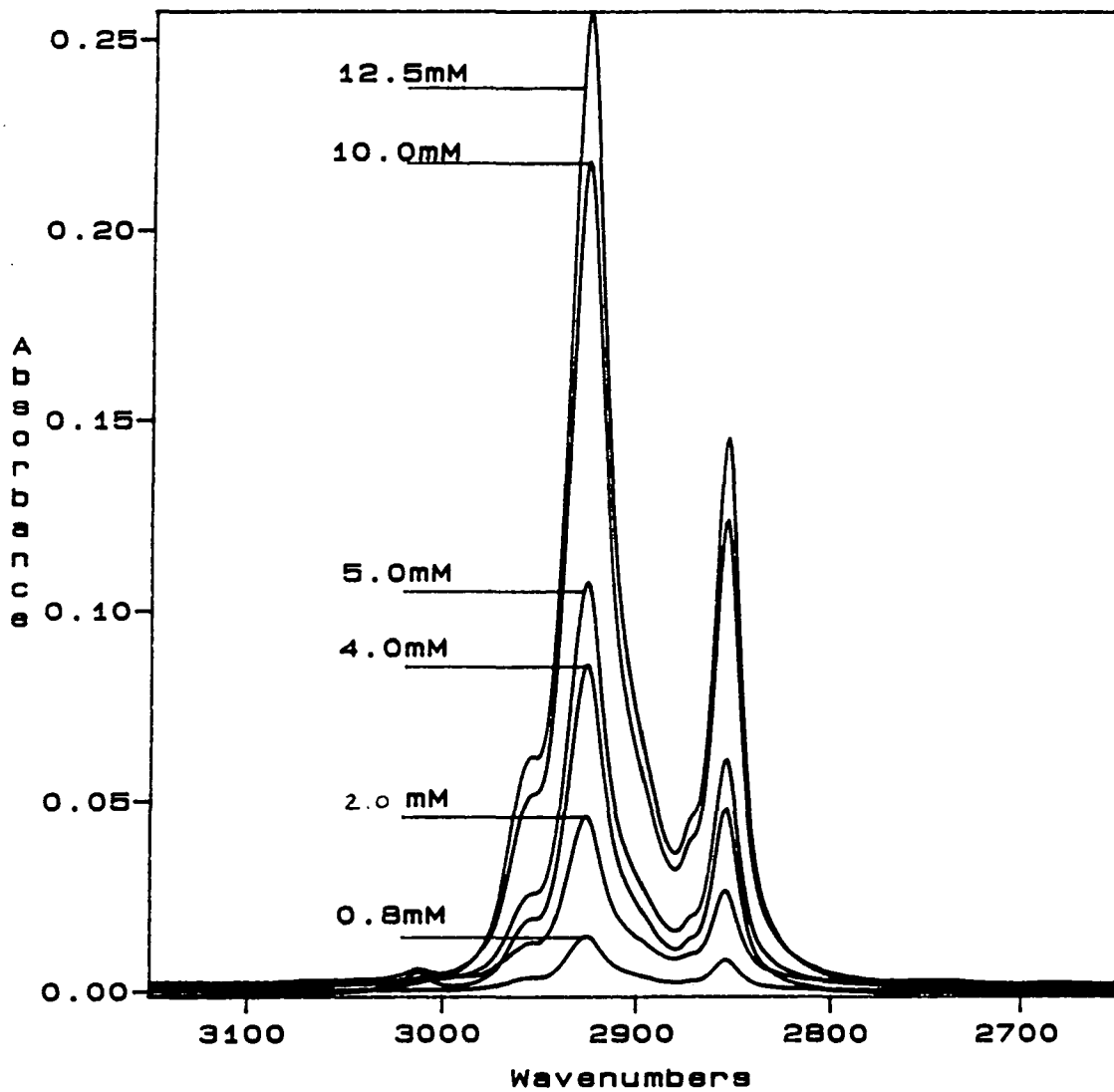
Figure 6.4   Unpolarized ATR Spectrum of 12.5mM Hexadecylamine
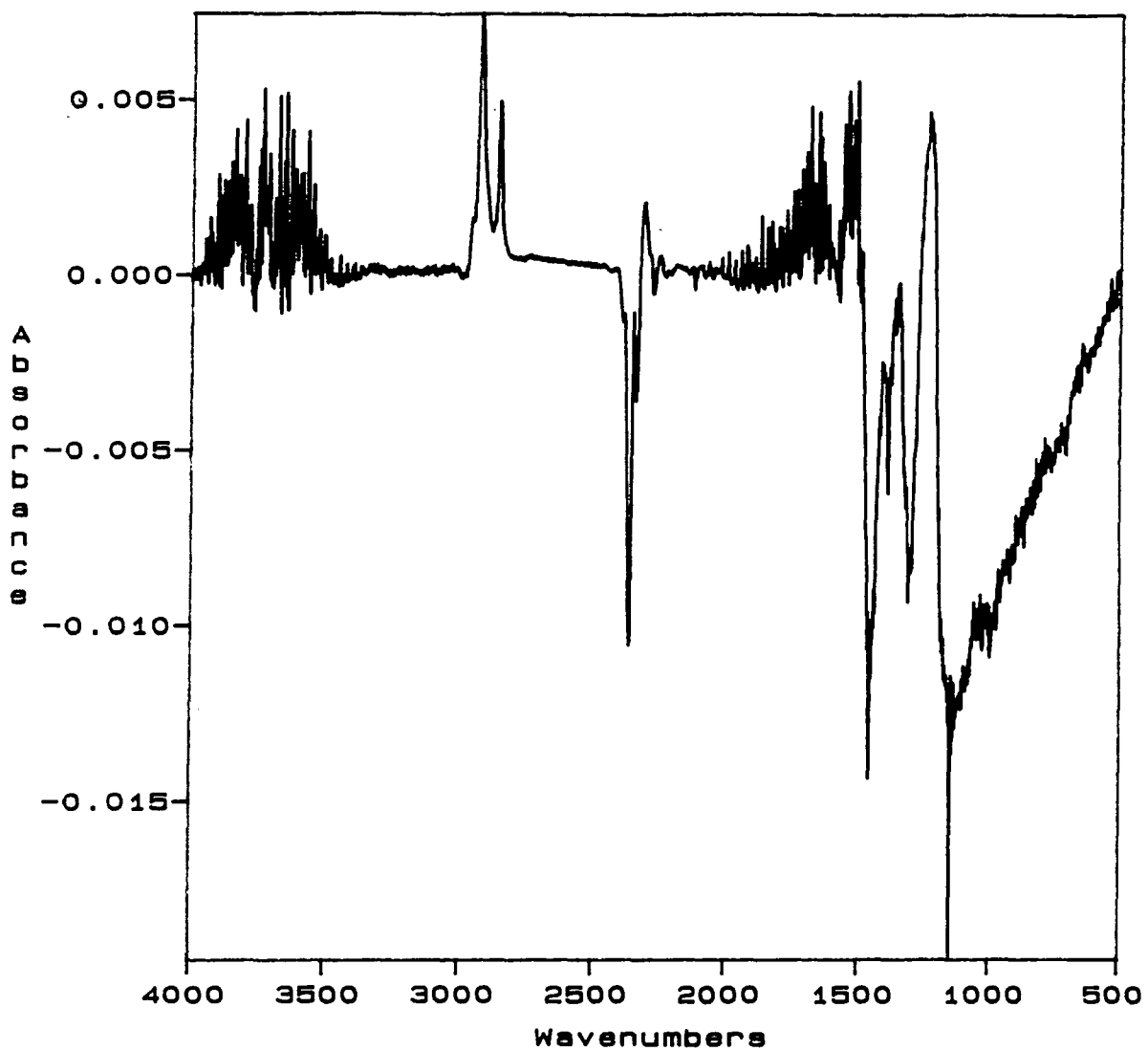
Figure 6.5   Unpolarized ATR Spectrum of 0.8mM Hexadecylamine
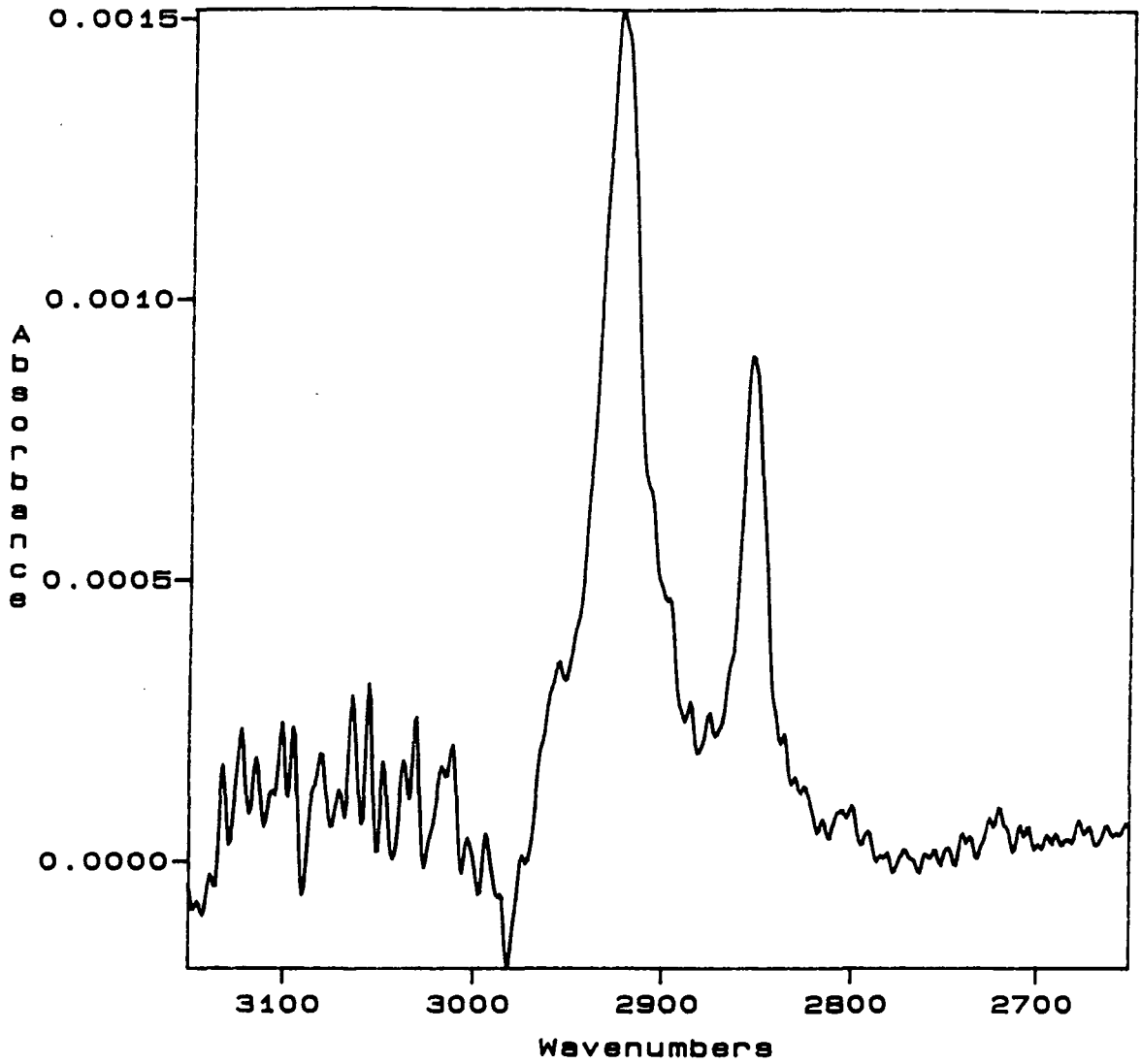
Figure 6.6   Unpolarized ATR Spectrum of 2.0mM Hexadecylamine
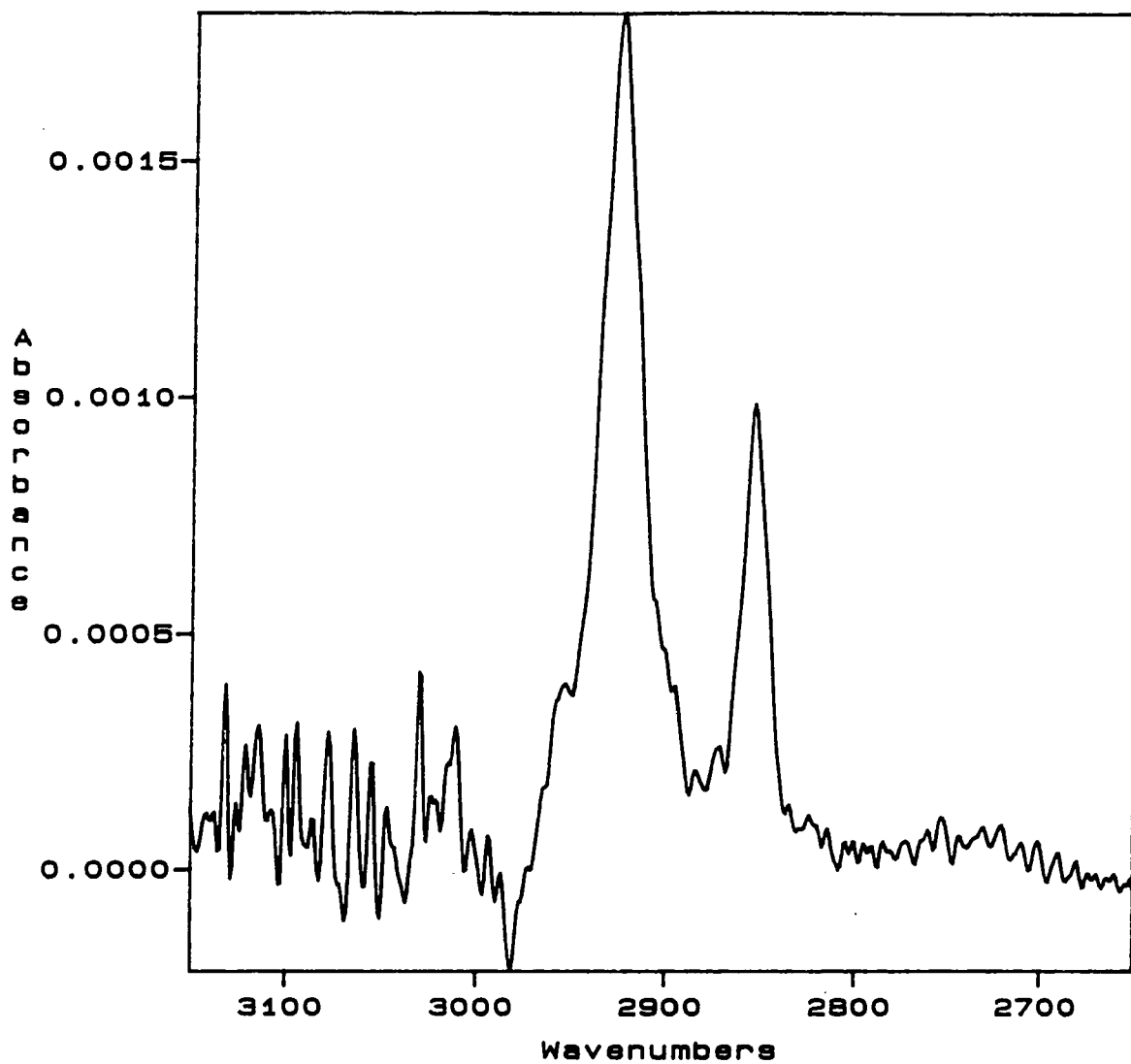
Figure 6.7   Unpolarized ATR Spectrum of 3.5mM Hexadecylamine
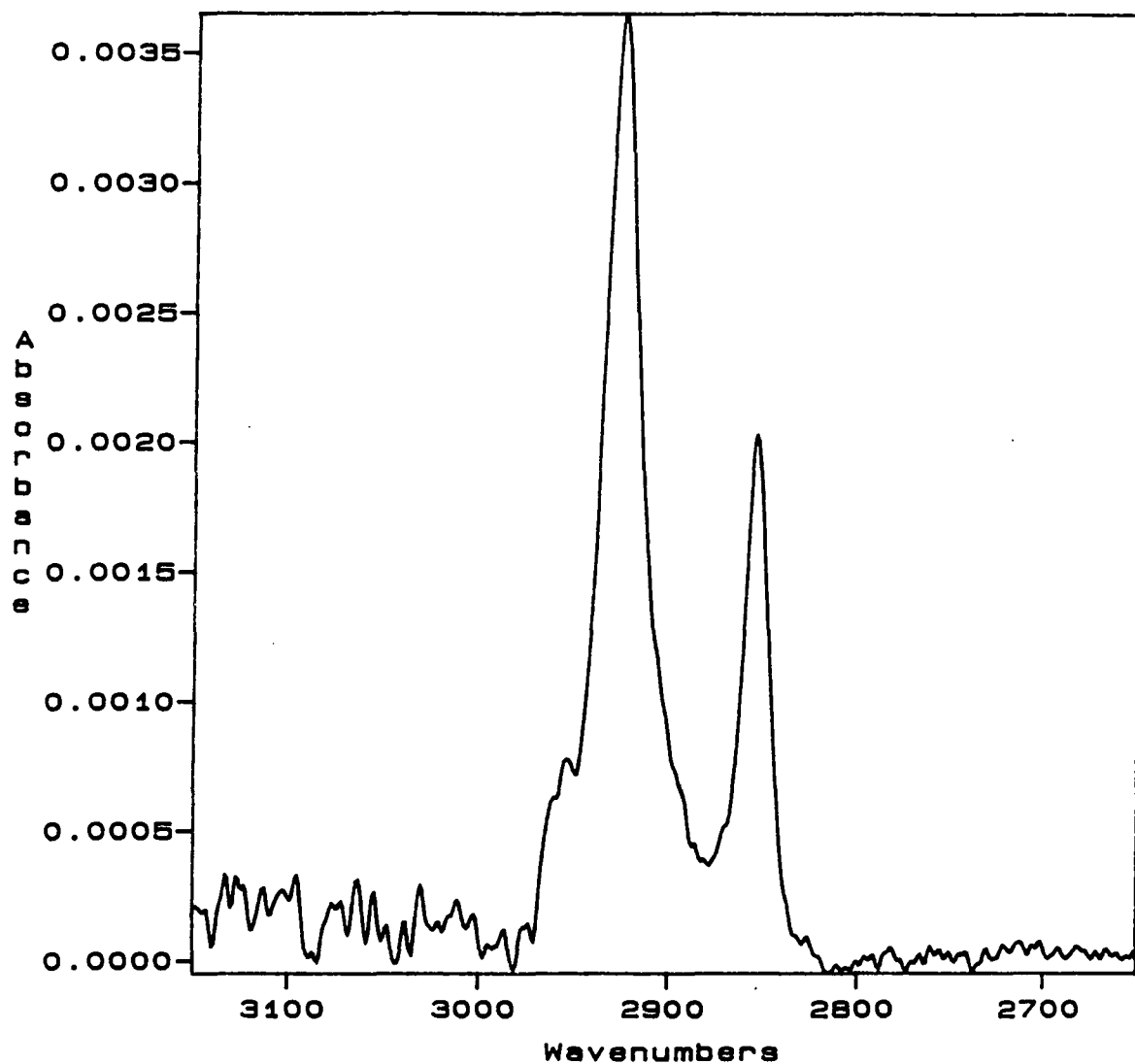
Figure 6.8   Unpolarized ATR Spectrum of 4.0mM Hexadecylamine
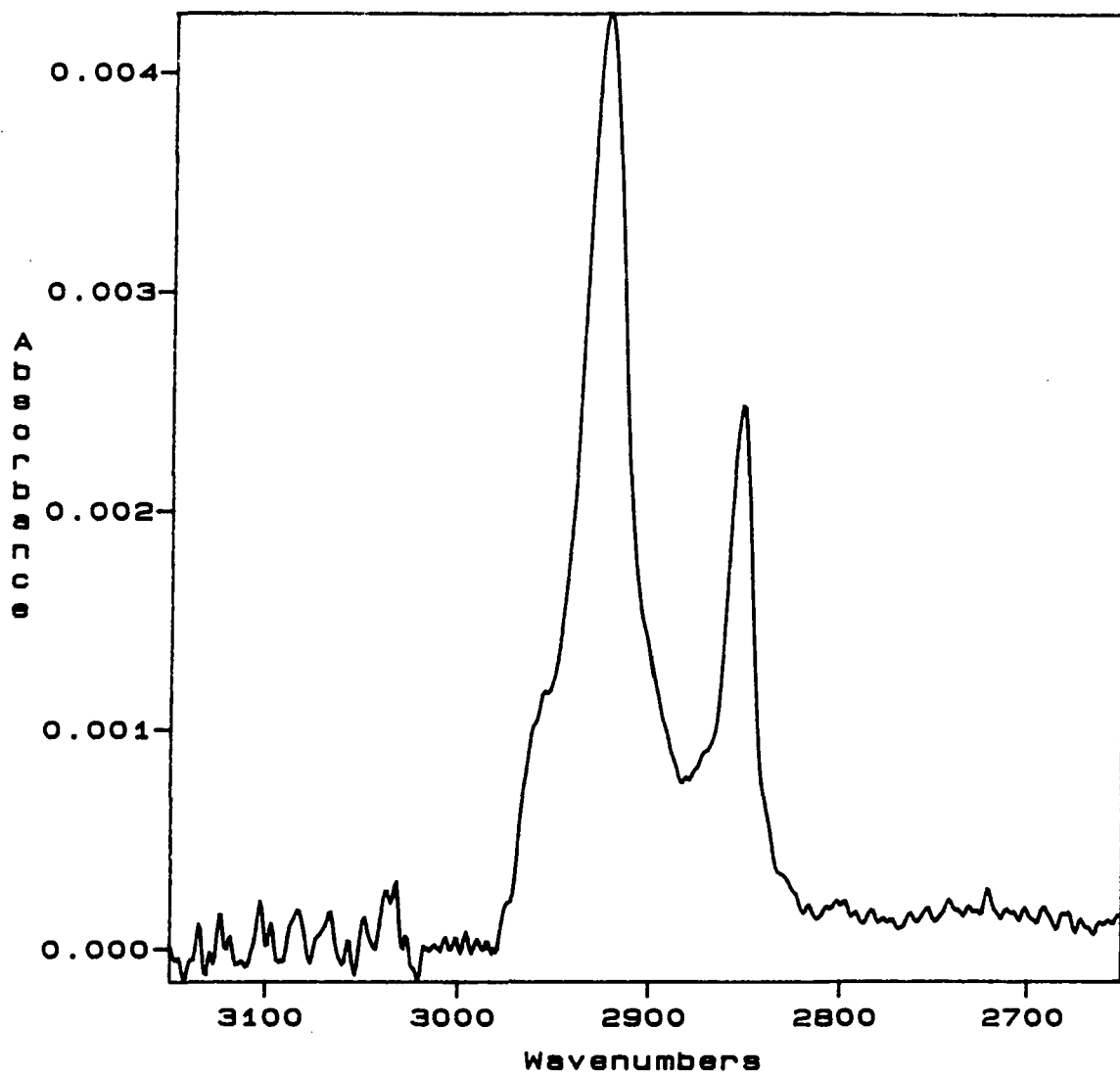
Figure 6.9   Unpolarized ATR Spectrum of 10.0mM Hexadecylamine
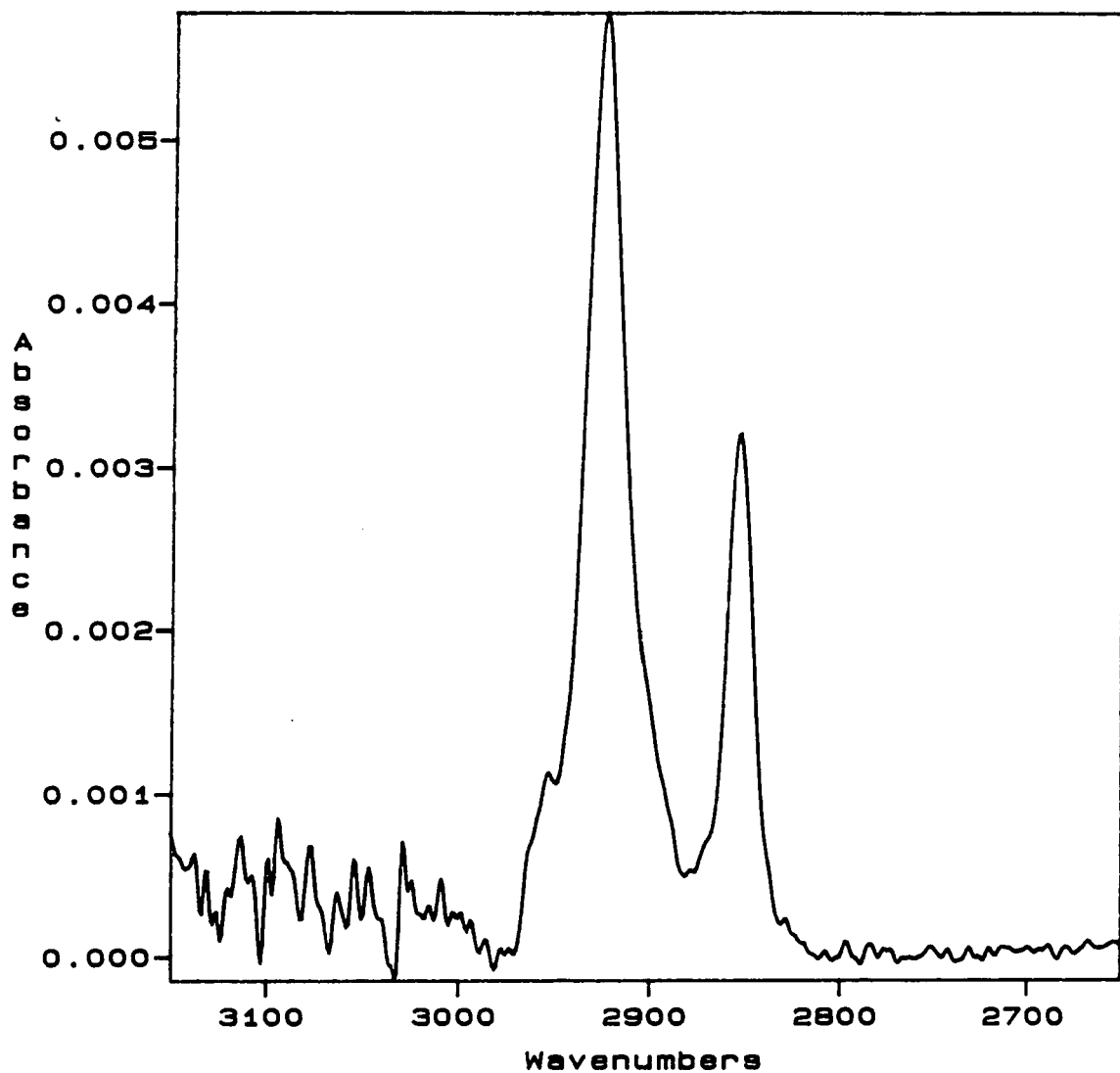
Figure 6.10   Unpolarized ATR Spectrum of 12.5mM Hexadecylamine
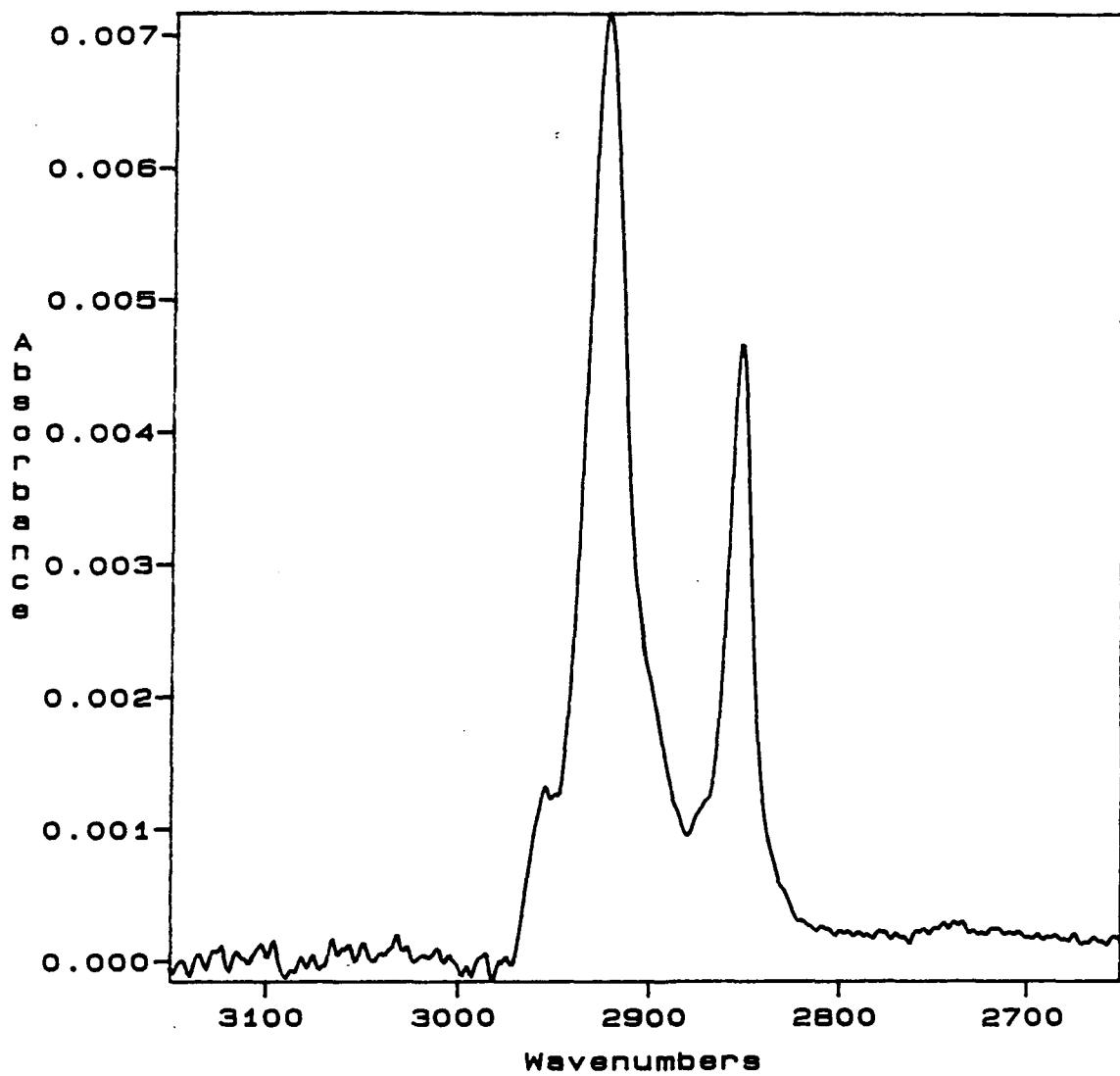
Figure 6.11   Unpolarized ATR Spectrum of 15.0mM Hexadecylamine
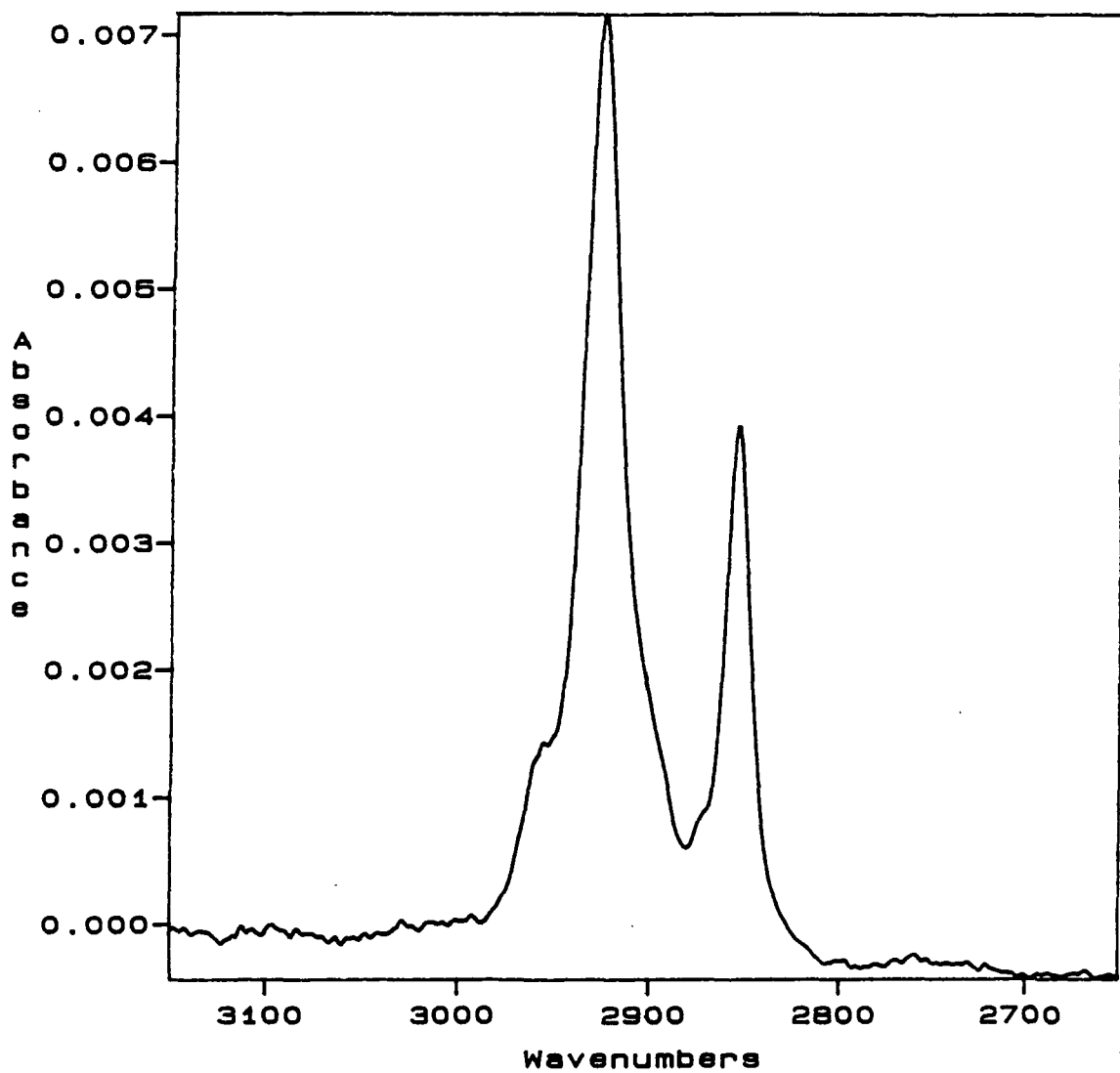
Figure 6.12   Unpolarized ATR Spectra of 12.5mM Hexadecylamine at 0, 1 and 2

Hours After Injection into the Squarecol Cell
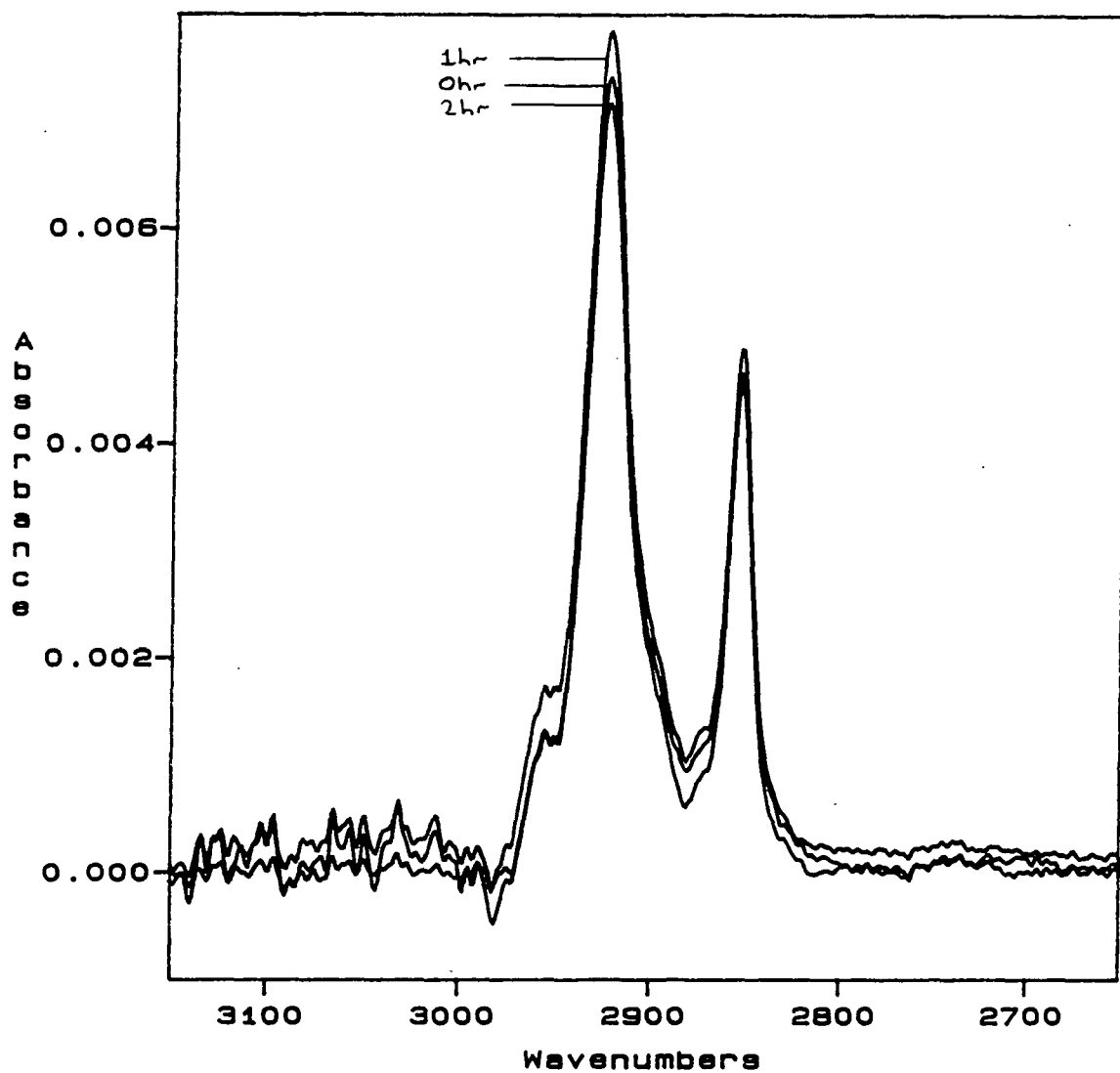
Figure 6.13
Adsorption Isotherm for Hexadecylamine
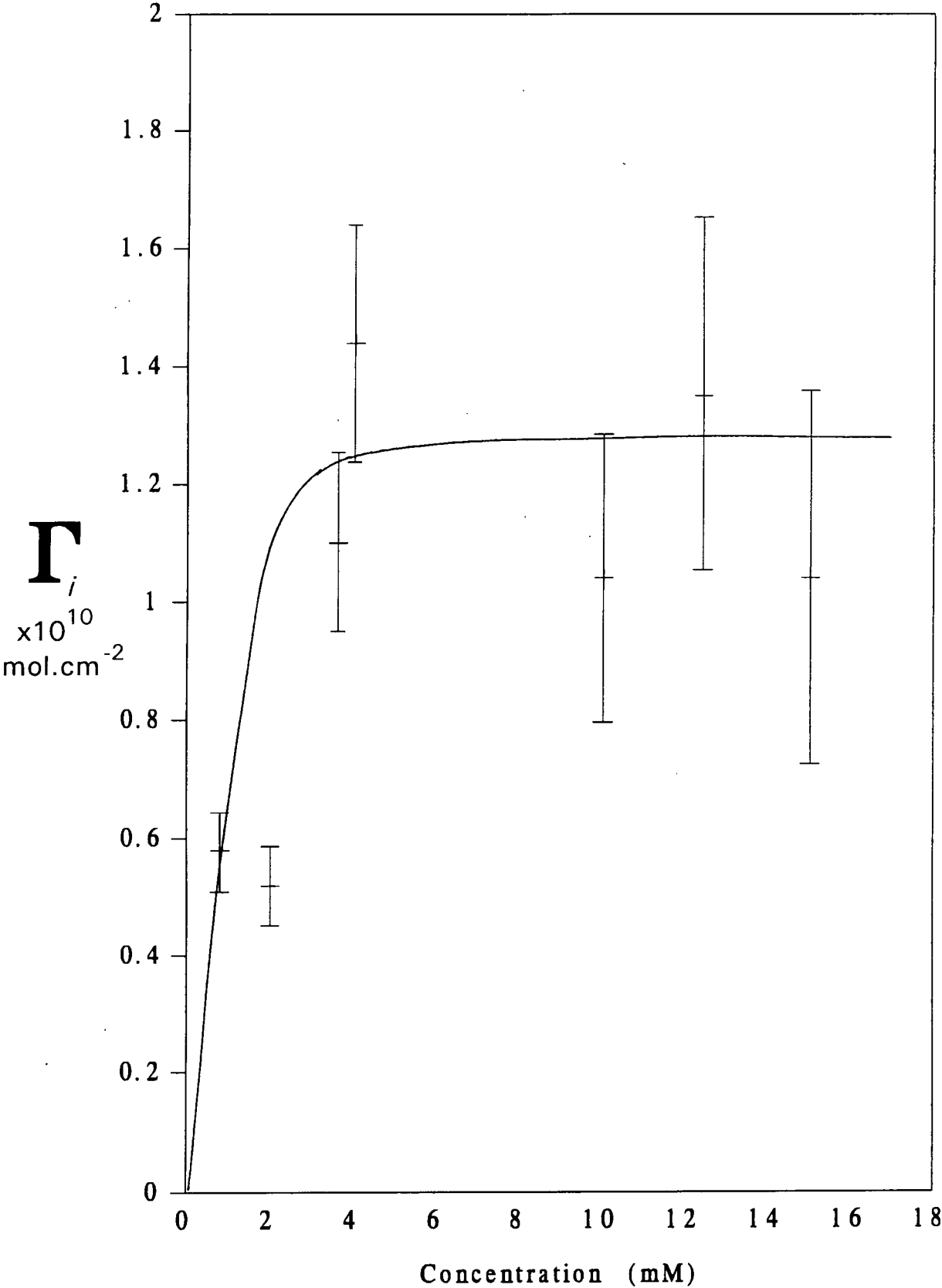
Figure 6.14   TE and TM Polarized Spectra of 0.8mM Hexadecylamine
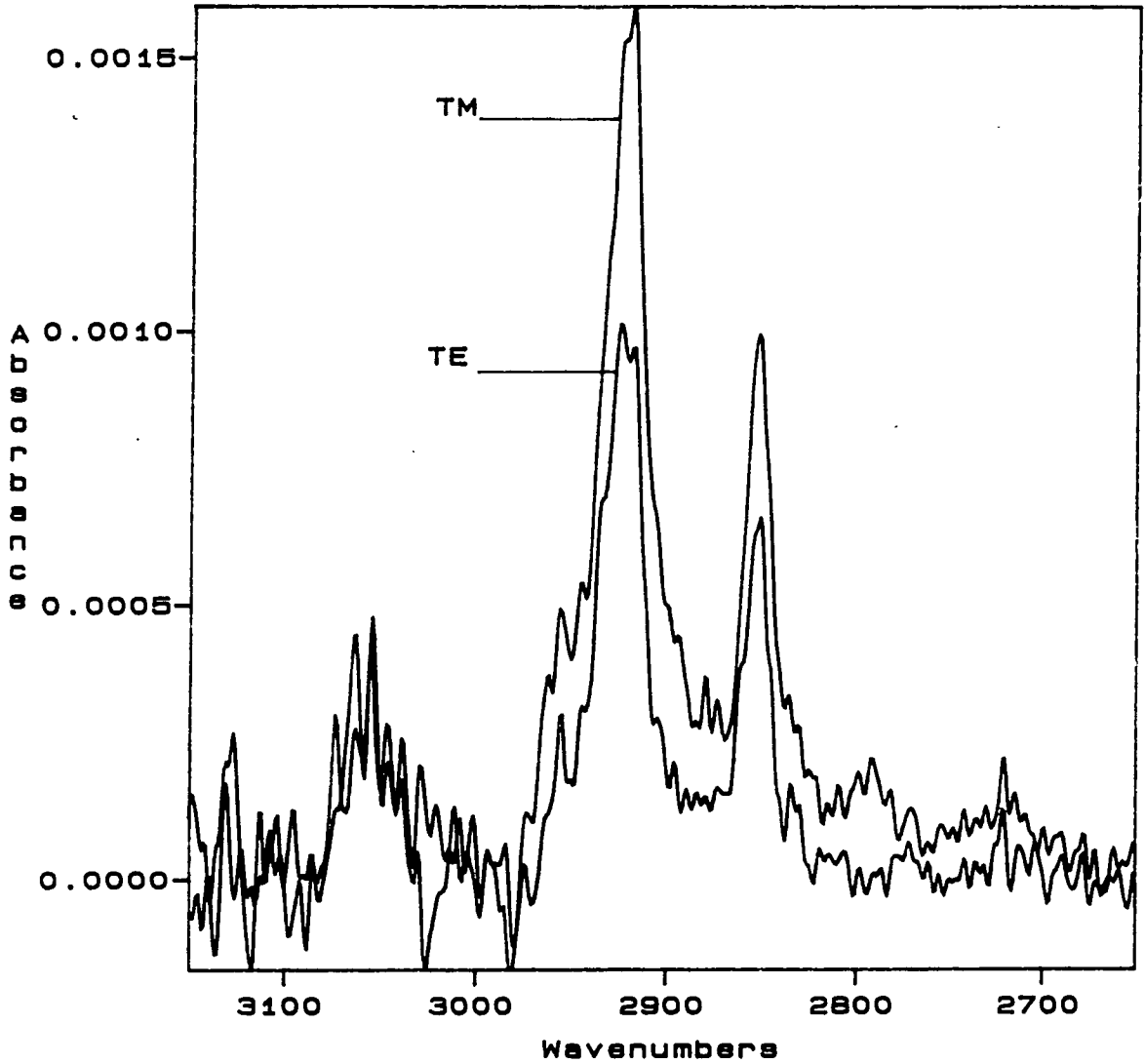
Figure 6.15   TE and TM Polarized Spectra of 2.0mM Hexadecylamine
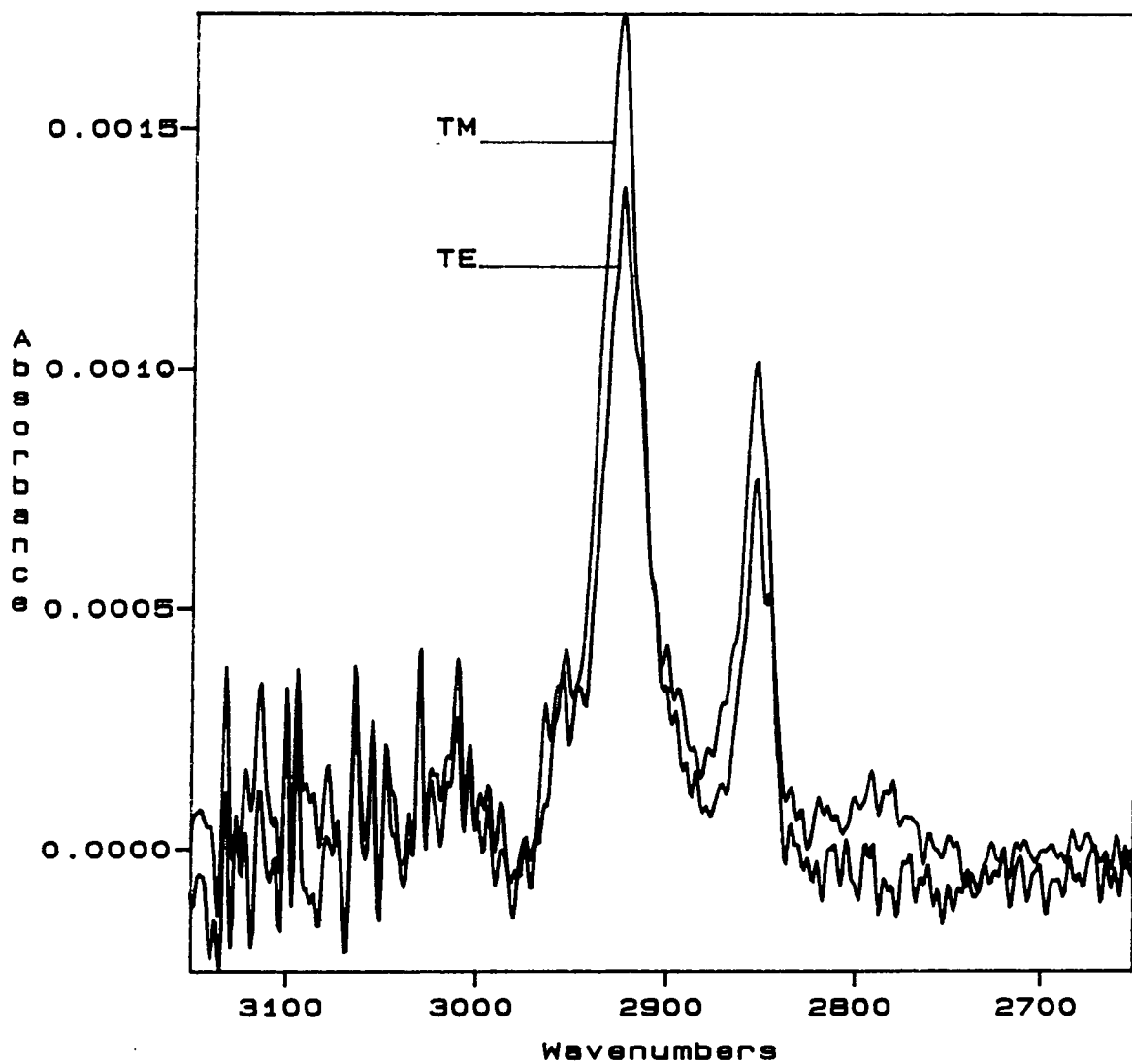
Figure 6.16   TE and TM Polarized Spectra of 3.5mM Hexadecylamine
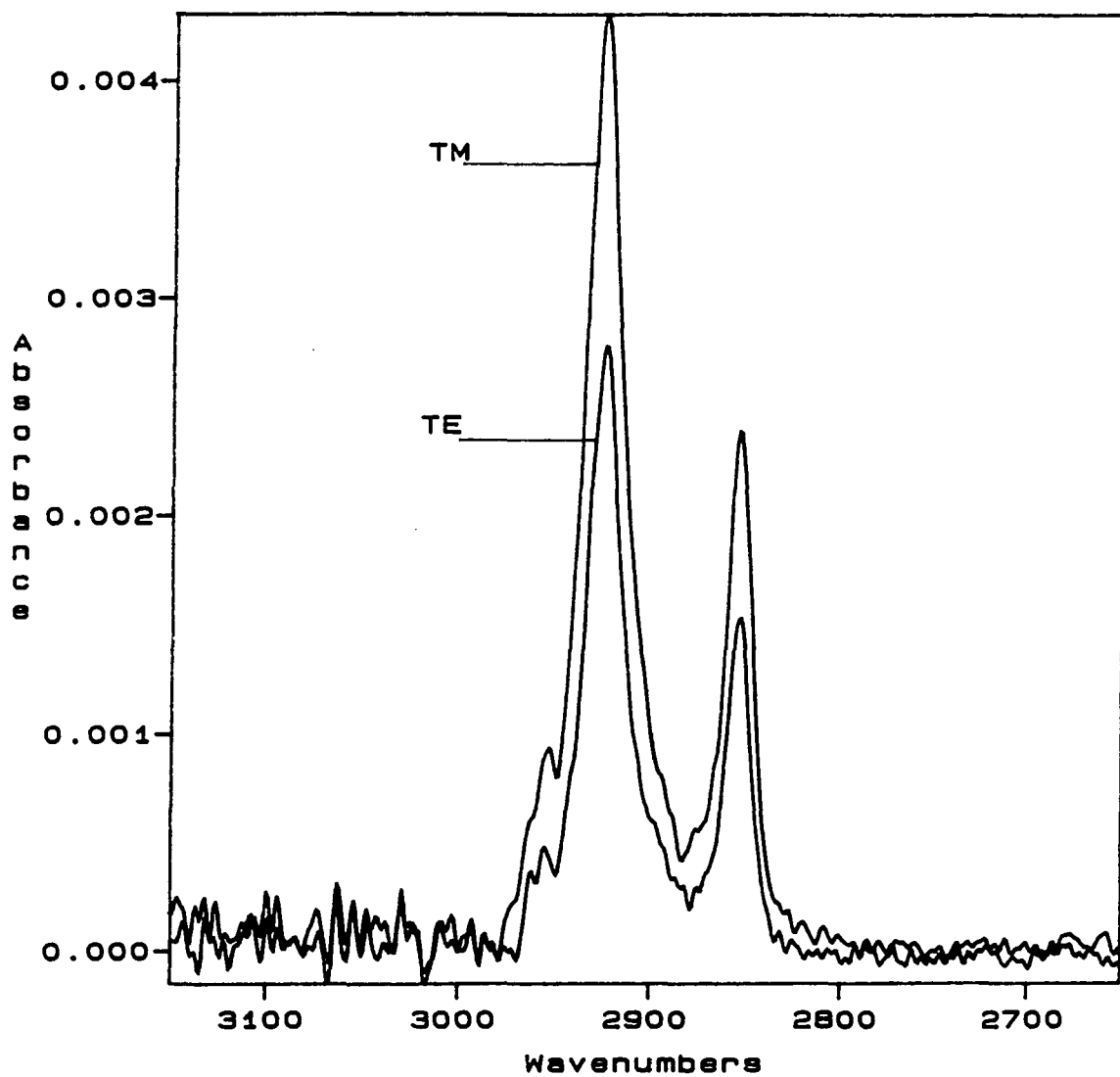
Figure 6.17 TE and TM Polarized Spectra of 4.0mM Hexadecylamine
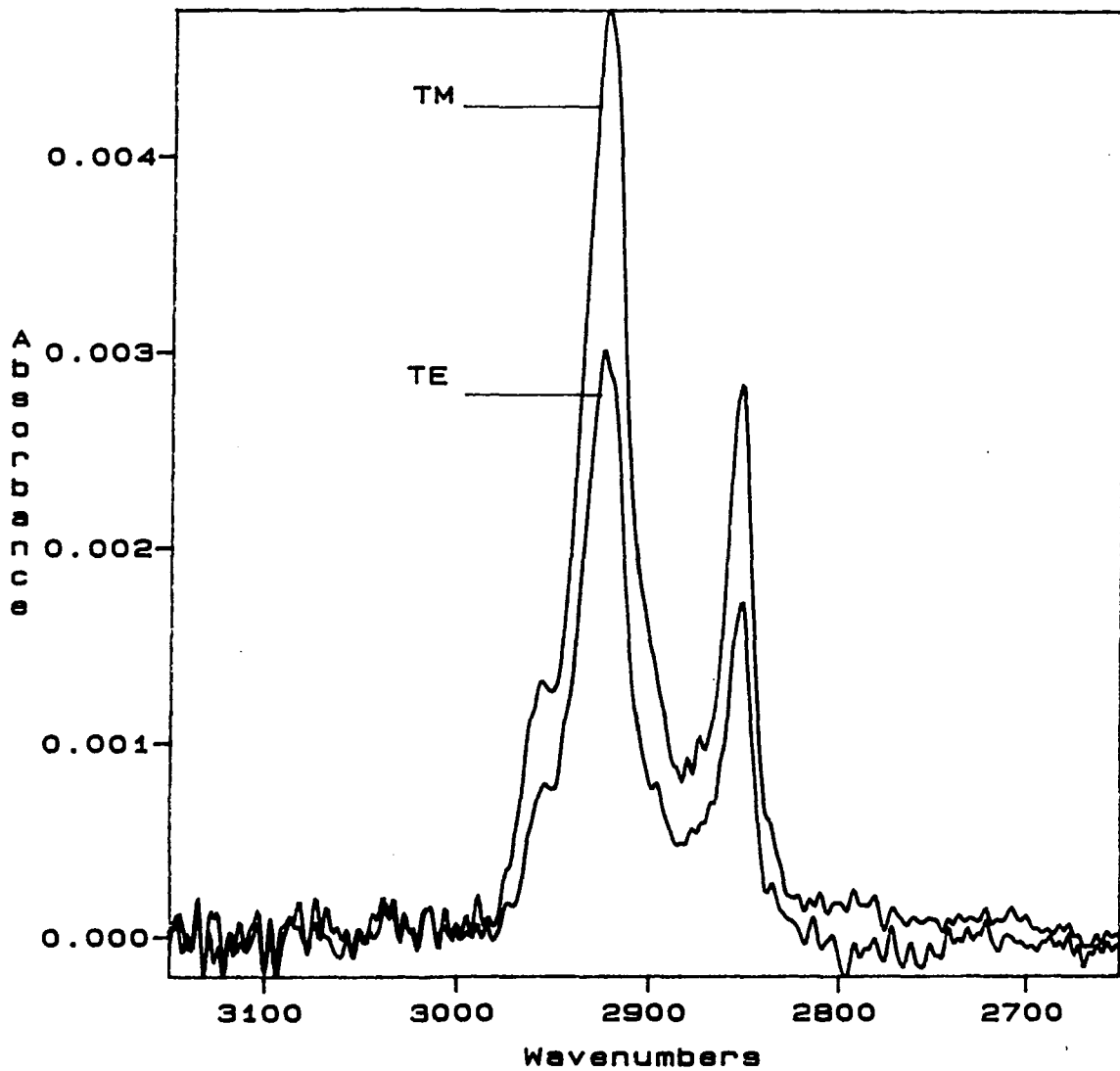
Figure 6.18   TE and TM Polarized Spectra of 10.0mM Hexadecylamine
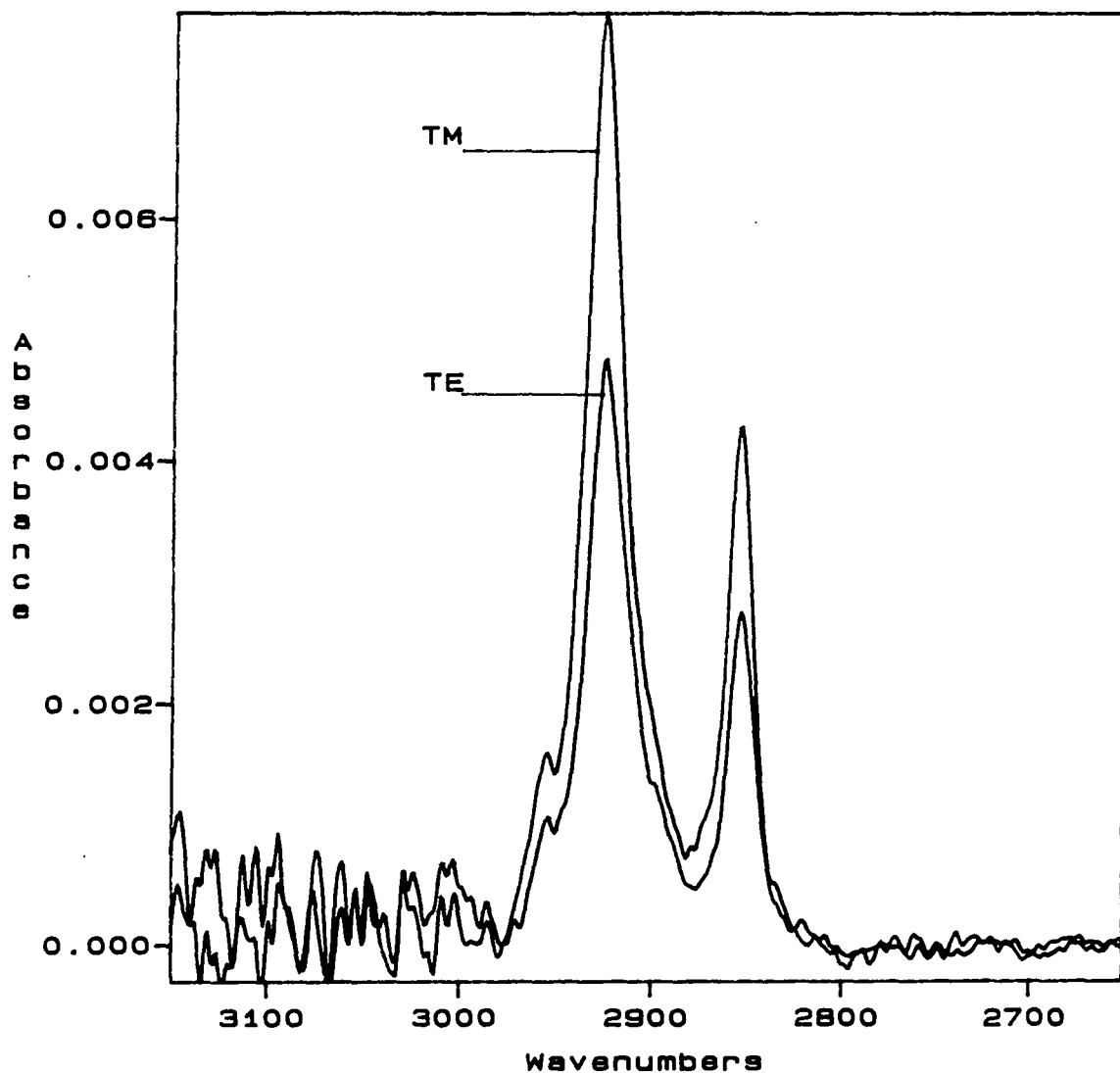
Figure 6.19   TE and TM Polarized Spectra of 12.5mM Hexadecylamine
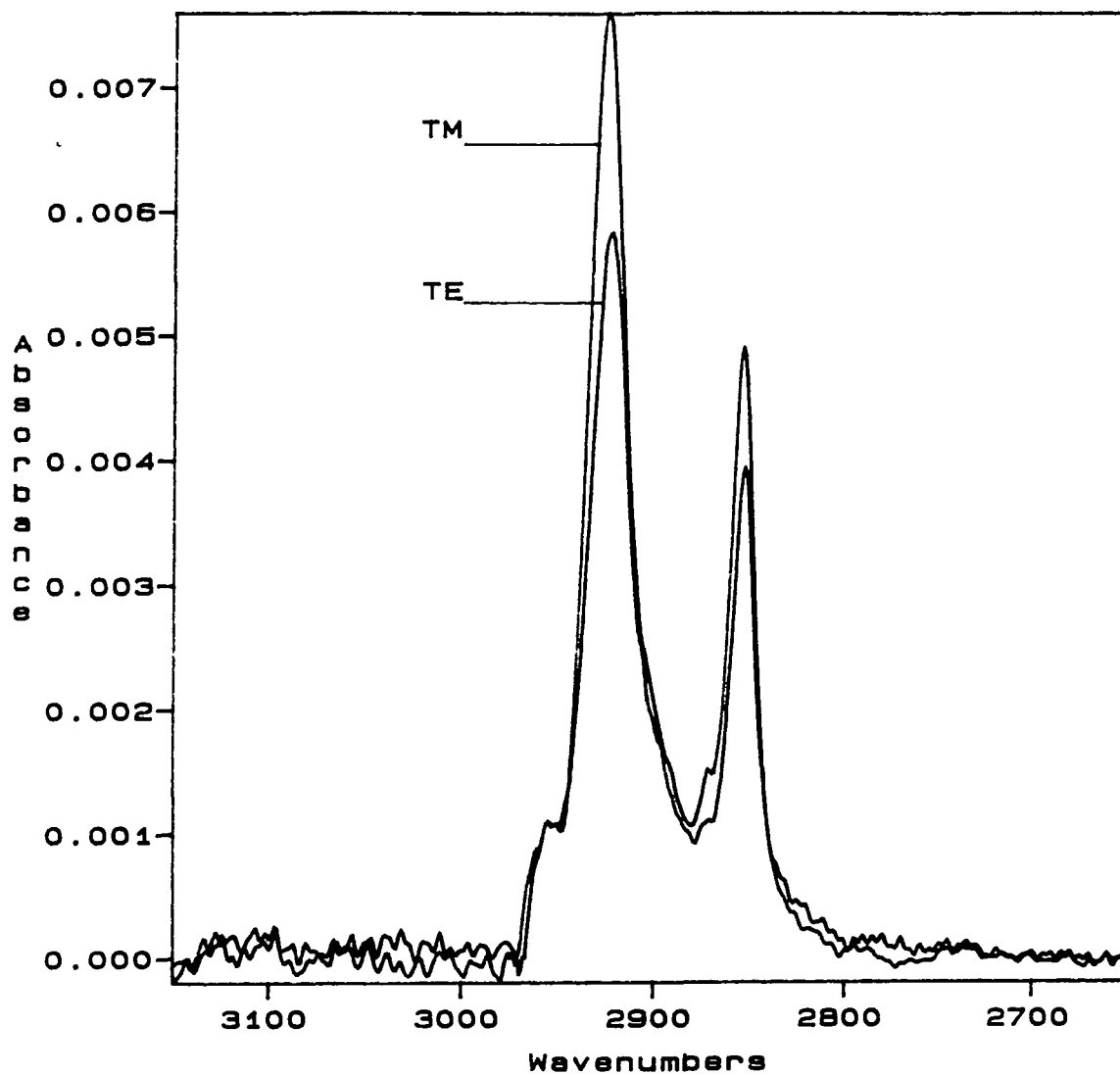
Figure 6.20   TE and TM Polarized Spectra of 15.0mM Hexadecylamine
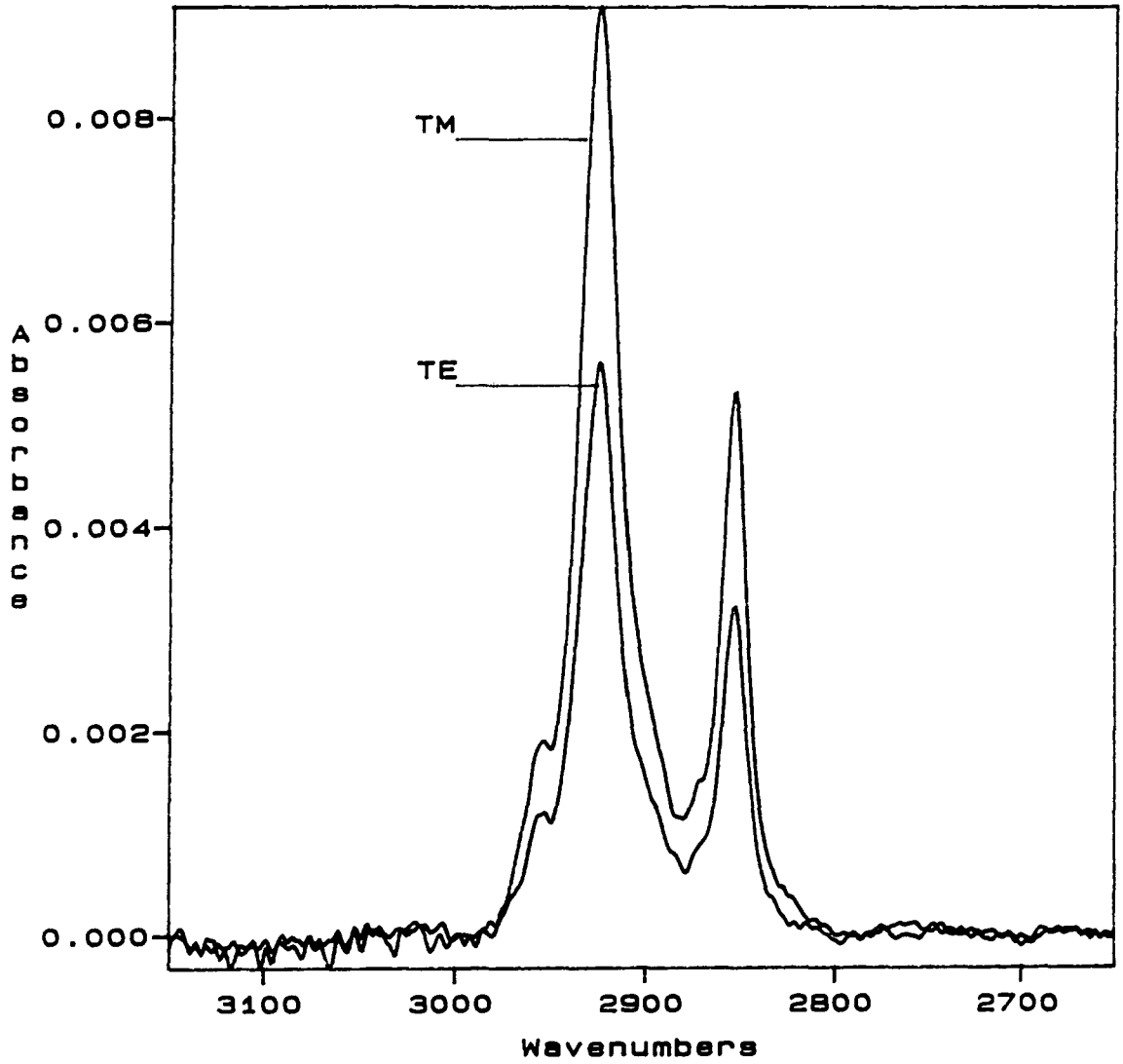
Figure 6.21   TE and TM Polarized Spectra of 18.6mM Hexadecane
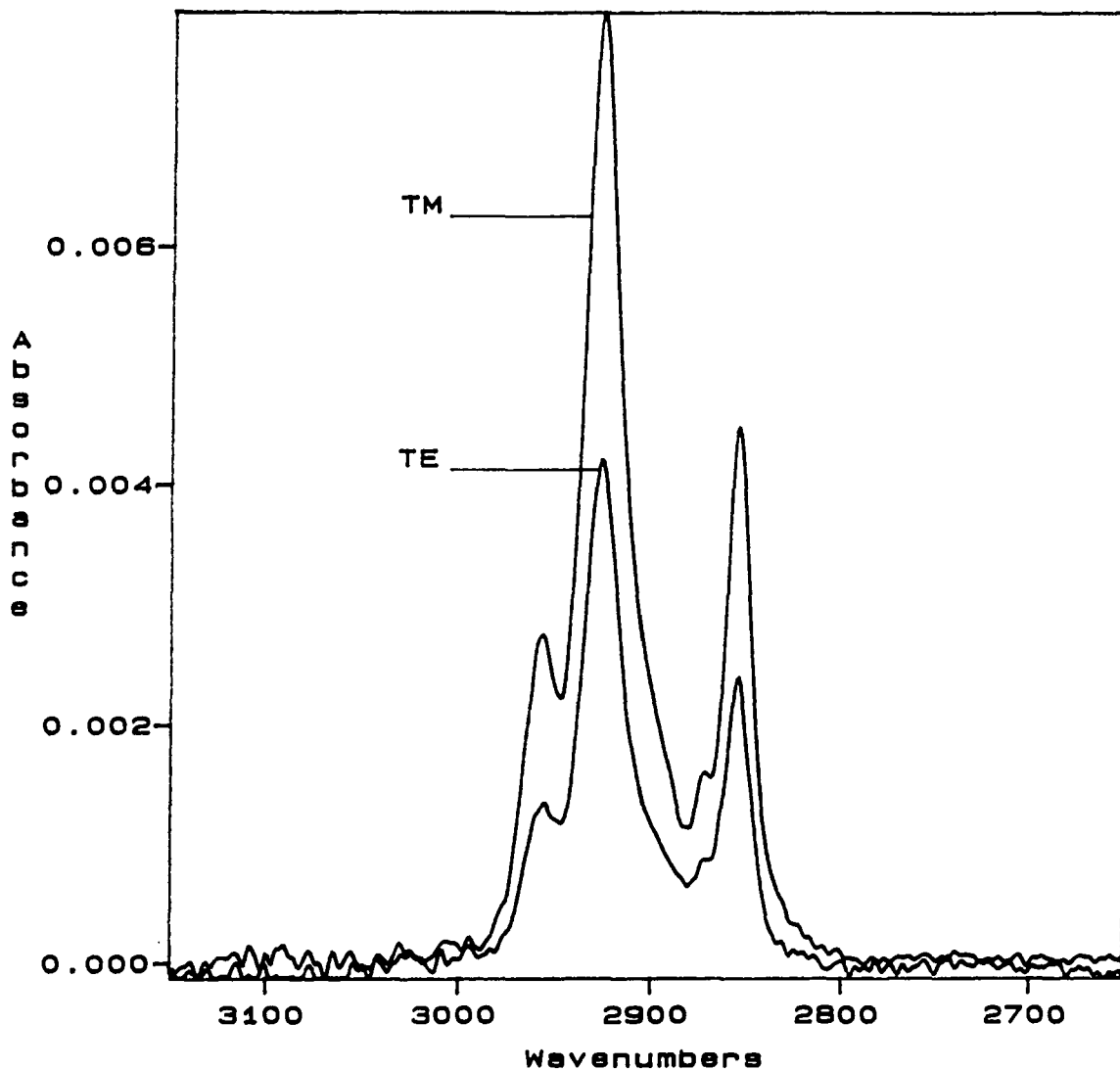
Figure 6.22   TE and TM Single Beam Spectra Ratioed Against an Unpolarized

Background
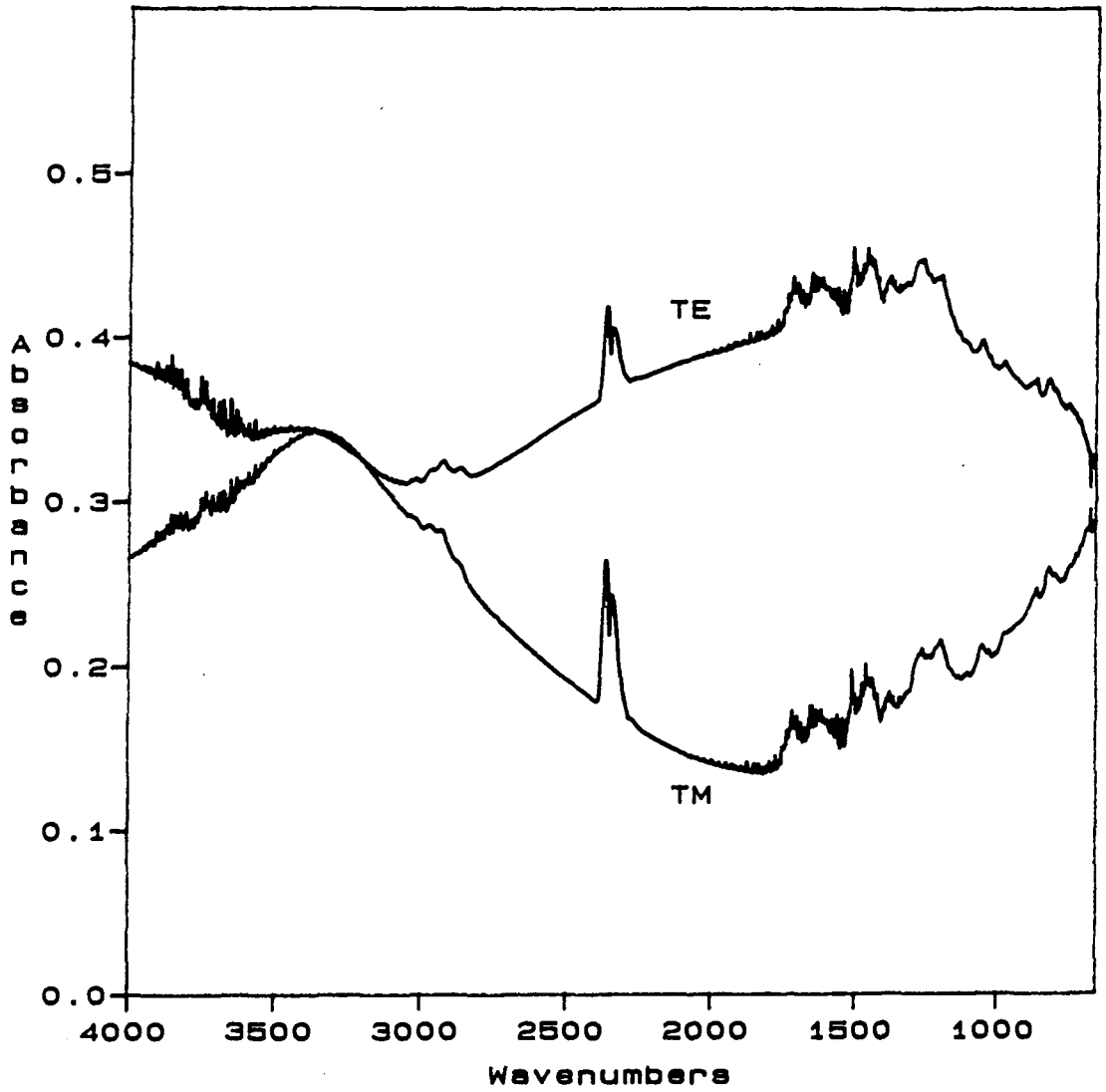
Figure 6.23   Unpolarized ATR Spectra of 11.9mM Hexadecane, 12.5mM

Hexadecylamine and the Difference
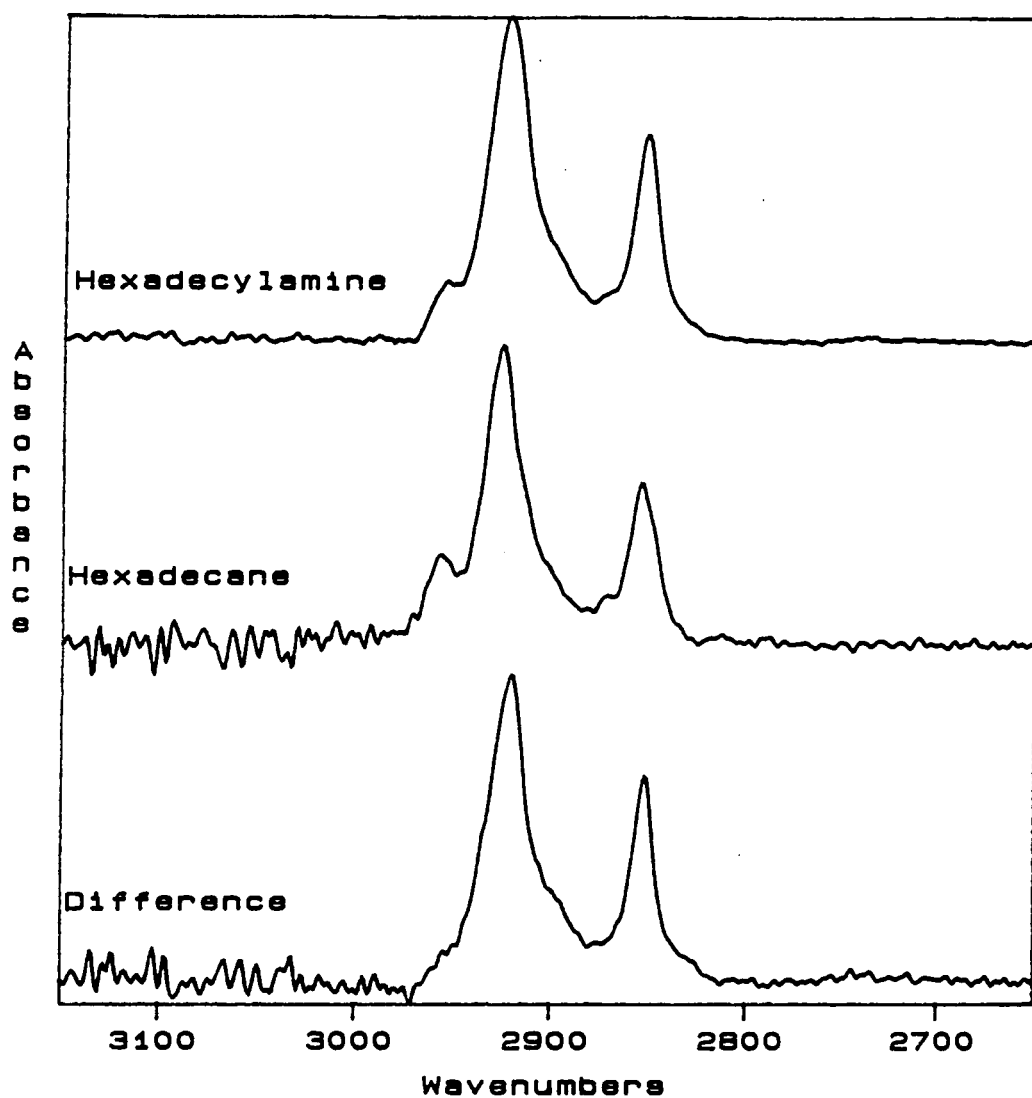
Figure 6.24   Unpolarized ATR Spectra of 3.5mM Hexadecane, 3.5mM

Hexadecylamine and the Difference
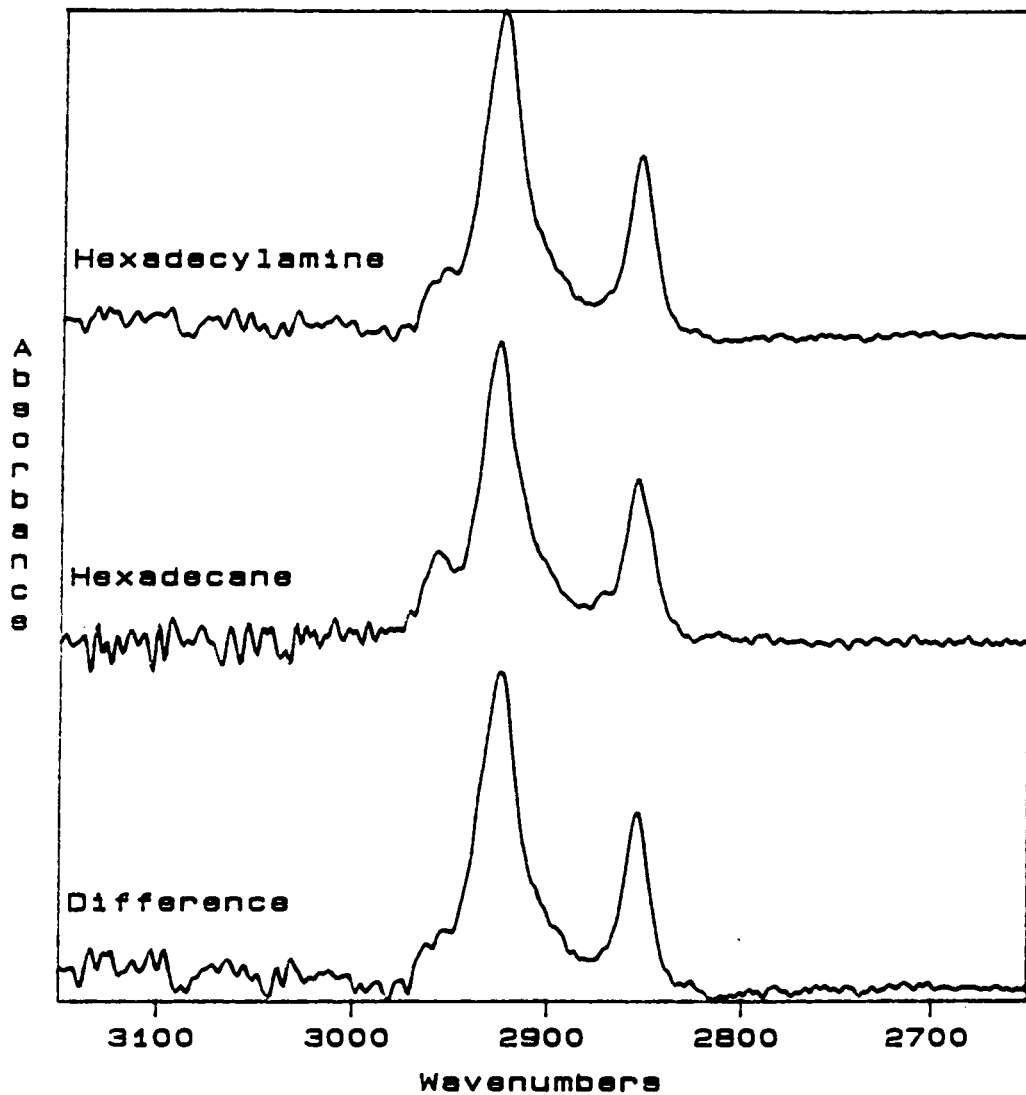
Figure 6.25   Transmission Spectrum of 20mM 1,12-diaminododecane
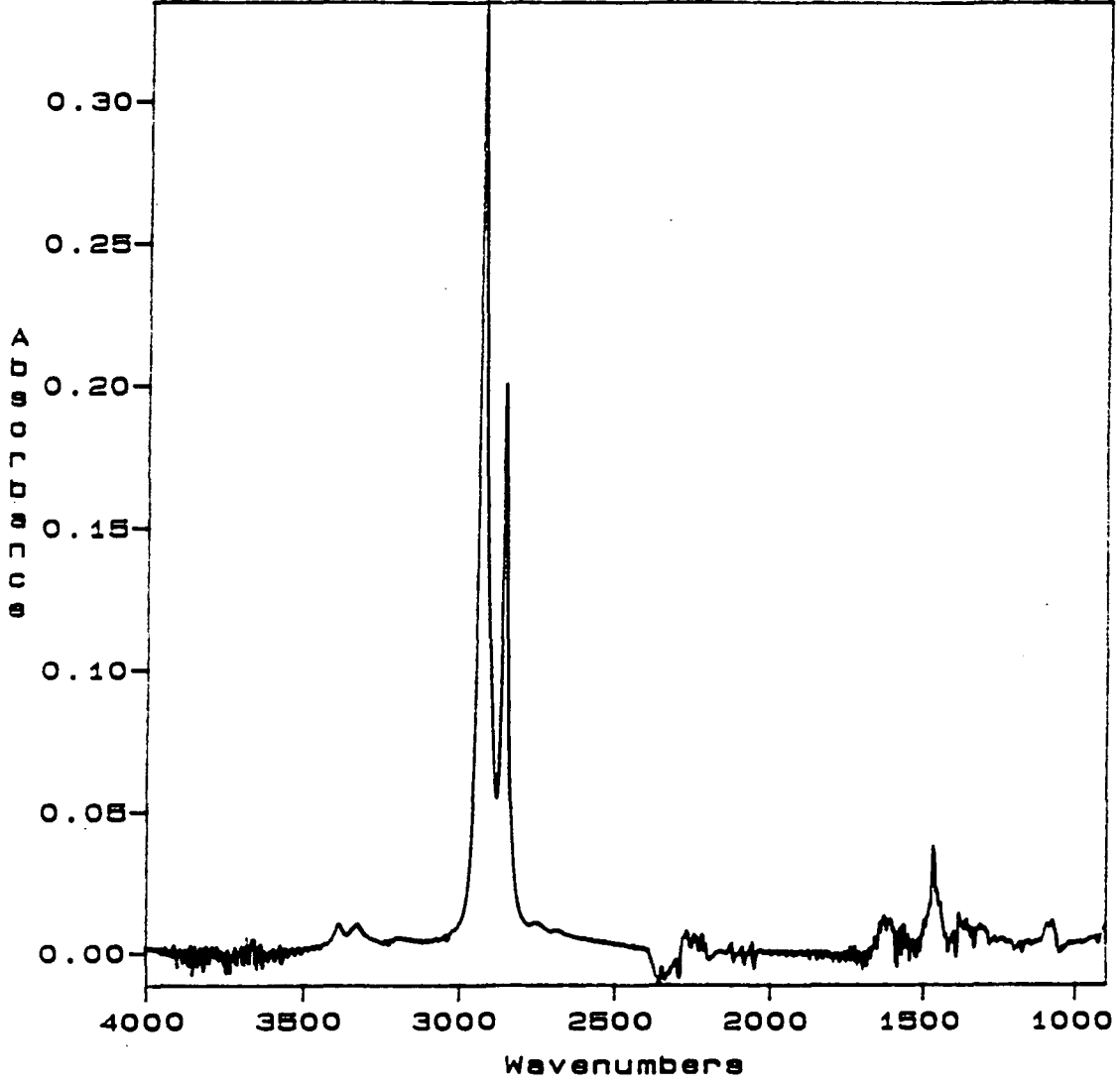
Figure 6.26   Transmission Spectrum of 20mM 1,12-diaminododecane Expanded in

the CH Stretching Region
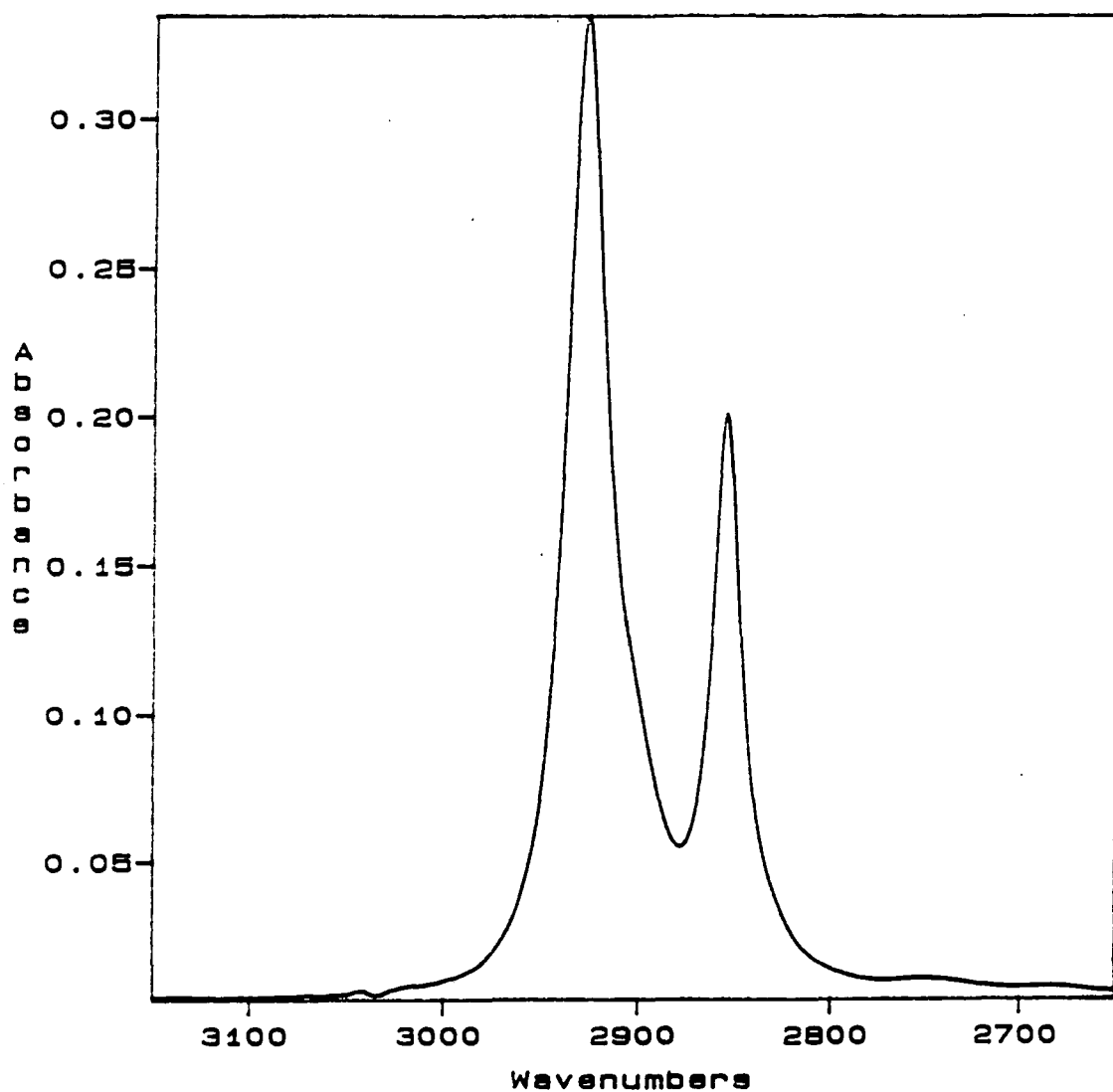
Figure 6.27   Unpolarized ATR Spectrum of 1.9mM 1,12-diaminododecane
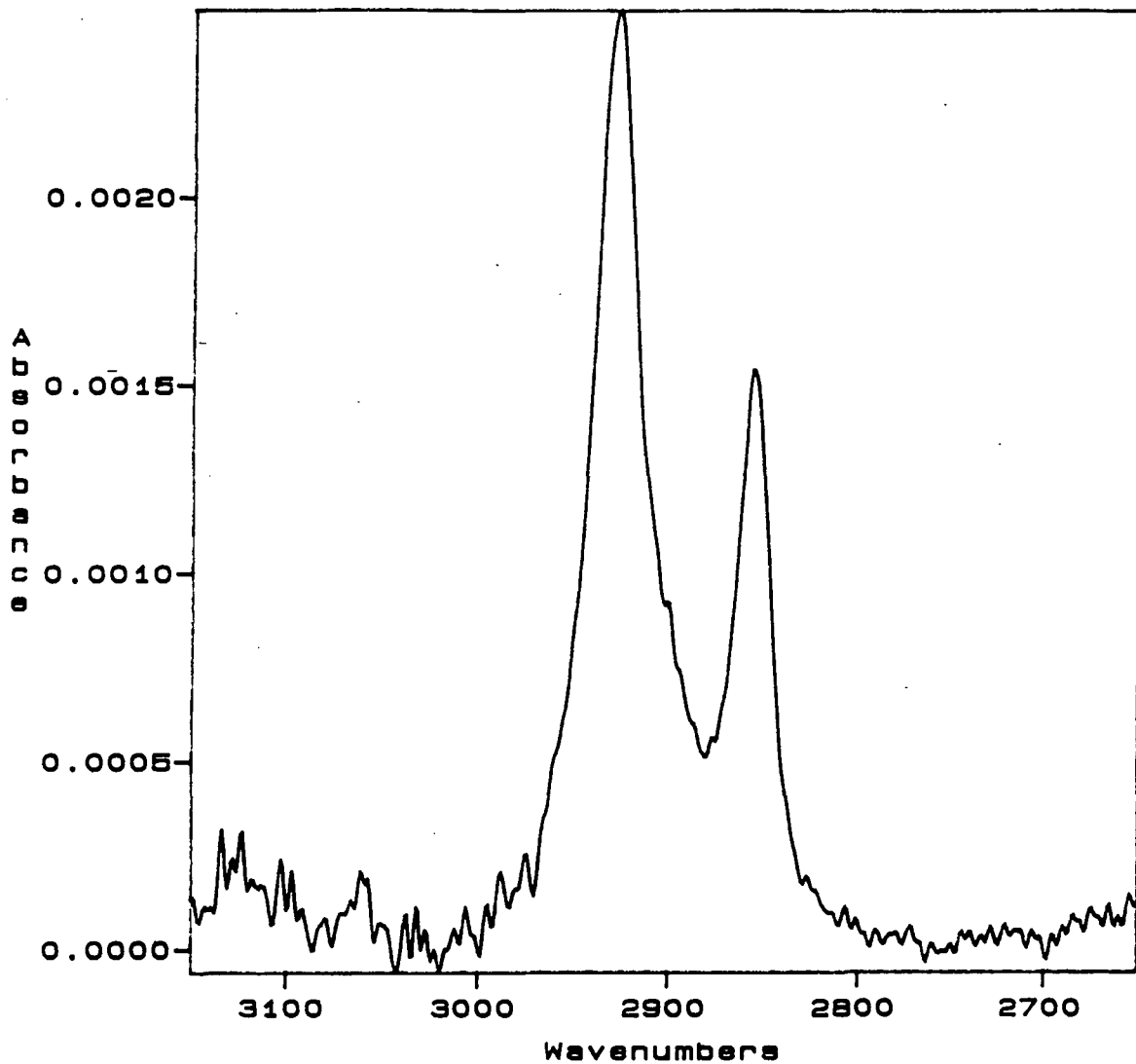
Figure 6.28   Unpolarized ATR Spectrum of 3.7mM 1,12-diaminododecane
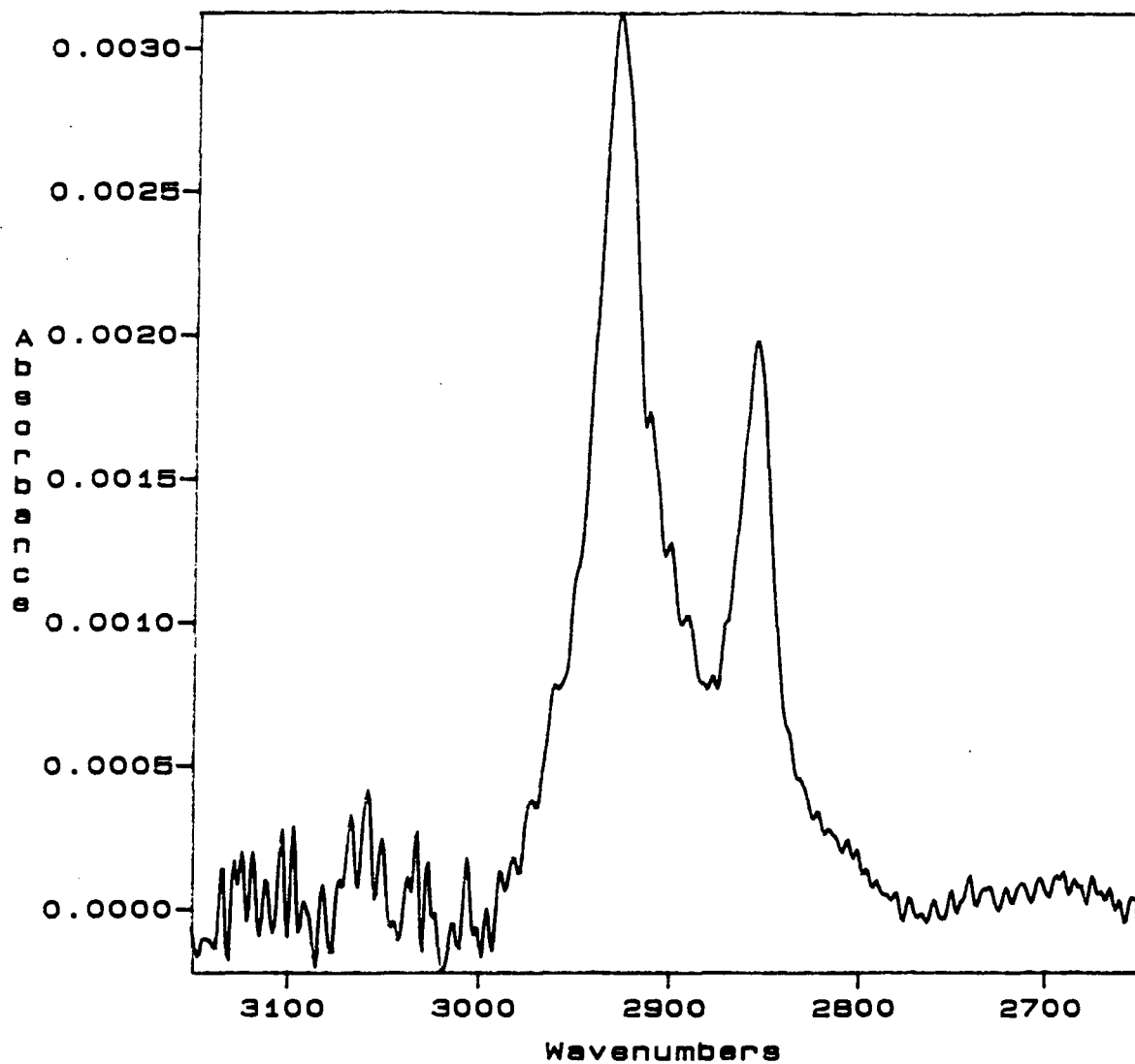
Figure 6.29   Unpolarized ATR Spectrum of 5.8mM 1,12-diaminododecane
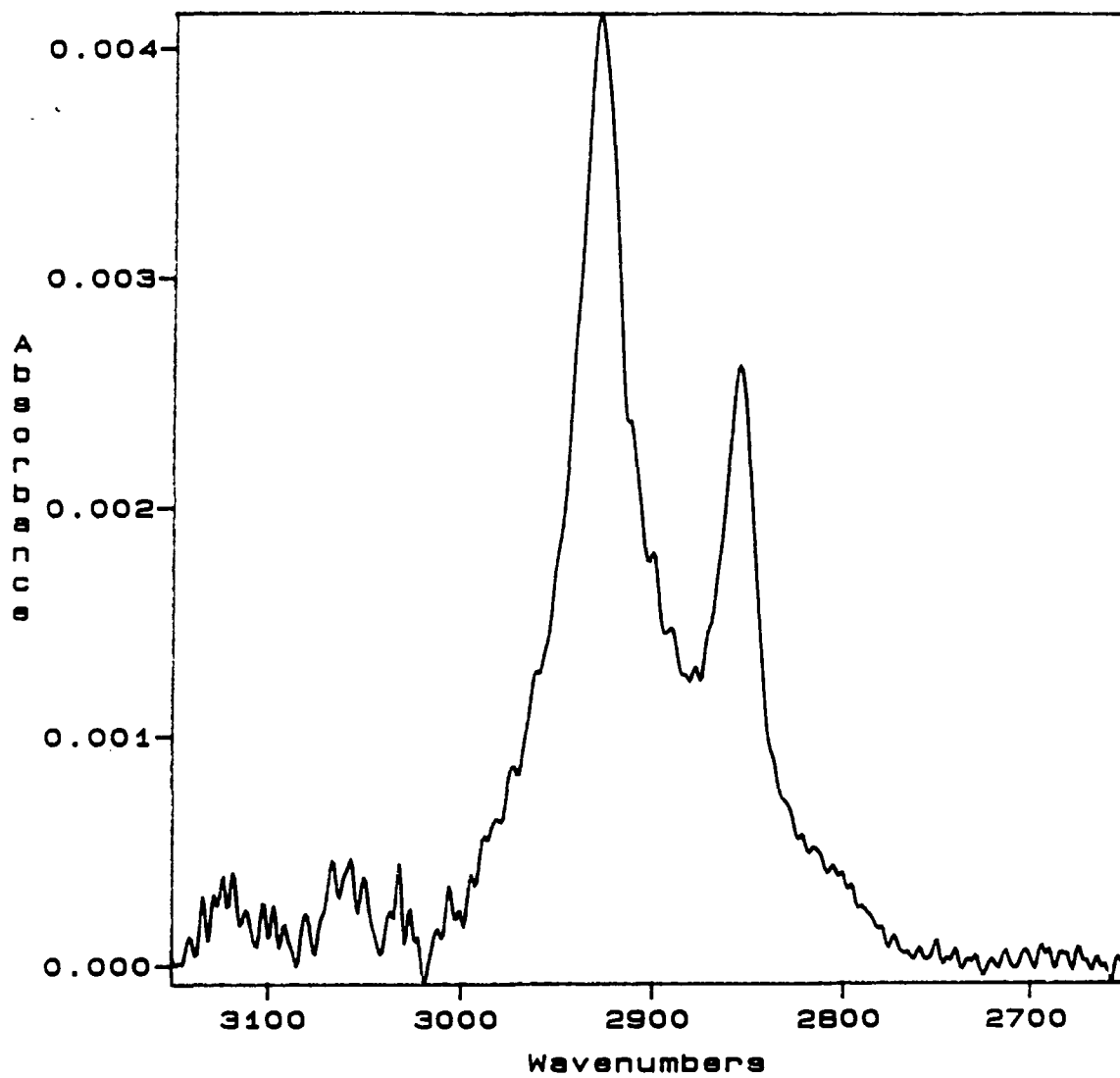
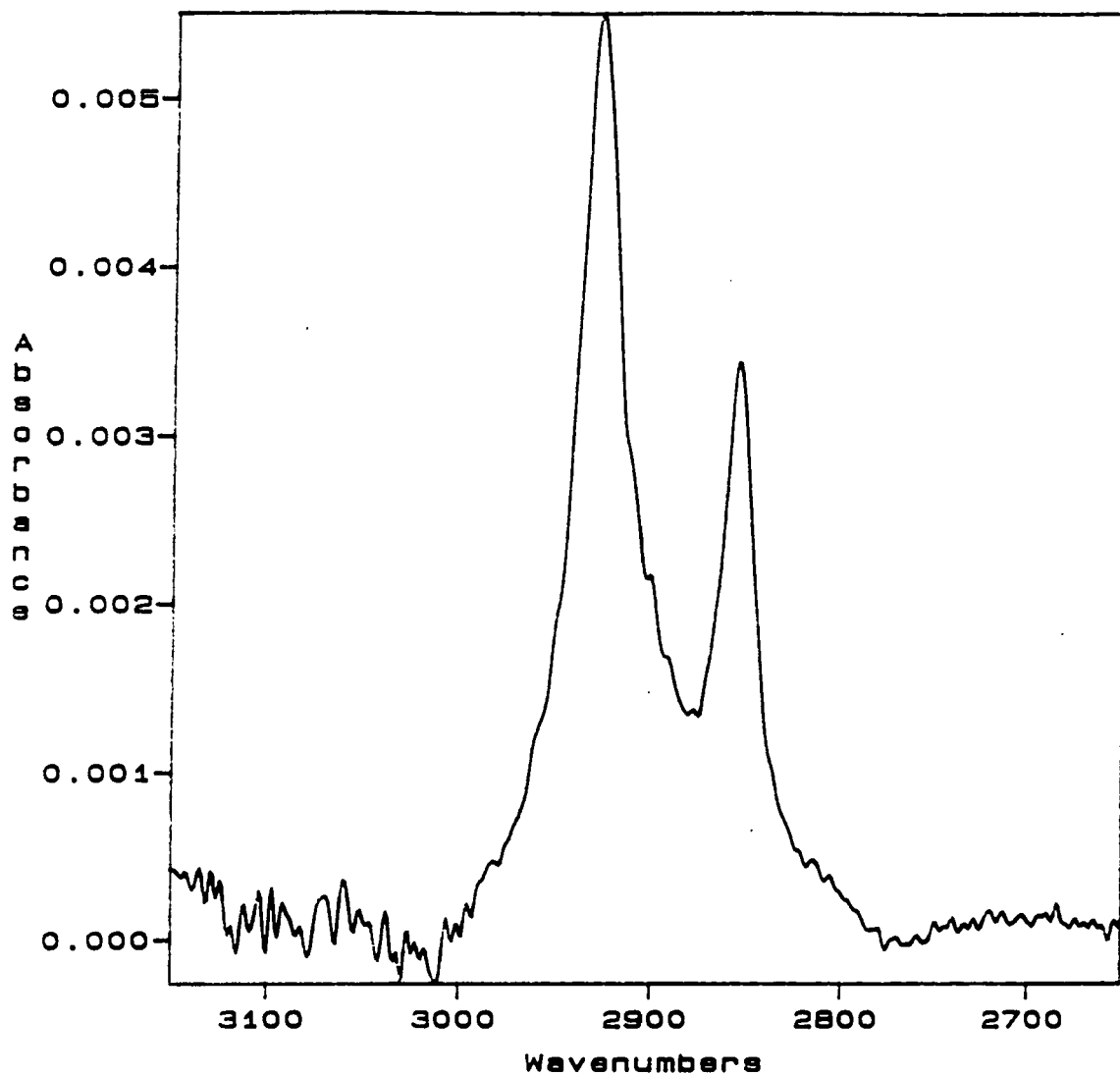Figure 6.30   Unpolarized ATR Spectrum of 7.4mM 1,12-diaminododecane
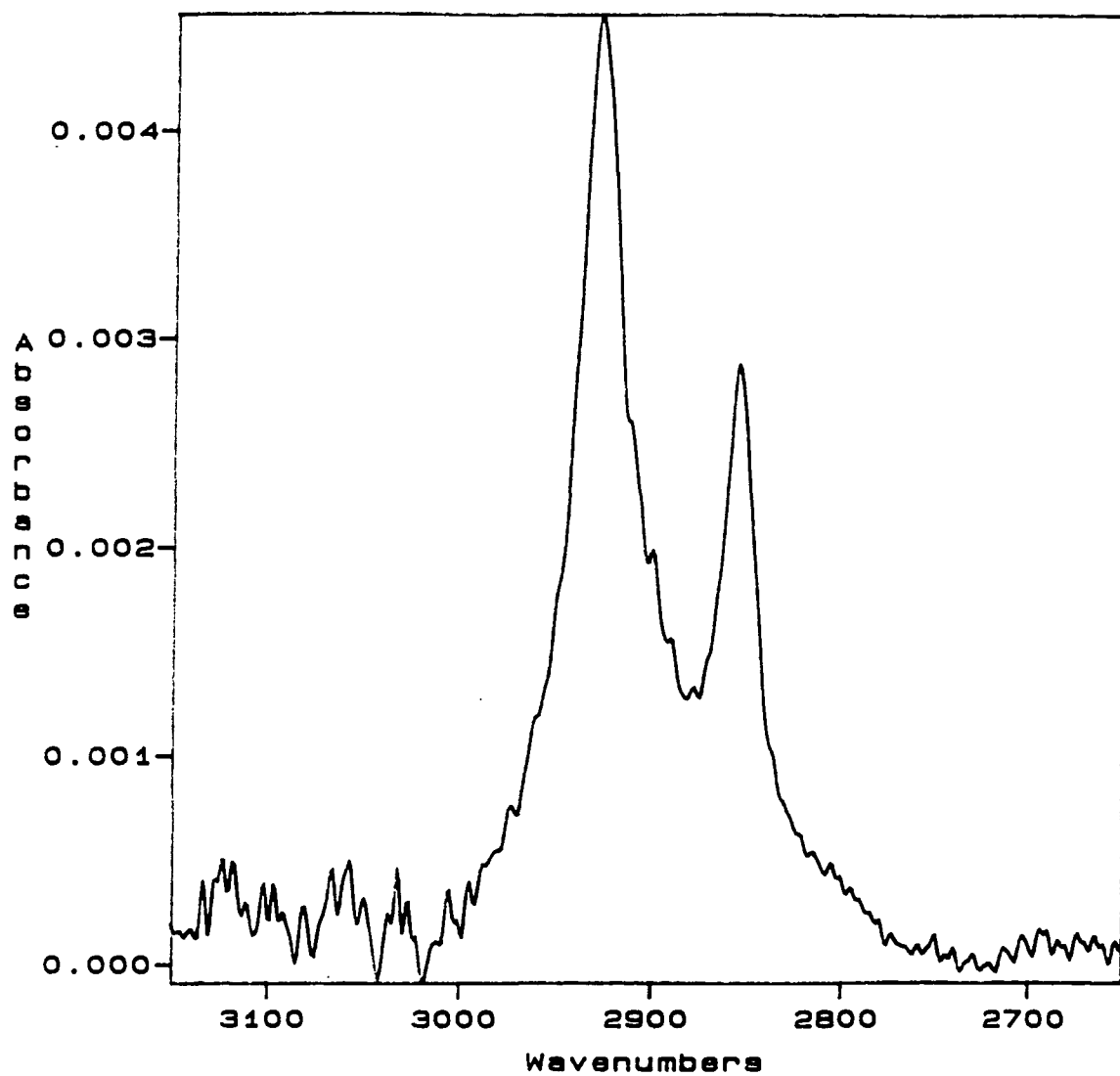
Figure 6.31   Unpolarized ATR Spectrum of 11.7mM 1,12-diaminododecane

Figure 6.32
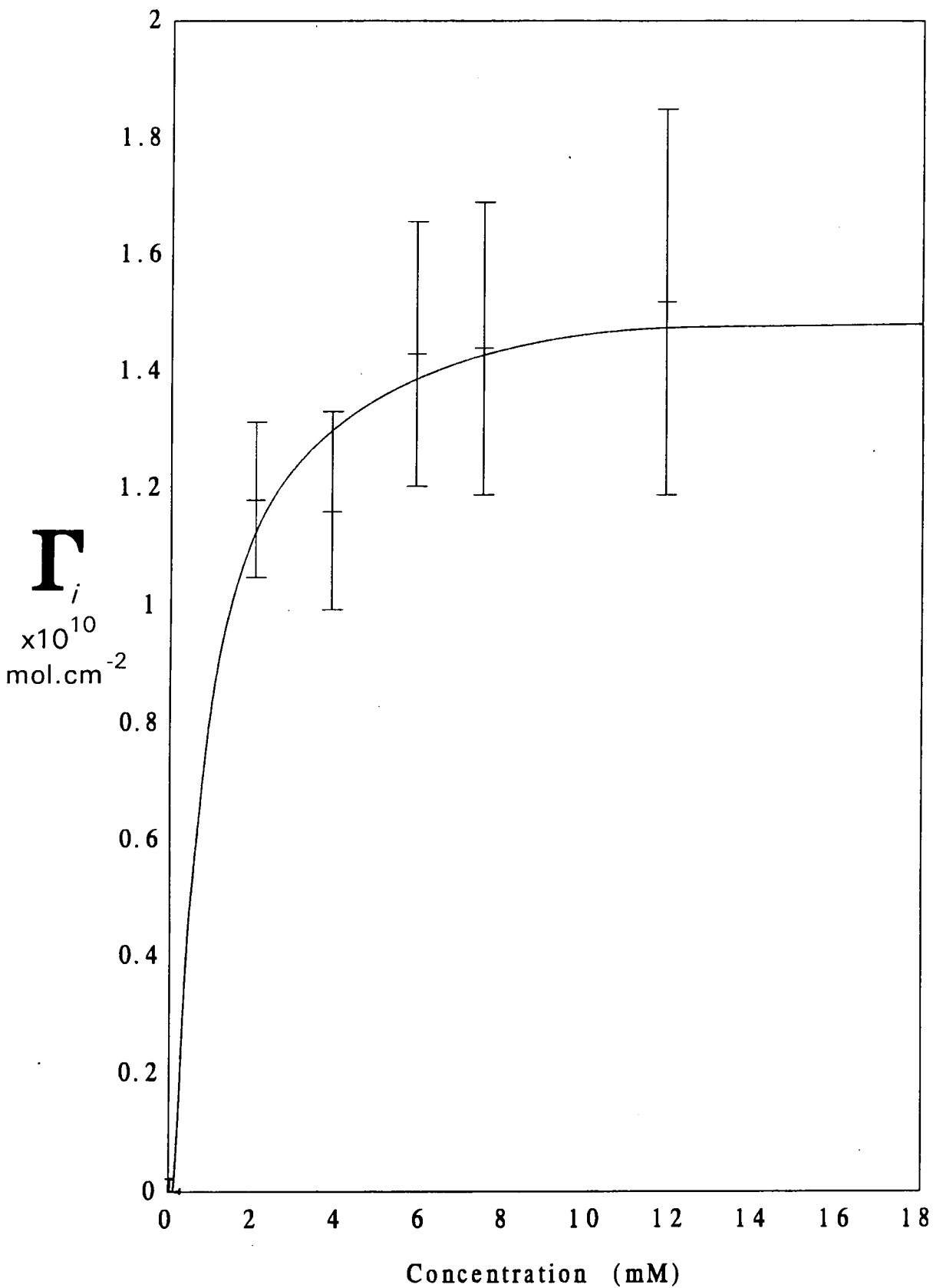Adsorption Isotherm for 1,12-diaminododecane

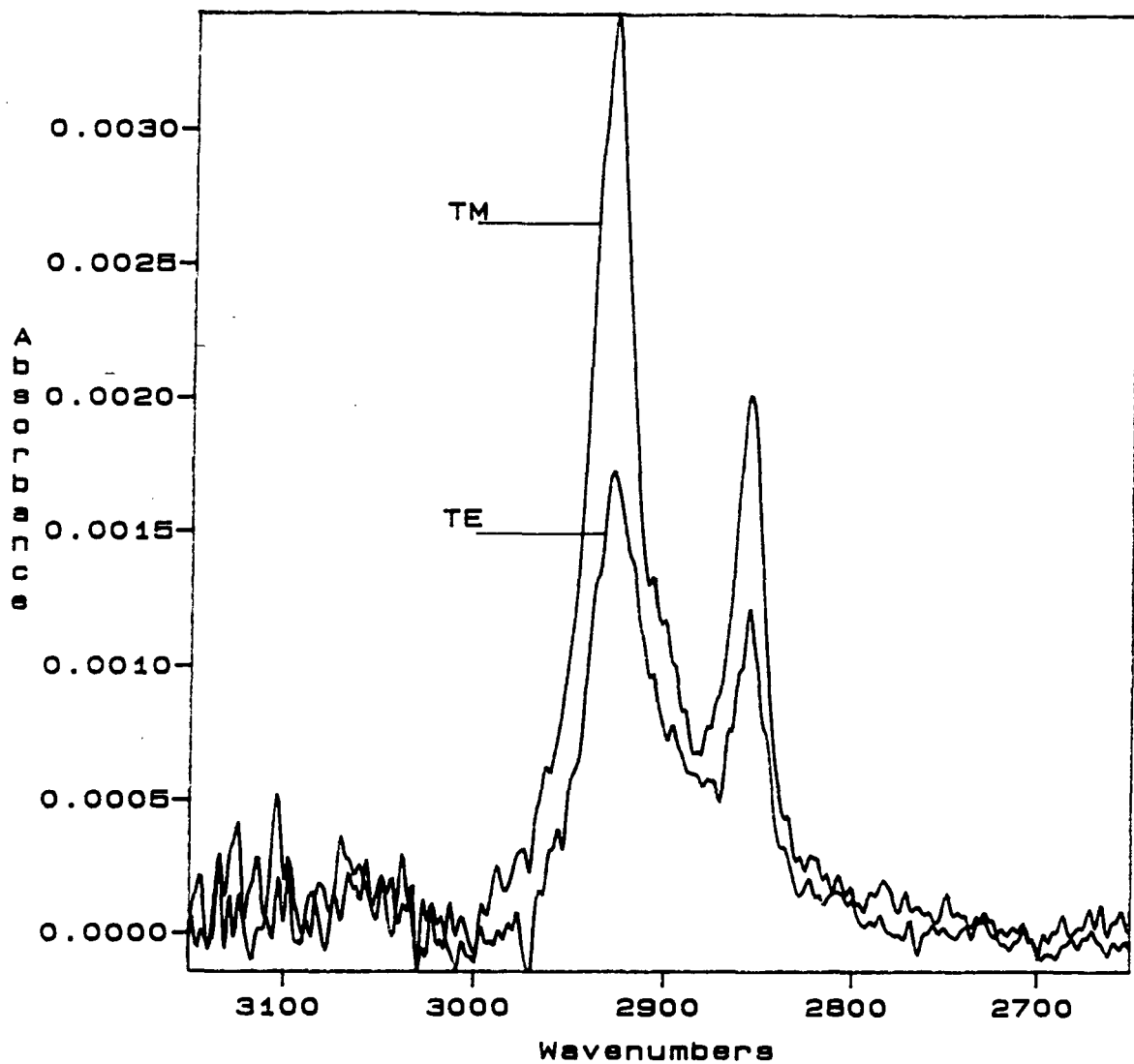Figure 6.33   TE and TM Polarized Spectra of 1.9mM 1,12-diaminododecane

Figure 6.34   TE and TM Polarized Spectra of 3.7mM 1,12-diaminododecane
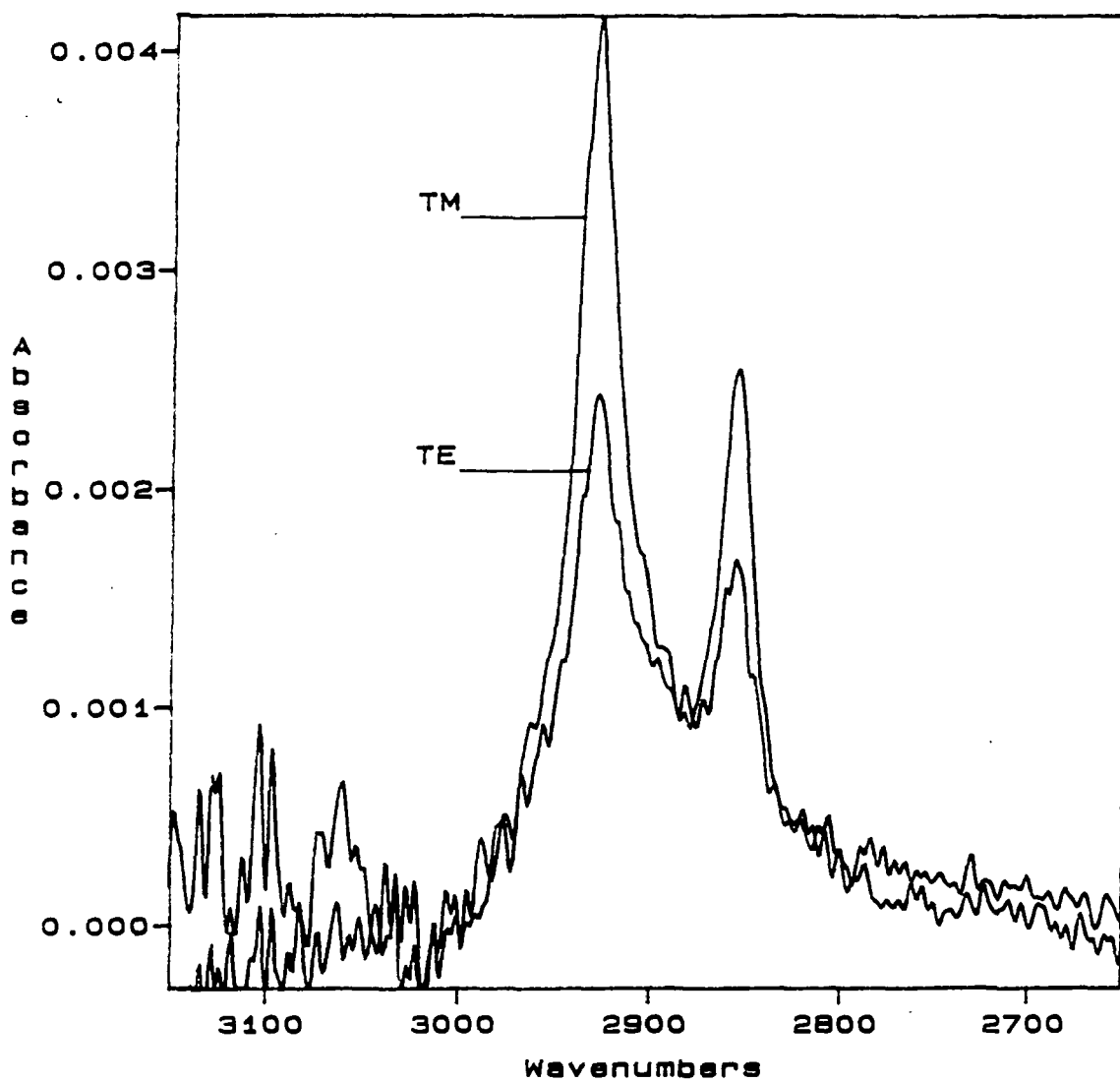
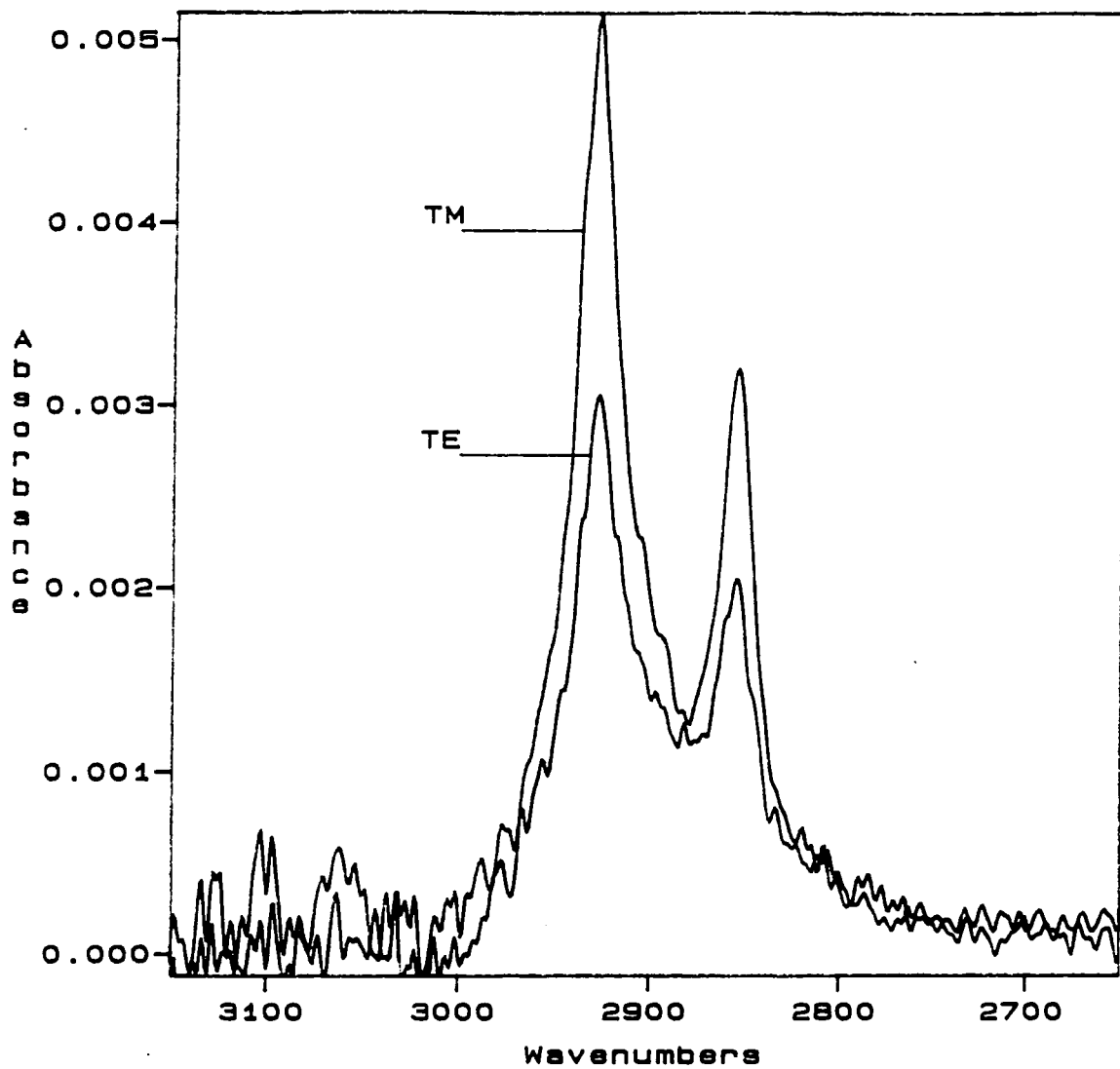Figure 6.35   TE and TM Polarized Spectra of 5.8mM 1,12-diaminododecane

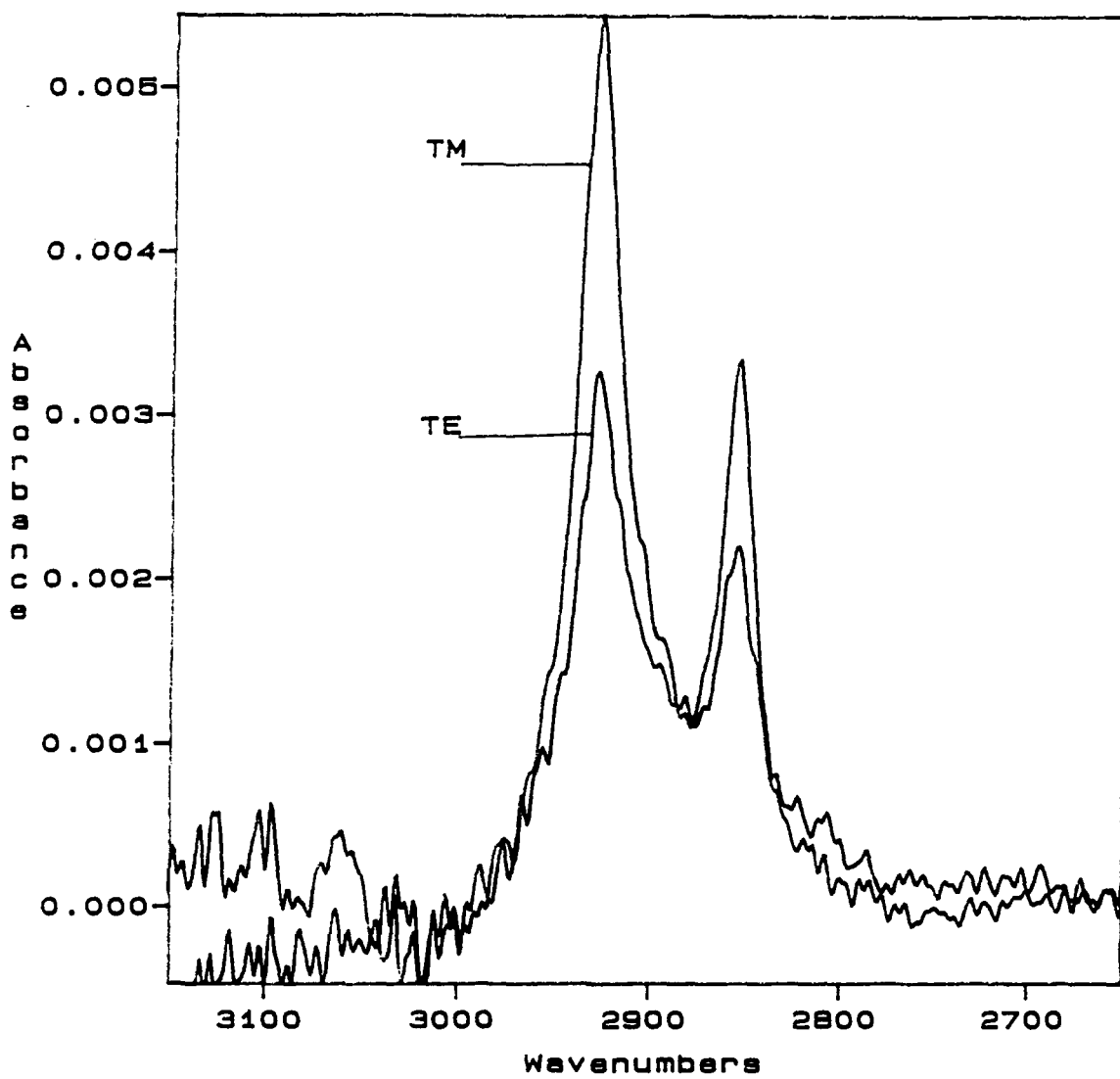Figure 6.36   TE and TM Polarized Spectra of 7.4mM 1,12-diaminododecane

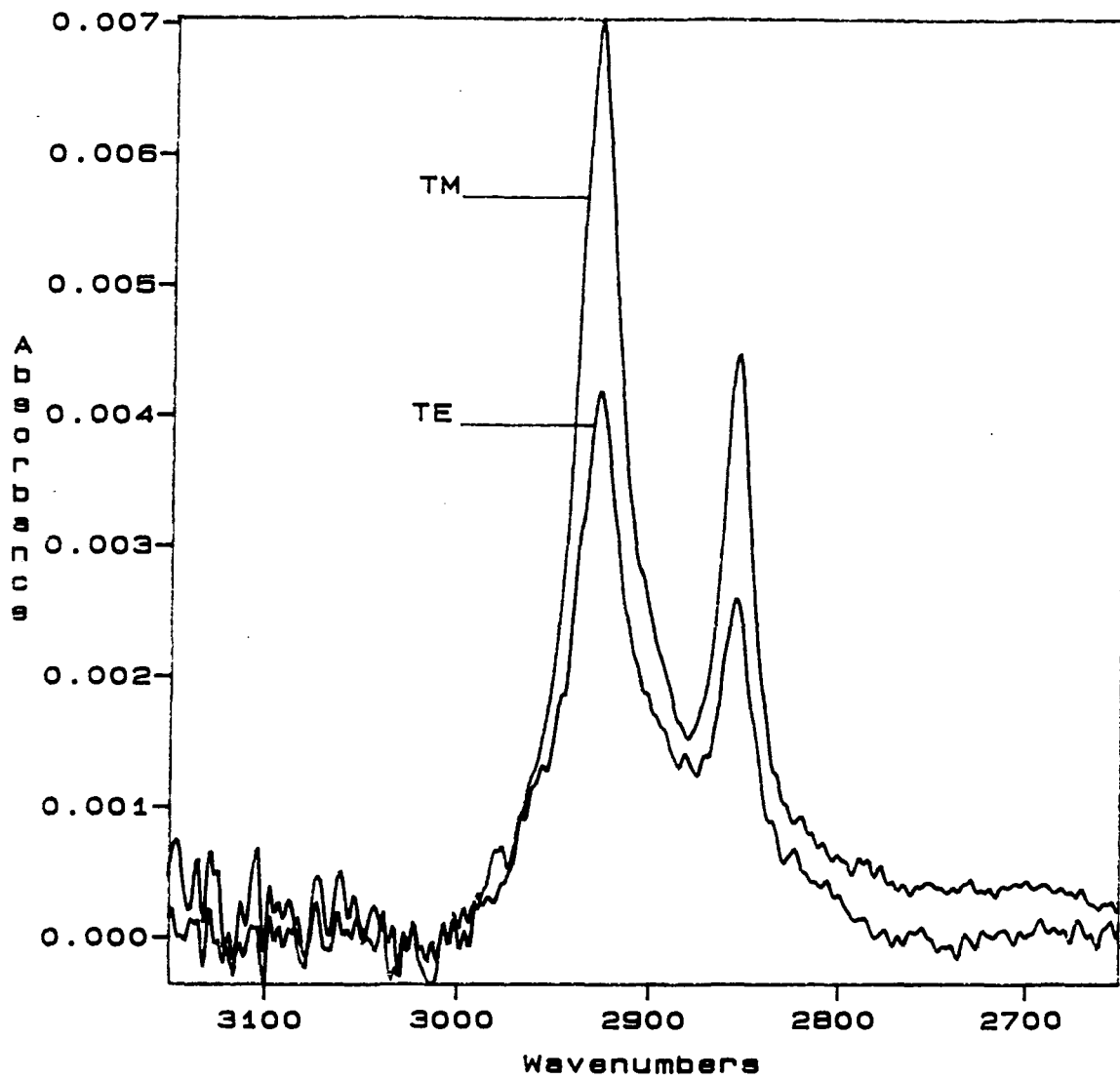Figure 6.37   TE and TM Polarized Spectra of 11.7mM 1,12-diaminododecane

Figure 6.38   ATR Spectra of 11.7mM 1,12-diaminododecane, 11.9mM Hexadecane

and the Difference
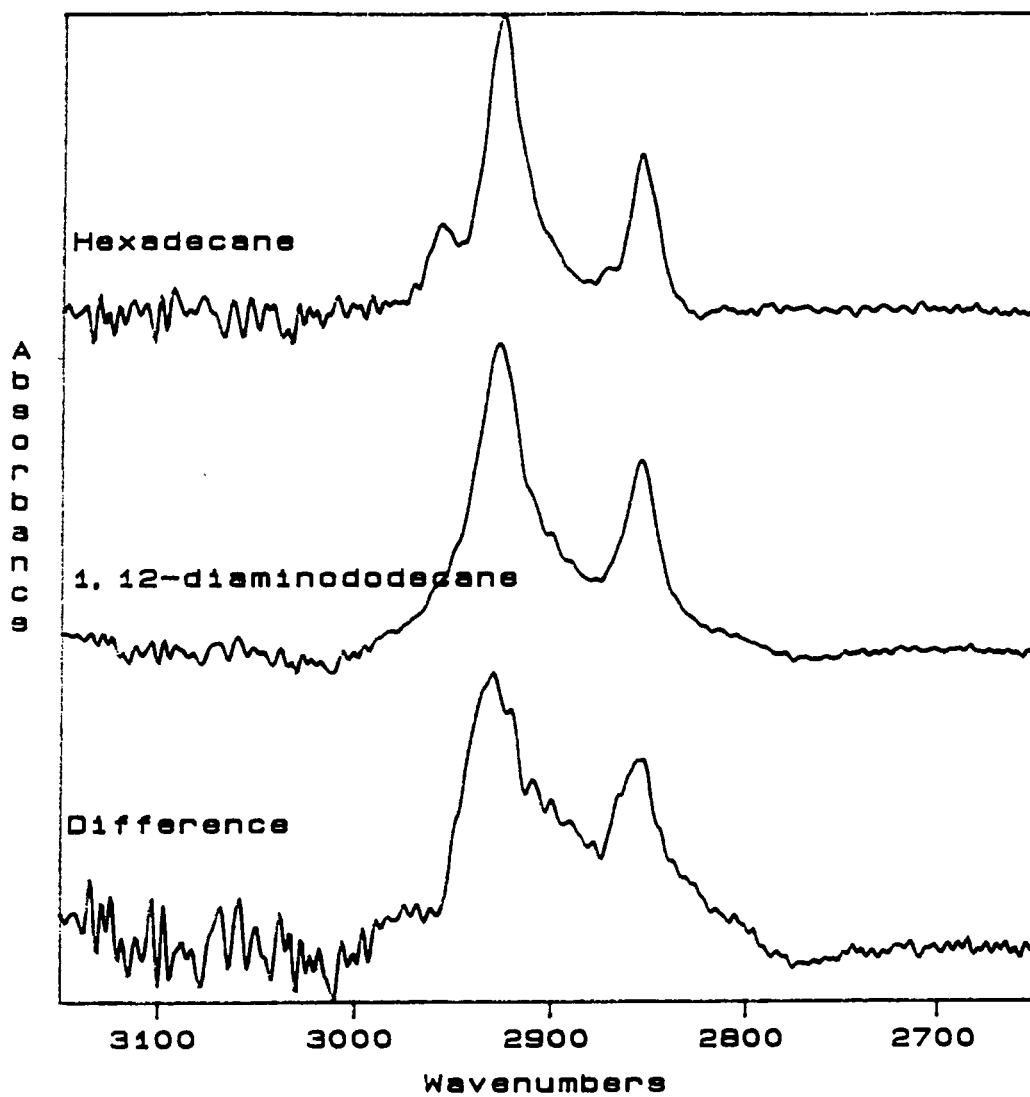
Figure 6.39   Transmission Spectrum of 15mM Didecylamine
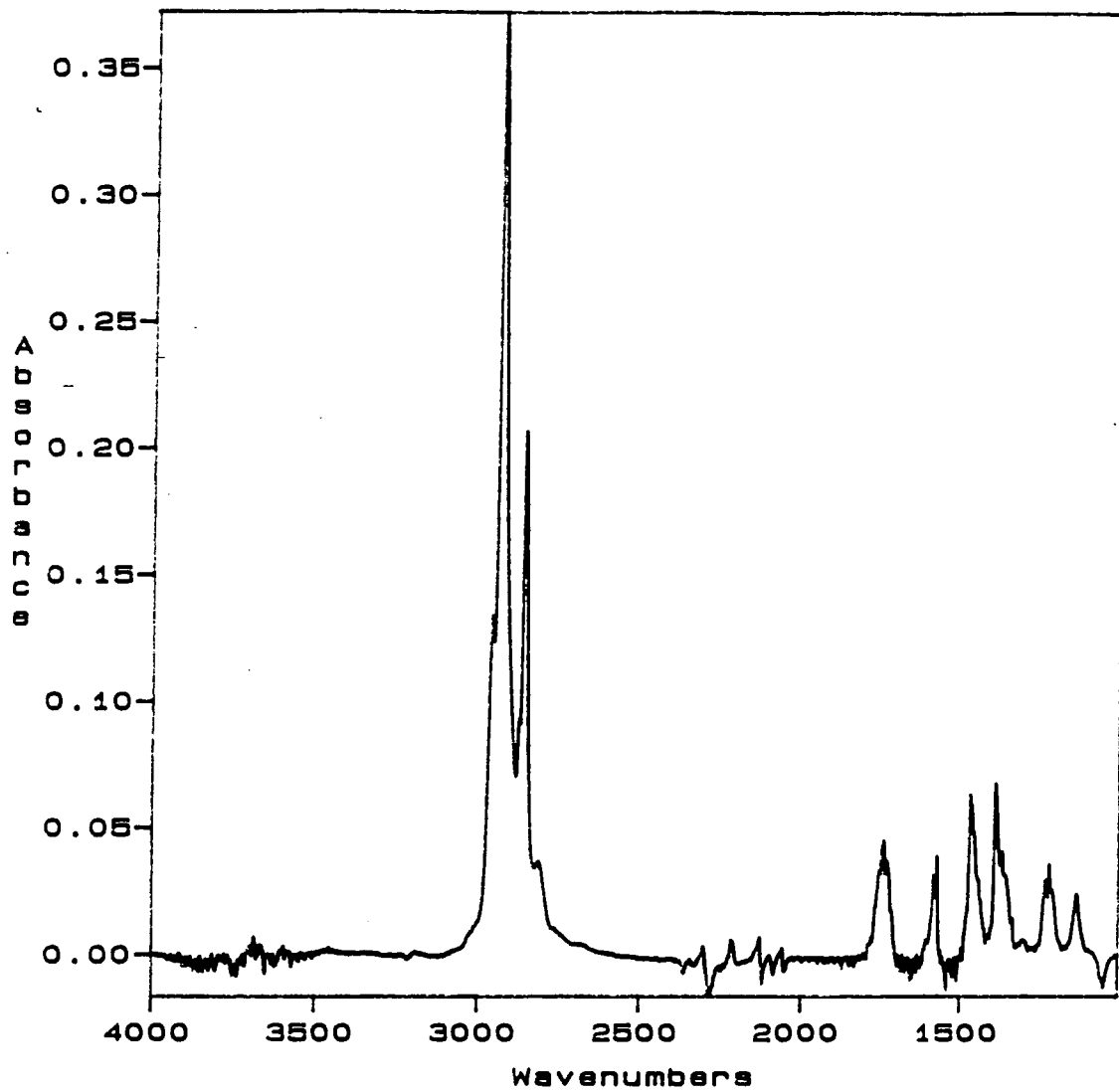
Figure 6.40   Expanded Transmission Spectrum of 15mM Didecylamine
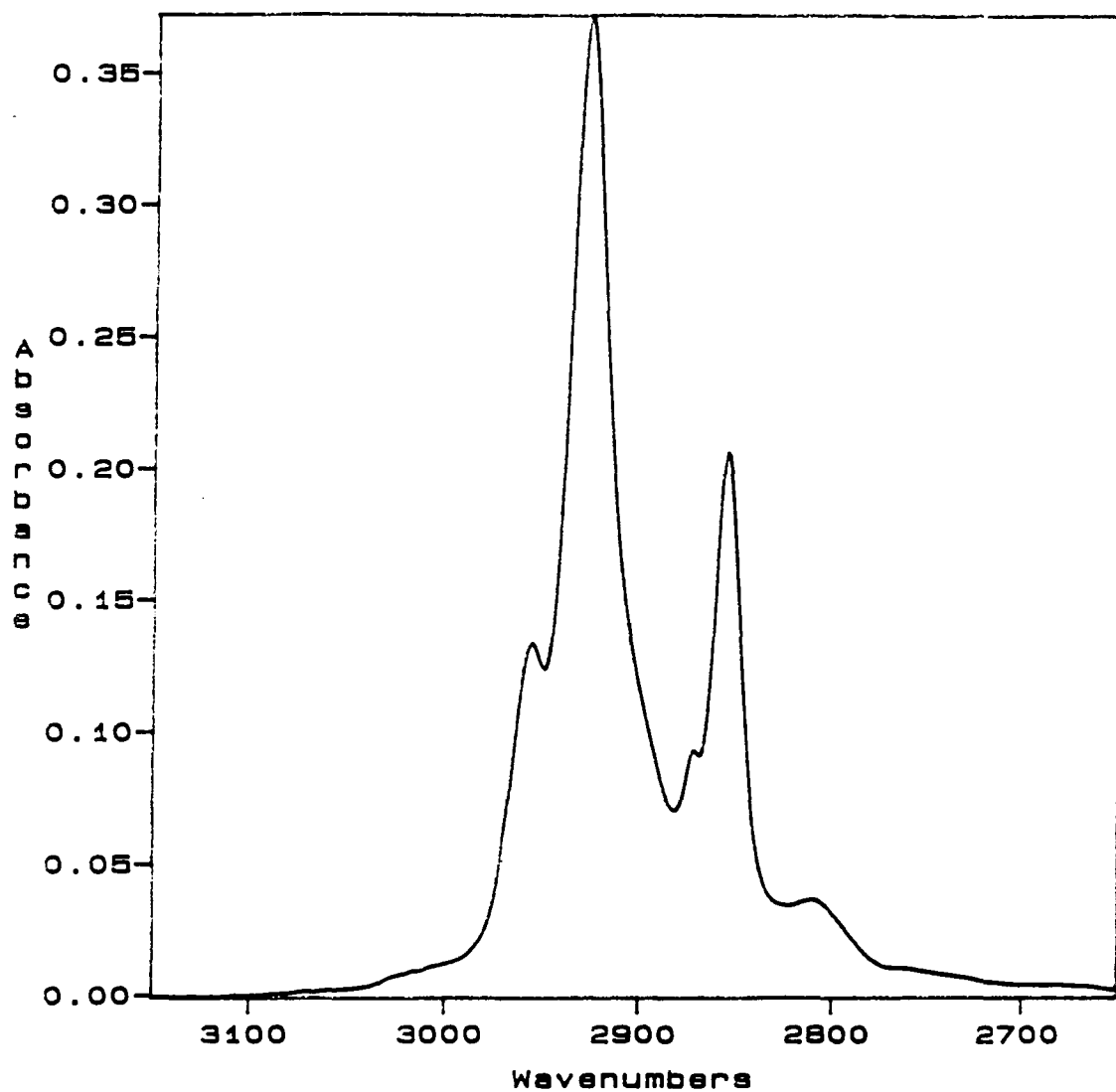
Figure 6.41   Unpolarized ATR Spectrum of 4.5mM Didecylamine
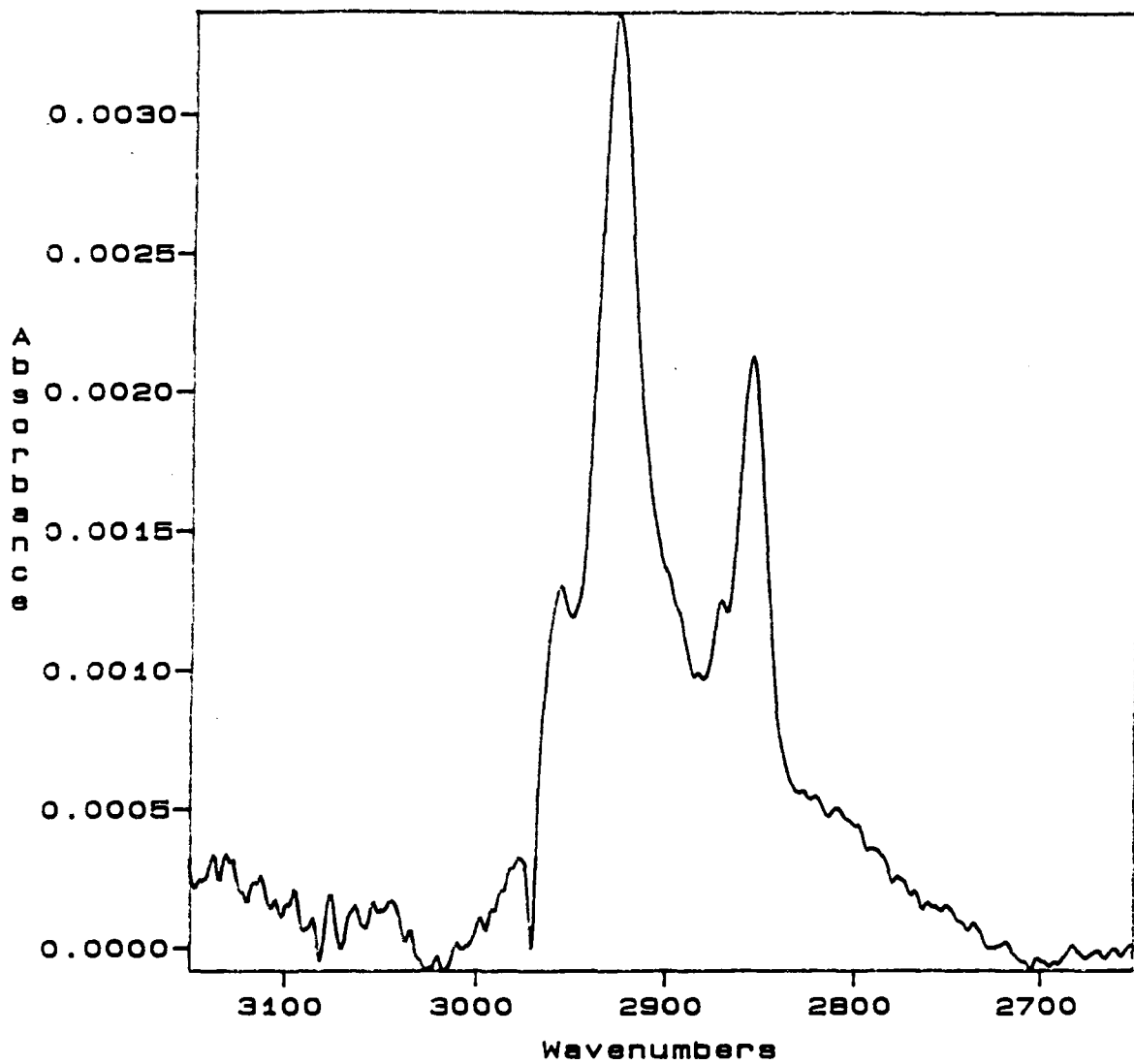
Figure 6.42   Unpolarized ATR Spectrum of 8.4mM Didecylamine

164
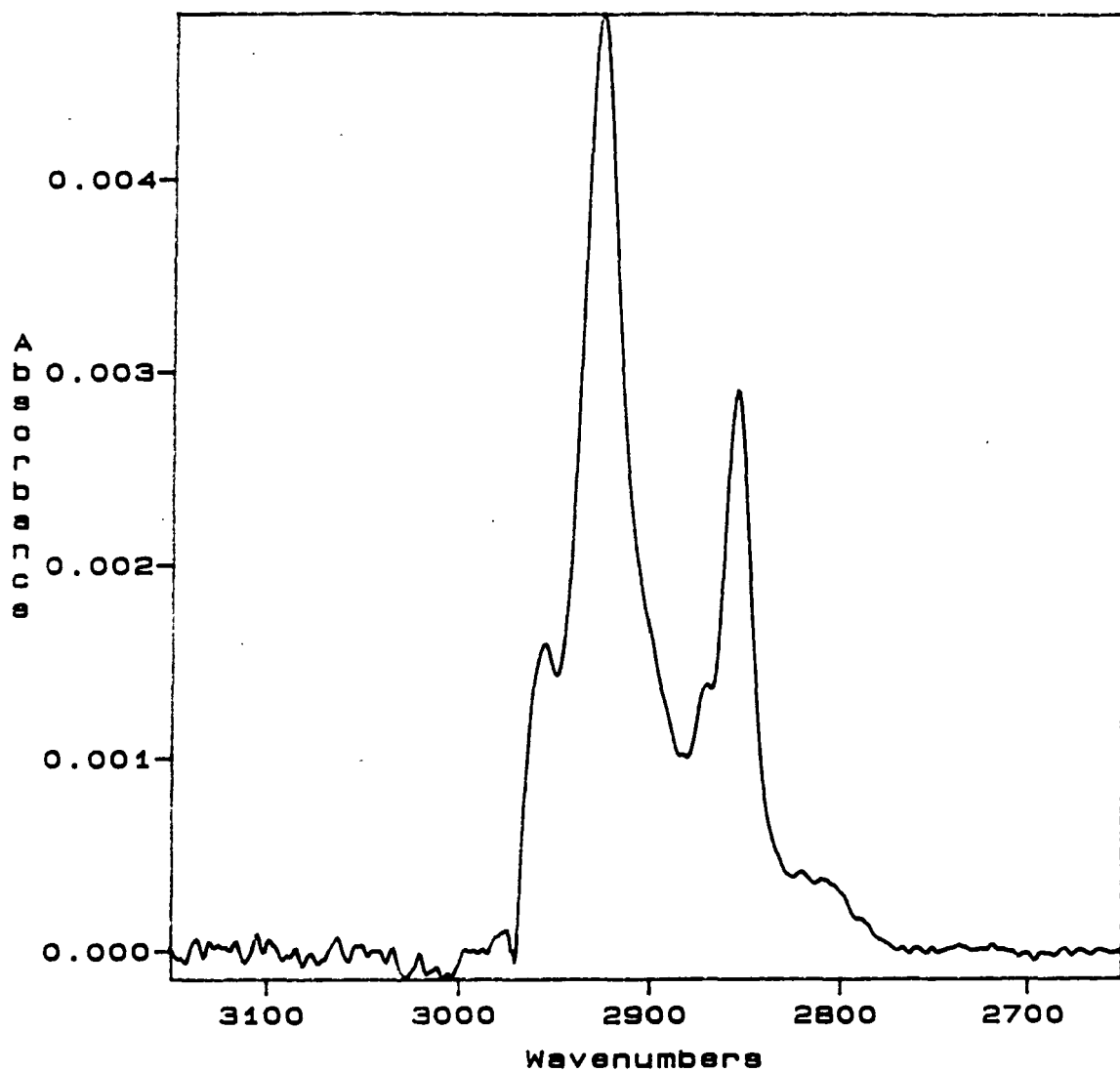
Figure 6.43   Unpolarized ATR Spectrum of 11.7mM Didecylamine

Figure 6.44   Unpolarized ATR Spectrum of 15.0mM Didecylamine
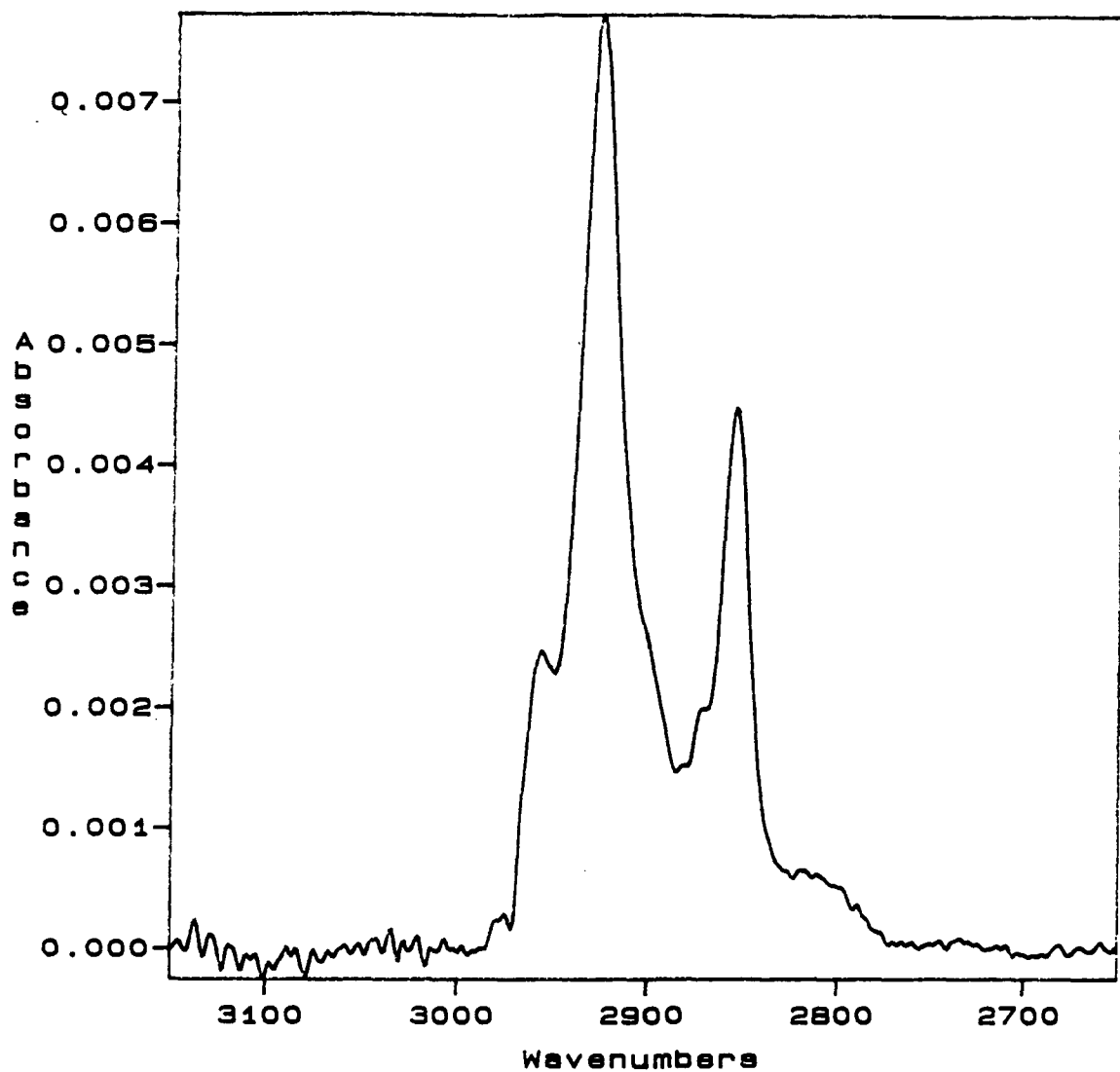
Figure 6.45
Adsorption Isotherm for Didecylamine

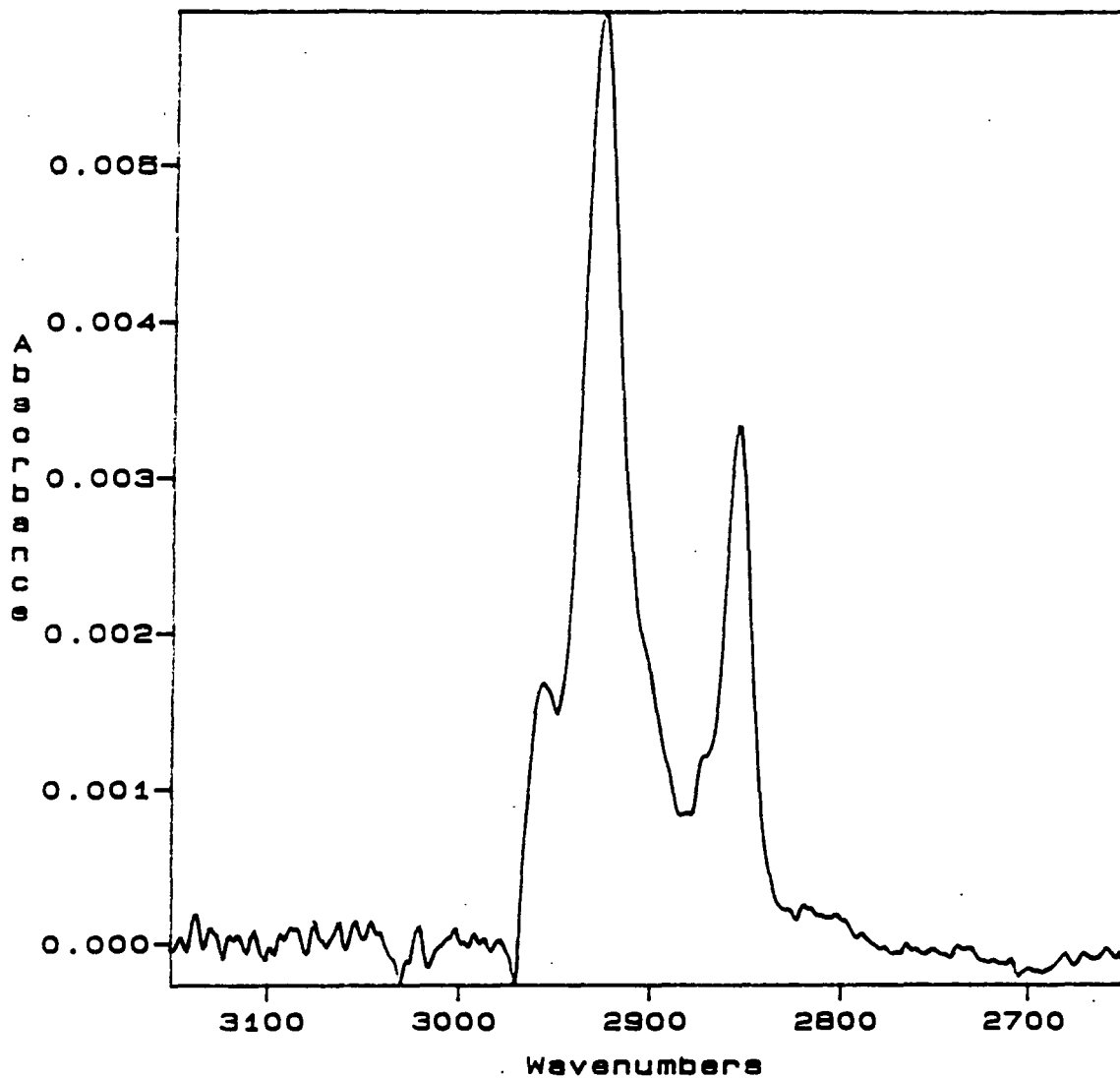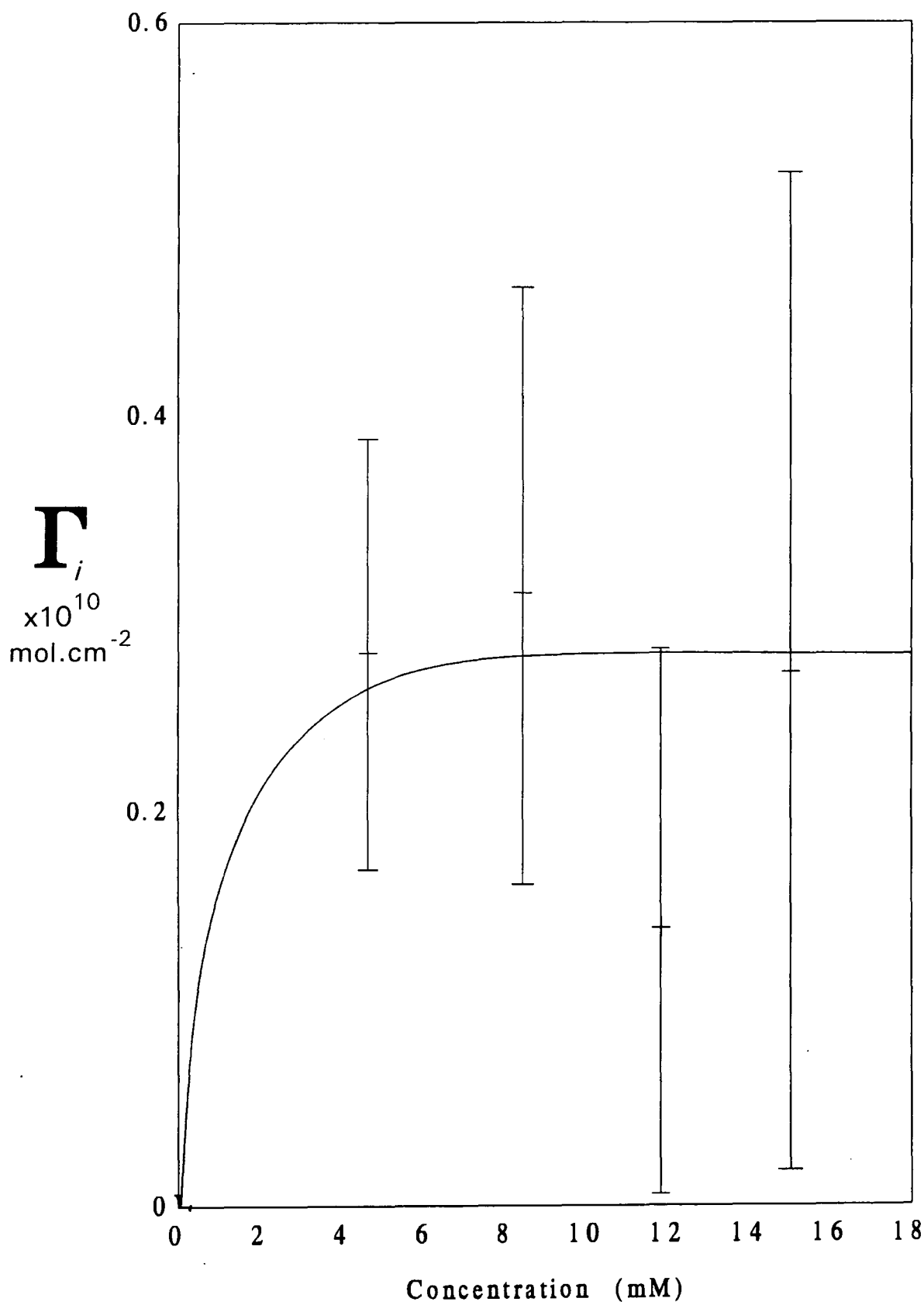Figure 6.46   TE and TM Polarized Spectra of 4.5mM Didecylamine
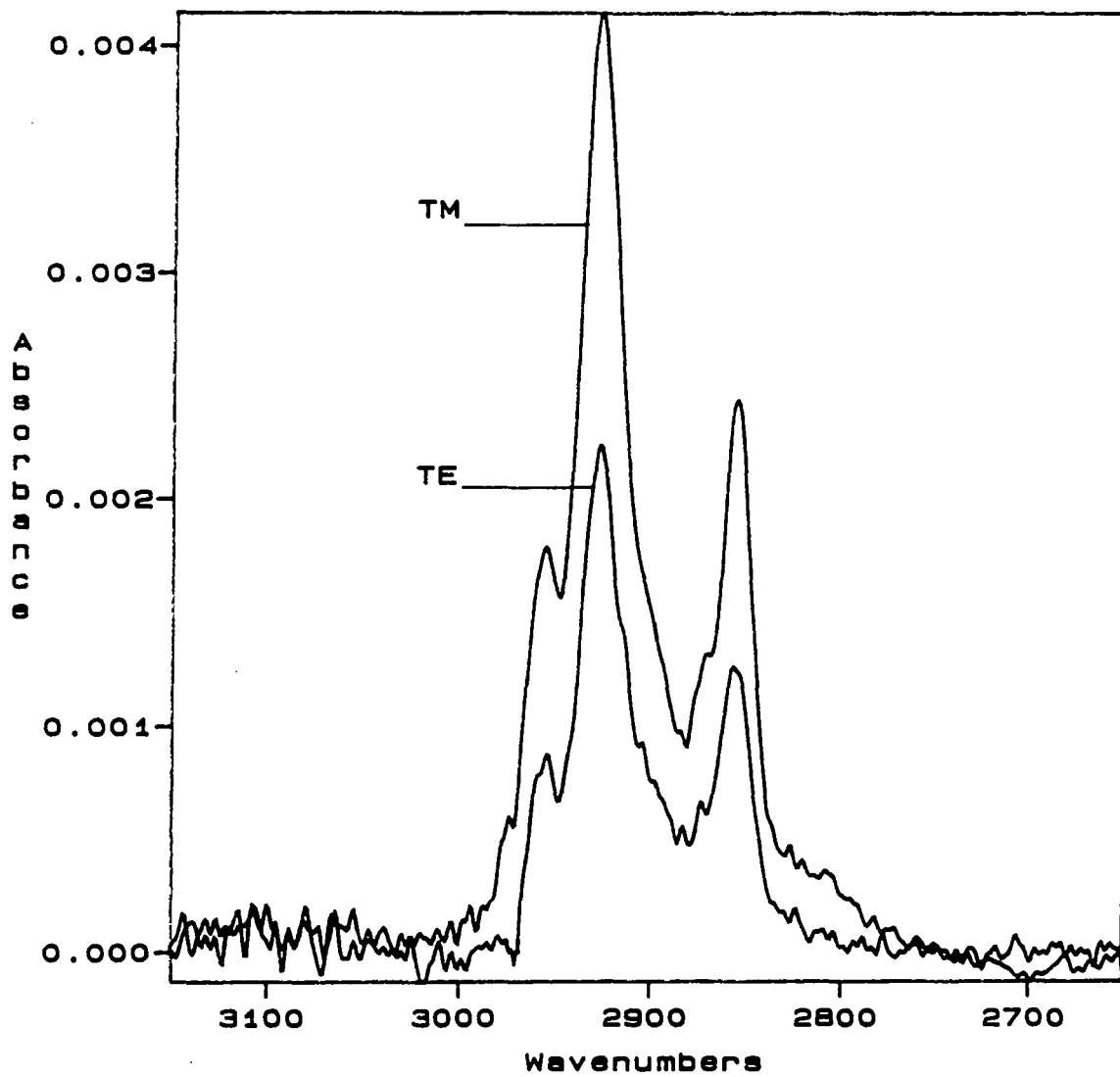
Figure 6.47   TE and TM Polarized Spectra of 8.4mM Didecylamine
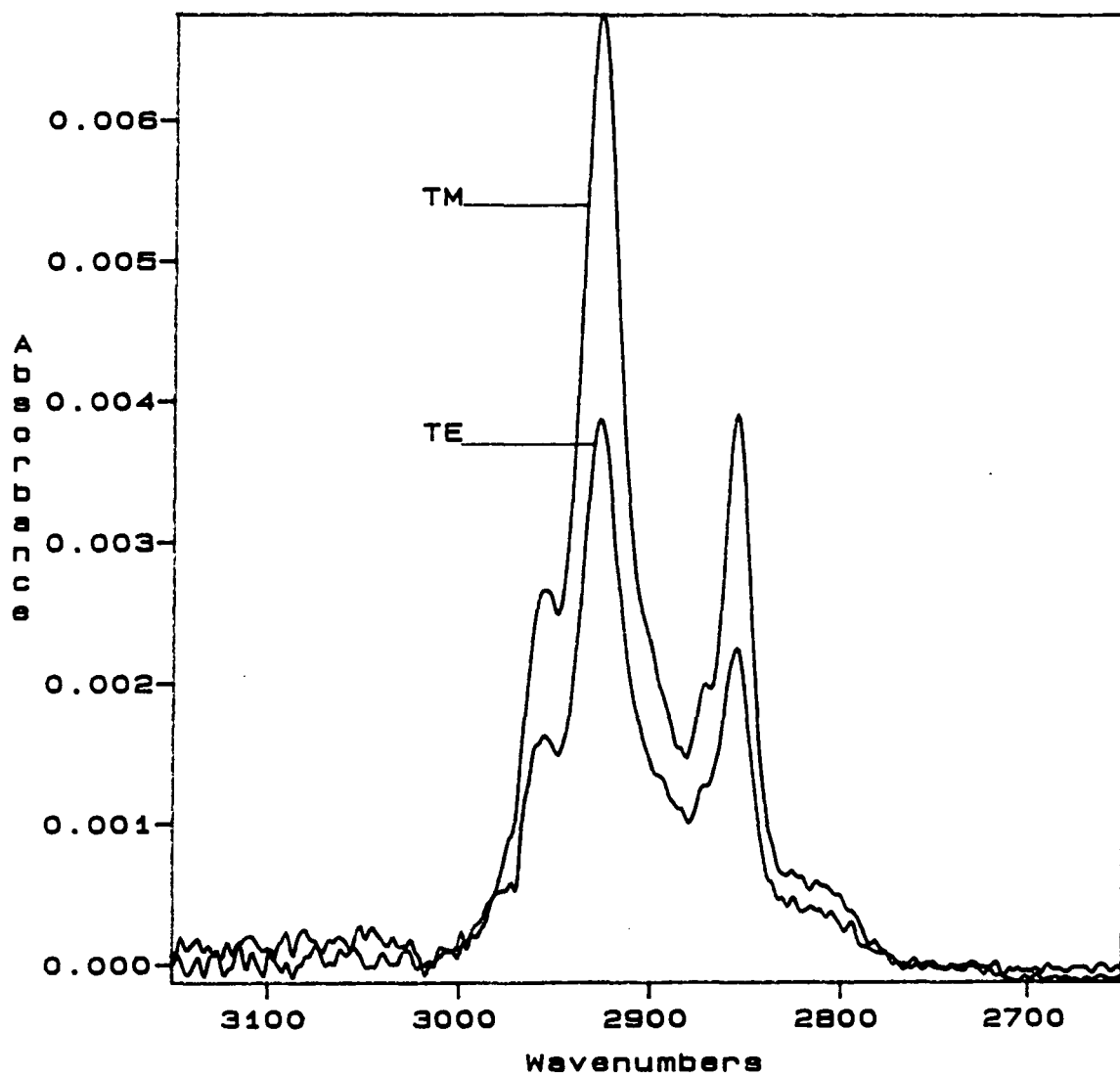
Figure 6.48   TE and TM Polarized Spectra of 11.7mM Didecylamine
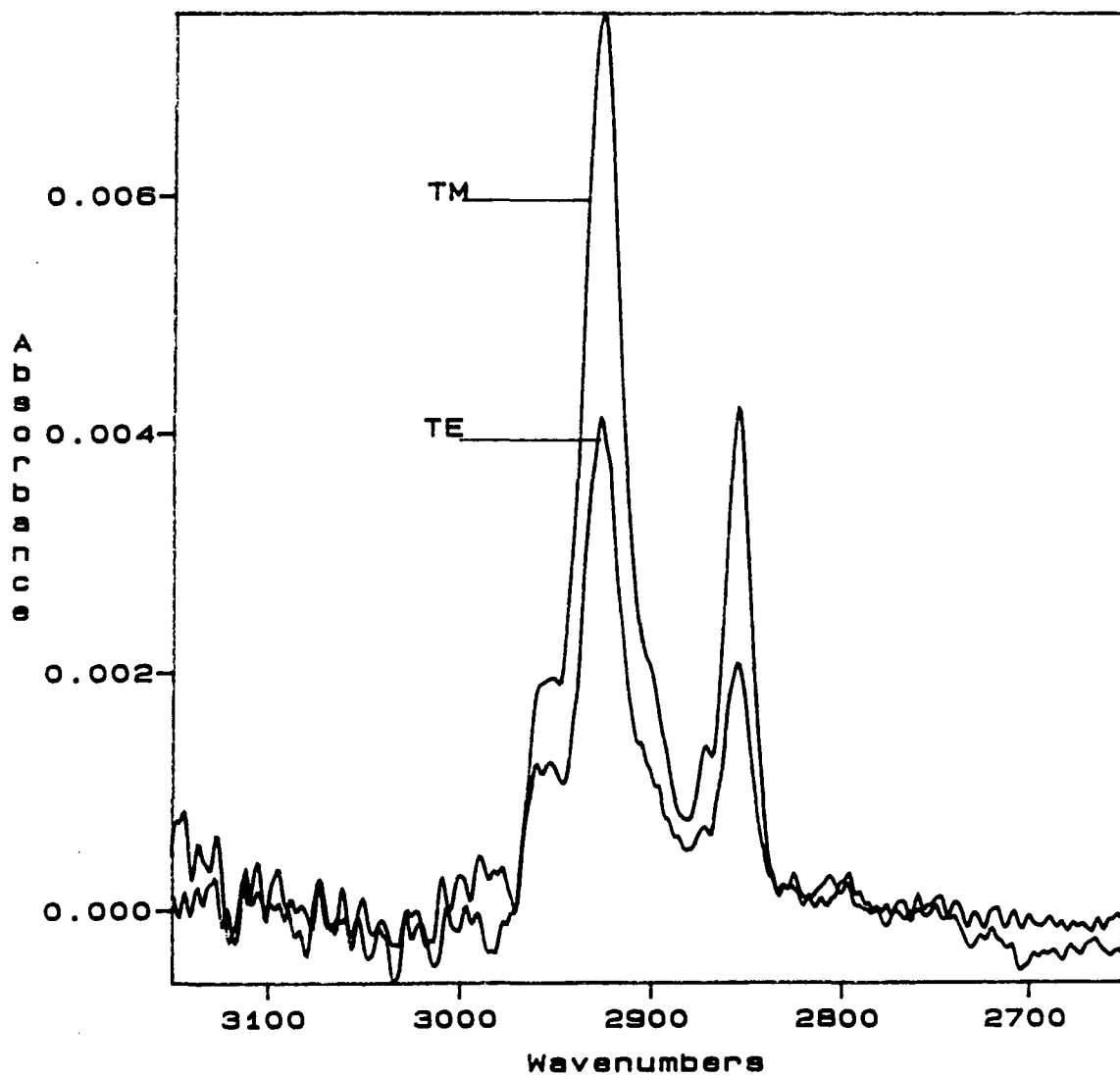
Figure 6.49   TE and TM Polarized Spectra of 15.0mM Didecylamine
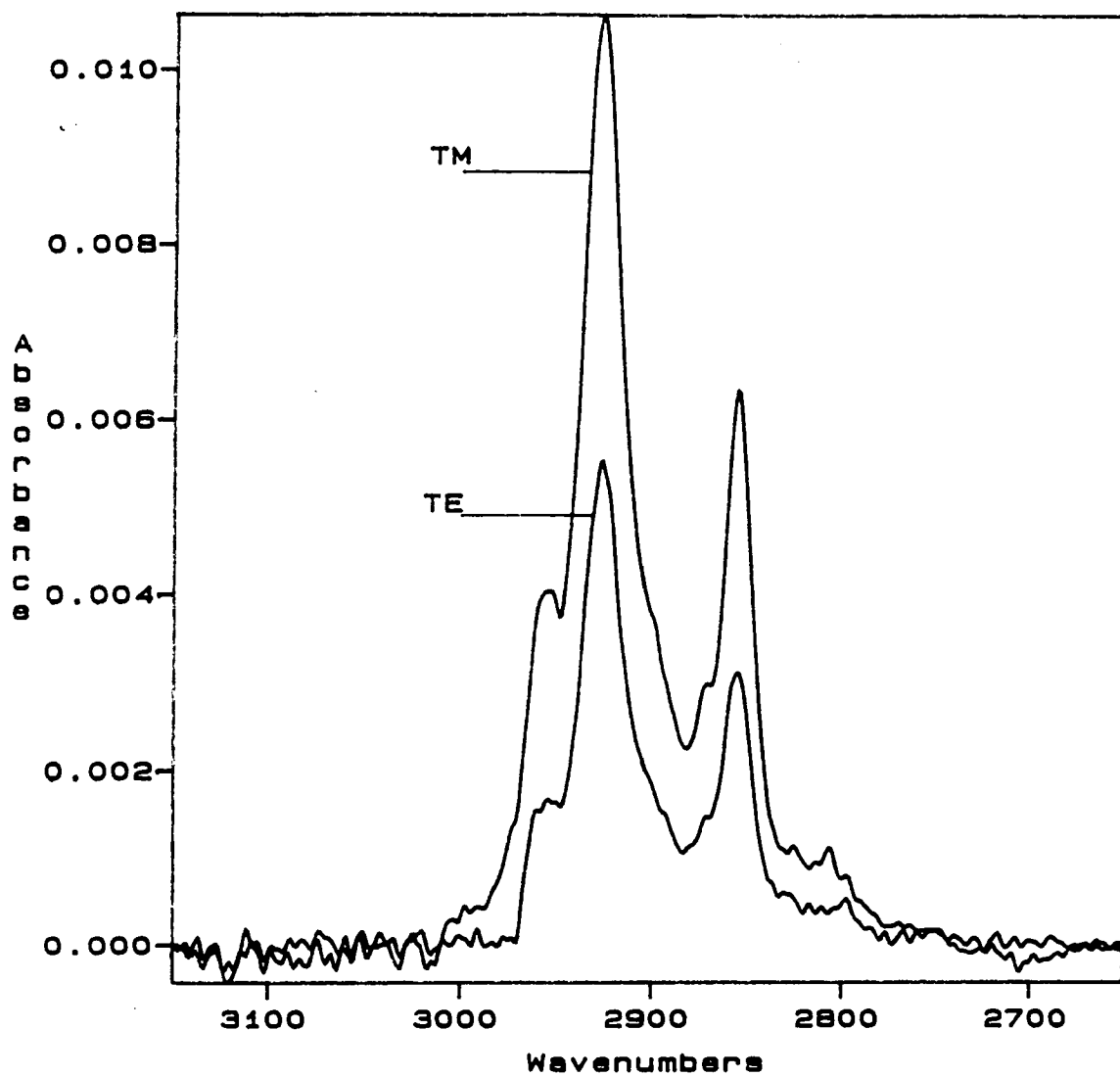
Chapter 7   Studies of the Adsorption Behaviour of Sorbitan Monopalmitate

7.1   Introduction

The previous chapter dealt with the adsorption of surfactants with amine headgroups from deuterated toluene onto a silica surface. This chapter describes studies of the adsorption of a surfactant with a sorbitan (sugar) headgroup in the same solvent/surface system. In the amine studies the bands associated with the headgroup were too weak to enable the nature of the interaction between the headgroup and the surface to be studied. However, the CH stretching bands associated with the aliphatic tail allowed quantification of the adsorbed amount and the orientation of the tails within the adsorbed layer. With sorbitan monopalmitate the opposite is true. Upon adsorption the infrared spectrum of sorbitan monopalmitate changes significantly. These changes allow the nature of the headgroup-surface interaction to be studied but prevent any truly quantitative analysis of the surface excess concentration. Due to the difficulties in quantifying Γ_i an adsorption isotherm is not presented.

7.2 Experimental

7.2.1 Materials

Sorbitan monopalmitate (a.k.a. Span 40) (Sigma) was used as received. Fully deuterated toluene (99+atom%, Aldrich) was distilled prior to use. Methanol (AnalR, BDH), chloroform (99.9% ACS HPLC grade, Aldrich) and 2-propanol (99.5% HPLC grade, Aldrich) were used as recieved.

7.2.2 Cleaning of the Squarecol Cell

The cell body, lid, 'O'-rings and Teflon gasket were rinsed sequentially with deionized water, methanol and chloroform prior to use. The silicon ATR crystal was rinsed sequentially with deionized water, methanol and chloroform prior to being refluxed for a minimum of four hours in 2-propanol.

The cell components and ATR prism were handled with polythene gloves (RS Components) during assembly. Care was taken to handle the prism by the non-sampling faces only.

All glassware was cleaned using the same series of rinses as used for the ATR prism.

7.2.3 Spectroscopy

In order to gain an understanding of the nature of the bonding in solid sorbitan monopalmitate a melt-cast film was prepared. Two KBr plates were polished and checked for cleanliness by IR spectroscopy. The plates were then place in an oven at 60°C. A few milligrammes of sorbitan monopalmitate were placed in the centre of one of the plates. The compound melted and the second plate was placed on top of the first. An even film, of indeterminate thickness was produced by applying gentle pressure to the upper plate. The assembly was allowed to cool and the sorbitan

monopalmitate layer solidified. A single beam spectrum of the film was recorded and ratioed against that of a single, clean, KBr plate.

A 7.5mM solution of sorbitan monopalmitate in D8-toluene was prepared. The spectrum of this solution in a 0.022cm pathlength transmission cell was recorded and ratioed against that of the open beam.

A spectrum of the empty Squarecol cell was recorded and ratioed against that of the open beam to check for cleanliness of the prism. The cell was then filled with D8-toluene and the spectrum recorded. A gold-wire polarizer (Graseby Specac) was placed in the beam and spectra were recorded with the polarizer in the TE and TM positions. These three spectra of D8-toluene provided the set of single-beam background spectra. The cell was emptied and blown dry in a stream of dry nitrogen. The cell was filled with the 7.5mM sorbitan monopalmitate solution and spectra were recorded without a polarizer and with the polarizer in the TE and TM positions. These spectra were then ratioed against the approprieate background spectrum. Spectra of the solution were recorded in this way at hourly intervals for the next five hours. The polarizer was then left in the instrument in the TM position and spectra were recorded at hourly intervals for a further ten hours.

The instrumental conditions under which the spectra were acquired are given in table 6.1.

7.3   Results and Discussion

7.3.1   Transmission Spectrum of Solid Sorbitan Monopalmitate

Sorbitan monopalmitate is one of the group of surfactants marketed under the name of Span, and is sometimes called Span 40. The Span surfactants consist of a sorbitan headgroup connected, *via* an ester linkage to an aliphatic chain. The headgroup is common to all the Spans but the aliphatic chain varies. Sorbitan monopalmitate (Span 40) consists of a sorbitan headgroup and a C_{16} chain. In fact, the commercial mixture used in this study also contains approximately 10% of the C_{18} derivative, sorbitan monostearate. The structure of sorbitan monopalmitate is shown in figure 7.1.

The full-range spectrum of the melt-cast film is shown in figure 7.2. The principal bands in this spectrum are assigned in table 7.1.

Table 7.1   Band Assignments in the Spectrum of a Sorbitan Monopalmitate Melt-Cast Film.

Band Position (cm^{-1})	Assignment
3385	OH Stretching
2918	Methylene Antisymmetric CH Stretching
2851	Methylene Symmetric CH Stretching
1736	Carbonyl CO Stretching
1468	Methylene CH Bending

The OH stretching band is very broad. Such breadth shows that the OH groups are hydrogen bonded, indicating that, in the solid, the hydroxyl groups on one headgroup form hydrogen bonds with those on a neighbouring headgroup.

The frequency of the methylene antisymmetic and symmetric stretching vibrations (2918 and 2851cm^{-1} respectively) indicate that the aliphatic chains are largely in the all-trans conformation. Such conformations occur when the chains exist in crystalline domains. Further evidence for crystalline packing of the aliphatic chains can be found in the region of the spectrum between 1350 and 1200cm^{-1}. This region is shown expanded in figure 7.3. A series of regularly spaced bands can be observed. This *band progression* is associated with perturbed CH$_2$ wagging vibrations [30, 103-107]. When methylene groups are arranged in a coplanar, trans conformation they may interact with one another such that they vibrate with various phase differences. In the solid phase then, sorbitan monopalmitate exists in a crytalline state with extensive hydrogen bonding between hydroxyl groups.

7.3.2   Transmission Spectrum of Sorbitan Monopalmitate in Solution

The transmission spectrum of a 7.5mM solution of sorbitan monopalmitate in a 0.022cm pathlength cell is shown in figure 7.4. The region 4000-2700cm^{-1} is shown expanded in figure 7.5. The antisymmetric and symmetric methylene CH stretching bands are centred at 2926 and 2854cm^{-1} respectively. These frequencies are typical of aliphatic chains in solution and indicate a high proportion of gauche conformers. The area under these peaks from 3000-2800cm^{-1} is 8.547cm^{-1}. As the pathlength is 0.022cm, the molar extinction coefficient, ε, is 51800dm^{3}mol^{-1}cm^{-2}.

The OH stretching region looks quite different to that of the melt-cast film. A band can be seen at 3575cm^{-1} which is at a higher frequency and is narrower than the broad OH stretching band which was observed in the spectrum of the melt-cast film. This band is associated with the OH stretching of "free" (i.e. non-hydrogen-bonded) hydroxyls. A weak, broad band can be seen on the low frequency side of this hydroxyl band. This is due to some hydrogen-bonded hydroxyls. These species may arise from the formation of hydrogen bonded sorbitan monopalmitate dimers (or higher aggregrates) or from the sorbitan headgroup associating with trace water. No special

precautions were taken to ensure that the surfactant was dry and so the hydrogen-bonded hydroxyls may be due to the partial hydration of the headgroup. The broad 'bonded' band is of lower intensity compared to the CH stretching peaks than in the spectrum of the melt-cast film. This, together with the presence of a free OH stretching band, indicates that upon dissolution, the sorbitan monopalmitate forms a solution in which single, unassociated molecules are present.

7.3.3   ATR Spectra of Sorbitan Monopalmitate Solutions

The unpolarized ATR spectrum of 7.5mM sorbitan monopalmitate obtained immediately after injection of the solution into the Squarecol is shown in figure 7.6. A distorted spectrum of atmospheric water vapour complicates the spectrum in the regions $4000\text{-}3560\text{cm}^{-1}$ and $1950\text{-}1500\text{cm}^{-1}$. The spectrum of water vapour displays rotational fine-structure and therefore consists of a number of narrow bands. The spectrum of water vapour is shown in figure 7.7. A change in the relative humidity within the spectrometer from one single-beam spectrum to the next leads to the appearance of water vapour bands in the resulting ratioed spectrum. These bands may be subtracted from the spectrum if a reference water vapour spectrum is available. However, if both the intensity and the *frequency* of the water vapour bands change from one spectrum to the next then the bands will not overlay perfectly. Ratioing one single-beam spectrum against a second in which the frequencies of the water vapour absorption bands have changed will lead to a distorted spectrum. The same argument applies to spectral subtraction. Subtracting a reference spectrum of water vapour from a sample spectrum will result in a distorted spectrum unless the peak frequencies match exactly. The resulting distortion takes the form of narrow peaks which are alternately positive and negative. Water vapour bands are particularly susceptible to such distortion as they are narrow. As the bands are narrow, small changes in the absorption frequency i.e. spectral distortion, between one spectrum and the next leads to spectra which will not overlay perfectly. Such spectral disortion can arise from a

distortion of the infrared beam caused by, for example, the placement of an ATR accessory in the instrument.

At frequencies below 1500cm^{-1} there is no useful spectral information as the silicon ATR prism is opaque in this region.

The region 4000-2700cm^{-1} is shown in figure 7.8. For comparison purposes, the transmission spectrum is also shown. The most obvious difference between the two spectra is the growth of a broad band centred at 3390cm^{-1}. This band arises from the OH stretching of a hydrogen-bonded hydroxyl group. Therefore, it seems probable that upon adsorption, the hydroxyl groups on the sorbitan headgroup form hydrogen bonds with the silanol groups on the silica surface.

Another, less obvious, difference between the spectra is that the methylene antisymmetric and symmetric bands appear less well resolved in the ATR spectrum than in the transmission spectrum. In order to make this more clear, both spectra are shown expanded and superimposed in figure 7.9. The spectrum of the adsorbed compound appears to show at least one extra band, located between the methylene antisymmetric and symmetric bands. Therefore the value of ε, calculated from the transmission spectrum in section 7.3.2, no longer applies. As a result of the change of ε upon adsorption quantitative analysis of the adsorbed amount is impossible. As adsorption leads to the growth of new band(s) it seems likely that ε increases by an uncertain amount upon adsorption. Using the value of ε calculated from the transmission experiment would lead to an overestimate of Γ_i. In this case, the area under the CH stretching bands in the ATR spectrum is 0.484cm^{-1} which, using a value of ε of 51800dm^{3}mol^{-1}cm^{-2} yields:

$\Gamma_i = 3.17 \times 10^{-10}$mol.cm^{-2}

%bulk = 26%

Area per molecule = 52Å^2

The value of Γ_i is more than double that obtained for either of the primary amines, and, as has been discussed, is likely to have been overestimated. However, even this overestimated Γ_i is not so high that multilayers must be considered. In other words, the adsorbed layer is a monolayer.

The TM polarized spectra obtained at 0 and 15 hours after injection of the solution into the cell are shown in figure 7.10. Over the 15 hour time period the area of the OH stretching band at 3370cm^{-1} increases and the CH stretching bands become less well resolved. The areas under the OH and CH stretching bands were measured from the TM polarized ATR spectra obtained at hourly intervals. The results of these measurements are given in table 7.2. A plot of the area under the OH stretching band as a function of time is shown in figure 7.11. The area under the CH stretching bands is shown in figure 7.12. The area of the OH stretching band increases with time for eleven hours, after which time it remains essentially constant. The area of the peak more than doubles over the time period. The growth of the area under the CH stretching bands is rather less marked. The area increases during the first eight hours, after which time it is contant. The growth of these bands is in marked contrast to the behaviour of the amines studied in the previous chapter. The spectrum obtained immediately after introduction of the amine solution to the cell was the same as that obtained after several hours. This showed that the adsorption was rapid, occuring over, at most, a few minutes. Therefore, it is somewhat surprising that the sorbitan monopalmitate appears to adsorb over a timescale of several hours. Figure 7.13 shows the CH stretching region of the ATR spectra of the sorbitan monopalmitate solution immediately after injection into the cell, after fifteen hours and the difference between the two. The difference spectrum reveals that the increase in intensity in the CH stretching region is due to the growth of two broad, overlapping, bands centred at 2943cm^{-1} and 2883cm^{-1}. The assignment of these bands is somewhat problematical. The width of the bands is greater than that usually observed for CH

179

stretching and the frequencies are not those expected for methylene or methyl stretching bands.

Table 7.2   Areas Under OH and CH Stretching Peaks in the TM Polarized ATR Spectrum of 7.5mM Sorbitan Monopalmitate as a Function of Time

Time After Injection (hours)	Area 3580-3000cm^{-1} (cm^{-1})	Area 3000-2800cm^{-1} (cm^{-1})
0	3.312	0.586
1	4.013	0.642
2	4.335	0.767
3	4.594	0.732
4	5.596	0.764
5	5.613	0.797
6	6.555	0.791
7	6.442	0.803
8	6.801	0.828
9	7.064	0.823
10	7.336	0.878
11	7.481	0.720
12	7.400	0.835
13	7.412	0.848
14	7.182	0.826
15	7.333	0.819

The bands arise upon adsorption and therefore it seems reasonable to suggest that they are due to a vibration associated with the sorbitan headgroup. There is one CH, one CH_2 and two HCOH groups on the sugar ring. In addition there is a CH_2 and an HCOH unit between the ring and the ester linkage. The new bands may be due to the stretching vibrations of such CH units which become perturbed when the headgoup hydrogen bonds to the silica surface.

Whatever the assignment of the growing bands in the CH stretching region of the spectrum it is clear that they are not associated with the aliphatic tail of the compound. These vibrations have been studied and described in the previous chapter. The spectrum of adsorbed hexadecylamine, for example, did not exhibit a similar set of new bands. So, whilst the area under the bands in the CH stretching region of the spectrum of sorbitan monopalmitate increases with time, none of that increase is attributable to the tails of the surfactant. In other words, over the time period studied, there is no evidence for an increase in the amount of surfactant adsorbed. Therefore, it is proposed that sorbitan monopalmitate adsorbs rapidly onto the silica surface of the ATR prism, as did the amines. This initial rapid adsorption is followed by a slow rearrangement of the molecules within the adsorbed layer such that the hydrogen-bonding interactions between the surface silanols and the headgroup hydroxyls are maximized.

Another possible interpretation of the observed spectral changes is that following adsorption the sorbitan monopalmitate undergoes some reaction and then desorbs. This process is repeated until equilibrium is reached and the spectra show no further change with time. This may happen if the sorbitan headgroup bonded to a water molecule on the silica surface and then desorbed in a hydrated state. In order to investigate this, a sample of the solution was removed from the cell after the fifteen hour time period. The transmission spectrum of this solution in a 0.022cm cell was recorded and compared to that of the original solution. The results of these

measurements are presented in figure 7.14. The spectra are virtually identical, showing that the adsorption-reaction-diffusion process does not occur and that the process is one which is associated with adsorption at the interface.

7.3.4   Orientational Meaurements

Since an accurate value of Γ_i is impossible to determine for sorbitan monopalmitate, the contribution made to the spectrum by bulk solution cannot be calculated. Hence the dichroic ratios expected for various combinations of ordered film and bulk solution cannot be calculated. In addition to this difficulty, the new bands in the CH stretching region are not assigned and so the direction of their dipole moment with respect to the molecular geometry cannot be determined. Therefore no accurate model for calculating theoretical dichroic ratios can be constructed.

However, the contribution made by the methylene stretching vibrations to the CH stretching region of the ATR spectra is considerable and a simple model for calculating theoretical dichroic ratios for oriented films of such chains has been described in chapters 3 and 5. Futhermore, in the systems studied in this thesis, completely random samples will give a dichroic ratio of 0.50. Consequently, a dichroic ratio of >0.50 in the CH stretching region shows that there is some order in the system, with the chains aligned preferentially parallel to the surface normal.

The TE and TM polarized spectra of the sorbitan monopalmitate solution acquired hourly over four hours are shown in figures 7.15 to 7.19. The areas under the CH stretching bands were integrated and the dichroic ratios calculated. The results of these measurements and calculations are given in table 7.3.

Table 7.3   Dichroic Ratio Measurements of the CH Stretching Region in the ATR

Spectra of Sorbitan Monopalmitate

Time After Injection (hours)	A_{TE} (cm^{-1})	A_{TM} (cm^{-1})	D_{exptl}
0	0.442	0.586	0.754
1	0.491	0.642	0.765
2	0.548	0.767	0.714
3	0.531	0.737	0.725
4	0.553	0.764	0.723

The measured dichroic ratios are all significantly greater that 0.50. This shows that there is some alignment of the aliphatic tails parallel to the surface normal. The amount of ordering does not change significantly with time. This may be expected as it has been asserted that the amount of surfactant adsorbed, and therefore the density of the packing of the molecules within the adsorbed layer, remains constant.

Conclusions

Sorbitan monopalmitate adsorbs onto the silica surface. Upon adsorption, significant changes can be observed in the infrared spectrum of the compound. These spectral changes prohibit quantitative determination of the surface excess concentration of the surfactant. However, it is possible to estimate that the coverage is no greater than a monolayer. The nature of the headgroup-surface interaction appears to be hydrogen bonding between the headgroup hydroxyls and the surface silanols. Adsorption is rapid and results in the formation of an adsorbed layer in which the aliphatic tails are aligned to some extent parallel to the surface normal. Following the initial rapid adsorption there is a slow rearrangement of the molecules within the adsorbed layer such that the hydrogen-bonding interactions with the surface are maximized.

Figure 7.1   The Structure of Sorbitan Monopalmitate

$$
\begin{array}{c}
\quad\quad\quad\quad \overset{\displaystyle O}{\underset{\displaystyle \|}{}} \\
H_2C\text{-}O\text{-}C\text{-}CH_2\,(CH_2)_{13}\,CH_3 \\
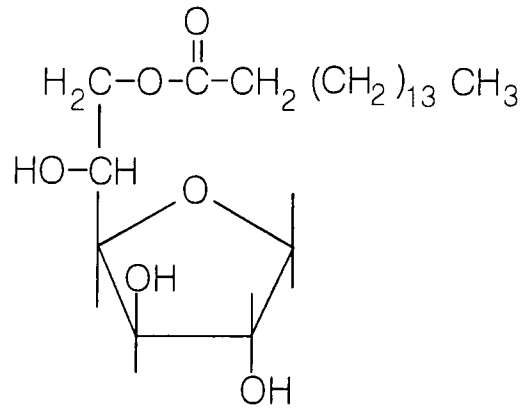HO\text{-}CH
\end{array}
$$

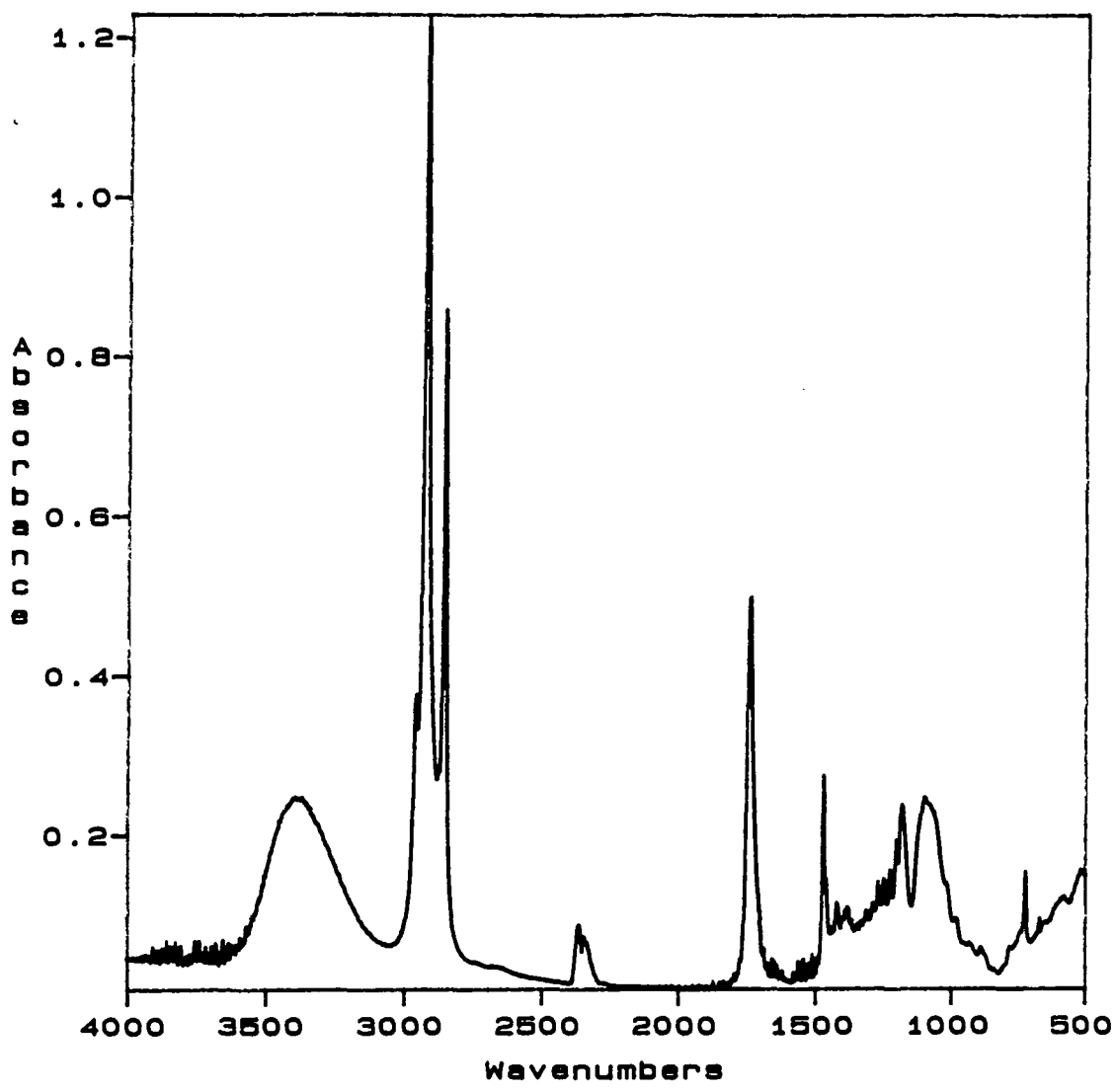Figure 7.2   Transmission Spectrum of a Melt-Cast Film of Sorbitan Monopalmitate

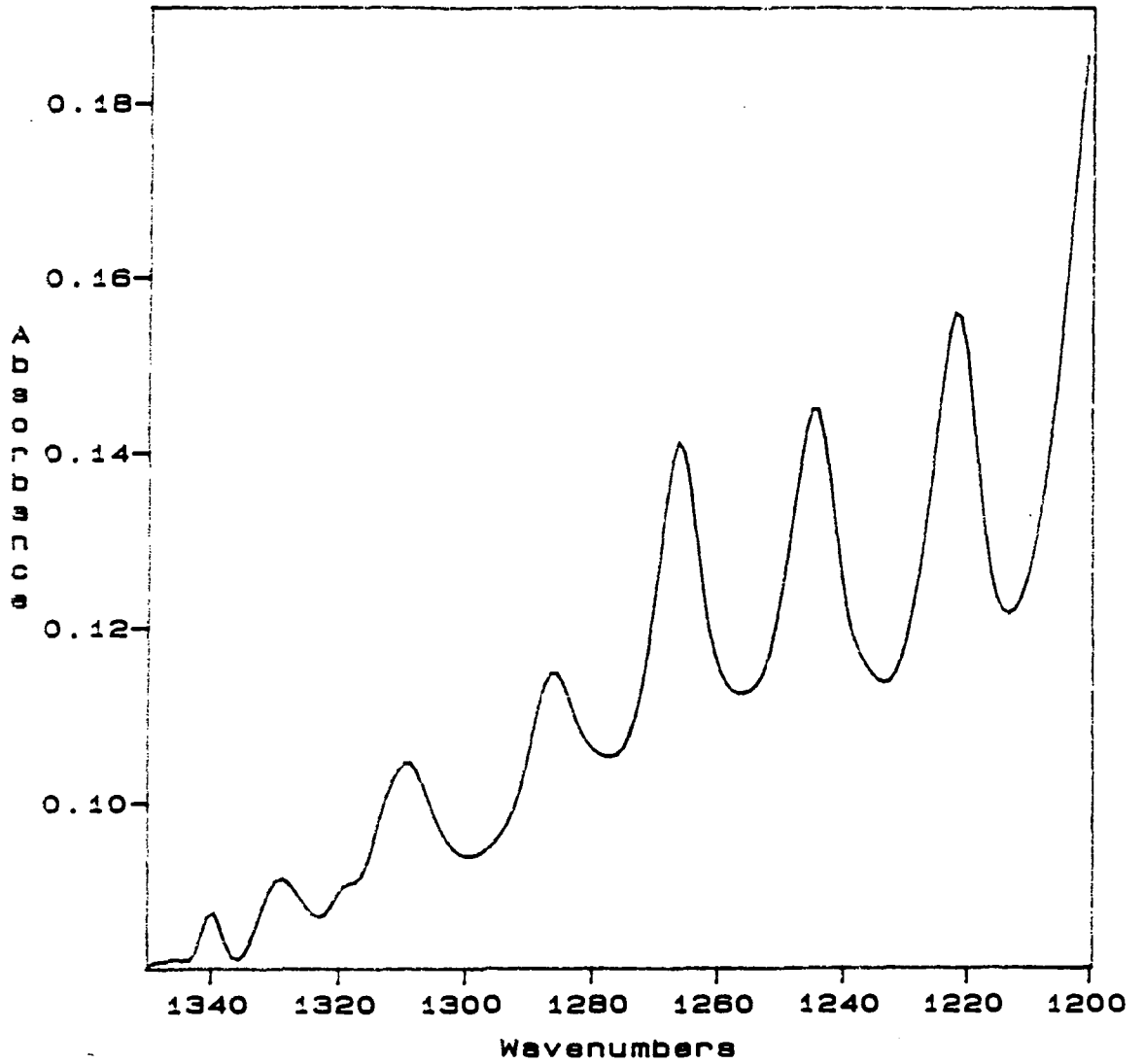Figure 7.3 Progression Bands in the Spectrum of Solid Sorbitan Monopalmitate
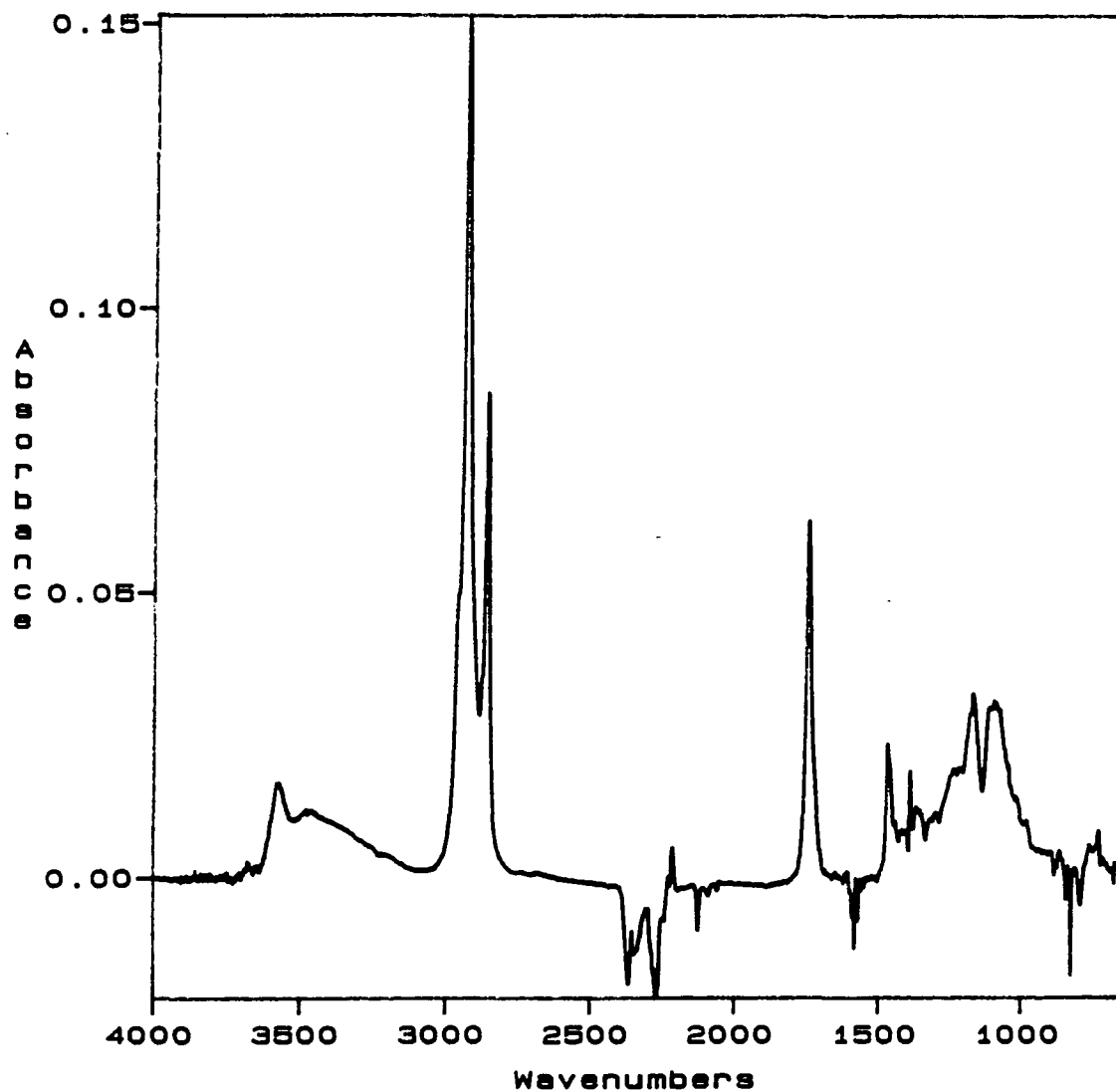
Figure 7.5   Transmission Spectrum of a 7.5mM Solution of Sorbitan

Monopalmitate Expanded in the Region 4000-2700cm^{-1}
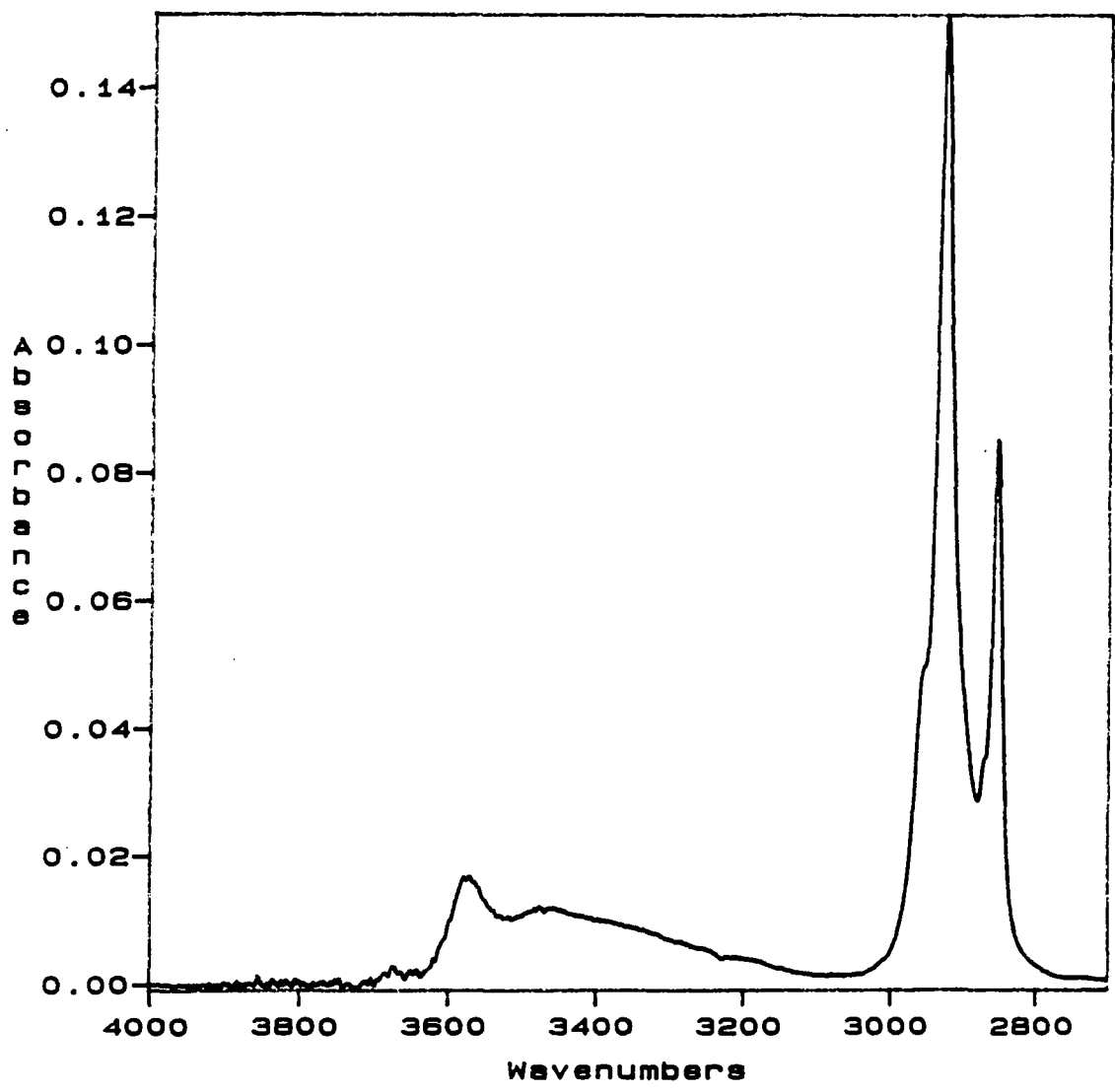
Figure 7.6   Unpolarized ATR Spectrum of 7.5mM Sorbitan Monopalmitate
Solution
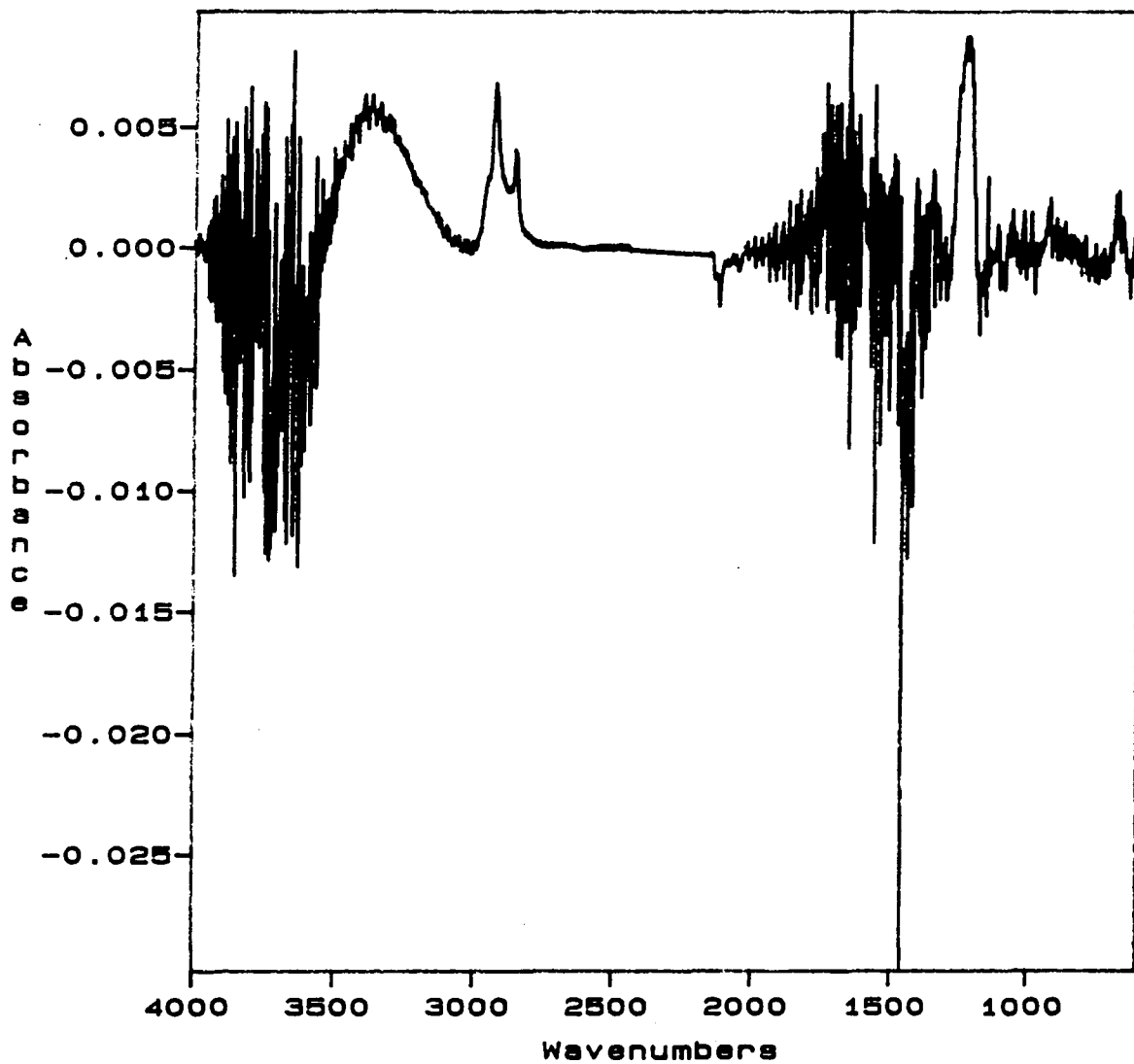
Figure 7.7   Spectrum of Atmospheric Water Vapour
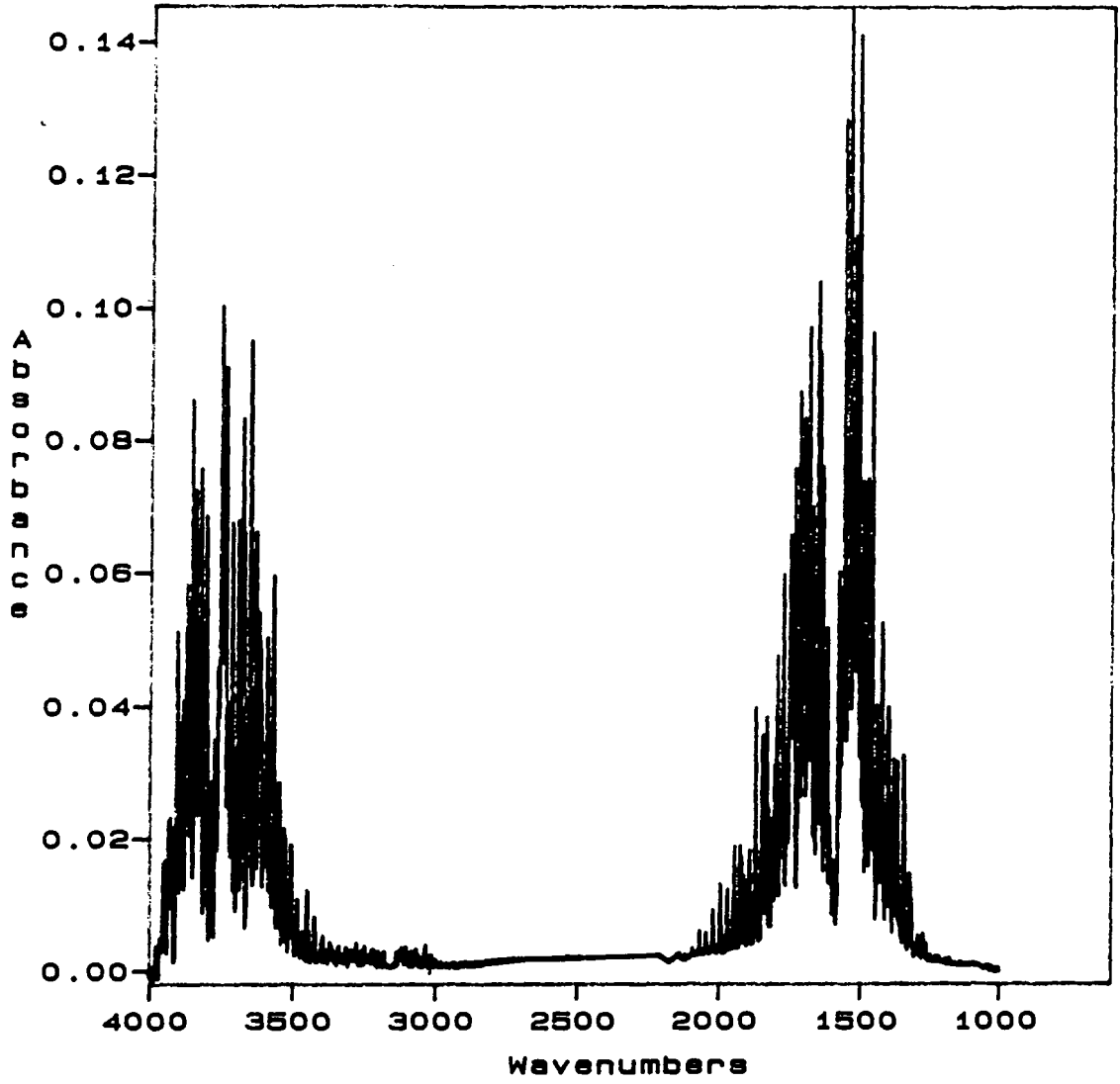
Figure 7.9   Transmission and ATR Spectra of 7.5mM Sorbitan Monopalmitate

Superimposed
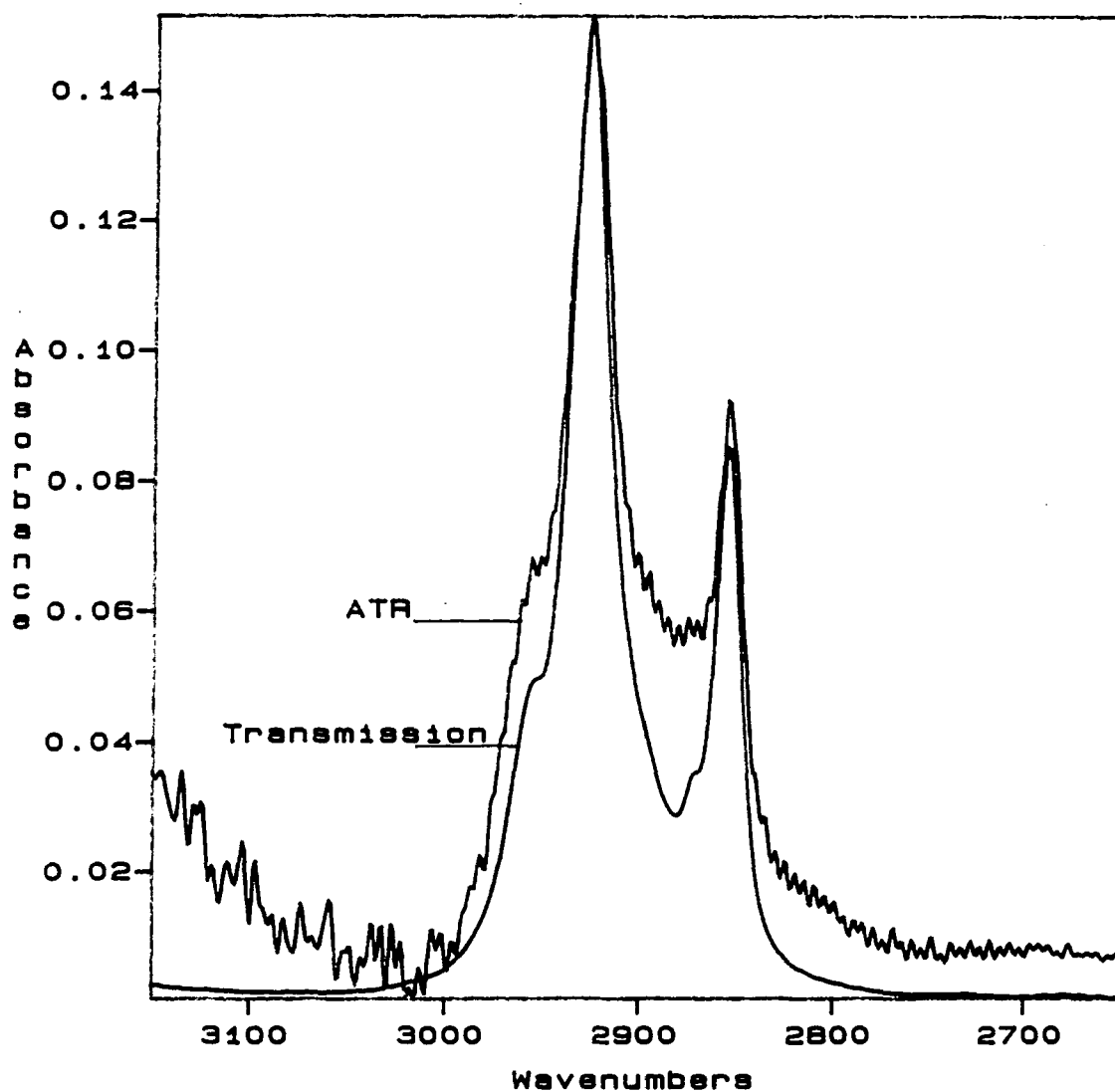
Figure 7.10   TM Polarized Spectra of 7.5mM Sorbitan Monopalmitate 0 and 15
Hours after Injection of the Solution into the Cell

Area (cm−1)

Time (hours)

Area (cm-1)

Time (hours)
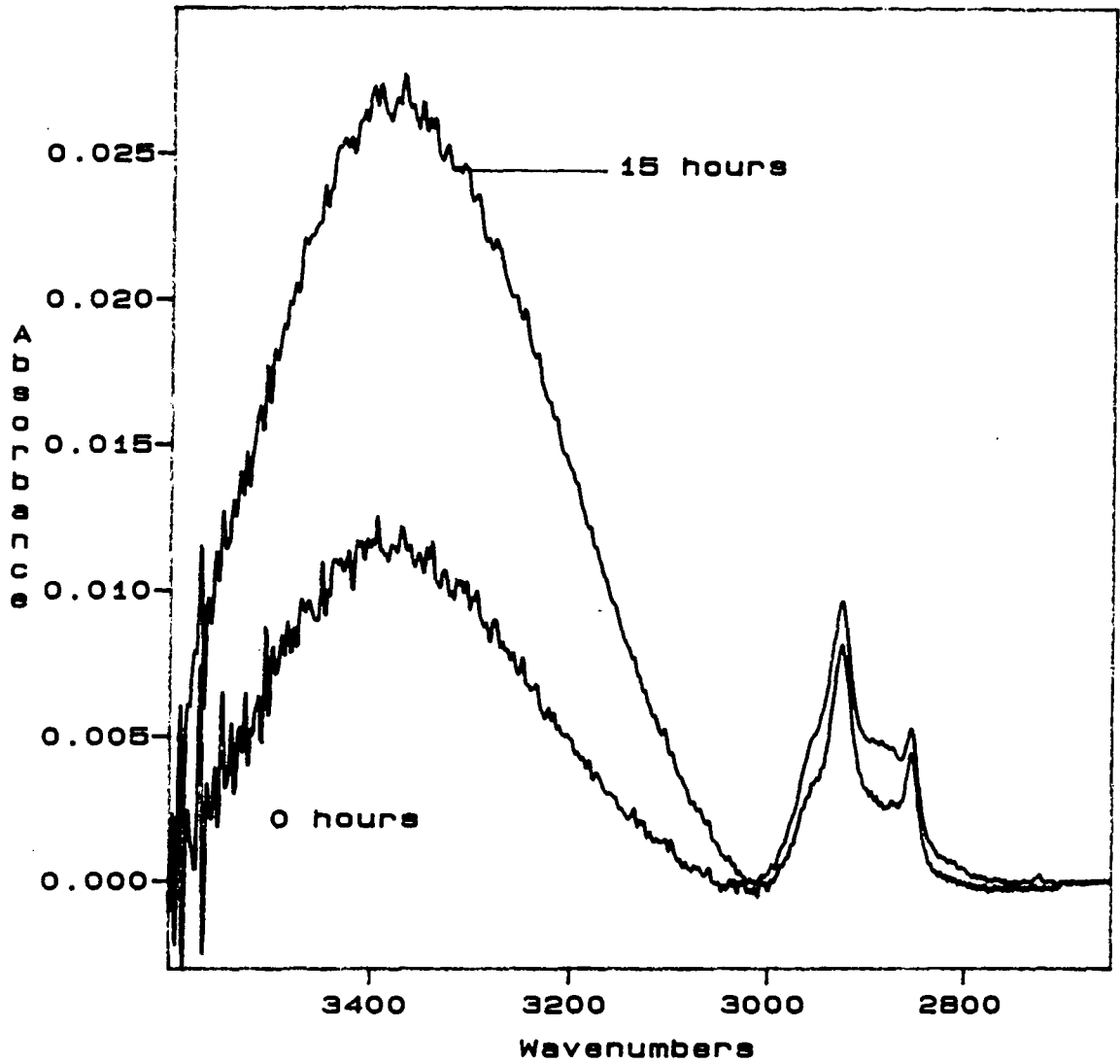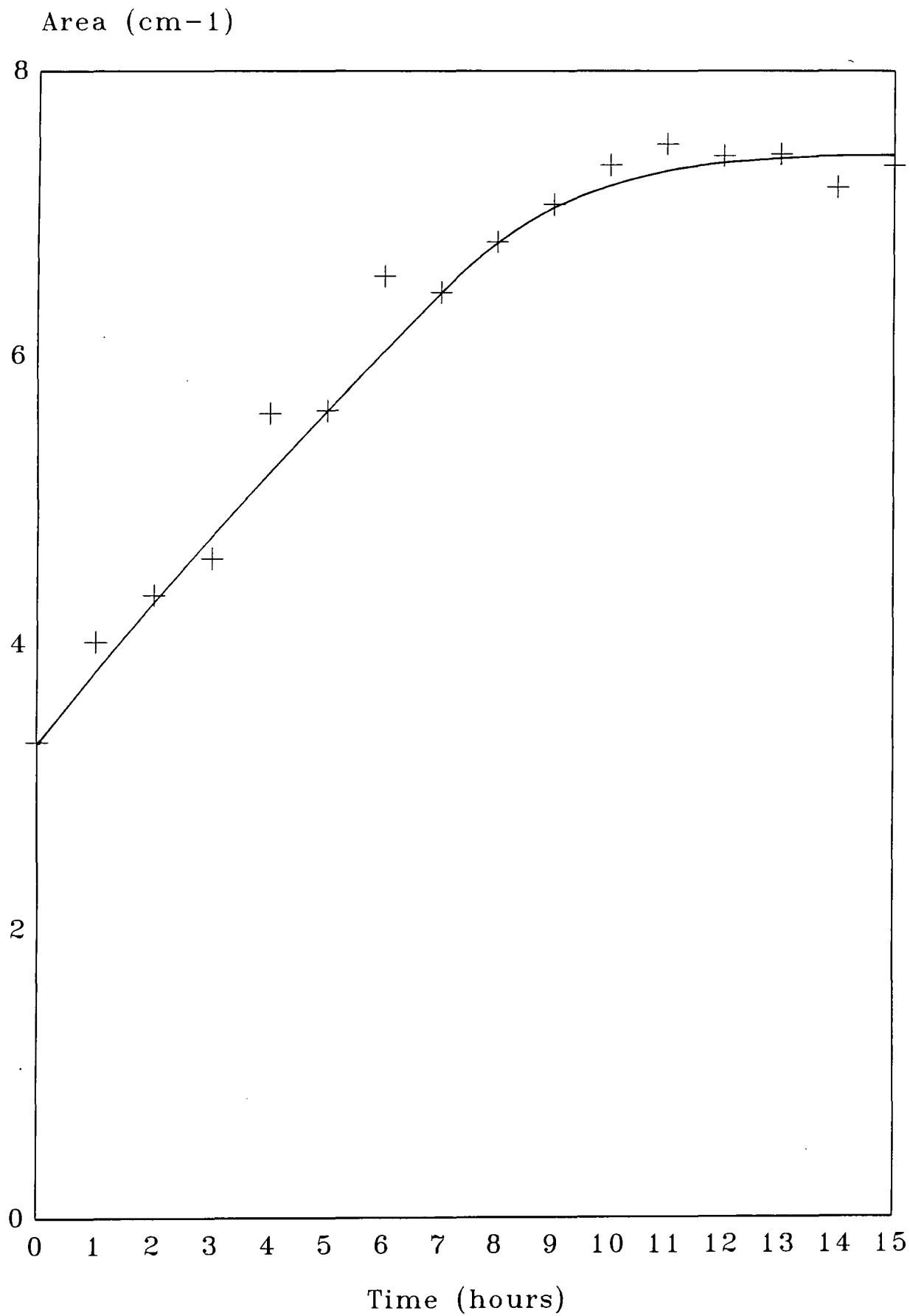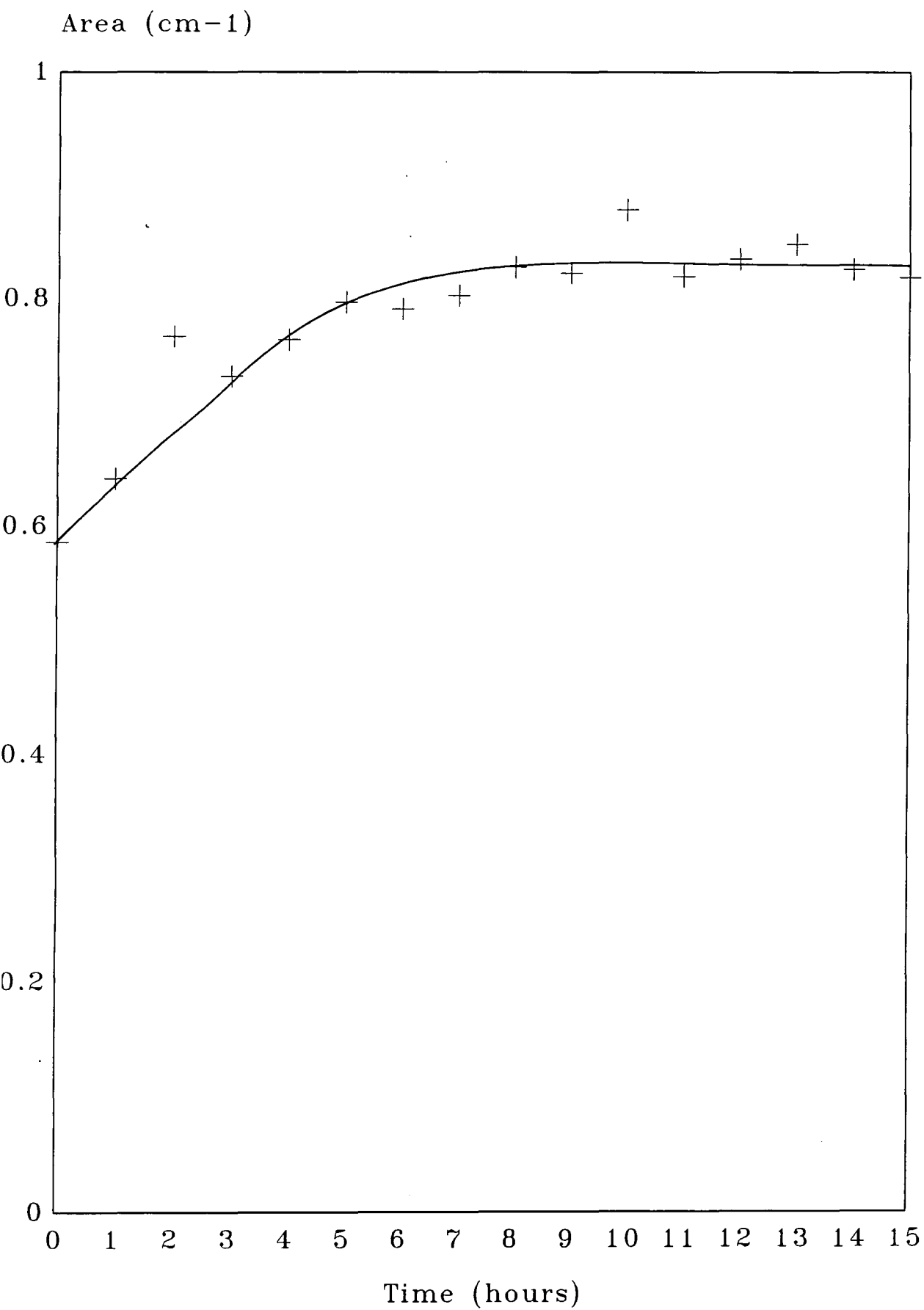
Figure 7.13   TM Polarized Spectra of 7.5mM Sorbitan Monopalmitate 0 and 15

Hours after Injection of the Solution into the Cell and the Difference
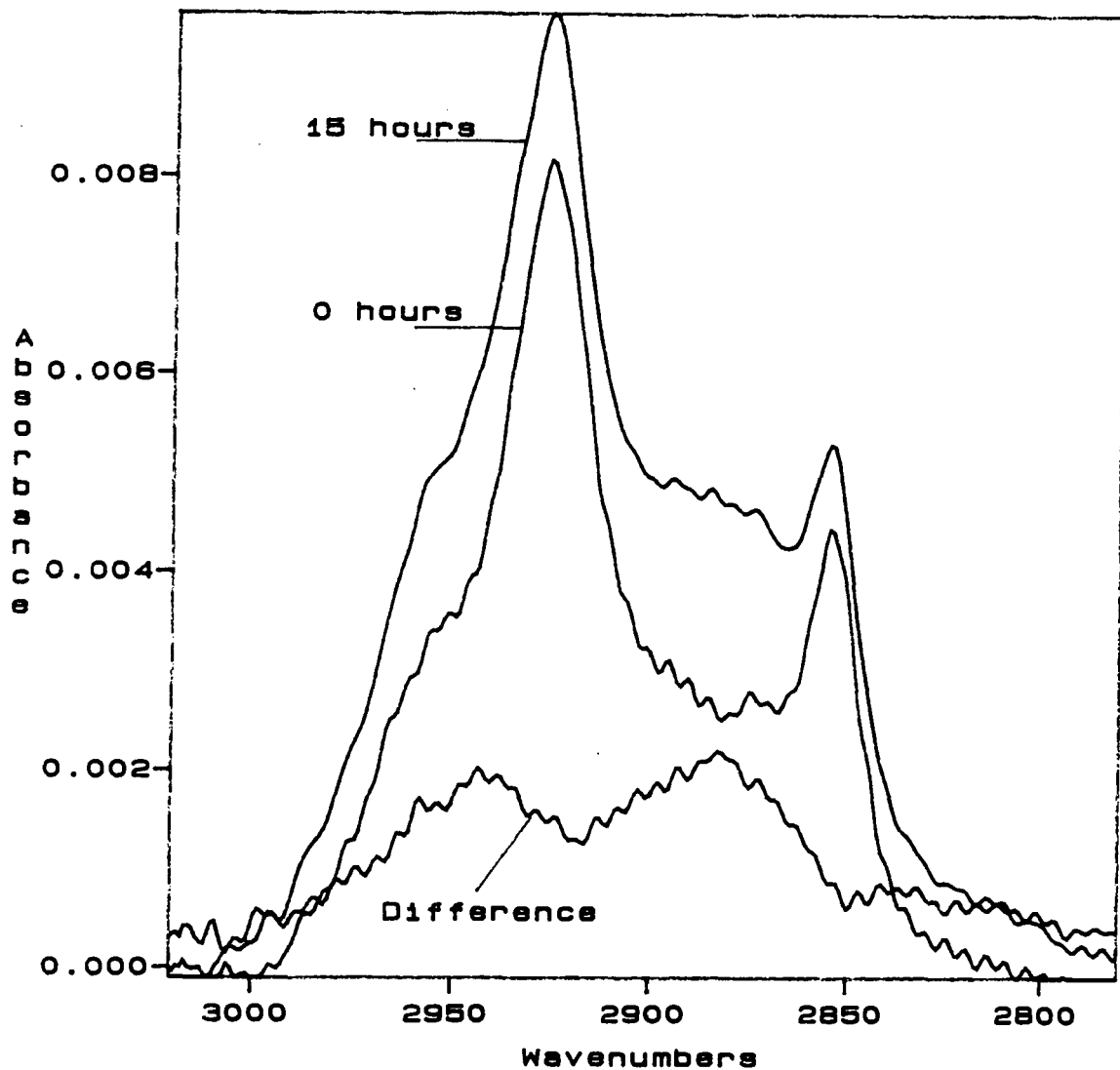
Figure 7.14   Transmission Spectra of 7.5mM Sorbitan Monopalmitate before and after Adsorption Experiment
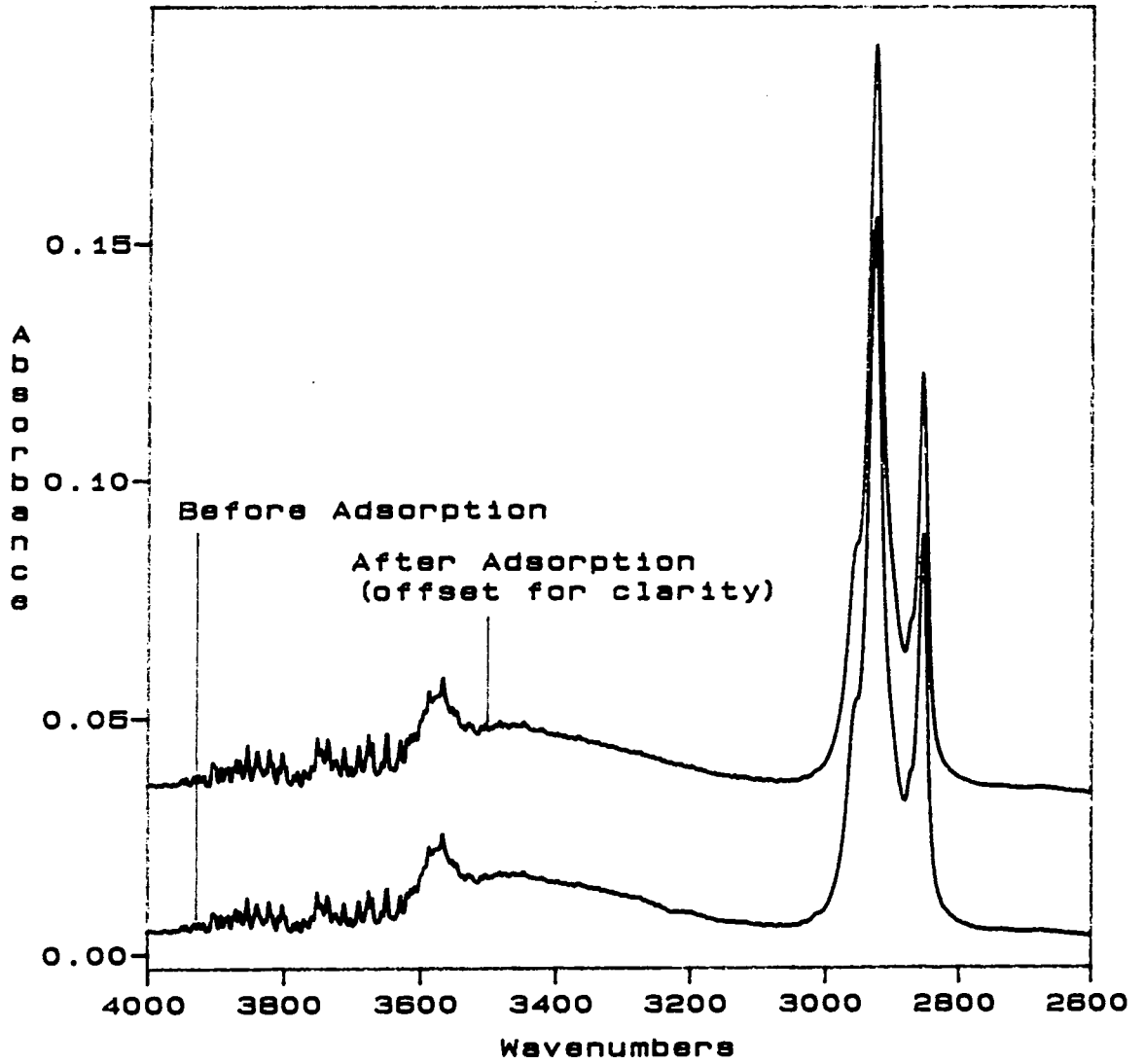
Figure 7.15   TE and TM Polarized ATR Spectra of 7.5mM Sorbitan Monopalmitate

Immediately After Injection into the Cell
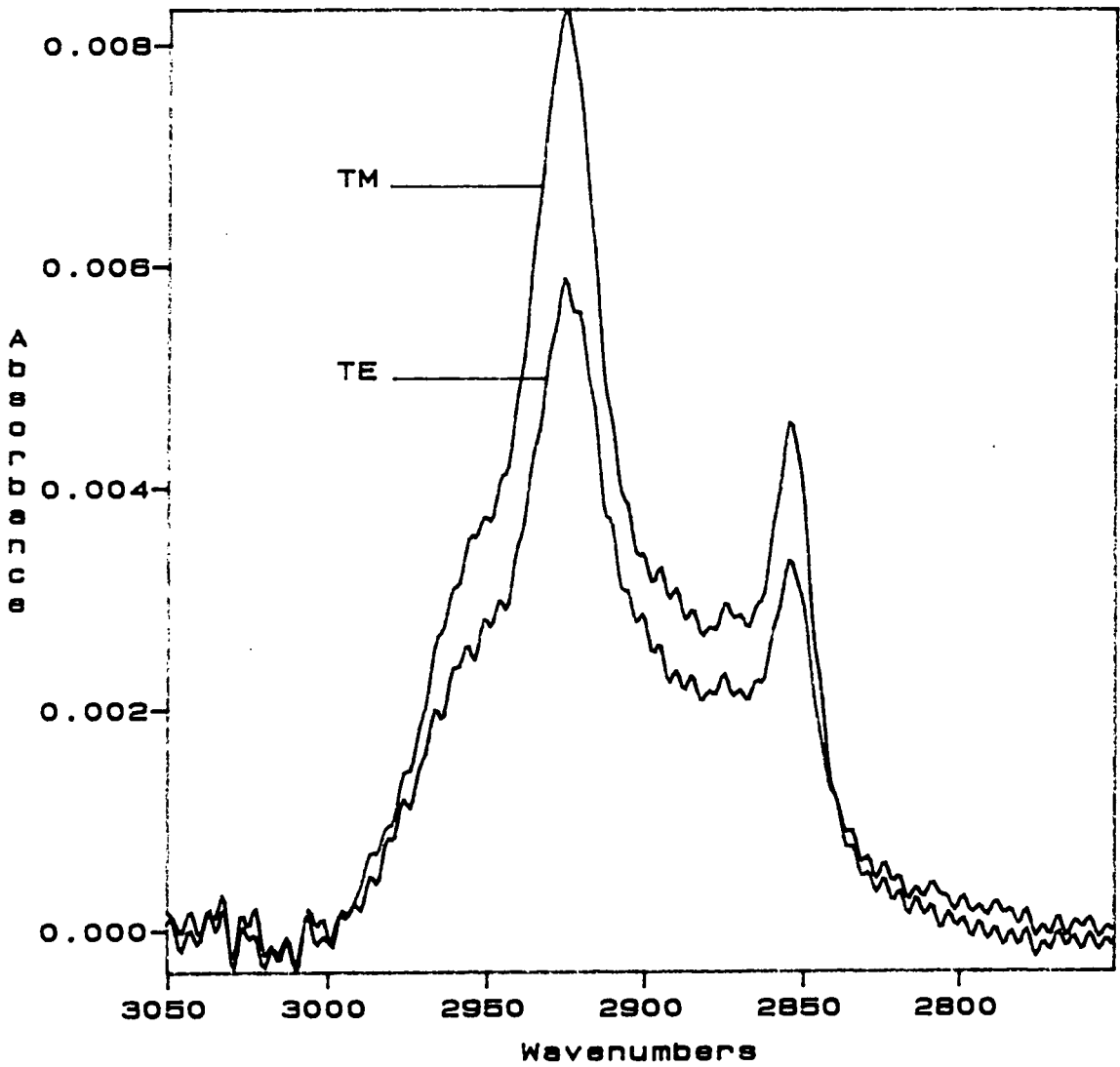
Figure 7.16   TE and TM Polarized ATR Spectra of 7.5mM Sorbitan Monopalmitate
1 Hour After Injection into the Cell
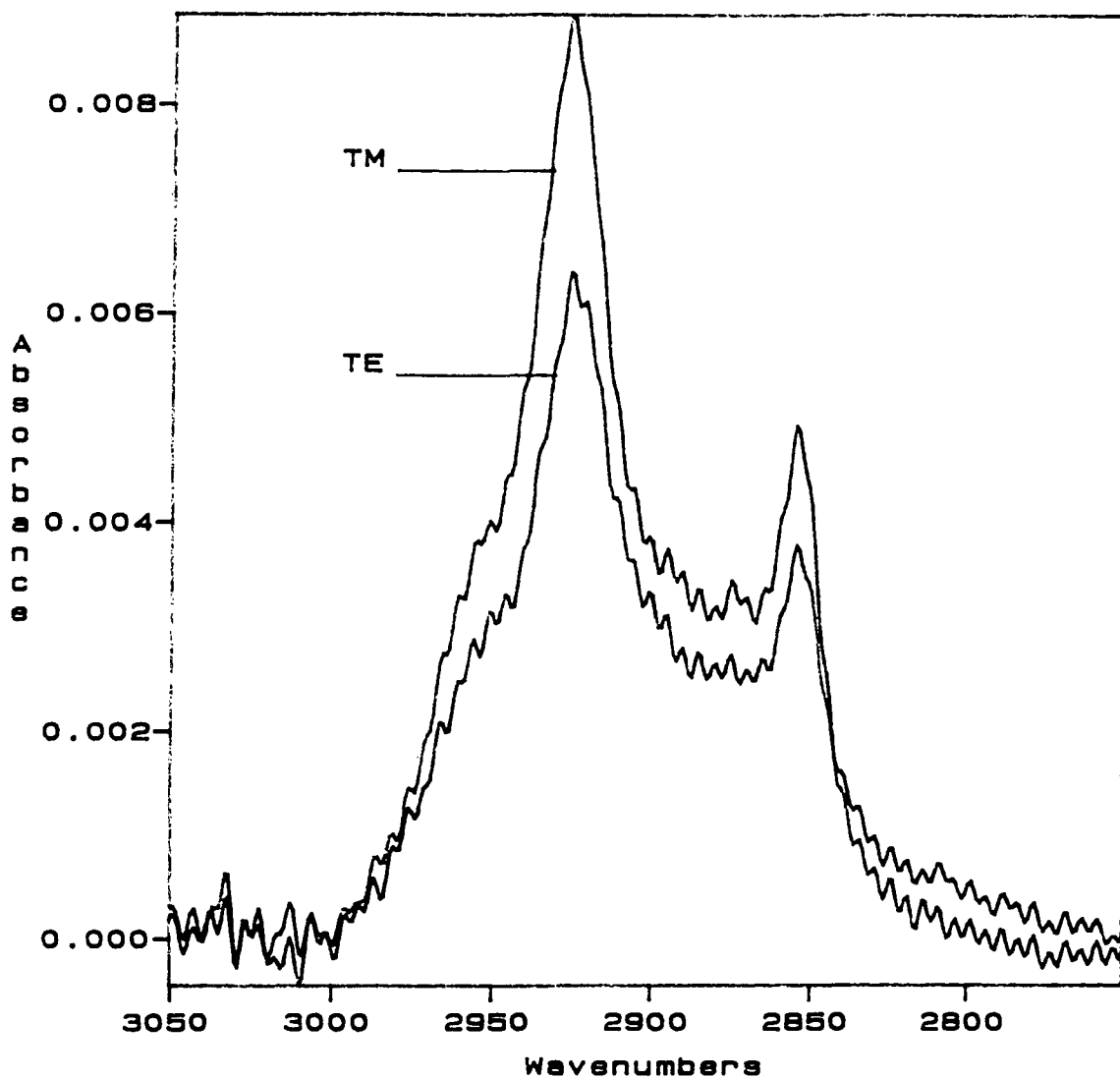
Figure 7.17　　TE and TM Polarized ATR Spectra of 7.5mM Sorbitan Monopalmitate
2 Hours After Injection into the Cell
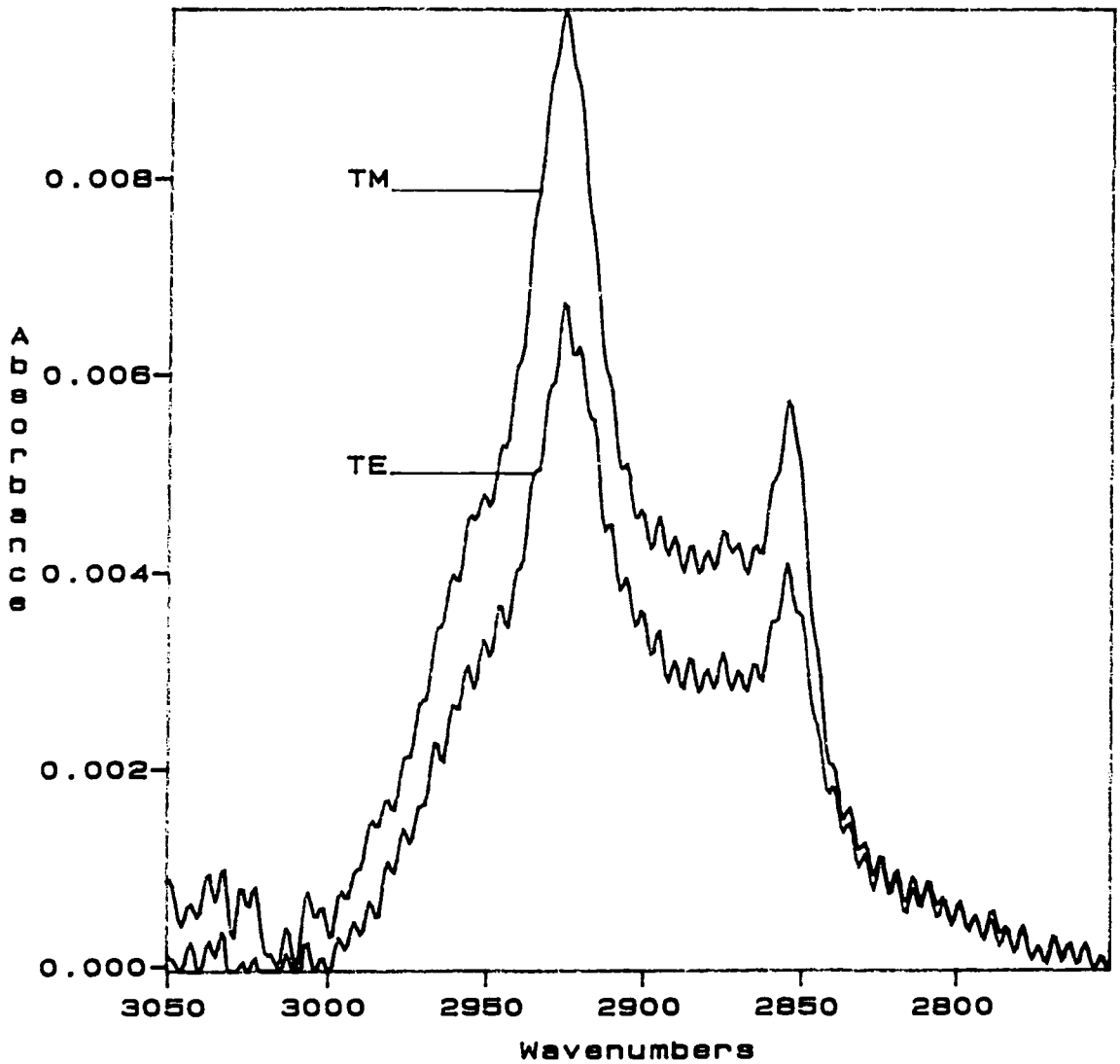
Figure 7.18   TE and TM Polarized ATR Spectra of 7.5mM Sorbitan Monopalmitate

3 Hours After Injection into the Cell
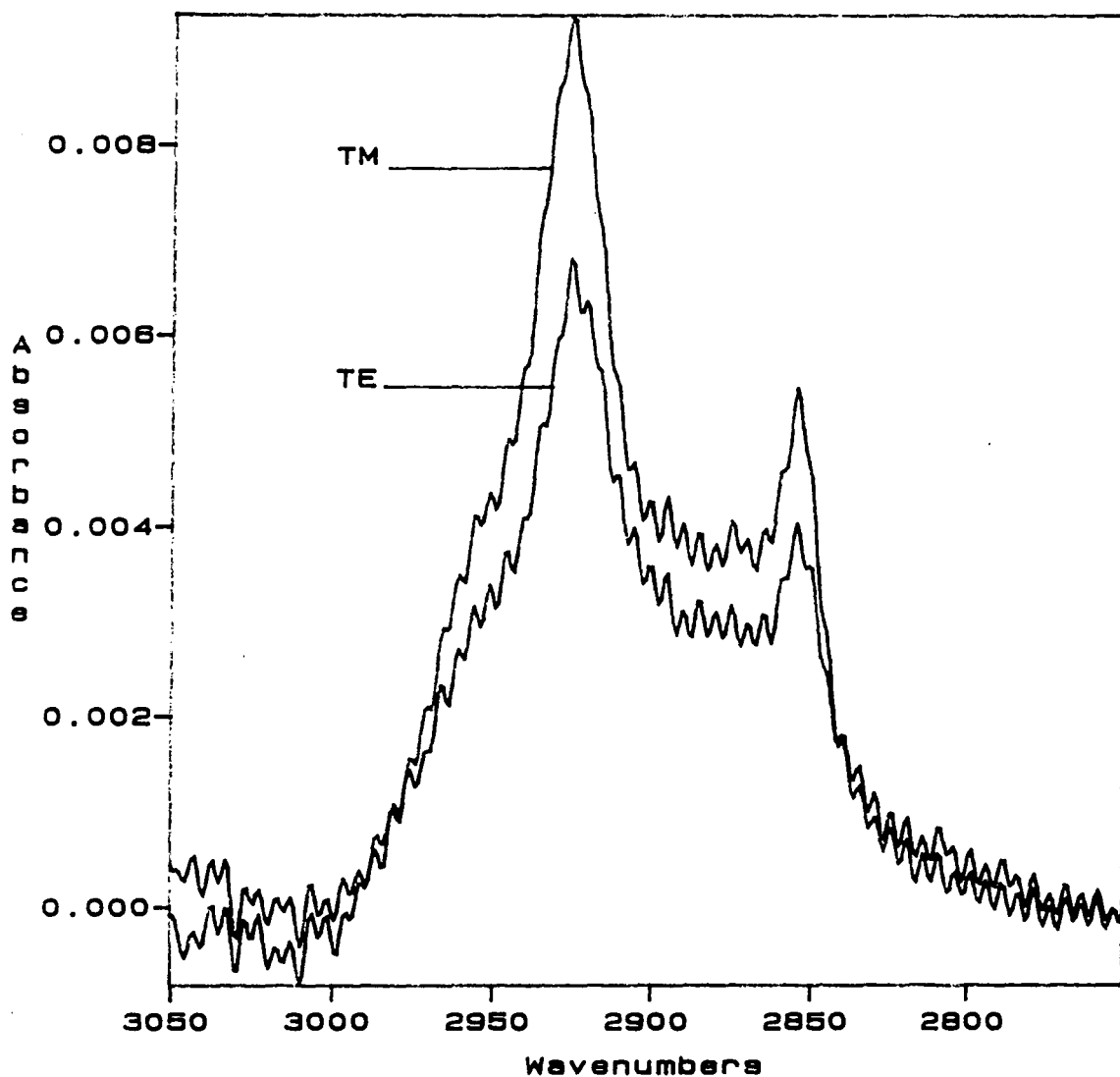
Figure 7.19   TE and TM Polarized ATR Spectra of 7.5mM Sorbitan Monopalmitate

4 Hours After Injection into the Cell
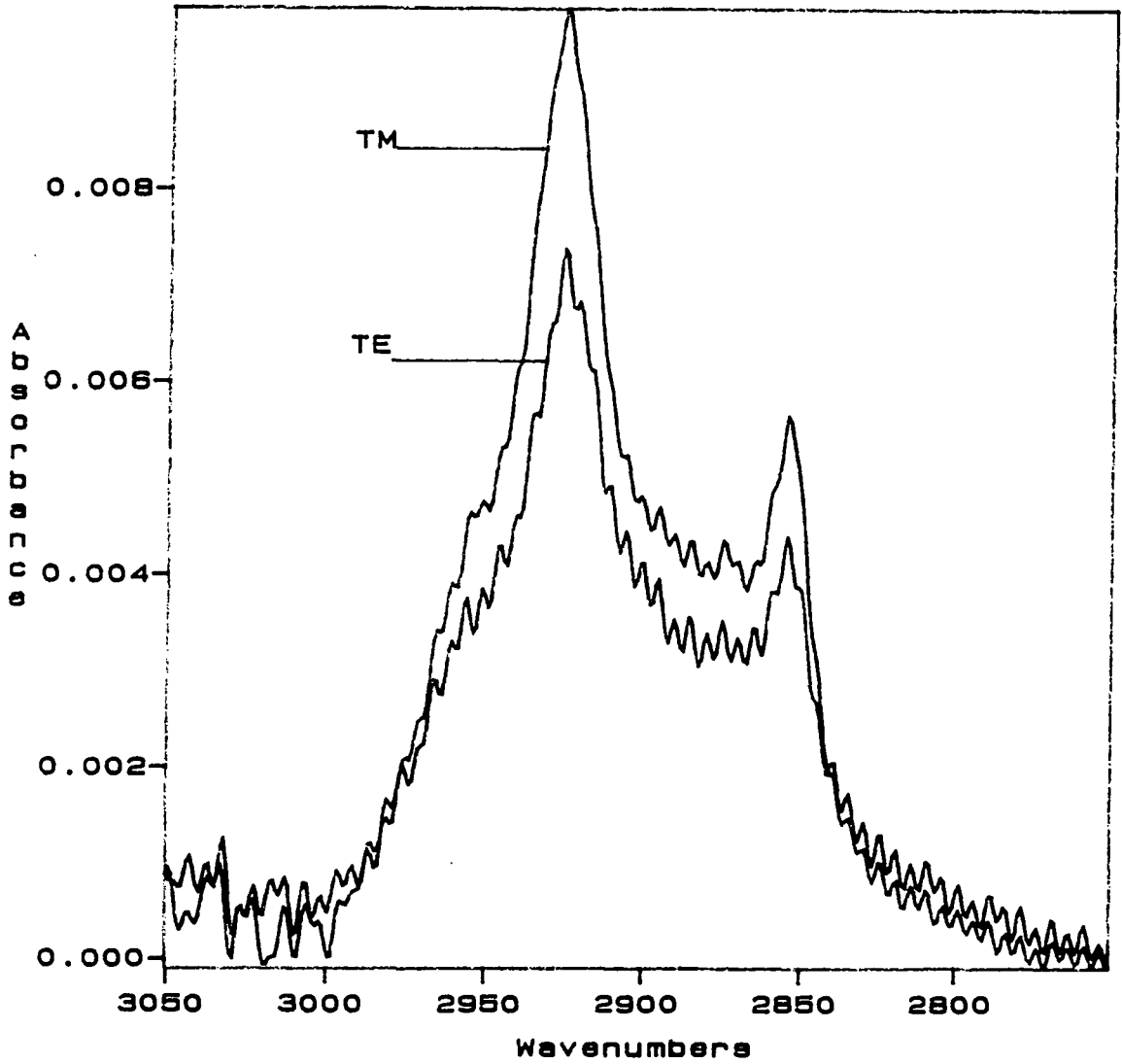
Chapter 8   Rheological Studies of Silica Dispersions

8.1   Introduction

The aim of this Ph.D. project is to relate the macroscopic properties of colloidal dispersions stabilized by model surfactants to adsorption processes occuring at the molecular level. The rheological behaviour of dispersions is one such macroscopic property.

This chapter describes effect of the degree of surface coverage by four surfactants on the rheology of silica-in-toluene dispersions. One sorbitan ester and three amine based surfactants have been used in this study. Dispersions were prepared by equilibrating a fixed mass of Aerosil 200 silica with surfactant solutions over a range of concentrations, such that the amount of silica in the final dispersion was $20g/dm^{-3}$. The viscosity of each dispersion was measured over a range of shear rates using a Bohlin VOR rheometer.

Following the rheological measurements, the amount of surfactant adsorbed onto the silica was determined by a solution depletion technique. In this way, an adsorption isotherm was constructed for each surfactant. The adsorption isotherms allow the rheological data to be related to the degree of surface coverage.

A comparison of the rheological data and the ATR data is presented in the chapter 9.

8.2 Experimental

8.2.1 Materials

Aerosil 200 silica (Degussa Ltd.) was kept in an oven at 60°C prior to use.

Hexadecylamine (Pfaltz & Bauer), sorbitan monopalmitate (a.k.a. SPAN 40) (Sigma), didecylamine (Aldrich), 1,12-diaminododecane (Aldrich), tetrabromophenolphthalein ethyl ester (a.k.a. BPM-E) (Kodak) and toluene (AnalR Grade, BDH) were used as received.

8.2.2 Preparation of Dispersions

Surfactant solutions of concentration 5, 10, 15, 20, 25 and 30mM were prepared by weighing an appropriate amount of compound into a 50cm^3 volumetric flask and making up to the mark with toluene. The 20mM and higher concentration solutions of 1,12-diaminododecane required a few minutes in an ultrasonic bath to promote complete dissolution.

Into a glass sample vial was weighed 0.4±0.01g Aerosil 200 silica. To this was added 20cm^{-3} of surfactant solution. The mixture was shaken by hand and wet readily. A sonication probe was inserted in the mixture. The mixture was then sonicated for 3 minutes at 18μm. Throughout the sonication process, the sample vial was immersed in a beaker of cold water to prevent overheating.

The mixtures were left overnight to cool and equilibrate prior to rheological study.

8.2.3 Rheological Measurements

All rheological measurements were made at 25°C using a Bohlin VOR rheometer equipped with large cup & bob (C25) geometry. A cap was fitted to the rheometer

cup to minimize solvent evaporation. Following introduction of the sample to the apparatus, the system was allowed to equilibrate for 10 minutes.

A shear rate sweep from $0.146s^{-1}$ to $921s^{-1}$ and down again to $0.146s^{-1}$ was employed. This up/down sweep allowed hysteresis effects to be investigated. The shear stress was measured at regular intervals and from this the viscosity was calulated and plotted as a function of shear rate.

8.2.4 Solution Depletion Measurements

8.2.4.1 Centrifugation

The dispersions were transfered to $10cm^3$ centrifuge tubes and spun down at 3000rpm for 10 minutes using a standard bench centrifuge. This process satisfactorily separated the dispersions into a clear supernatant and a compact gel, except in the case of the 25 and 30mM hexadecylamine dispersions, which required a further 10 minute spin.

8.2.4.2 Sorbitan Monopalmitate

The infrared spectrum of each supernatant and each stock surfactant solution (the blank) in a 0.02cm pathlength cell was recorded using a Mattson Sirius FTIR spectrometer.

Each spectrum was ratioed against that of pure toluene and converted to absorbance units. The area of the carbonyl band at $1745cm^{-1}$ was measured using Mattson's FIRST software.

8.2.4.3 Hexadecylamine

From each stock (blank) and supernatant solution was taken a 1cm^3 aliquot. Each aliquot was diluted by a factor of 50. From each diluted solution, 2cm^3 were transferred to a 1cm pathlength glass cuvette for spectrophotometric analysis. To the cuvette was added 0.1cm^1 of a 0.743mM solution of tetrabromophenolphthalein ethyl ester (BPM-E) in toluene.

The cuvette was capped and placed in the sample compartment of a Pye-Unicam SP-800 spectrometer, thermostatted at 25°C, and allowed to equilibrate for 10 minutes.

The absorbance at 570nm was measured.

8.2.4.4 Didecylamine

As for hexadecylamine except that the original solutions were diluted 250 times prior to analysis, rather than 50.

8.2.4.5 1,12-diaminododecane

As for hexadecylamine except that the original solutions were diluted 500 times prior to analysis.

8.3   Results and Discussion

8.3.1   Adsorption Isotherms

8.3.1.2 Sorbitan Monopalmitate

The infrared spectrum of the 30mM sorbitan monopalmitate solution is shown in figure 8.1. In chapter 7 the infrared spectra of sorbitan monopalmitate in fully deuterated toluene were studied. The deuterated solvent allows the bands due to the methylene

CH stretching of the surfactant to be studied. The rheological measurements require much larger volumes of solvent to be used than the ATR studies. Therefore, the cost of using deuterated solvent for rheological measurents is prohibitive. Hence H_8-toluene is used. This solvent has bands in the 2800-3000cm^{-1} region of the infrared spectrum and therefore the CH stretching region cannot be used to quantify the amount of sorbitan monopalmitate in solution. The spectrum of sorbitan monopalmitate shows a strong band due to the stretching of the ester carbonyl C=O at 1745cm^{-1}. Toluene has no bands in this region and so the carbonyl stretching band may be used to determine the concentration of sorbitan monopalmitate in solution. The region of the carbonyl band at 1745cm^{-1} is shown expanded in figure 8.2.

The integrated areas of the carbonyl band for both the stock and the supernatant solutions are tabulated in table 8.1. The figures in the concentration column refer to the concentration of the sorbitan monopalmitate in the stock solutions from which the dispersions were prepared. A plot of peak area *versus* concentration is shown in figure 8.3. The upper line was obtained from the stock solutions from which the dispersions were prepared and is linear, indicating that Beer's law applies to the carbonyl band over the range of concentrations studied. Adsorption of the sorbitan monopalmitate onto the silica reduces the concentration of the surfactant in the supernatant with respect to the stock solution. The curve obtained from the supernatant solutions therefore lies below that obtained from the stock solutions.

Drawing a line parallel to the concentration axis from the supernatant curve to the blank curve allows the concentration in the supernatant following adsorption to be determined. The difference in concentration of surfactant in solution before and after adsorption, ΔC, allows the adsorbed amount to be determined thus:

Specific surface area of silica = 200m^{2}g^{-1}

Total surface area of silica = 0.4 x 200 = 80m^2

Volume of surfactant solution added = 20cm^3

$\therefore$ Number of moles adsorbed = ΔC x (20/1000)

If ΔC is expressed in mM then :

Number of moles adsorbed = ΔC x (20/1000) x (1/1000)

Number of moles adsorbed per square centimetre = Γ_i, the Gibbs surface excess concentration.

Hence:

$$\Gamma_i = \Delta C \times \frac{20}{10^6} \times \frac{1}{8 \times 10^5}$$

$$= \Delta C \times \frac{20}{8 \times 10^{11}}$$

And the area available per adsorbed molecule, A:

$$A = \frac{1}{N_A \times \Gamma_i \times 10^{-16}} \quad Å^2$$

where N_A is Avogadro's constant.

The results of these calculations are tabulated in table 8.2.

Plotting Γ_i *versus* concentration in supernatant yields an adsorption isotherm. This is shown in figure 8.4.

8.3.1.2 Hexadecylamine

The infrared spectrum of hexadecylamine was described in chapter 5. The NH stretching vibration is very weak and so, unlike sorbitan monopalmitate, there is no

band in the spectrum which is strong and well separated from solvent (toluene) bands. Therefore infrared spectroscopy is not suitable for determining the concentration of hexadecylamine in toluene. A colorimetric technique has therefore been used. Tertabromophenolphthalein ethyl ester (also known as bromophthalein magenta ethyl ester (BPM-E)) was chosen as the indicator. This compound is a red solid which dissolves in toluene to yield a yellow solution. The visible absorption spectrum of the solution shows a strong band at 402nm and a weaker band at 495nm. The interaction between the indicator and a number of organic bases, including amines, has been studied [108]. Upon addition of an amine to the indicator solution a new band in the visible spectrum appears at 570nm. Depending upon the ratio of this band to that at 402nm, the solutions of indicator an amine may appear yellow, purple, or intense blue. The absorbance at 570nm may be used to quantify the concentration of amine in the solution. The colorimetric reaction between indicator and amine is temperature dependent [108] and so all measurements must be made in a temperature controlled cell. All measurements were taken fifteen minutes after the solution was introduced to a cell thermostatted to 25.0±0.1°C.

The optical absorption data for for the stock and supernatant solutions of hexadecylamine are tabulated in table 8.3. A plot of absorbance *versus* concentration is shown in figure 8.5.

The adsorption data for hexadecylamine may be calculated in the same way as for sorbitan monopalmitate. This data is tabulated in table 8.4.

The adsorption isotherm for hexadecylamine is shown in figure 8.6.

8.3.1.3 Didecylamine

The optical absorption data for for the stock and supernatant solutions of didecylamine are tabulated in table 8.5. A plot of absorbance *versus* concentration is shown in figure 8.7.

The adsorption data for didecylamine may be calculated in the same way as for sorbitan monopalmitate. This data is tabulated in table 8.6.

The adsorption isotherm for didecylamine is shown in figure 8.8.

8.3.1.4   1,12-diaminododecane

The optical absorption data for for the stock and supernatant solutions of 1,12-diaminododecane are tabulated in table 8.7. A plot of absorbance *versus* concentration is shown in figure 8.9.

The adsorption data for 1,12-diaminododecane may be calculated in the same way as for sorbitan monopalmitate. This data is tabulated in table 8.8.

The adsorption isotherm for 1,12-diaminododecane is shown in figure 8.10.

8.3.1.5 Discussion of Adsorption Isotherms

In order to facilitate comparison of the adsorption isotherms, all four are plotted together in figure 8.11.

The adsorption isotherms of the two primary amines, namely hexadecylamine and 1,12-diaminododecane are very similar. Both rise very sharply to a plateau when the equilibrium concentration is around 3mM. The surface excess concentration at the plateau is 2×10^{-10}mol.cm^{-2}. This corresponds to an area per molecule of 80Å^2.

The isotherm of the secondary amine, didecylamine, is quite different. The initial rise is somewhat less steep than that of the primary amines. A plateau is reached when the equilibrium concentration is around 7mM. The surface excess concentration at the plateau is 0.7×10^{-10}mol.cm^{-2}, less than half that of the primary amines. The corresponding area per molecule is 237Å².

The isotherm of sorbitan monopalmitate rises much more slowly than those of the amines. The isotherm reaches a maximum of 1.5×10^{-10}mol.cm^{-2} when the equilibrium concentration is 20mM. The reason for the comparatively slow rise of the sorbitan monopalmitate adsorption isotherm is probably due to it being a weaker base than the amines.

8.3.2   Rheology

8.3.2.1 Aerosil 200 in Toluene

A plot of viscosity *versus* shear rate for 20g.dm^{-3} Aerosil 200 in toluene is shown in figure 8.12. Note the log scales. The upper curve was obtained by increasing the shear rate and the lower curve was obtained by decreasing the shear rate.

The system shows shear thinning behaviour; i.e. as the shear rate is increased the viscosity decreases. This is the result of silica aggregates being broken down as shear rate increases. The curves do not flatten out, indicating that some structure remains even at the highest shear rates employed.

The curve obtained by increasing the shear rate lies above that obtained by decreasing the shear rate. This implies that the aggregates broken up during the increasing shear rate regime were not completely reformed as the shear rate was reduced. The difference betwen the curves is particularly marked at low shear rates. This is most

probably due to a few large aggregates being broken down as the shear rate was initially increased.

At the lowest shear rate used, $0.146s^{-1}$, the viscosity of the dispersion was around 10Pa.s. Physically, such a dispersion has the appearence of a gel, such as hair-styling gel.

8.3.2.2 Hexadecylamine

A plot of viscosity *versus* shear rate for 20g.dm^{-3} Aerosil 200 in 5mM hexadecylamine is shown in figure 8.13. This plot is very similar to that for silica with no surfactant present. Shear thinning is observed over the entire range of shear rates employed. The viscosity of the dispersion at low shear is similar to but slightly less than that of the silica in pure toluene system.

Figure 8.14 is a plot of viscosity *versus* shear rate for 20g.dm^{-3} Aerosil 200 in 25mM hexadecylamine solution. This plot is quite different to the 5mM and 0mM plots.

The viscosity at the lowest shear rate, 0.146s^{-1}, is around 50mPa.s, some two orders of magnitude lower than that of either the 5mM or 0mM dispersions. Physically, this dispersion was a free-flowing liquid. Such a low viscosity at low shear indicates that the presence of hexadecylamine has significantly reduced the size of the silica aggregates in the dispersion.

Shear thinning occurs rapidly and the curves bottom-out at a shear rate of around 20s^{-1}. This suggests that the silica aggregates are readily broken up and reach a minimum size at this shear rate.

Taken together, the low viscosity and rapid shear thinning indicate that the 25mM hexadecylamine solution is highly effective in hindering the aggregation of the Aerosil particles.

8.3.2.3 Didecylamine, 1,12-diaminododecane and Sorbitan Monopalmitate

The plots of viscosity *vesus* shear rate for all concentrations of didecylamine, 1,12-diaminododecane and sorbitan monopalmitate are visually similar. All resemble the plot for Aerosil 200 in pure toluene and a detailed description for each compound is therefore unnecessary. However, for reference purposes the following figures are

included. Each figure is a plot of viscosity *versus* shear rate for 20g.dm^{-3} Aerosil 200 in a solution of the stated composition.

Figure 8.15   5mM   Didecylamine

Figure 8.16   25mM Didecylamine

Figure 8.17   5mM   1,12-diaminododecane

Figure 8.18   25mM 1,12-diaminododecane

Figure 8.19   10mM   Sorbitan Monopalmitate

Figure 8.20   25mM Sorbitan Monopalmitate

Unfortunately, there is no plot of 5mM sorbitan monopalmitate as the computer crashed before the plot could be generated and so the 10mM trace has been used in its place.

8.3.2.4 Comparison of Rheological Properties

The effect of the various surfactants upon the rheology of the Aerosil dispersions may be compared. One rheological parameter which may be chosen for comparison is the viscosity at a given shear rate. Figure 8.21 shows a plot of viscosity at a shear rate of $1.46s^{-1}$ as a function of equilibrium concentration of surfactant.

Didecylamine and 1,12-diaminododecane reduce the viscosity slightly as concentration is increased, but their effect is minimal. For comparison, the viscosity of 20g.dm^{-3} Aerosil 200 in pure toluene at a shear rate of $1.46s^{-1}$ is 1Pa.s.

Sorbitan monopalmitate appears to reduce the viscosity of the dispersion slightly with repect to a dispersion in pure toluene but its effect is independent of concentration.

In contrast to the other three surfactants, hexadecylamine shows a marked effect on viscosity. When the equilibrium concentration is around 15mM, the viscosity of the dispersion falls by two orders of magnitude.

8.3.2.5 Relationship between Surface Coverage and Rheology

8.3.2.5.1 Hexadecylamine

Figure 8.22 shows plots of surface excess and viscosity *versus* concentration of hexadecylamine on the same axes. The figure shows that the viscosity decreases rapidy once the adsorption isotherm reaches a plateau. In fact, the adsorption isotherm reaches a plateau at a somewhat lower equilibrium concentration than the point at which the sudden fall in viscosity is observed. This indicates that a complete monolayer of hexadecylamine is necessary to significantly reduce aggregation of the silica particles.

8.3.2.5.2 1,12-diaminododecane

Figure 8.23 shows plots of surface excess and viscosity *versus* concentration of 1,12-diaminododecane on the same axes. The adsorption isotherm, as has been mentioned previously, is very similar to that of hexadecylamine. However, the plot of viscosity *versus* concentration is very different. A slight decrease in viscosity with increasing concentration is observed but nothing like the two orders of magnitude drop show by hexadecylamine.

As 1,12-diaminododecane has an amino group at either end of the aliphatic chain the possibility of bridging arises. Two amino groups on the same molecule may both adsorb onto the surface of a single silica particle but if only one adsorbs, the non-adsorbed group is free to bind either to a silanol group or to a similarly free amino

216

group on an adjacent particle. In the case where both amino groups are adsorbed onto the same particle, the aliphatic chain has to bend back upon itself and therefore will not extend far into solution. "Steric" repulsion between two such coated silica particles is therefore likely to be minimal. There is, of course, likely to be both bridging and adsorption onto a single particle. None of the adsorption schemes provide an effective method for preventing aggregation thereby reducing viscosity. Hence the viscosity of the system is only slightly affected by 1,12-diaminododecane despite the adsorption isotherm being similar to that of hexadecylamine.

The relationship between the rheological properties of the dispersions and the structure of the adsorbed layer will be discussed further in the next chapter.

8.3.2.5.3 Didecylamine

Figure 8.24 shows plots of surface excess concentration and viscosity *versus* concentration of didecylamine. The didecylamine appears to have little effect upon the rheology of the silica dispersions. It must be emphasized that the variation in viscosity is minimal compared to that shown by the hexadecylamine system. Indeed, the variation may possibly be accounted for by experimental error. The adsorption isotherm of didecylamine shows that the coverage of the silica particles by didecylamine is low and a surface excess concentration as low as $0.7 \times 10^{-10} mol.cm^{-2}$ would not be expected to significantly affect the aggregation of the silica.

8.3.2.5.4   Sorbitan Monopalmitate

Figure 8.25 shows plots of surface excess concentration and viscosity *versus* concentration of sorbitan monopalmitate.

The presence of sorbitan monopalmitate has no significant affect on the viscosity. The isotherm shows very slow approach to a plateau compared to the primary amines. This suggests that the sorbitan headgroup has less affinity for the silica surface than the amino group and hence the adsorbed sorbitan monopalmitate layer is less tightly bound than the amine layer. The surface excess concentration at the plateau is slightly greater than $1.5 \times 10^{-10} \text{mol.cm}^{-2}$. This is less than the value of $2 \times 10^{-10} \text{mol.cm}^{-2}$ shown by the primary amines. Sorbitan monopalmitate is therefore expected to be less effective at preventing aggregation than hexadecylamine.

8.4   Conclusions

Solution depletion measurements have shown that hexadecylamine adsorbs strongly onto the surface of Aerosil 200 silica from toluene. Rheological measurements on such dispersions have shown that a complete monolayer of hexadecylamine significantly hinders the aggregation of of silica particles. The assertion that such a monolayer imparts some stability to the dispersions is supported by the observation that at high equilibrium concentrations of hexadecylamine, the dispersions are difficult to serparate by centrifugation.

The adsorption isotherm of 1,12-diaminododecane resembles that of hexadecylamine but the former compound has little effect on the rheology of the silica dispersions. This may be due to bridging by the diamine.

The adsorption isotherm of didecylamine exhibits a maximum, the origin of which is uncertain. The effect of didecylamine on the rheology is minimal.

Sorbitan monopalmitate also has neglible effect on the rheology of the silica dispersions. The adsorption isotherm approaches a plateau much more slowly than those of the primary amines.

In order to significantly reduce the aggregation of silica particles it is necessary to adsorb a tightly bound monolayer of a surfactant which is incapable of bridging to neighbouring particles.

Table 8.1   Area under Carbonyl Band in the Spectra of Sorbitan Monopalmitate

Concentration of Original Stock Solution mM	Absorbance (cm^{-1}) Stock Solution	Absorbance (cm^{-1}) Supernatant
5	1.183	0.807
10	2.418	1.625
15	3.494	2.693
20	4.712	3.463
25	6.294	4.684
30	7.530	5.745

Table 8.2   Adsorption Data for Sorbitan Monopalmitate

Concentration in Original Stock Solution mM	Concentration in Supernatant mM	ΔC mM	$\Gamma_i \times 10^{10}$ $mol.cm^{-2}$	Area per Molecule Å^2
5	3.2	1.8	0.46	375
10	6.4	3.6	0.90	185
15	10.2	4.8	1.20	139
20	14.4	5.6	1.40	119
25	19.1	5.9	1.48	112
30	23.9	6.1	1.53	109

Table 8.3   Optical Absorption Data for Hexadecylamine

Original Concentration of Stock Solution mM	Absorbance of Stock Solution at 570nm	Absorbance of Supernatant at 570nm
5	0.262	0.013
10	0.670	0.111
15	0.864	0.411
20	1.024	0.761
25	1.118	0.900
30	1.138	1.055

Table 8.4   Adsorption Data for Hexadecylamine

Concentration in Original Stock Solution mM	Concentration in Supernatant mM	ΔC mM	$\Gamma_i \times 10^{10}$ mol.cm^{-2}	Area per Molecule Å^2
5	0.5	4.5	1.15	151
10	1.8	8.2	2.05	81
15	6.4	8.6	2.15	77
20	12.4	7.6	1.90	87
25	16.9	8.1	2.00	82
30	21.0	9.0	2.25	74

Table 8.5   Optical Absorption Data for Didecylamine

Original Concentration of Stock Solution mM	Absorbance of Stock Solution at 570nm	Absorbance of Supernatant at 570nm
5	0.241	0.162
10	0.511	0.372
15	0.675	0.582
20	0.784	0.748
25	0.902	0.861
30	1.021	0.957

Table 8.6   Adsorption Data for Didecylamine

Concentration in Original Stock Solution mM	Concentration in Supernatant mM	ΔC mM	$\Gamma_i \times 10^{10}$ mol.cm^{-2}	Area per Molecule Å^2
5	3.2	1.8	0.45	369
10	7.2	2.8	0.70	237
15	12.0	3.0	0.75	221
20	17.4	2.6	0.65	255
25	22.4	2.6	0.65	255
30	27.4	2.6	0.65	255

Table 8.7   Optical Absorption Data for 1,12-diaminododecane

Original Concentration of Stock Solution mM	Absorbance of Stock Solution at 570nm	Absorbance of Supernatant at 570nm
5	0.350	0.000
10	0.800	0.129
15	0.900	0.605
20	0.950	0.840
25	0.970	0.900
30	1.020	0.970

Table 8.8   Adsorption Data for 1,12-diaminododecane

Concentration in Original Stock Solution mM	Concentration in Supernatant mM	ΔC mM	$\Gamma_i \times 10^{10}$ mol.cm^{-2}	Area per Molecule Å^2
5	0.6	4.4	1.1	156
10	2.2	7.8	2.0	83
15	7.0	8.0	2.0	83
20	12.0	8.0	2.0	83
25	17.0	8.0	2.0	83
30	22.0	8.0	2.0	83

Figure 8.1   Full Range IR Transmission Spectrum of Sorbitan Monopalmitate with

Toluene Subtracted
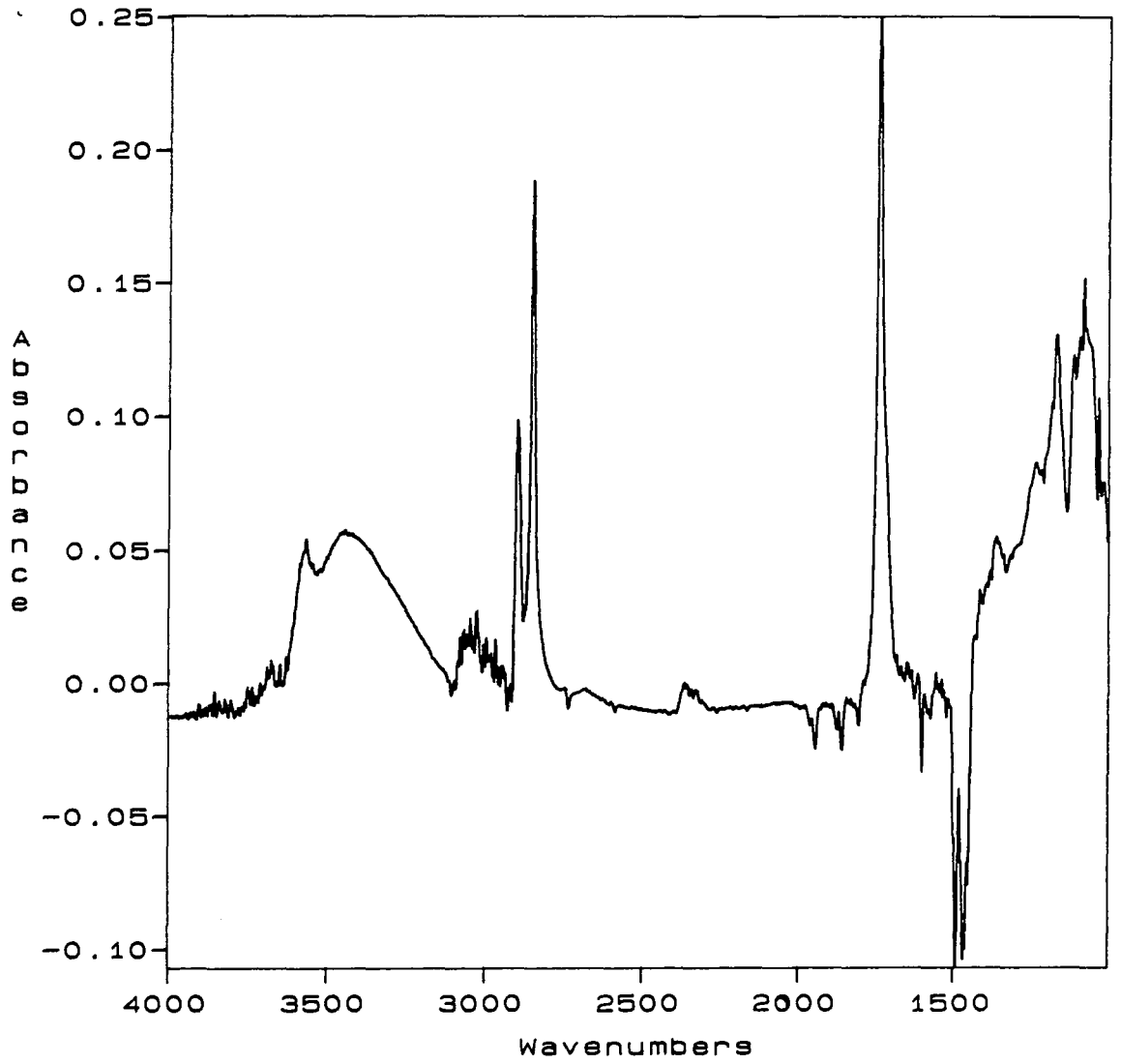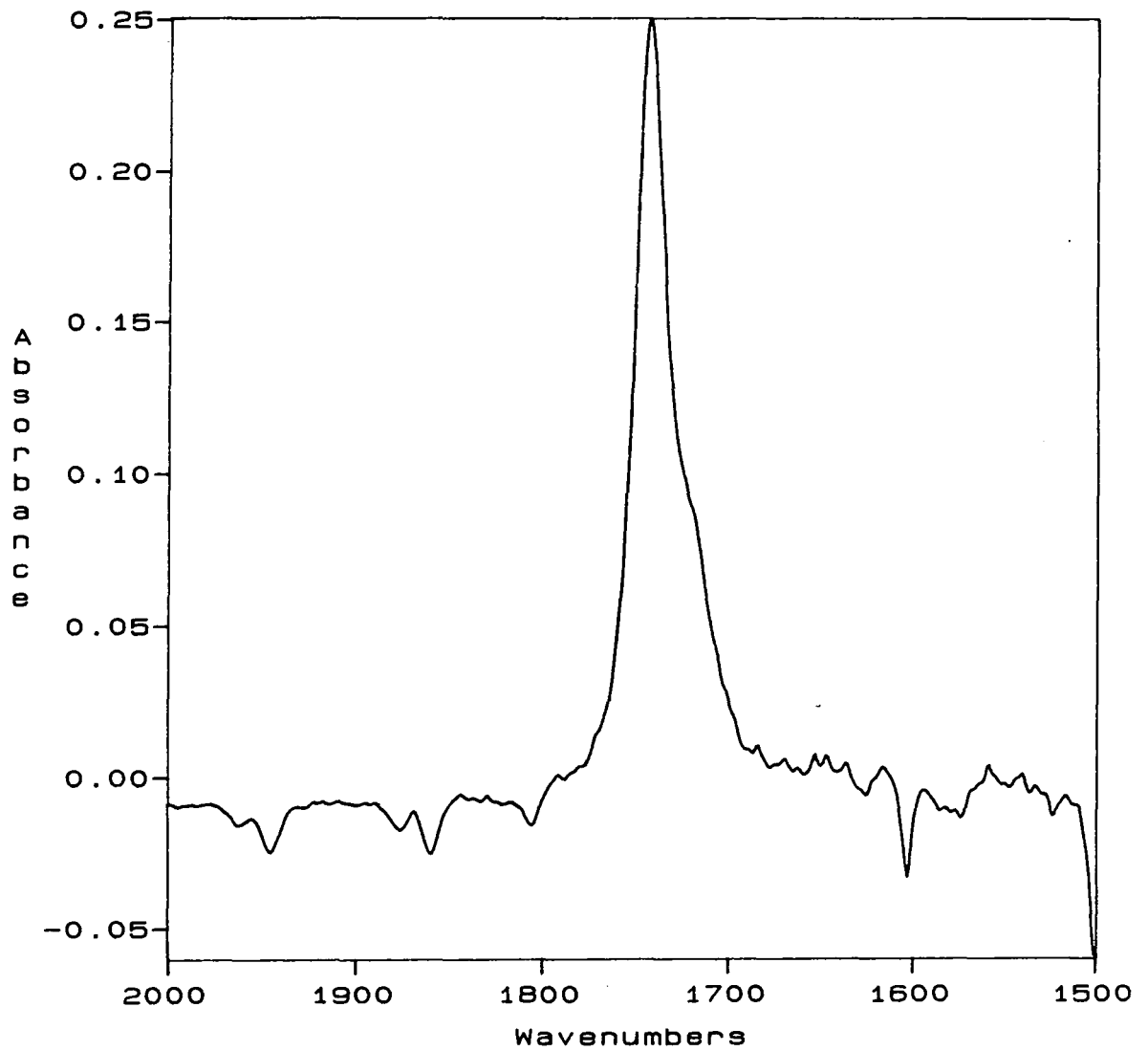
Figure 8.3
Area of Carbonyl Peak vs. Concentration for Sorbitan Monopalmitate

Absorbance (cm-1)

Concentration (mM)
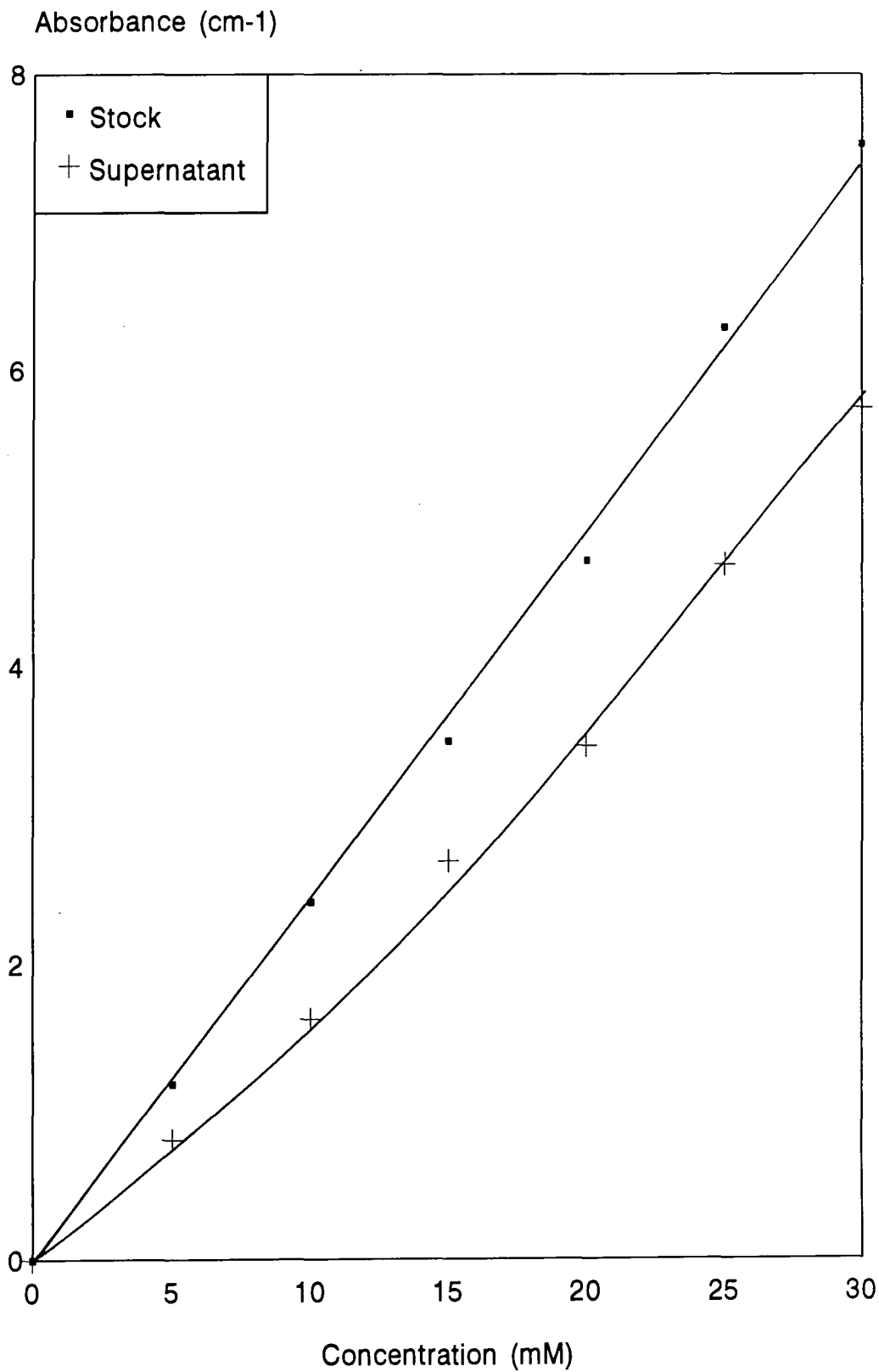
Figure 8.5
Optical Absorbance Data for Hexadecylamine
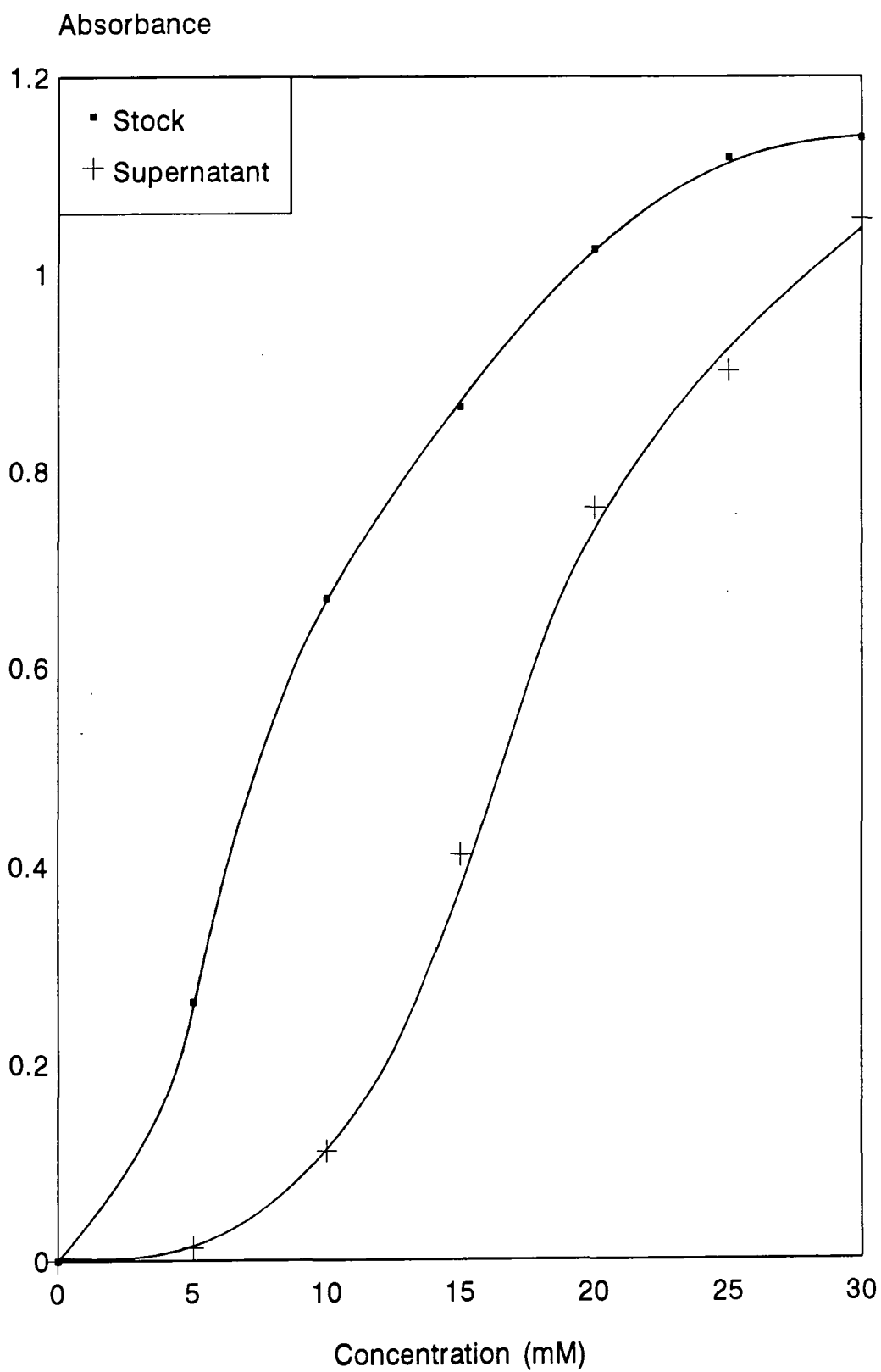
Figure 8.6 Adsorption Isotherm for Hexadecylamine
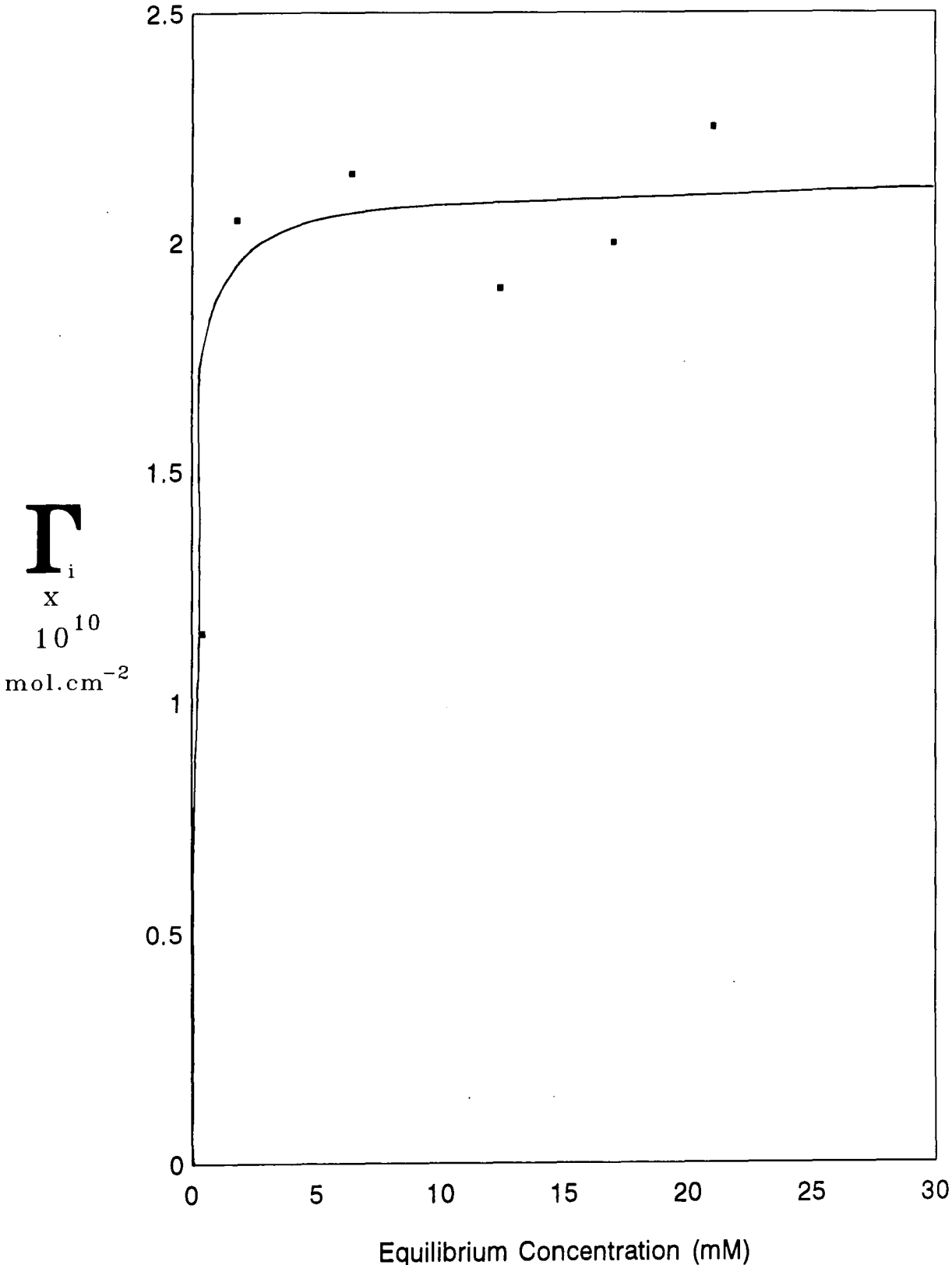
Figure 8.7
Optical Absorbance Data for Didecylamine
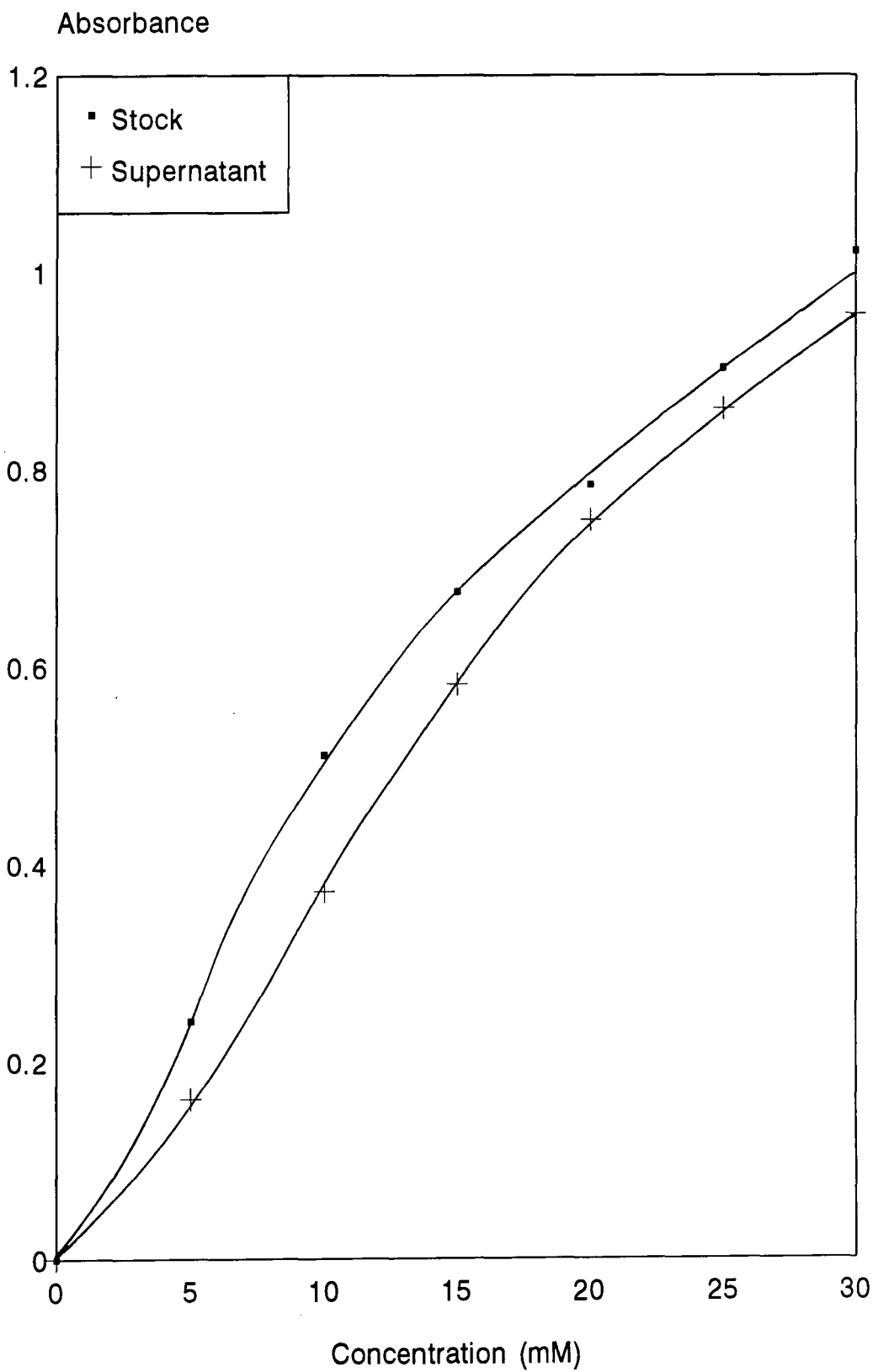
Figure 8.8 Adsorption Isotherm for Didecylamine
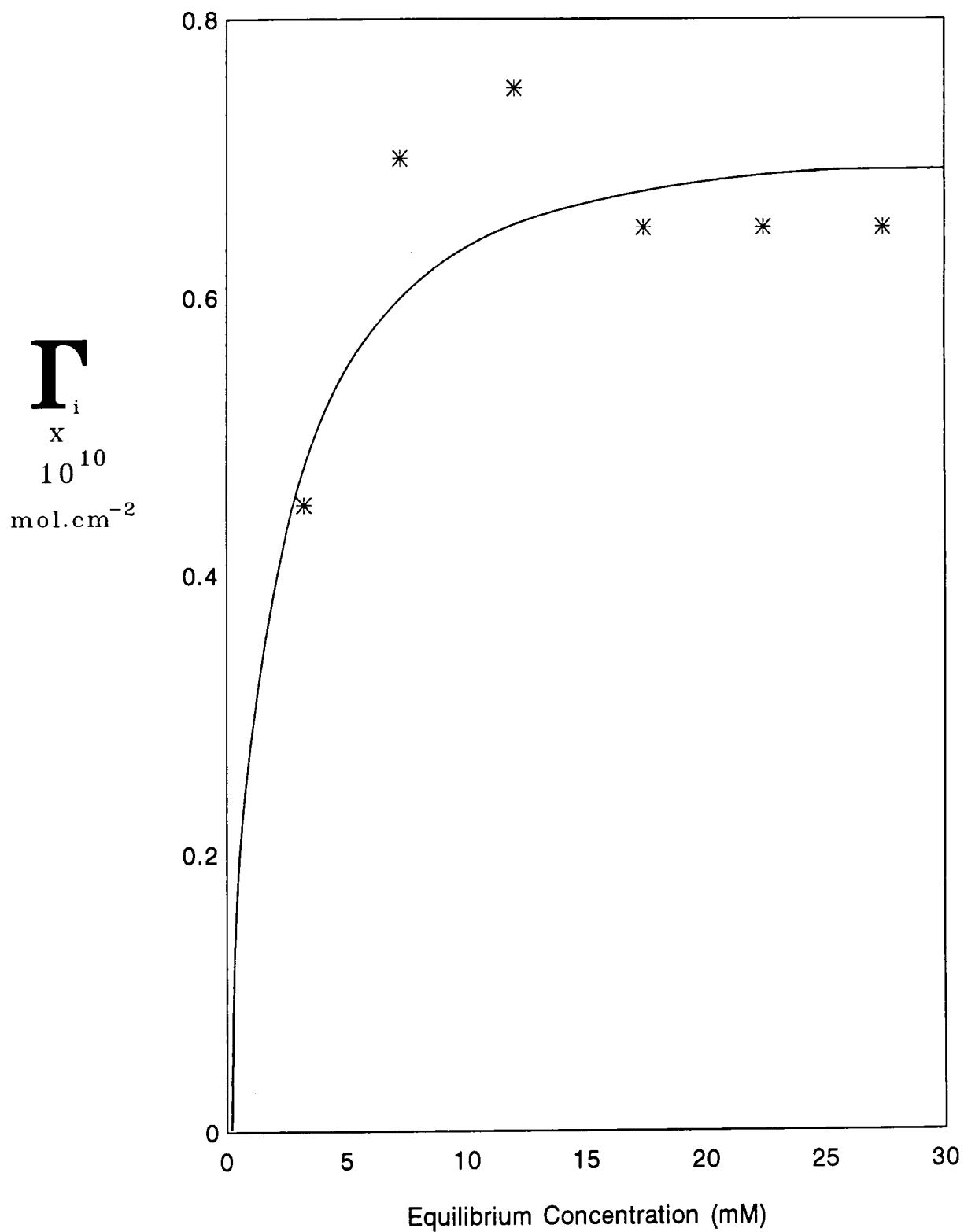
Figure 8.9
Optical Absorbance Data for 1,12-diaminododecane
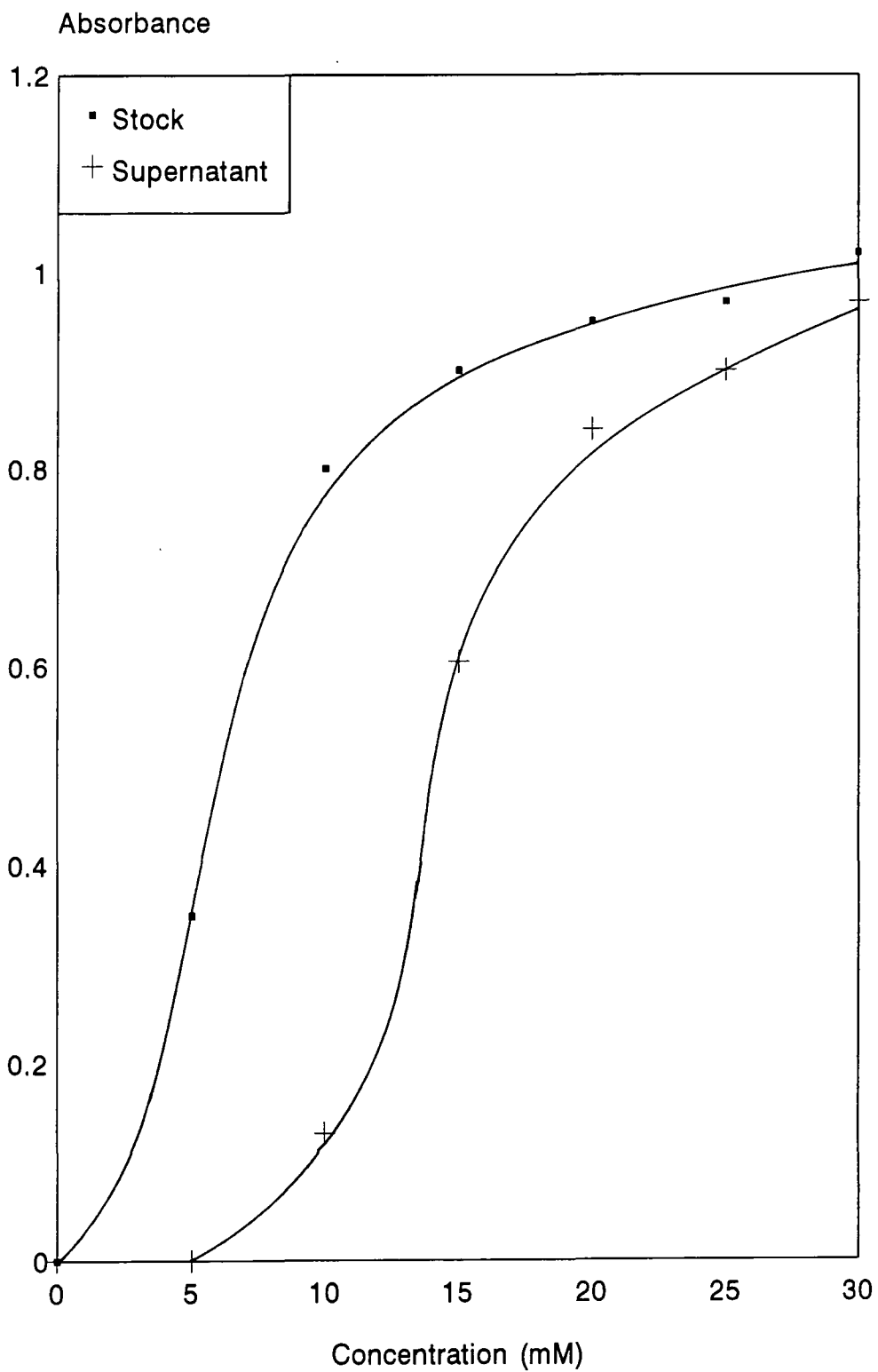
Figure 8.10 Adsorption Isotherm for 1,12-diaminododecane
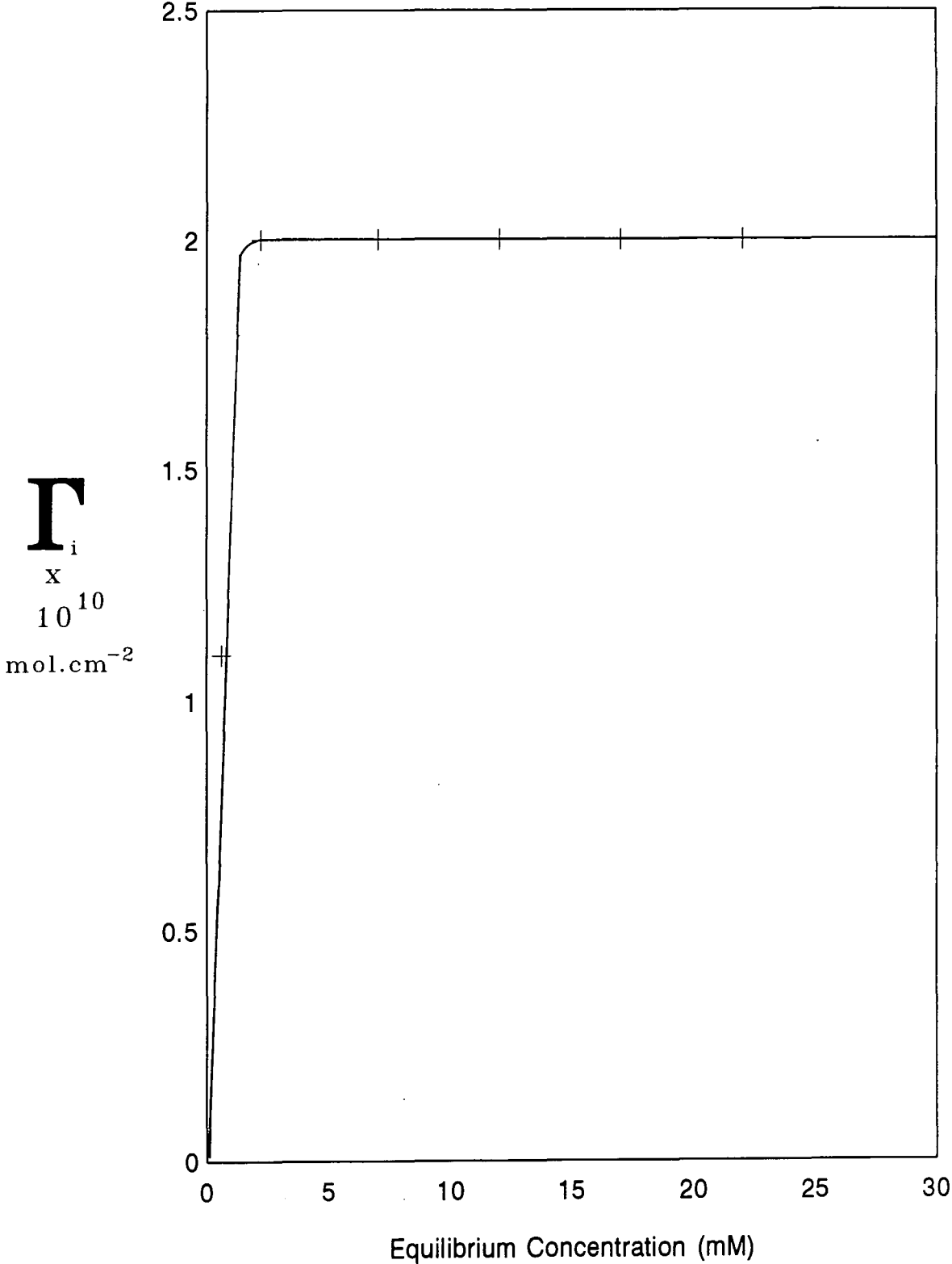
Figure 8.11
Adsorption Isotherms for all four Surfactants
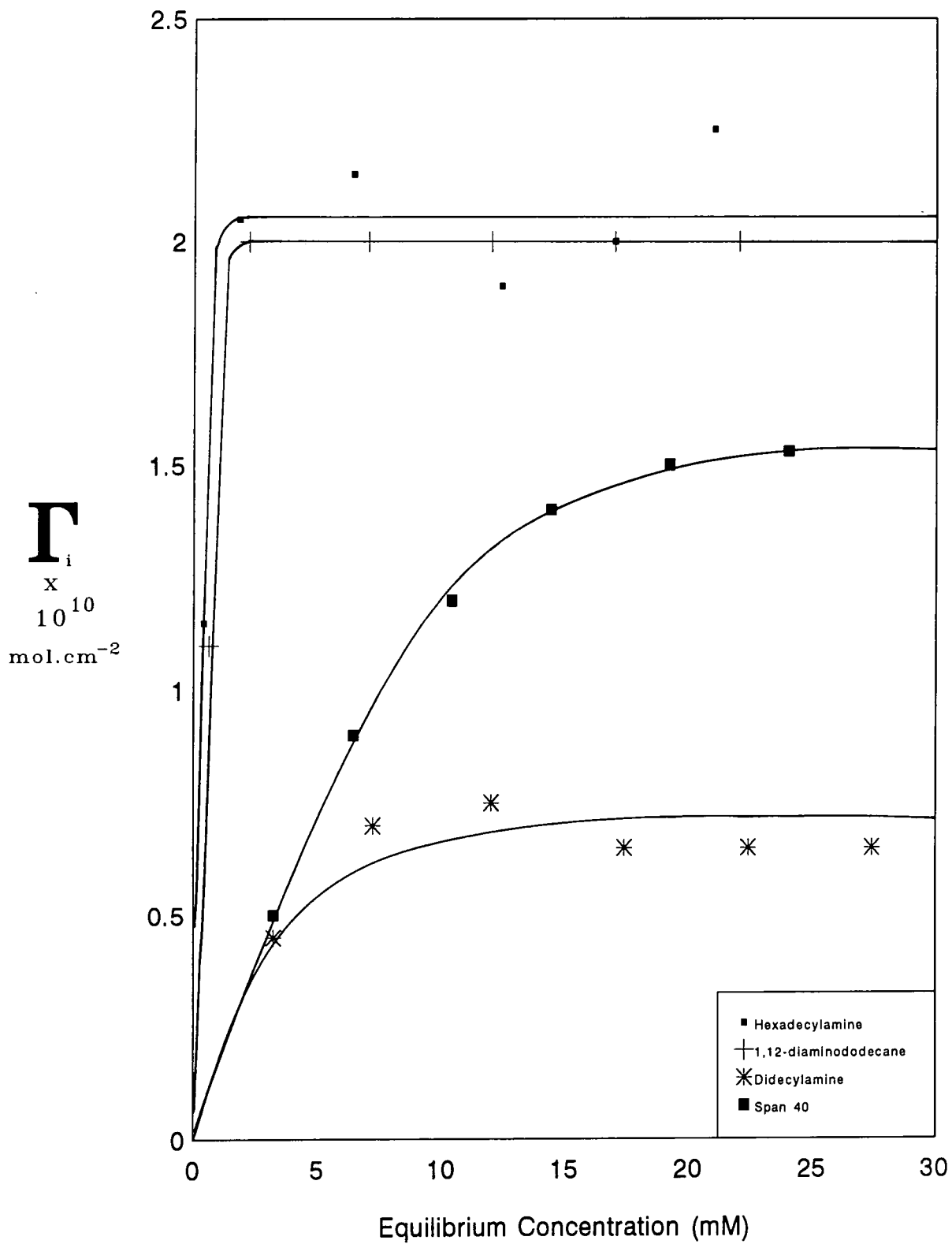
Figure 8.12

BOHLIN RHEOMETER SYSTEM   Shell Research, Thornton, Surface and Colloid Group
Viscometry test
1993-02-12   10:20:10 #   1

20g/L Aerosil 200 in Toluene

✕—✕ Viscosity

C 25
3.99 g/cm   1 ✕

No A zero

SDt 30 s   It 30 s
No of M 1
MI 30 s

T   24.3 -   25.3 C
H   17.38 -   81.78 %

234

Figure 8.13

✳✳ Viscosity

5mM Hexadecylamine 20g/L Aerosil200 No.1/2

C 25
3.99 g cm   1 x

No A zero

SDt 30 s   It 30 s
No of M 1
MI 30 s

T   24.0 -   25.2 C
R   6.23 -   85.93 % -

Viscosity   Pas

Shear rate   1/s

Figure 8.14

✳✳ Viscosity

25mM Hexadecylamine 20g/L Aerosil200 No.1/2

C 25
0.233 g cm   1 x

No A zero

CDt 30 s   It 30 s
No of M 1
MI 30 s

T   24.1 -   25.2 C
R   0.96 -   90.74 %

Viscosity   mPas

Shear rate   1/s

Figure 8.15

×—× Viscosity

5mM Didecylamine 20g/L Aerosil200

C 25
3.99 g cm   1 ×

No A zero

SDt 30 s   It 30 s
No of M 1
MI 30 s

T   24.1 -   25.3 C
R   1.61 -   82.03 %

Figure 8.16

×—× Viscosity

25mM Didecylamine 20g/L Aerosil200

C 25
1.723 g cm   1 ×

No A zero

SDt 30 s   It 30 s
No of M 1
MI 30 s

T   24.1 -   25.2 C
R   4.64 -   94.63 %

Figure 8.17

5mM 1,12-diaminododecane 20g/L Aerosil200 1

x-x Viscosity

C 25
3.99 g cm   1 x

No A zero

SDt 30 s   It 30 s
No of M 1
MI 30 s

T   24.2 - 25.1 C
R   11.40 - 90.55 %

Viscosity Pas

Shear rate   1/s

Figure 8.18

25mM 1,12-diaminododecane 20g/L Aerosil200 1

x-x Viscosity

C 25
3.99 g cm   1 x

No A zero

SDt 30 s   It 30 s
No of M 1
MI 30 s

T   24.0 - 25.2 C
R   0.71 - 71.35 %

Viscosity Pas

Figure 8.19

×-× Viscosity

C 25
3.99 g cm   1 x

No A zero

SDt 30 s   It 30 s
No of M 1
MI 30 s

T 24.0 - 25.2 C
R   3.30 - 51.98 %

10mM Span40 20g/L Aerosil200

Shear rate   1/s

Figure 8.20

×-× Viscosity

C 25
3.99 g cm   1 x

No A zero

SDt 30 s   It 30 s
No of M 1
MI 30 s

T 24.2 - 25.3 C
R   4.08 - 48.92 %

25mM Span40 20g/L Aerosil200
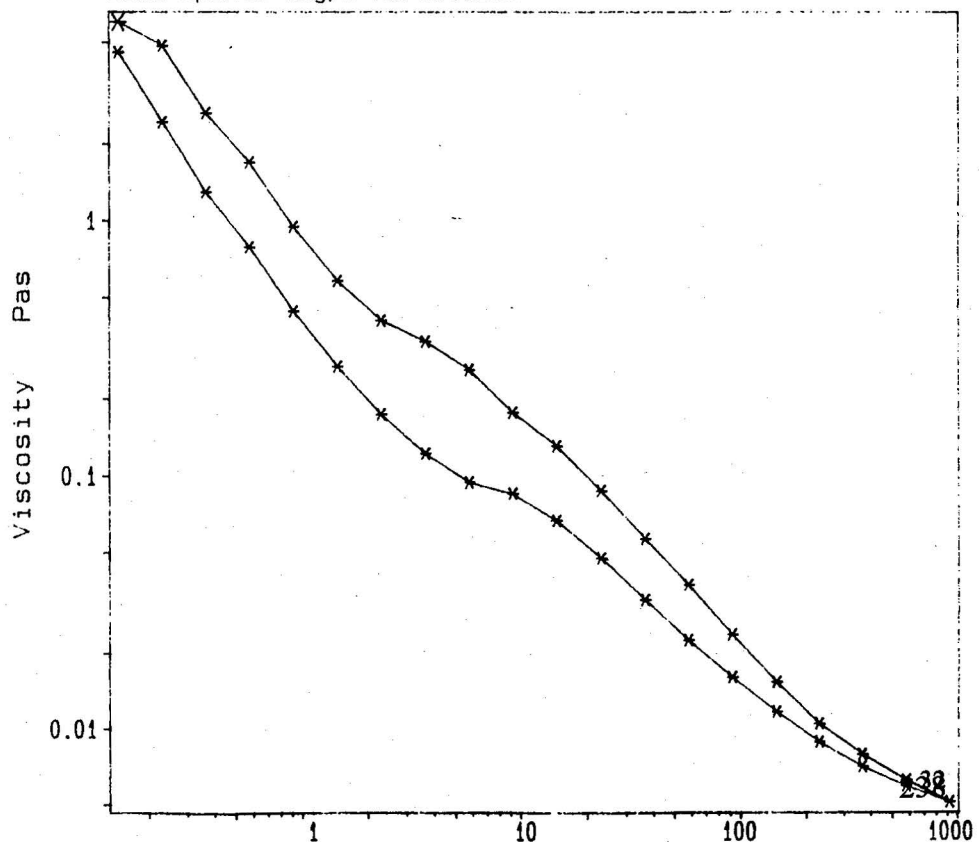
Figure 8.21 Viscosity as a Function of Surfactant Concentration
Shear Rate = 1.46 s-1
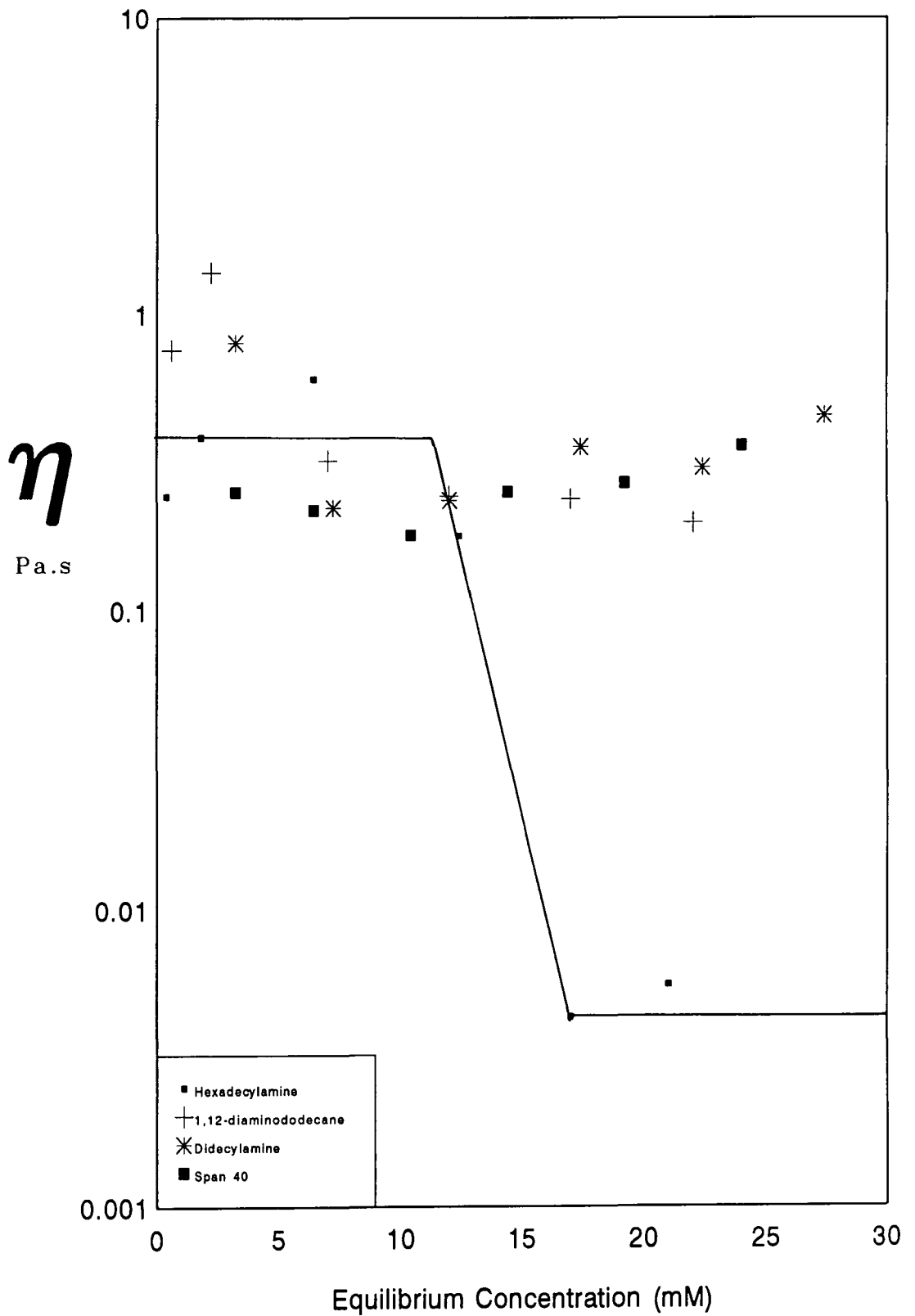
Figure 8.22 Adsorption and Viscosity Data for Hexadecylamine
Shear Rate = 1.46 s-1
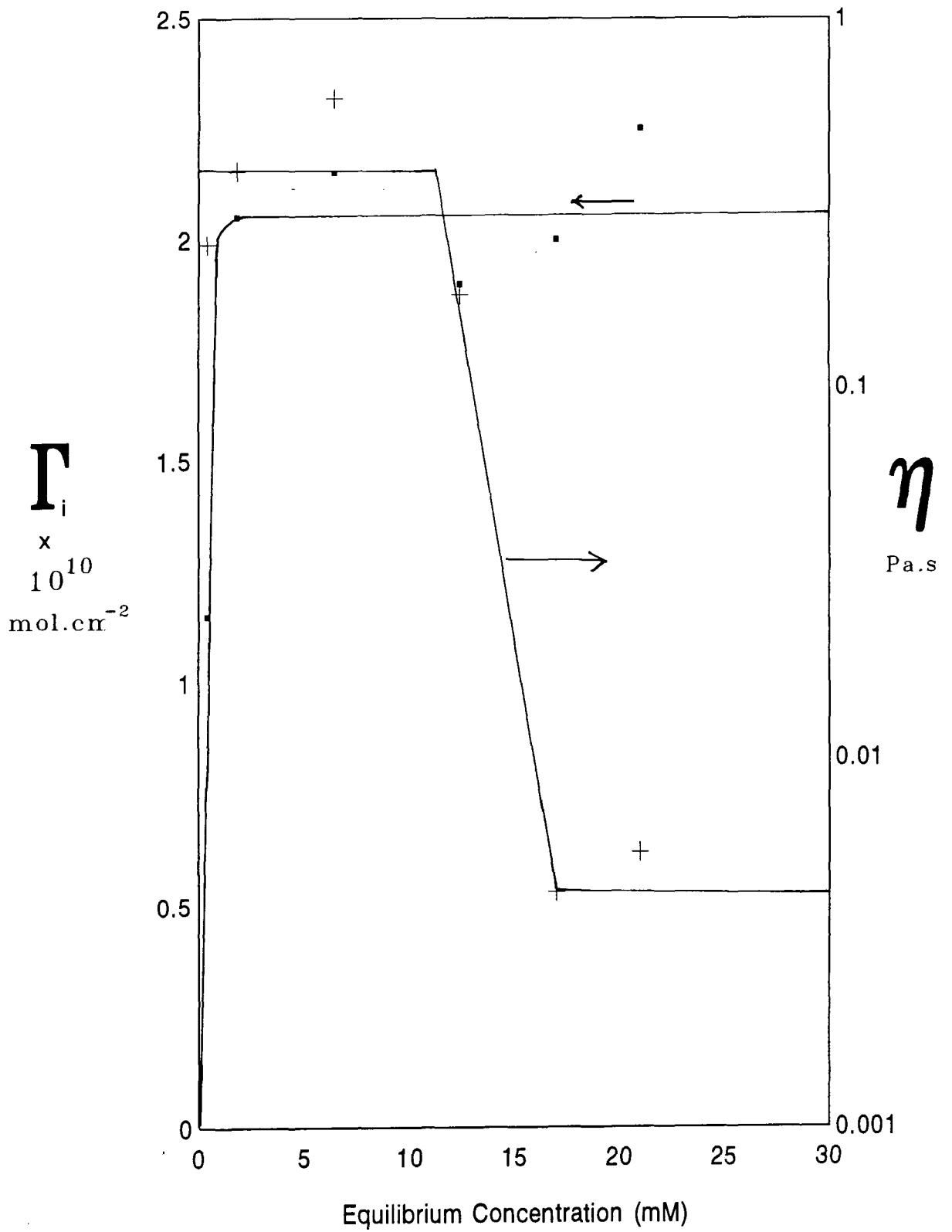
Figure 8.23 Adsorption and Viscosity Data for 1,12-diaminododecane
Shear Rate = 1.46 s-1
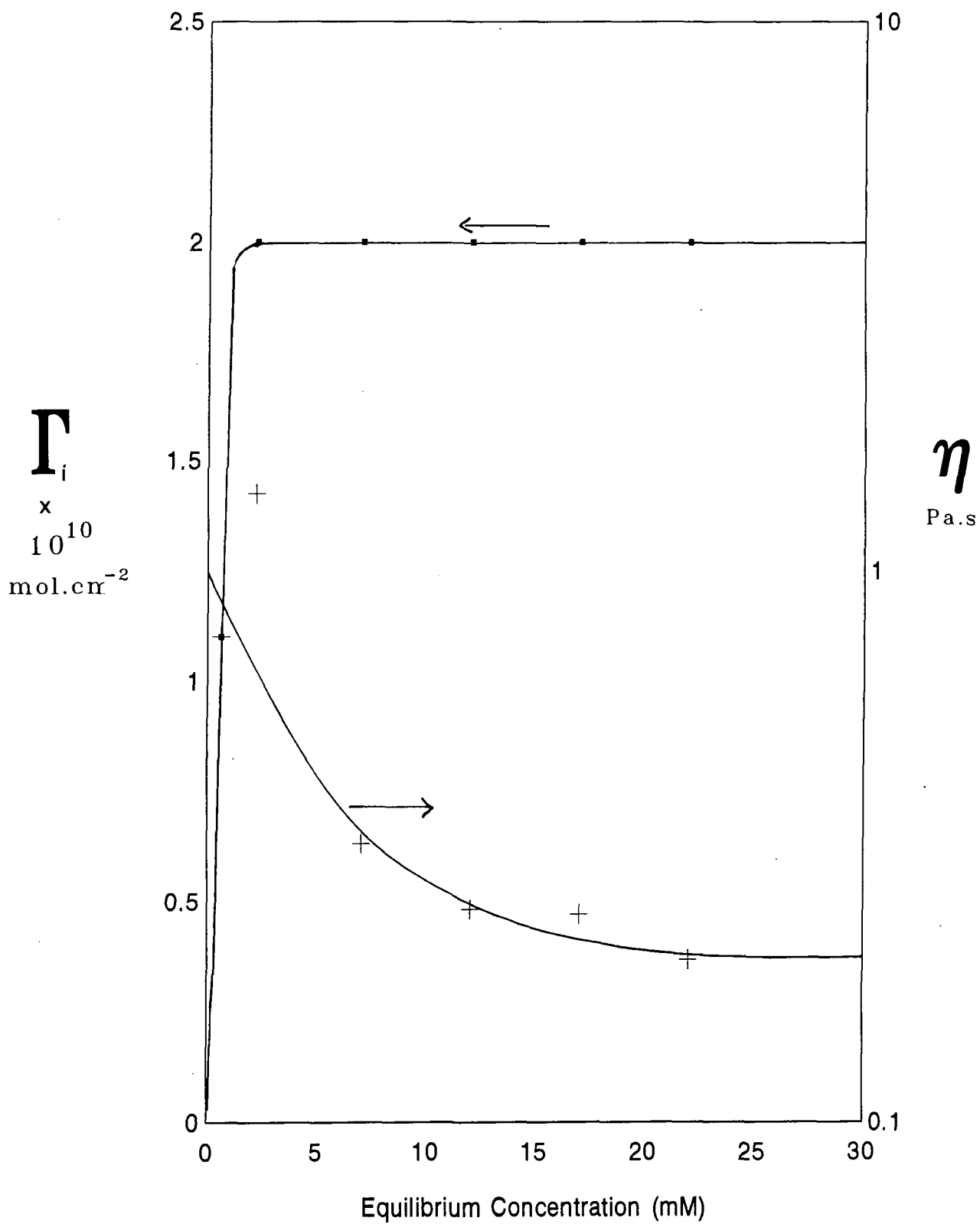
Figure 8.24 Adsorption and Viscosity Data for Didecylamine
Shear Rate = 1.46 s-1
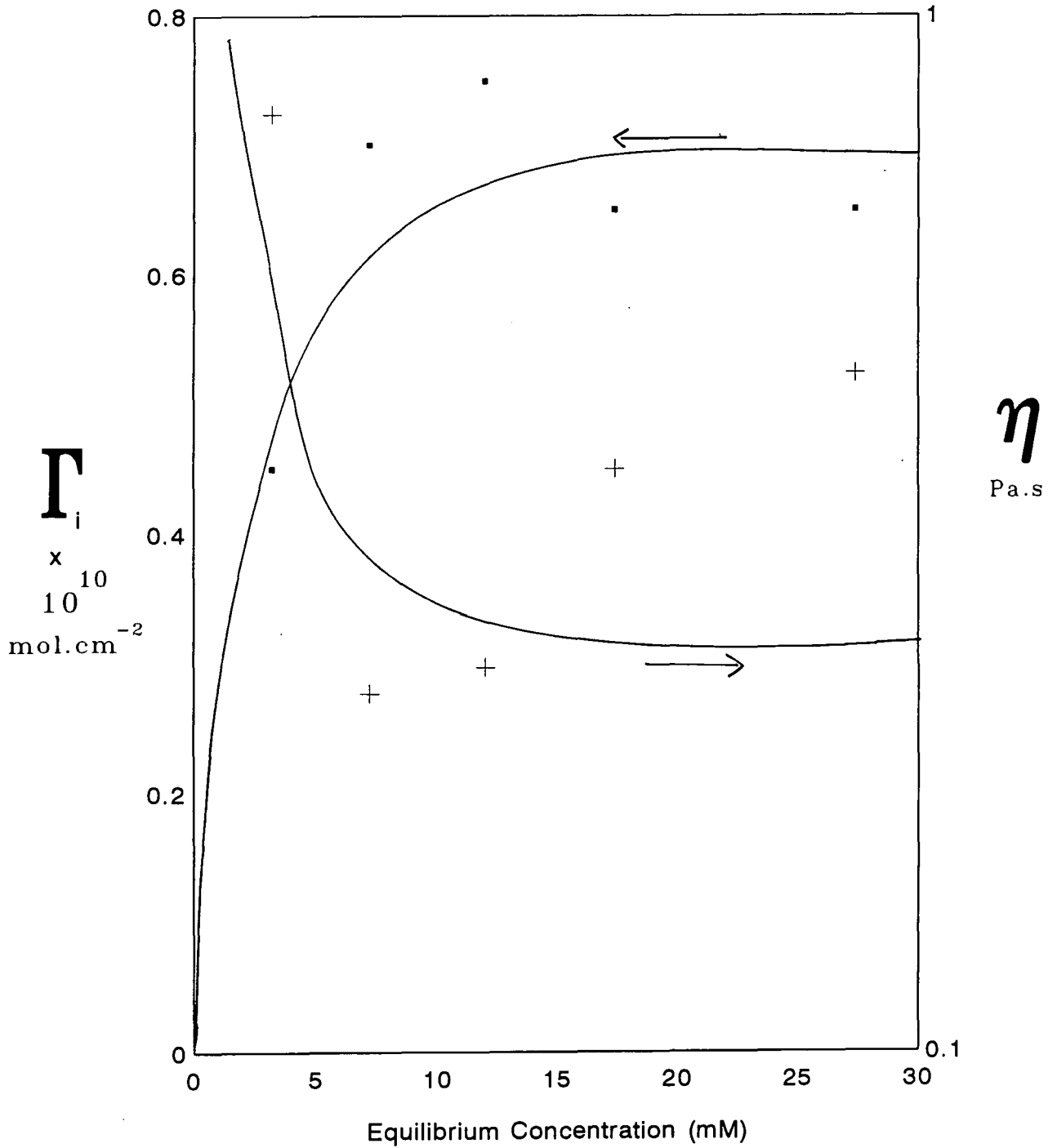
Figure 8.25 Adsorption and Viscosity Data for Sorbitan Monopalmitate
Shear Rate = 1.46 s-1
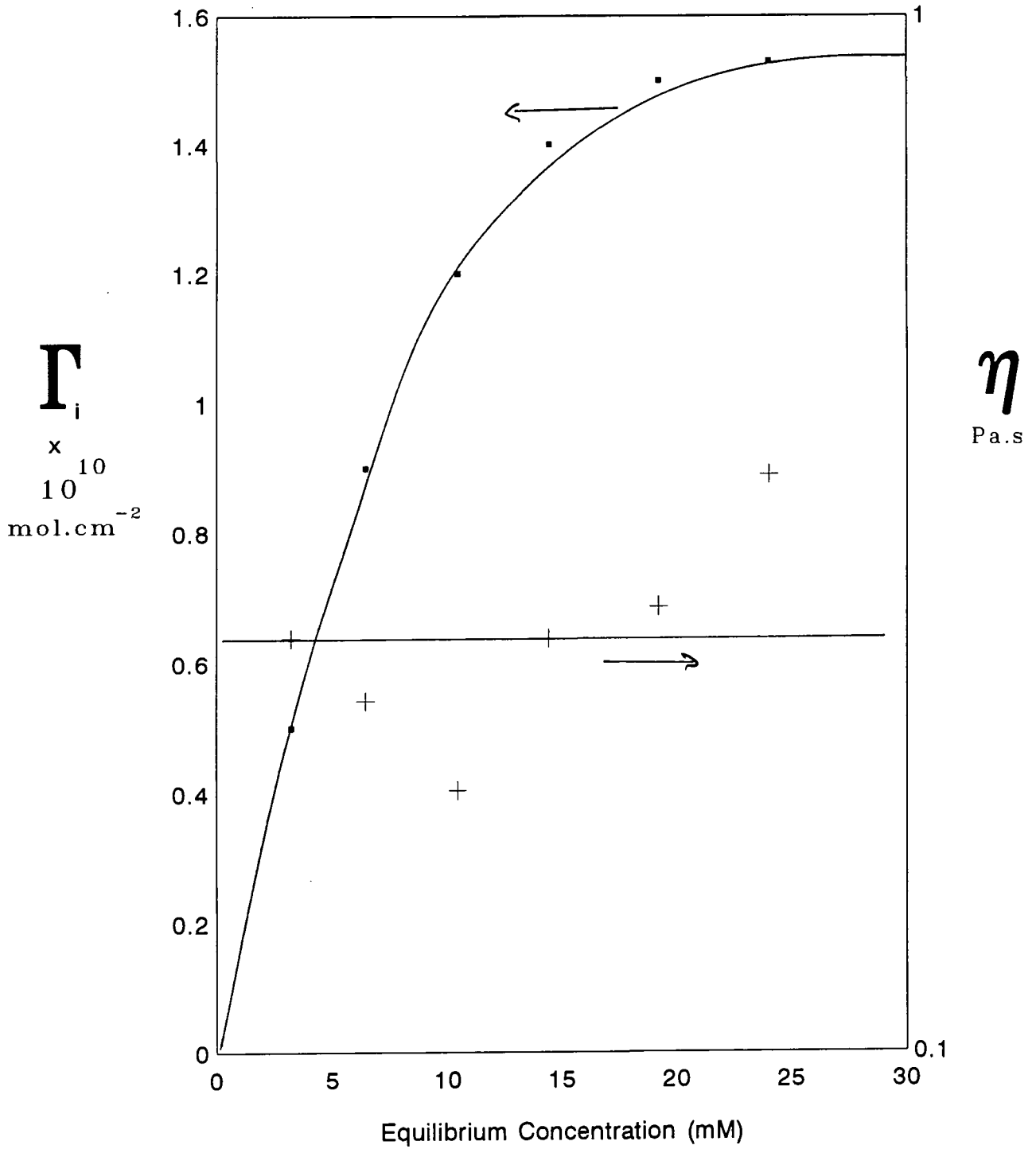
Chapter 9   Comparison of Infrared and Rheological Data

9.1   Introduction

Chapters 6 and 7 described infrared studies of the structure of layers of surfactant molecules adsorbed at the silica/toluene interface. The effect of those surfactants on the behaviour of dispersions of Aerosil 200 in toluene was described in chapter 8. In this chapter the two sets of results are compared. Firstly, the adsorption isotherms obtained from the ATR experiments are compared with those obtained from solution depletion measurements on the dispersions. This gives some measure of how good a model the surface of the silicon ATR prism is for the Aerosil 200 surface. Providing that the prism surface is a good model for the Aerosil 200 surface, the rheological behaviour of dispersions treated with the surfactants may be related to the structures of the adsorbed layers of those surfactants, as determined by FTIR-ATR.

Quantitative ATR data is only available for the amine-based surfactants and so the following discussion concentrates on these compounds.

9.2   Comparison of Adsorption Isotherms of the Amine Based Surfactants

The adsorption isotherms for the amine-based surfactants as determined by FTIR-ATR and solution depletion techniques have been presented in chapters 6 and 8 respectively. All these isotherms reached a plateau. The values of the surface excess concentration, Γ_i, for each surfactant at the isotherm plateau, together with the corresponding area per molecule, as determined by the two techniques are given in table 9.1.

The plateau values of Γ_i for the two primary amines as determined by ATR are comparable whilst that for didecylamine is significantly lower. The same pattern is found by the solution depletion technique. However, for a given surfactant, the value of Γ_i determined by the ATR technique is lower than that determined by the solution depletion method. The agreement is poorest for didecylamine. This is probably

because the low adsorption of the secondary amine gives rise to greater errors in the determination of Γ_i than in the determination of Γ_i for the primary amines.

Table 9.1   Adsorption Data as Determined by FTIR-ATR and Solution Depletion Techniques

Surfactant	$\Gamma_i \times 10^{-10}$ (mol.cm^{-2}) ATR	$\Gamma_i \times 10^{-10}$ (mol.cm^{-2}) Solution Depletion	Area per Molecule (Å^2) ATR	Area per Molecule (Å^2) Solution Depletion
Hexadecyl-amine	1.2	2.0	138	83
1,12-diamino-dodecane	1.5	2.0	111	83
Didecylamine	0.3	0.7	553	237

In a study of the adsorption of cetylpyridinium chloride (CPC) from solution in CH_2Cl_2 onto zinc selenide, Sperline et al [46] obtained a value for Γ_i of 5.7×10^{-10}mol.cm^{-2} by ATR and 9.0×10^{-10}mol.cm^{-2} by solution depletion. Sperline considered this agreement to be 'fairly close'. In the current study a similar agreement was obtained: The value of the surface excess as determined by the ATR measurement is of the order of half that obtained by the solution depletion technique.

As discussed in chapter 6, the nature of the surface of the ATR prism is poorly characterized. From studies on silicon wafers produced for the semiconductor industry, it is known that there exists a native silicon oxide layer, approximately 50Å thick [99], on the silicon surface. The surface of this silica layer is unlikely to be identical to that of the Aerosil silica. However, on smooth, non-porous, amorphous silica the area per silanol group is typically 25Å^2 [24] and it is unlikely that the silanol density on the prism surface is much lower than this. Sagiv and co-workers [58] have produced self-assembled monolayers of octadecyltrichlorosilane on the native silicon

oxide layer on the surface of a silicon ATR prism in which the area per silane molecule is 25Å², suggesting that the silanol group density is sufficient to allow the formation of close-packed layers. An area per SiOH group of 25Å² also applies to the Aerosil 200 surface [25]. Clearly, from the area per molecule values presented in table 9.1, not every silanol group is bonded to an amine molecule. The silanol group density is not uniform on the amorphous silica surface; the SiOH groups are separated by a range of distances. Infrared studies of the silica surface [26, 27, 28 and Chapter 1] have identified both free and hydrogen-bonded silanol groups. It may be that the amine headgroup only forms a hydrogen bond with one type of silanol group, perhaps forming a bridge between two groups.

The values of the area available per molecule obtained by both techniques for all amines are greater than that expected for a close-packed monolayer (ca. 25Å²). This indicates that the molecules adsorbed on the ATR prism and those on the Aerosil surface do not exist in tightly packed, well-ordered films. Therefore, it is not unreasonable to speculate that the conformational order present in the films studied by ATR is likely to be similar to that in the adsorbed layer on the Aerosil particles.

In summary, the ATR measurements show similar trends in the adsorption behaviour of the three amines to the solution depletion measurements. The isotherms obtained by the solution depletion technique show higher plateau values of Γ_i than those obtained by ATR. This may be attributable to differences between the surface of the ATR prism and that of Aerosil silica. The plateau values of Γ_i obtained by both techniques show that not every available silanol group has an amine molecule bonded to it and that the area per adsorbed molecule is sufficiently large to allow conformational disorder in the aliphatic chains. The ATR data may therefore be used, with some caution regarding the density of the adsorbed layers, in the interpretation of the rheological behaviour of the silica/amine/toluene systems.

9.3   Structural Data and Rheology

The infrared studies of the adsorbed amines described in chapter 6 yielded information about their conformation and orientation. This information may help to explain differences in the rheological behaviour of dispersions 'stabilized' by the three amines which are not readily explicable from the adsorption isotherms.

The adsorption isotherm for hexadecylamine is very similar to that for 1,12-diaminododecane. This is true whether the isotherms are determined by ATR or solution depletion. Both isotherms rise monotonically to a plateau at a value of Γ_i which is less than that expected for a close-packed monolayer. The plateau values of Γ_i for hexadecylamine and 1,12-diaminododecane are comparable. However, the rheological behaviour of the silica/hexadecylamine/toluene system is very different to that of the silica/1,12-diaminododecane/toluene system. As shown in figure 8.22, the viscosity of the silica/hexadecylamine/toluene system falls by two orders of magnitude as the adsorption isotherm reaches a plateau. This suggests that the presence of a monolayer of hexadecylamine inhibits the aggregation of the silica particles, preventing the formation of a three-dimensional network, as described in chapter 4. The reduction of the viscosity of the silica/1,12-diaminododecane/toluene system as the plateau of the adsorption isotherm is reached is less dramatic, as shown in figure 8.23. A slight reduction is observed. This shows that 1,12-diaminododecane is less effective at hindering the aggregation of silica particles than the hexadecylamine, despite being present at the same surface excess concentration.

The ATR data presented in chapter 6 showed that the adsorbed layers of hexadecylamine were more ordered than those of 1,12-diaminododecane. The peak positions of the antisymmetric methylene stretching bands in the ATR spectra of the adsorbed layers of the two amines and (non-adsorbed) hexadecane are given in table 9.2. As the gauche content of the chains increase, ν_{max} moves to higher frequency. The value of ν_{max} for the adsorbed layer of hexadecylamine is lower than that of

hexadecane, indicating that the chains in the adsorbed layer have a higher trans content than the totally random chains in solution. The value of v_{max} for adsorbed 1,12-diaminododecane is greater than that of hexadecane or the compound in solution, indicating that the adsorbed chains have a higher gauche content than the chains in solution. This may be to allow the chains to bend around such that both amine groups are bonded to the surface.

Table 9.2   Position of the Maximum of the Antisymmetric Methylene Stretching Band in the ATR Spectra of Three Compounds

Compound	v_{max} (cm^{-1})
Hexadecane (non-adsorbed)	2926
Hexadecylamine (adsorbed)	2920-2924
1,12-diaminododecane (adsorbed)	2930

The dichroic ratios calculated in chapter 6 showed that the molecules in the adsorbed layer of hexadecylamine were to some extent oriented perpendicular to the surface plane. The perfection of this alignment was variable and this is reflected by the range of values of v_{max} quoted in table 9.2. In one of the measurements (that of the 12.5mM solution), the dichroic ratio suggested that the alignment was perfect, and this corresponds to the lowest value of v_{max}. Dichroic studies of the adsorbed layer of 1,12-diaminododecane showed no such orientation. If the 1,12-diaminododecane molecules do loop around, no orientation of the chains perpendicular to the surface is expected. If both ends of the molecule adsorb then each molecule occupies two adsorption sites and therefore one may expect the surface excess concentration to be approximately half that of hexadecylamine. This is not the case. The area per molecule is large enough to allow both ends to adsorb and it may be that once one amine group has adsorbed onto a favourable site the second group then adsorbs onto a

less favourable site. There is certainly sufficient spectroscopic evidence to suggest that some of the adsorbed molecules exists in a looped configuration, from the $v(CH_2)$ values. It seems likely that the adsorbed layer of 1,12-diaminododecane contains some molecules with both ends adsorbed and some with one end free. The structure of the adsorbed layer of 1,12-diaminododecane is clearly quite different to that of hexadecylamine. Possible structures of the adsorbed layers of hexadecylamine and 1,12-diaminododecane as suggested by the ATR results are shown schematically in figure 9.1.

Figure 9.1   Schematic of the Structures of the Adsorbed Layers of the Primary Amines

I. Hexadecylamine
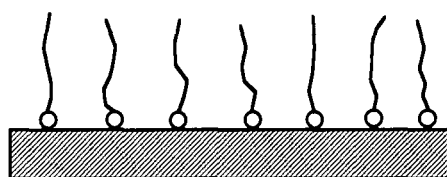
II. 1,12-diaminododecane

Aliphatic Tail   Amine Headgroup
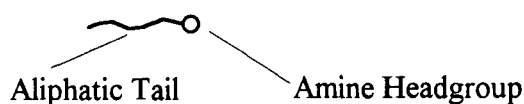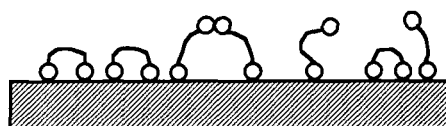
The adsorption isotherms of hexadecylamine and 1,12-diaminododecane show that the surface excess concentrations of the two molecules are comparable. The spectroscopic studies reveal, however, that the structures of the adsorbed layers are different. These differences in the adsorbed layer structure are reflected by the rheological behaviour of the systems. The hexadecylamine layer is quite well ordered and, despite not being

close-packed, inhibits the formation of three-dimensional networks in the system. The poorly ordered 1,12-diaminododecane layer is much less effective at inhibiting aggregation. As the diamine layer is poorly ordered and appears to contain molecules in looped configurations, the spatial extension of the layer will be less than that of the (ordered) hexadecylamine layer. This difference in spatial extension is over and above the difference in chain length. The sharp rise in the V_s curve will therefore occur closer to the particle surface in the case of the 1,12-diaminododecane than it will with the hexadecylamine layer (see figure 4.9). The depth of the secondary minimum, V_{min}, will therefore be greater with 1,12-diaminododecane than with hexadecylamine. Hexadecylamine will therefore stabilize the silica dispersion more effectively than 1,12-diaminododecane. As 1,12-diaminododecane has a headgroup at either end, the possibility of one molecule bridging two silica particles arises. This will also reduce the efficiency of the diamine as a stabilizer.

The adsorption isotherms for didecylamine obtained by both ATR and solution depletion techniques show that the plateau value of Γ_i is much lower that those of the primary amines. The area per molecule values are very much larger than those expected for a close-packed monolayer. Surface coverage by didecylamine, then, is poor and there are large areas of bare silica surface. The orientational measurements made by ATR show that the adsorbed layer is completely random. The spatial extension of the adsorbed molecules into the dispersion medium will therefore be much less than that of the hexadecylamine layer. Didecylamine would, therefore, not be expected to inhibit the aggregation of silica particles. This is supported by the rheological data. The viscosity of the silica/didecylamine/toluene system remains essentially constant over the range of didecylamine concentrations studied.

9.4   Conclusions

The rheological properties of dispersions of silica in toluene in the presence of an aliphatic amine may be related to the structure of the adsorbate layer, as determined by

in situ FTIR-ATR. The adsorption isotherms of hexadecylamine and 1,12-diaminododecane are very similar but their effects on the rheological properties of silica-in-toluene dispersions are quite different. Hexadecylamine forms an adsorbed layer which, while not close-packed, is capable of inhibiting the aggregation of silica particles. The molecules in the adsorbed layer are quite well ordered and are, on average, oriented perpendicular to the surface. Hence the spatial extension of the aliphatic chains into the dispersion medium is maximized. In contrast to this, 1,12-diaminododecane forms poorly ordered layers. There is spectroscopic evidence to suggest that some of the adsorbate molecules form a looped configuration such that both amine groups are bonded to the surface. The spatial extension of the chains into the dispersion medium is therefore much less than that of the hexadecylamine chains. The diamine is therefore less effective at hindering aggregation than the hexadecylamine.

Didecylamine forms disordered layers in which there are large voids between neighbouring molecules. As the layer is poorly ordered, the spatial extension of the adsorbate tails into the dispersion medium is poor. The low spatial extension and the low surface coverage make didecylamine ineffective as an inhibitor of silica aggregation.

Quantitative information about the structure of the adsorbed layer of sorbitan monopalmitate proved impossible to obtain by *in situ* FTIR-ATR because the value of the extinction coefficient, ε, changed for all bands upon adsorption. The rheological properties of the silica/sorbitan monopalmitate/toluene system cannot, therefore, be related to structural properties.

9.5   Future Work

The techniques described in this thesis may be applied to the study of a great number of molecules onto the silica surface and it would be pointless to list them. However, in the context of the current study, it would be of use to investigate the adsorption of a series of primary aliphatic amines with a variety of chain lengths. Molecular order in the adsorbed layer and the effect of a monolayer on the rheology of dispersion as function of chain length should be investigated. This would give information about the importance of the spatial extension of the adsorbed layer to the rheological properties of the dispersions. Secondly, the effect of variations in chain branching should be investigated.

The modified Squarecol cell allows the temperature to be varied. In the present study the unit was used simply to maintain the cell temperature at 25°C. However, the effect of increasing or decreasing the temperature could be investigated.

The ability to confidently compare the ATR data to the rheological data requires that the surfaces of both the ATR prism and the Aerosil are well characterized and are similar. The surface of the silicon ATR prism is poorly characterized. In order to fully understand the difference between adsorption onto the ATR prism and the Aerosil surface it is necessary to obtain a reproducible, fully characterized prism surface. Of particular interest is the density of the silanol groups. The effect of surface treatments other than the 2-propanol reflux on the silanol group density and hence the adsorption behaviour of the amine molecules should be investigated. Such treatments as exposure to an RF oxygen plasma could be used.

References

1.   Hunter, R.J.; "*Foundations of Colloid Science: Volume 1*" Oxford Science Publications, Oxford, 1989.

2.   Lyklema, J.; "*Fundamentals of Interface and Colloid Science: Volume 1: Fundamentals*" Academic Press, 1991.

3.   London, F.; *Z. Phys.*, **89**, 736, 1934.

4.   Hamaker, H.C.; *Physica*, **4**, 1058, 1937.

5.   Lifshitz, E.M.; *Sov. Phys. JETP*, **2**, 73, 1956.

6.   Napper, D.H.;"*Polymeric Stabilization of Colloidal Dispersions*", Academic Press, London, 1983.

7.   Cosgrove, T.; *J. Chem. Soc. Faraday Trans*, **86**(9), 1323-1332, 1990.

8.   Evers, O.A.; Scheutjens, J.M.H.M. and Fleer, G. J.; *J. Chem. Soc. Faraday Trans*, **86**(9), 1333-1340, 1990.

9.   Scheutjens, J.M.H.M. and Fleer, G.J.; *J. Phys. Chem.*, **83**, 1619, 1979.

10.   Scheutjens, J.M.H.M. and Fleer, G.J.; *J. Phys. Chem.*, **84**, 178, 1980.

11.   Scheutjens, J.M.H.M. and Fleer, G.J.; *Macromolecules*, **18**, 1882, 1985.

12.   Dickinson, E.; *Mol. Phys.*, **65**, 895, 1988.

13.   Dickinson, E.; *Mol. Phys.*, **68**, 407, 1989.

14.   Fleer, G.J. and Scheutjens, J.M.H.M.; *Colloids and Surfaces*, **51**, 281, 1991.

15.   Lee, J-J. and Fuller, G.G.; *J. Coll. Int. Sci.*, **103**(2), 569, 1985.

16.   Dijt, J.C.; Cohen-Stuart, M.A.; Hofman, J.E. and Fleer, G.J.; *Colloids and Surfaces*, **51**, 141, 1990.

17.   Munch, M.R. and Gast, A.P.; *J. Chem. Soc. Faraday Trans*, **86**(9), 1341,1990.

18.   Kawaguchi, M; Kawaarabayashi, M.; Nagata, N.; Kato, T.; Yoshioka, A and Takahashi, A; *Macromolecules*, **21**, 1059, 1988.

19.   Kawaguchi, M; Hanai, H.; Takahashi, A.; Nagata, N. and Yoshioka, A.; *Colloids and Surfaces*, **37**, 319,1989.

20.   Kawaguchi, M.; Kawarabayashi, M.; Takahashi, A.; Nagata, N. and Yoshioka, A.; *Colloids and Surfaces*, **48**, 363, 1990.

21.   Kawaguchi, M.; Yamagiwa, S.; Takahashi, A. and Kato, T.; *J. Chem. Soc. Faraday Trans*, **86**(9), 1383, 1990.

22.   Cosgrove, T.; Prestidge, C.A. and Vincent, B.; *J. Chem. Soc. Faraday Trans*, **86**(9), 1377, 1990.

23.   Killmann, Fulka, C. and Reiner, M.; *J. Chem. Soc. Faraday Trans*, **86**(9), 1389, 1990.

24.   Iler, R.K.; *The Chemistry of Silica*, Wiley-Interscience, N.Y. 1990.

25.   *Basic Characteristics and Applications of AEROSIL®*;Technical Bulletin Pigments No. 11; Degussa AG., Frankfurt.

26.   Hair, M.L.; *Infrared Spectroscopy in Surface Chemistry*; Marcel Dekker, N.Y., 1967.

27.   Kunath, D and Schultz, D.; *J. Colloid and Interface Science*, **66**, 379, 1978.

28.   McFarlan, A.J. and Morrow, B.A.; *J. Phys. Chem.*, **95**(14), 5388, 1991.

29.   Low, M.J.D. and Hasegawa, M.; *J. Colloid and Interface Science*, **26**, 95, 1968.

30.   Hasegawa, M. and Low, M.J.D.; *J. Colloid and Interface Science*, **29**(4), 593, 1969.

31.   Hasegawa, M. and Low, M.J.D.; *J. Colloid and Interface Science*, **30**(3), 378, 1969.

32.   Low, M.J.D. and Lee, P.L.; *J. Colloid and Interface Science*, **45**(1), 148, 1973.

33.   Rochester, C.H.; *Adv. Colloid and Interface Science*, **12**(1), 43, 1980.

34.   Yang, R.T.; Low, M.J.D.; Haller, G.L. and Fenn, J.; *J. Colloid and Interface Science*, **44**(2), 249, 1973.

35.   Harrick, N.J.; *Phys. Reviews Lett.*, **4**(5), 224, 1960.

36.   Harrick, N.J.; *J. Phys. Chem.*, **64**, 1110, 1960.

37.   Fahrenfort, J.; *Spectrochim. Acta*, **17**, 698, 1961.

38.   Swalen, J.D.; Allara, D.L.; Andrade, J.D.; Chandross, E.A.; Garoff, S.; Israelachvili, J.; McCarthy, T.J.; Murray, R.; Pease, R.F.; Rabolt, J.F.; Wynne, K.J. and Yu, H.; *Langmuir*, **3**, 932, 1987.

39.   Kimura, F.; Umemura, J. and Takenaka, T.; *Langmuir*, **2**, 96, 1986.

40.   Okamura, E.; Umemura, J. and Takenaka, T.; *Biochimica et Biophysica Acta*, **812**, 139, 1985.

41.   Okamura, E.; Umemura, J. and Takenaka, T.; *Biochimica et Biophysica Acta*, **856**, 68, 1986.

42.   Ter-Minassian-Saraga, L.; Okamura, E.; Umemura, J. and Takenaka, T.; *Biochimica et Biophysica Acta*, **946**, 417, 1988.

43.   Matsuzaki, K.; Shioyama, T; Okamura, E.; Umemura, J.; Takenaka, T.; Takaishi, Y.; Fujita, T. and Miyajima, K.; *Biochimica et Biophysica Acta*, **1070**, 419, 1991.

44.   Vaughan, M. H.; Frogatt, E.S.; Swart, R. M. and Yarwood, J.; *Thin Solid Films*, **210/211**, 574, 1992.

45.   Haller, G.L. and Rice, R.W.; *J. Phys. Chem.*, **74**, 4386, 1970.

46.   Sperline, R. P.; Muralidharan, S. and Freiser, H.; *Langmuir*, **3**, 198, 1987.

47.   Kellar, J. J.; Cross, W. M. and Miller, J. D.; *Applied Spectroscopy*, **43**(8), 1456, 1989.

48.   Kellar, J. J.; Young, C. A.; Knutson, K. and Miller, J. D.; *J. Colloid and Interface Science*, **144**(2), 381, 1991.

49.   Pluedemann, E. P.; *Silane Coupling Agents*, 2nd Edition, Plenum Press, New York, 1990.

50.   Skoog, D. A.; *Principles of Instrumental Analysis*, 3rd Edition. Saunders College Publishing, 1985.

51.   Sagiv, J.; *J. Amer. Chem. Soc.*, **102**, 92, 1980.

52.   Sagiv, J.; *Israel J. Chemistry*, **18**(3-4), 339, 1980.

53.   Sagiv, J.; *Israel J. Chemistry*, **18**(3-4), 346, 1980.

54.   Netzer, L.; Iscovici, R. and Sagiv, J.; *Molecular Crystals and Liquid Crystals*, **93**(1-4), 415, 1983.

55.   Netzer, L.; Iscovici, R. and Sagiv, J.; *Thin Solid Films*, **99**(1-3), 235, 1983.

56.   Netzer, L.; Iscovici, R. and Sagiv, J.; *Thin Solid Films*, **100**(1), 67, 1983.

57.   Netzer, L. and Sagiv, J.; *J. Amer. Chem. Soc.*, **105**(3), 674, 1983.

58.   Maoz, R. and Sagiv, J; *J. Colloid and Interface Science*, **100**(2), 465, 1984.

59.   Gun, J.; Iscovici, R. and Sagiv, J.; *J. Colloid and Interface Science*, **101**(1), 201, 1984.

60.   Gun, J. and Sagiv, J.; *J. Colloid and Interface Science*, **112**(2), 457, 1986.

61.   Maoz, R. and Sagiv, J.; *Langmuir*, **3**(6), 1034, 1987.

62.   Maoz, R. and Sagiv, J.; *Langmuir*, **3**(6), 1045, 1987.

63.   Maoz, R. and Sagiv, J.; *Thin Solid Films*, **132**(1-4), 135, 1985.

64.   Tripp, C. P. and Hair, M. L.; *Langmuir*, **7**(5), 923, 1991.

65.   Angst, D. L. and Simmons, G. W.; *Langmuir*, **7**(10), 2236, 1991.

66.   Silberzan, P.; Léger, L.; Ausseré, D. and Benattar, J. J.; *Langmuir*, **7**, 1647, 1991.

67.   Tripp, C. P. and Hair, M. L., *Langmuir*, **8**(4), 1120, 1992.

68.   Parry, D. B. and Harris, J. M.; *Applied Spectroscopy*, **42**(6), 997, 1988.

69.

g, S. S.; Scherson, D. A. and Sukenik, C. N.; *J. American Chem. Soc.*, **114**, 5436, 1992.

70.   Herzberg, G; *Infrared and Raman Spectra of Polyatomic Molecules*, Van Nostrand, Princeton, New Jersey, 1945.

71.   Banwell, C. N.; *Fundamentals of Molecular Spectroscopy*, 3rd. Ed., McGraw-Hill,1983.

72.   Potts, W. J. Jr.; *Chemical Infrared Spectroscopy, Volume 1: Techniques*, John Wiley, New York, 1963.

73.   Brame, E. G. Jr. and Grasselli, J. G.; *Infrared and Raman Spectroscopy, Parts A, B and C;* Marcel Dekker, NewYork, 1976.

74.   Woodward, L. A.; *Introduction to the Theory of Molecular Vibrations and Vibrational Spectroscopy*, Oxford University Press, Oxford, 1972.

75.   Straughan, B. P. and Walker, S.; *Spectroscopy: Volume 2*, 1976.

76.   Griffiths, P. R. and deHaseth, J. A.; *Fourier Transform Infrared Spectroscopy*, Wiley-Interscience, New York, 1986.

77.   Chamberlain, J. E.; *The Principles of Interferometric Spectroscopy*, Wiley-Interscience, 1979.

78.   Ferraro, J. R. and Basile, L. J.; *Fourier Transform Infrared Spectroscopy, Applications to Chemical Systems, Vol. 1-4*, Academic Press, London, 1978.

79.   Mackenzie, M. W. (ed.); *Advances in Applied Fourier Transform Infrared Spectroscopy*; Wiley-Interscience, 1988.

80.   Bell, R. J.; *Introductory Fourier Transform Spectroscopy*, Academic Press, 1972.

81.   Griffiths, P. R.; *Chemical Infrared Fourier Transform Spectroscopy*, Wiley-Interscience, 1975.

82.   Ferraro, J. R. and Krishnan, K.; *Practical Fourier Transform Infrared Spectroscopy - Industrial and Laboratory Chemical Analysis*, Academic Press, 1990.

83.   Johnston, S. F.; *Fourier Transform Infrared - A Constantly Evolving Technology*, Ellis Horwood Ltd., 1991.

84.   Harrick, N. J.; *Internal Reflection Spectroscopy*, Wiley Interscience, 1967.

85.   Born, M. and Wolf, E.; *Principles of Optics*, 2nd Ed., Macmillan, New York, 1964.

86.   Harrick, N. J.; *J. Optical Soc. Am.*; **55**, 851, 1965.

87.   Kane, J. and Osterberg, H.; *J. Optical Soc. Am.*; **54**, 347, 1964.

88.   Song, Y. P.; *Reports on Electromagnetic Wave Considerations for FTIR and Waveguiding Raman Spectroscopy*, University of Durham Department of Chemistry Internal Report, Durham, 1992.

89.   Goos, F. and Hänchen, H.; *Ann. Physik*, **1**, 333, 1947.

90.   Goos, F. and Lindberg-Hänchen, H; *Ann. Physik*, **5**, 251, 1949.

91.   Müller, G.; Abraham, K. and Schaldach, M.; *Applied Optics*, **20**(7), 1182, 1981.

92.   Mirabella, F. M. Jr.; *Applied Spectroscopy Reviews*, **21**(1/2), 45, 1985.

93.   Tompkins, H. G.; *Applied Spectroscopy*, **28**, 335, 1974.

94.   Ohta, K., and Iwamoto, R.; *Analytical Chemistry*, **57**, 2491, 1985.

95.   Ohta, K., and Iwamoto, R.; *Applied Spectroscopy*, **39**, 418, 1985.

96.   Sperline, R. P.; Muralidharan, S. and Freiser, H.; *Applied Spectroscopy*, **40**, 1019, 1986.

97.   Braue, E. H. Jr. and Pannella, M. G.; *Applied Spectroscopy*, **41**(6), 1057, 1987.

98.   Braue, E. H. Jr. and Pannella, M. G.; *Applied Spectroscopy*, **41**(7), 1213, 1987.

99.   Mott, N. F.; *Philosophical Magazine B*, **55**(2), 117, 1987.

100.   Sperline, R. P.; *Applied Spectroscopy*, **45**(4), 677, 1991.

101.   Bellamy,; *The Infrared Spectra of Complex Molecules*, Volume 1

102.   Bellamy,; *The Infrared Spectra of Complex Molecules*, Volume 2

103.   Jones, R. N.; McKay, A. F. and Sinclair, R. G.; *J. American Chemical Society*, **74**, 2575, 1952.

104.   Kohno, M.; *J. Chemical Society of Japan*, **81**, 1805, 1960.

105.   Meiklejohn, R. A.; Meyer, R. J.; Aronovic, S. M.; Schuette, H. A. and Meloch, V. W.; *Analytical Chemistry*, **29**, 329, 1957.

106.   Kuroda, Y.; *J. Chemical Society of Japan*, **81**, 1624, 1961.

107.   Goto, R. and Takenaka, T.; *J. Chemical Society of Japan*, **84**, 392, 1963.

108.   Davis, M. M. and Schuhmann, P. J.; *J. Res. Nat. Bureau Standards Research Paper RP1825*, **39**, 221, 1947.

109.   *AEROSIL® as a Thickening Agent for Liquid Systems*, Technical Bulletin Pigments No. 23, Degussa A.G., Frankfurt.

110.   Fina, L. J. and Chen, G.; *Vibrational Spectroscopy*, **1**, 353, 1991.

111.   Rochester, C. H. and Trebilco, D.-A.; *J. Chem. Soc. Chem. Communications*, 621, 1977.

Appendix A

GWBASIC computer program to facilitate the calibration of the Squarecol ATR Cell

```
1000 REM SPERLINE
1010 REM Author-Simon Nunn-JY Group-Durham U Chem
Dept-30.5.91
1020 REM To perform an iterative calibration of an
 ATR cell using
1030 REM the method set out by Sperline et al in A
pplied Spectroscopy
1040 REM 40(7),1986,1019-1022
1050 CLS
1060 PRINT"SPERLINE - The program to perform an it
erative calibration of"
1070 PRINT"an ATR cell using the method set out by
 Sperline et al in"
1080 PRINT"Applied Spectroscopy 40(7) 1986 1019-10
22."
1090 PRINT:PRINT"Author - N S Nunn - Durham Univer
sity Chemistry Department"
1100 PRINT:PRINT:PRINT"This version 30.5.1991"
1110 PRINT:PRINT:PRINT:INPUT"Press ENTER to contin
ue......";DUMMY$
1120 CLS
1130 NIT=1
1140 PRINT"Refractive index of IRE";:INPUT RII
1150 PRINT
1160 INPUT"Refractive index of analyte";RIA
1170 PRINT
1180 INPUT"Angle of incidence ";THETA
1190 PRINT
1200 INPUT"Frequency (cm-1) ";CM
1210 PRINT:INPUT"Concentration of reference compou
nd (mol/dm^3)";CR
1220 PRINT:INPUT"INTEGRATED molar absorptivity (dm
3/mol/cm2)";ER
1230 PRINT:INPUT"INTEGRATED absorbance of referenc
e band (cm-1)";AR
1240 PRINT:INPUT"Solution contact length of prism
(cm) ";L
1250 PRINT:INPUT"Thickness of prism (cm) ";T
1260 PRINT:PRINT"Select polarization :-"
1270 PRINT:PRINT"1) TM (p polarized)"
1280 PRINT"2) TE (s polarized)"
1290 PRINT"3) Unpolarized"
1300 PRINT:INPUT CHOICE
1310 C=10000/CM
1320 PI=3.14159
1330 THETAR=(THETA/360)*(2*PI)
1340 D=COS(THETAR)
1350 E=SIN(THETAR)
1360 A=RIA/RII
1370 B=A*A
1380 F=E*E
1390 G=D*D
1400 H=A*A*A*A
1410 DPERP=A*C*D/(RII*PI*(1-B)*SQR(F-B)*10000)
1420 DPAR=(D*A*(2*F-B)*(C/RII))/(PI*(1-B)*((1+B)*F
-B)*SQR(F-B)*10000)
1430 DUP=(DPERP+DPAR)/2
1440 IF CHOICE=1 THEN DE=DPAR
```

```
1450  IF CHOICE=2 THEN DE=DPERP
1460  IF CHOICE=3 THEN DE=DUP
1470  N=AR/(ER*CR*DE)
1480  THETACALC=ATN(L/(N*T))
1490  THETANEW=(2*THETAR+THETACALC)/3
1500  TEST=(THETANEW-THETACALC)/THETANEW
1510  IF TEST>-.0002 AND TEST<.0002 THEN GOTO 1550
1520  THETAR=THETANEW
1530  NIT=NIT+1
1540  GOTO 1340
1550  CLS
1560  PRINT"Number of iterations = ";NIT
1570  THETAX=THETANEW*360/(2*PI)
1580  PRINT:PRINT"Calculated angle of incidence = "
;THETAX
1590  PRINT:PRINT"Calculated number of reflections
= ";N
1600  END
```

Appendix B

GWBASIC computer program to calculate the electromagnetic field intensities at the ATR prism/sample interface using Harrick's semi-infinite bulk approximation. The effective thickness is also calculated.

```
1000 REM ATRCALC
1010 REM Author-Simon Nunn-JY Group-Durham U Chem
Dept-28.5.91
1020 REM Program to calculate penetration depth. d
ecay constant.
1030 REM effective thickness. electric field ampli
tudes at the
1040 REM sample/IRE interface and at a defined dep
th.
1050 CLS
1060 PRINT"ATRCALC - To calculate ATR parameters "
;
1070 PRINT"for the semi-infinite bulk case."
1080 PRINT:PRINT"Author - N S Nunn  - Durham Unive
rsity Chemistry Dept."
1090 PRINT:PRINT"This version 29 May 1991"
1100 PRINT:PRINT
1110 REM Data input
1120 INPUT"Refractive index of IRE ";RII
1130 PRINT
1140 INPUT"Refractive index of analyte ";RIA
1150 PRINT
1160 INPUT"Angle of incidence (degrees) ";THETA
1170 PRINT
1180 INPUT"Frequency (cm-1) ";CM
1190 PRINT
1200 INPUT"Depth of interest (microns) ";MICRON
1210 PRINT
1220 C=10000/CM
1230 PI=3.14159
1240 D=COS((THETA/360)*(2*PI))
1250 E=SIN((THETA/360)*(2*PI))
1260 A=RIA/RII
1270 B=A*A
1280 F=E*E
1290 G=D*D
1300 H=A*A*A*A
1310 REM Calculate electric field intensities at i
nterface
1320 EY=2*D/SQR(1-B)
1330 EX=2*(SQR(F-B))*D/(SQR(1-B)*SQR((1+B)*F-B))
1340 EZ=2*D*E/(SQR(1-B)*SQR((1+B)*F-B))
1350 REM Calculate decay constant
1360 GAMMA=(2*PI*SQR(F-B)*RII)/C
1370 EXFN=EXP(-1*GAMMA*MICRON)
1380 REM Calculate effective thicknesses
1390 DPERP=A*C*D/(RII*PI*(1-B)*SQR(F-B))
1400 DPAR=(D*A*(2*F-B)*(C/RII))/(PI*(1-B)*((1+B)*F
-B)*SQR(F-B))
1410 DUP=(DPERP+DPAR)/2
1420 CLS
1430 REM Calculate penetration depth
1440 DP=C/(RII*2*PI*SQR(F-B))
1450 REM Display results
1460 PRINT"Penetration depth (microns) = ";DP
1470 PRINT:PRINT:PRINT"Effective thicknesses (micr
ons) :-"
1480 PRINT:PRINT"de (P wave)       = ";DPAR
```

```
1490 PRINT"de (S wave)         = ";DPERP
1500 PRINT"de (unpolarised) = ";DUP
1510 PRINT:PRINT
1520 PRINT"Decay constant (micron-1) = ";GAMMA
1530 PRINT:PRINT:PRINT
1540 INPUT"Press ENTER for electric field data....
.";DUMMY
1550 CLS
1560 PRINT"Electric field amplitudes at surface fo
r unit incident amplitude :-"
1570 PRINT
1580 PRINT"Eyo = ";EY;"    Eyo^2 = ";EY*EY
1590 PRINT"Exo = ";EX;"    Exo^2 = ";EX*EX
1600 PRINT"Ezo = ";EZ;"     Ezo^2 = ";EZ*EZ
'1610 REM Calculate electric field intensites at de
pth
1620 EYD=EY*EXFN
1630 EXD=EX*EXFN
1640 EZD=EZ*EXFN
1650 PRINT:PRINT
1660 PRINT"Electric field amplitudes at a depth of
 ";MICRON;" microns :-"
1670 PRINT:PRINT"Ey = ";EYD;"    Ey^2 = ";EYD*EYD
1680 PRINT"Ex = ";EXD;"    Ex^2 = ";EXD*EXD
1690 PRINT"Ez = ";EZD;"    Ez^2 = ";EZD*EZD
1700 REY=EYD/EY
1710 PRINT:PRINT
1720 PRINT"Ratio of field at depth to surface fiel
d :-"
1730 PRINT:PRINT"E/Eo = ";REY
1740 PRINT:PRINT
1750 INPUT"Do you want a hard copy (y/n)";REPLY$
1760 IF REPLY$="y" THEN GOTO 1780 ELSE GOTO 2060
1770 REM Produce hard copy
1780 LPRINT"For the following system :-"
1790 LPRINT:LPRINT"Refractive index of IRE
= ";RII
1800 LPRINT"Refractive index of Sample     = ";RIA
1810 LPRINT"Angle of incidence          = ";THE
TA;" degrees"
1820 LPRINT"Frequency                   = ";CM;
" cm-1"
1830 LPRINT
1840 LPRINT"Penetration depth (microns) = ";DP
1850 LPRINT
1860 LPRINT"Effective thicknesses (microns) :-"
1870 LPRINT:LPRINT"de (S wave)      = ";DPERP
1880 LPRINT"de (P wave)      = ";DPAR
1890 LPRINT"de (unpolarised) = ";DUP
1900 LPRINT:LPRINT"Decay constant = ";GAMMA
1910 LPRINT
1920 LPRINT"Electric field amplitudes at substrate
/IRE interface :-"
1930 LPRINT
1940 LPRINT"Eyo = ";EY;"    Eyo^2 = ";EY*EY
1950 LPRINT"Exo = ";EX;"    Exo^2 = ";EX*EX
1960 LPRINT"Ezo = ";EZ;"     Ezo^2 = ";EZ*EZ
1970 LPRINT
1980 LPRINT"Electric field amplitudes at a depth o
```

```
f ":MICRON;" microns :-"
1990 LPRINT:LPRINT"Ey = ";EYD;"    Ey^2 = ":EYD*EY
D
2000 LPRINT"Ex = ";EXD;"    Ex^2 = ":EXD*EXD
2010 LPRINT"Ez = ";EZD;"    Ez^2 = ":EZD*EZD
2020 LPRINT:LPRINT
2030 LPRINT"Ratio of E at depth to E at surface :-
"
2040 LPRINT:LPRINT"E/Eo = ";REY
2050 LPRINT:LPRINT:LPRINT
2060 END
```

GWBASIC computer program to calculate surface excess concentrations from ATR spectra.

```basic
1000 REM EXCESS version 1
1010 REM Author-Simon Nunn-JY Group-Durham U Chem Dept-30.5.91
1020 REM To calculate Gibbs Surface Excess from ATR measurements
1030 REM according to the method set out in Langmuir 3(2) 1987 198-202
1040 REM pp 1019-1022.
1050 CLS
1060 PRINT"EXCESS - The program to calculate the surface excess concentration"
1070 PRINT"at the sample/IRE interface in an ATR experiment according to the"
1080 PRINT"method set out by Sperline et al in Langmuir 3(2) 1987 198-202."
1090 PRINT:PRINT"Author - N S Nunn - Durham University Chemistry Department."
1100 PRINT:PRINT"This version 30.5.1991"
1110 PRINT:PRINT:PRINT:INPUT"Press ENTER to continue ";DUMMY$
1120 CLS
1130 PRINT"Refractive index of IRE";:INPUT RII
1140 PRINT
1150 INPUT"Refractive index of analyte";RIA
1160 PRINT
1170 INPUT"Angle of incidence ";THETA
1180 PRINT
1190 INPUT"Frequency (cm-1) ";CM
1200 PRINT:INPUT"Concentration of sample compound (mol/dm^3)";CS
1210 PRINT:INPUT"INTEGRATED molar absorptivity (dm3/mol/cm2)";ES
1220 PRINT:INPUT"INTEGRATED absorbance of sample band ";AS
1230 PRINT:INPUT"Number of Reflections ";N
1240 PRINT:PRINT"Select polarization :-"
1250 PRINT:PRINT"1) TM (p polarized)"
1260 PRINT"2) TE (s polarized)"
1270 PRINT"3) Unpolarized"
1280 PRINT:INPUT CHOICE
1290 C=1/CM
1300 PI=3.14159
1310 THETAR=(THETA/360)*(2*PI)
1320 D=COS(THETAR)
1330 E=SIN(THETAR)
1340 A=RIA/RII
1350 B=A*A
1360 F=E*E
1370 G=D*D
1380 H=A*A*A*A
1390 DP=C/(RII*2*PI*SQR(F-B))
1400 DPERP=A*C*D/(RII*PI*(1-B)*SQR(F-B))
1410 DPAR=(D*A*(2*F-B)*(C/RII))/(PI*(1-B)*((1+B)*F-B)*SQR(F-B))
1420 DUP=(DPERP+DPAR)/2
1430 IF CHOICE=1 THEN DE=DPAR
1440 IF CHOICE=2 THEN DE=DPERP
1450 IF CHOICE=3 THEN DE=DUP
1460 CIT=((AS/N)-(ES*CS*DE))/(ES*(2*DE/DP))
1470 GIBB=CIT/1000
1480 BULK=100*(CS*DP/(CS*DP+2000*GIBB))
1490 AREA=10^16/(GIBB*6.022*10^23)
1500 CLS
1510 PRINT"Gibbs Surface Excess = ";GIBB;" mol cm-2"
1520 PRINT
1530 PRINT"Proportion of absorbance band due to bulk species = ";BULK;" % "
1540 PRINT
1550 PRINT"Area available per molecule = ";AREA;"Angstrom^2"
1560 END
```

Appendix D

List of colloquia, lectures and seminars given by invited speakers at Durham from 1st August 1990 to 31st July 1993.

Those lectures marked * were attended by the author.

List of conferences attendended.

UNIVERSITY OF DURHAM

Board of Studies in Chemistry

COLLOQUIA, LECTURES AND SEMINARS GIVEN BY INVITED SPEAKERS
1ST AUGUST 1990 TO 31ST JULY 1991

* ALDER, Dr. B.J. (Lawrence Livermore Labs., California) 15th January, 1991
    Hydrogen in all its Glory

* BELL[+], Prof. T. (SUNY, Stoney Brook, U.S.A.) 14th November, 1990
    Functional Molecular Architecture and Molecular
    Recognition

BOCHMANN[+], Dr. M. (University of East Anglia) 24th October, 1990
    Synthesis, Reactions and Catalytic Activity of
    Cationic Titanium Alkyls

BRIMBLE, Dr. M.A. (Massey University, New Zealand) 29th July, 1991
    Synthetic Studies Towards the Antibiotic
    Griseusin-A

BROOKHART, Prof. M.S. (University of N. Carolina) 20th June, 1991
    Olefin Polymerizations, Oligomerizations and
    Dimerizations Using Electrophilic Late Transition
    Metal Catalysts

BROWN, Dr. J. (Oxford University) 28th February, 1991
    Can Chemistry Provide Catalysts Superior to Enzymes?

* BUSHBY[+], Dr. R. (Leeds University) 6th February, 1991
    Biradicals and Organic Magnets

COWLEY, Prof. A.H. (University of Texas) 13th December, 1990
    New Organometallic Routes to Electronic Materials

CROUT, Prof. D. (Warwick University) 29th November, 1990
    Enzymes in Organic Synthesis

* DOBSON[+], Dr. C.M. (Oxford University) 6th March, 1991
    NMR Studies of Dynamics in Molecular Crystals

* GERRARD[+], Dr. D. (British Petroleum) 7th November, 1990
    Raman Spectroscopy for Industrial Analysis

HUDLICKY, Prof. T. (Virginia Polytechnic Institute) 25th April, 1991
  . Biocatalysis and Symmetry Based Approaches to the
    Efficient Synthesis of Complex Natural Products

JACKSON[+], Dr. R. (Newcastle University) 31st October, 1990
    New Synthetic Methods: α-Amino Acids and Small
    Rings

KOCOVSKY[+], Dr. P. (Uppsala University) 6th November, 1990
    Stereo-Controlled Reactions Mediated by Transition
    and Non-Transition Metals

* LACEY, Dr. D. (Hull University)   31st January, 1991
  Liquid Crystals

* LOGAN, Dr. N. (Nottingham University) 1st November, 1990
  Rocket Propellants

* MACDONALD, Dr. W.A. (ICI Wilton)   11th October, 1990
  Materials for the Space Age

 MARKAM, Dr. J. (ICI Pharmaceuticals) 7th March, 1991
  DNA Fingerprinting

*PETTY, Dr. M.C. (Durham University) 14th February, 1991
  Molecular Electronics

PRINGLE[+], Dr. P.G. (Bristol University) 5th December, 1990
  Metal Complexes with Functionalised Phosphines

* PRITCHARD, Prof. J. (Queen Mary & Westfield College, 21st November, 1990
  London University)
  Copper Surfaces and Catalysts

*SADLER, Dr. P.J. (Birkbeck College London) 24th January, 1991
  Design of Inorganic Drugs: Precious Metals,
  Hypertension + HIV

*SARRE, Dr. P. (Nottingham University) 17th January, 1991
  Comet Chemistry

SCHROCK, Prof.R.R. (Massachusetts Institute of Technology) 24th April, 1991
  Metal-ligand Multiple Bonds and Metathesis Initiators

SCOTT, Dr. S.K. (Leeds University) 8th November, 1990
  Clocks, Oscillations and Chaos

SHAW[+], Prof. B.L. (Leeds University) 20th February, 1991
  Syntheses with Coordinated, Unsaturated Phosphine
  Ligands

* SINN[+], Prof. E. (Hull University) 30th January, 1991
  Coupling of Little Electrons in Big Molecules.
  Implications for the Active Sites of (Metalloproteins
  and other) Macromolecules

SOULEN[+], Prof. R. (South Western University, Texas) 26th October, 1990
  Preparation and Reactions of Bicycloalkenes

* WHITAKER[+], Dr. B.J. (Leeds University) 28th November, 1990
  Two-Dimensional Velocity Imaging of State-Selected
  Reaction Products

[+] Invited specifically for the postgraduate training programme.

UNIVERSITY OF DURHAM

Board of Studies in Chemistry

COLLOQUIA, LECTURES AND SEMINARS FROM INVITED SPEAKERS

1991 – 1992 (August 1 – July 31)

1991

*October   17   Dr. J.A. Salthouse, University of Manchester
Son et Lumiere – a demonstration lecture

*October   31   Dr. R. Keeley, Metropolitan Police Forensic Science
Modern forensic science

* November   6   Prof. B.F.G. Johnson[†], Edinburgh University
Cluster–surface analogies

* November   7   Dr. A.R. Butler, St. Andrews University
Traditional Chinese herbal drugs: a different way of treating disease

November   13   Prof. D. Gani[†], St. Andrews University
The chemistry of PLP–dependent enzymes

November   20   Dr. R. More O'Ferrall[†], University College, Dublin
Some acid–catalysed rearrangements in organic chemistry

November   28   Prof. I.M. Ward, IRC in Polymer Science, University of Leeds
The SCI lecture: the science and technology of orientated polymers

December   4   Prof. R. Grigg[†], Leeds University
Palladium–catalysed cyclisation and ion–capture processes

December   5   Prof. A.L. Smith, ex Unilever
Soap, detergents and black puddings

December   11   Dr. W.D. Cooper[†], Shell Research
Colloid science: theory and practice

1992

*January   22   Dr. K.D.M. Harris[†], St. Andrews University
Understanding the properties of solid inclusion compounds

January   29   Dr. A. Holmes[†], Cambridge University
Cycloaddition reactions in the service of the synthesis of piperidine and indolizidine natural products

Board of Studies in Chemistry

COLLOQUIA, LECTURES AND SEMINARS FROM INVITED SPEAKERS

1992 - 1993 (August 1 - July 31)

1992

* October 15   Dr M. Glazer & Dr. S. Tarling, Oxford University & Birbeck College, London
It Pays to be British! - The Chemist's Role as an Expert Witness in Patent
Litigation

October 20   Dr. H. E. Bryndza, Du Pont Central Research
Synthesis, Reactions and Thermochemistry of Metal (Alkyl) Cyanide Complexes
and Their Impact on Olefin Hydrocyanation Catalysis

* October 22   Prof. A. Davies, University College London
The Ingold-Albert Lecture The Behaviour of Hydrogen as a Pseudometal

October 28   Dr. J. K . Cockcroft, University of Durham
Recent Developments in Powder Diffraction

October 29   –   Dr. J. Emsley, Imperial College, London
The Shocking History of Phosphorus

November 4   Dr. T. P. Kee, University of Leeds
Synthesis and Co-ordination Chemistry of Silylated Phosphites

* November 5   Dr. C. J. Ludman, University of Durham
Explosions, A Demonstration Lecture

November 11   Prof. D. Robins†, Glasgow University
Pyrrolizidine Alkaloids : Biological Activity, Biosynthesis and Benefits

* November 12   Prof. M. R. Truter, University College, London
Luck and Logic in Host - Guest Chemistry

* November 18   Dr. R. Nix†, Queen Mary College, London
Characterisation of Heterogeneous Catalysts

November 25   Prof. Y. Vallee. University of Caen
Reactive Thiocarbonyl Compounds

November 25   Prof. L. D. Quin†, University of Massachusetts, Amherst
Fragmentation of Phosphorous Heterocycles as a Route to Phosphoryl Species
with Uncommon Bonding

* November 26   Dr. D. Humber, Glaxo, Greenford
AIDS - The Development of a Novel Series of Inhibitors of HIV

December 2   Prof. A. F. Hegarty, University College, Dublin
Highly Reactive Enols Stabilised by Steric Protection

December 2   Dr. R. A. Aitken†, University of St. Andrews
The Versatile Cycloaddition Chemistry of $Bu_3P.CS_2$

* December 3   Prof. P. Edwards, Birmingham University
The SCI Lecture - What is Metal?

* December 9   Dr. A. N. Burgess†, ICI Runcorn
The Structure of Perfluorinated Ionomer Membranes

272

* January   30   Dr. M. Anderson, Sittingbourne Research Centre, Shell Research
Recent Advances in the Safe and Selective Chemical Control of Insect
Pests

* February   12   Prof. D.E. Fenton[†], Sheffield University
Polynuclear complexes of molecular clefts as models for copper biosites

* February   13   Dr. J. Saunders, Glaxo Group Research Limited
Molecular Modelling in Drug Discovery

February   19   Prof. E.J. Thomas[†], Manchester University
Applications of organostannanes to organic synthesis

* February   20   Prof. E.Vogel, University of Cologne
The Musgrave Lecture   Porphyrins: Molecules of Interdisciplinary
Interest

* February   25   Prof. J.F. Nixon, University of Sussex
The Tilden Lecture   Phosphaalkynes: new building blocks in inorganic
and organometallic chemistry

* February   26   Prof. M.L. Hitchman[†], Strathclyde University
Chemical vapour deposition

* March   5   Dr. N.C. Billingham, University of Sussex
Degradable Plastics – Myth or Magic?

March   11   Dr. S.E. Thomas[†], Imperial College
Recent advances in organoiron chemistry

* March   12   Dr. R.A. Hann, ICI Imagedata
Electronic Photography – An Image of the Future

March   18   Dr. H. Maskill[†], Newcastle University
Concerted or stepwise fragmentation in a deamination–type reaction

April   7   Prof. D.M. Knight, Philosophy Department, University of Durham
Interpreting experiments: the beginning of electrochemistry

May   13   Dr. J–C Gehret, Ciba Geigy, Basel
Some aspects of industrial agrochemical research

[†] Invited specially for the postgraduate training programme.

~3

<u>1993</u>

✻ January 20   Dr. D. C. Clary†, University of Cambridge
Energy Flow in Chemical Reactions

✻ January 21   Prof. L. Hall, Cambridge
NMR - Window to the Human Body

January 27   Dr. W. Kerr, University of Strathclyde
Development of the Pauson-Khand Annulation Reaction : Organocobalt Mediated
Synthesis of Natural and Unnatural Products

January 28   Prof. J. Mann, University of Reading
Murder, Magic and Medicine

February 3   Prof. S. M. Roberts, University of Exeter
Enzymes in Organic Synthesis

February 10   Dr. D. Gillies†, University of Surrey
NMR and Molecular Motion in Solution

February 11   Prof. S. Knox, Bristol University
The Tilden Lecture Organic Chemistry at Polynuclear Metal Centres

February 17   Dr. R. W. Kemmitt†, University of Leicester
Oxatrimethylenemethane Metal Complexes

February 18   Dr. I. Fraser, ICI Wilton
Reactive Processing of Composite Materials

February 22   Prof. D. M. Grant, University of Utah
Single Crystals, Molecular Structure, and Chemical-Shift Anisotropy

✻ February 24   Prof. C. J. M. Stirling†, University of Sheffield
Chemistry on the Flat-Reactivity of Ordered Systems

March 10   Dr. P. K. Baker, University College of North Wales, Bangor
'Chemistry of Highly Versatile 7-Coordinate Complexes'

✻ March 11   Dr. R. A. Y. Jones, University of East Anglia
The Chemistry of Wine Making

March 17   Dr. R. J. K. Taylor†, University of East Anglia
Adventures in Natural Product Synthesis

March 24   Prof. I. O. Sutherland†, University of Liverpool
Chromogenic Reagents for Cations

✻ May 13   Prof. J. A. Pople, Carnegie-Mellon University, Pittsburgh, USA
The Boys-Rahman Lecture Applications of Molecular Orbital Theory

May 21   Prof. L. Weber, University of Bielefeld
Metallo-phospha Alkenes as Synthons in Organometallic Chemistry

June 1   Prof. J. P. Konopelski, University of California, Santa Cruz
Synthetic Adventures with Enantiomerically Pure Acetals

June 2   Prof. F. Ciardelli, University of Pisa
Chiral Discrimination in the Stereospecific Polymerisation of Alpha Olefins

June 7   Prof. R. S. Stein, University of Massachusetts   274
Scattering Studies of Crystalline and Liquid Crystalline Polymers

June 16   Prof. A. K. Covington, University of Newcastle
               Use of Ion Selective Electrodes as Detectors in Ion Chromatography

✳ June 17   Prof. O. F. Nielsen, H. C. Ørsted Institute, University of Copenhagen
               Low-Frequency IR - and Raman Studies of Hydrogen Bonded Liquids

† Invited specially for the graduate training programme.

File Ref. CG137/E(CH)

Research Conferences Attended

Adsorption of Surfactants and Polymers, A Research Conference of the Colloid & Interface Science Group of the Royal Society of Chemistry, Bath University, 10-12th September, 1991.

Polymer Surfaces and Interfaces II, An International Symposium organized under the auspices of the Macro Group, U.K., University of Durham, 22nd-26th July 1991.

9th International Conference on Fourier Transform Spectroscopy, University of Calgary, Alberta, 23rd-27th August 1993.[†]

[†] Poster presented :

"F.T.I.R.-A.T.R. studies of surfactant adsorption at the solid/liquid interface"

N. Simon Nunn[†], Jack Yarwood[†*], Paul A. Stevenson[‡] and W. David Cooper[‡][†]Department of Chemistry, University of Durham, Durham, U.K, DH1 3LE[‡]Shell Research Ltd., Thornton Research Centre, P.O. Box 1, Chester, U.K.